UiO **: University of Oslo**

Maksym Teslyk

Information entropy and its applications in high-energy physics and astrophysics

Thesis submitted for the degree of Philosophiae Doctor

Department of Physics
The Faculty of Mathematics and Natural Sciences

Faculty of Physics
Taras Shevchenko National University of Kyiv

2023

Abstract

Today we are living in the Information Age. Amount of data influences reliability of models, validity of decisions and forecasts at any level from the one's everyday life to global economy. Information is a valuable resource of great demand in any sphere today.

Physics is not an exception from this general rule. Any experiment or finding increases our knowledge about reality. Any additional piece of information we collect improves our physical models and provides a deeper level of understanding.

It is easy to estimate how much we know about some process. This can be represented as the number of bytes encoding the data we have collected. For example, the LHC experiment generates more than 30 PB ($\mathcal{O}\left(10^{16}\right)$ bytes) annually.

Therefore, one comes to the obvious conclusion: the more we know, the more we understand. But how about what we *do not* know? Can we estimate our unawareness about a physical system? How can it help us to improve, validate or discard our models of some phenomena?

There is an answer to the first two questions: information entropy. It serves as a measure of how much we do not know. Attempts to find the answer to the third one have induced this study. It is focused on entropy and its role in relativistic heavy ion collisions and in the physics of black holes. Despite the items seem to differ a lot, both of them do have something in common: probability distributions of observables. And in what follows we will find out how our lack of information can be useful for expanding our knowledge about nature.

The main idea of this thesis is to demonstrate how both quantum and classical information entropies may help us to solve modern problems of high energy physics and astrophysics.

The thesis is a collection of eight papers, presented in chronological order separately for each of the considered topics. These are preceded by Part I, which is an introductory one. It contains reviews of topics serving as motivation for the research and brief discussions of open problems. A concise description of models and formalisms used throughout the study is included also. The papers can be found in Part II.

Information entropy is a basic tool used throughout the study. In order to set up the background, some basics and necessary concepts of information theory for entropy quantification are presented in Chapter 1. It includes also a brief discussion of entropy interpretation.

A deconfined state of matter, known as quark-gluon plasma, its signatures and fluid properties are discussed in Chapter 2. The chapter is accompanied by a brief description of equilibration and early entropy generation problems in

collision experiments; these are presented in Chapter 3. It also discusses particle momentum distributions and how these can be used to extract entropy even in a far-from-equilibrium state.

Chapter 4 contains models and formalisms used to study viscous properties of the plasma. The description of the performed investigation and main results on specific viscosity can be found in Chapter 5.

Chapter 6 is devoted to black hole thermodynamics, information loss and black hole entropy problems. These are deep issues inspiring a vast amount of theoretical findings with far-reaching consequences for modern physics. To give a taste, the Chapter briefly discusses popular approaches to some problems and open questions in gravity quantization.

Unruh effect is suggested as a promising solution for the black hole problems. Its description and the discussion of Unruh radiation entropy can be found in Chapter 7. The main results for this part of the study are presented in Chapter 8.

Finally, Chapter 9 contains the summary. It concludes on the role of information entropy in resolving the studied problems and efficiency of such a tool. At the end, one can find a brief outline of possible improvements and issues for further research.

Sammendrag

Vi lever i informasjonsalderen. Datamengden påvirker påliteligheten til modeller, gyldigheten av beslutninger og prognoser på alle nivåer fra ens hverdag til global økonomi. Informasjon er en verdifull ressurs med stor etterspørsel på alle områder i dag.

Fysikk er ikke et unntak fra denne generelle regelen. Ethvert eksperiment eller funn øker vår kunnskap om virkeligheten. All tilleggsinformasjon vi samler inn forbedrer våre fysiske modeller og gir et dypere nivå av forståelse.

Det er lett å anslå hvor mye vi vet om en prosess. Dette kan representeres som antall byte som koder for dataene vi har samlet inn. For eksempel genererer LHC-eksperimentet mer enn 30 PB ($\mathcal{O}\left(10^{16}\right)$ byte) årlig.

Derfor kommer man til den åpenbare konklusjonen: jo mer vi vet, jo mer forstår vi. Men hva med det vi *ikke* vet? Kan vi anslå vår uvitenhet om et fysisk system? Hvordan kan det hjelpe oss å forbedre, validere eller forkaste modellene våre for noen fenomener?

Det finnes et svar på de to første spørsmålene: informasjonsentropi. Denne fungerer som et mål på hvor mye vi ikke vet. Forsøk på å finne svaret på det tredje spørsmålet er motivasjonen bak denne avhandlingen. Den er fokusert på entropi og dens rolle i relativistiske tungionekollisjoner og i fysikken til sorte hull. Til tross for at disse to emnene kan virke veldig ulike, har de noe viktig til felles: sannsynlighetsfordelinger av observable. Og i det følgende skal vi finne ut hvordan vår mangel på informasjon kan være nyttig for å utvide vår kunnskap om naturen.

Hovedideen med denne oppgaven er å demonstrere hvordan både kvante- og klassiske informasjonsentropier kan hjelpe oss til å løse moderne problemer innen høyenergifysikk og astrofysikk.

Oppgaven er en samling av åtte artikler, presentert i kronologisk rekkefølge separat for hvert av hovedemnene. Del I er avhandlingens innledende del. Den inneholder en gjennomgang av bakgrunn og motivasjon for forskningen, samt korte diskusjoner av åpne problemer. En kortfattet beskrivelse av modeller og formalisme brukt gjennom hele studien er også inkludert. Selve artiklene utgjør Del II.

Informasjonsentropi er et grunnleggende verktøy som brukes gjennom hele studiet. For å gi den nødvendige bakgrunnen, presenteres grunnleggende begreper innen informasjonsteori for entropikvantifisering i Kapittel 1. Dette inkluderer også en kort diskusjon om tolkning av entropi.

Kvark-gluon plasma (en tilstand til materie hvor kvarker og gluoner kan bevege seg relativt fritt), dens signaturer og væskeegenskaper er diskutert i Kapittel 2. Kapittelet er ledsaget av en kort beskrivelse av ekvilibrering og problemer rundt tidlig entropigenerering i kollisjonseksperimenter; disse er presentert

i Kapittel 3. Dette kapitlet diskuterer også partikkelmomentumfordelinger og hvordan disse kan brukes til å trekke ut entropi selv i en tilstand langt fra likevekt.

Kapittel 4 inneholder modeller og formalisme som brukes til å studere viskøse egenskaper til plasma. Beskrivelsen av utført undersøkelse og hovedresultater på spesifikk viskositet finnes i Kapittel 5.

Kapittel 6 er viet til sorte hulls termodynamikk, informasjonstap og entropien til sorte hull. Dette er dype problemstillinger som inspirerer en enorm mengde teoretiske funn med vidtrekkende konsekvenser for moderne fysikk. For å gi en smakebit, diskuterer kapitlet kort populære tilnærminger til noen problemer og åpne spørsmål i gravitasjonskvantisering.

Unruh-effekten er foreslått som en lovende løsning for problemene med sorte hull. Beskrivelsen og diskusjonen om Unruh-strålingsentropi kan finnes i Kapittel 7. Hovedresultatene for denne delen av studien er presentert i Kapittel 8.

Til slutt inneholder Kapittel 9 sammendraget. Det konkluderer med informasjonsentropiens rolle i å løse de studerte problemene og effektiviteten til et slikt verktøy. Helt til slutt finnes en kort oversikt over mulige forbedringer og problemstillinger for videre forskning.

Acknowledgements

I am very thankful to all the people for help and critical remarks during the research work and while preparing the thesis. There are too many of them to list everyone here.

Especially I would like to thank Larissa Bravina and Evgeny Zabrodin, who have contributed a lot to my investigation of relativistic heavy ion collisions. Their support cannot be overestimated. I appreciate all our discussions during the research and hope we will have much more in the future.

I am deeply grateful to Eugene Belokolos who introduced me to information theory.

A great thanks goes out to my colleagues for all the discussions, remarks and advices during the research.

Last but not least I would like to express my deep gratitude to my family for all the support and belief in me while preparing this thesis.

Maksym Teslyk
Oslo, August 2023

List of Papers

Paper I

Teslyk, M., Bravina, L., Panova, O., Vitiuk, O., Zabrodin, E.
"Shear viscosity in microscopic calculations of $A + A$ collisions at energies available at the Nuclotron-based Ion Collider fAcility (NICA)".
In: *Physical Review C*. Vol. 101, no. 1 (2020), pp. 014904. DOI: 10.1103/PhysRevC.101.014904.

Paper II

Zabrodin, E., Teslyk, M., Vitiuk, O., Bravina, L.
"Calculation of shear viscosity in Au+Au collisions at NICA energies".
In: *Physica Scripta.* Vol. 95, no. 7 (2020), pp. 074009. DOI: 10.1088/1402-4896/ab9035.
International Conference on New Frontiers in Physics (ICNFP19) August 2019.

Paper III

Zabrodin, E., Teslyk, M., Vitiuk, O., Bravina, L.
"Shear viscosity of nucleons and pions in heavy-ion collisions at energies of NICA".
In: *Journal of Physics: Conference Series*. Vol. 1690, (2020), pp. 012106. DOI: 10.1088/1742-6596/1690/1/012106.

Paper IV

Zabrodin, E., Bravina, L., Teslyk, M., Vitiuk, O.
"Early thermalization and shear viscosity to entropy ratio in heavy-ion collisions at energies of BES, FAIR and NICA".
In: *Nuclear Physics A*. Vol. 1005, (2021), pp. 121861. DOI: https://doi.org/10.1016/j.nuclphysa.2020.121861.
XXVIIIth International Conference on Ultrarelativistic Nucleus-Nucleus Collisions (Quark Matter 2019).

Paper V

Teslyk, M., Bravina, L., Zabrodin, E.
"Total and Partial Shear Viscosity in Heavy-Ion Collisions at Energies of BES,

FAIR and NICA".
In: *Symmetry.* Vol. 14, no. 4 (2022), pp. 634. DOI: 10.3390/sym14040634.

Paper VI

Belokolos, E. D., Teslyk, M. V.
"Scalar field entanglement entropy of a Schwarzschild black hole from the Schmidt decomposition viewpoint".
In: *Classical and Quantum Gravity.* Vol. 26, no. 23 (2009), pp. 235008. DOI: 10.1088/0264-9381/26/23/235008.

Paper VII

Teslyk, M. V., Teslyk, O. M.
"Scalar field entanglement entropy for a small Schwarzschild black hole".
In: *Classical and Quantum Gravity.* Vol. 30, no. 12 (2013), pp. 125013. DOI: 10.1088/0264-9381/30/12/125013.

Paper VIII

Teslyk, M., Teslyk, O., Zadorozhna, L., Bravina, L., Zabrodin, E.
"Unruh Effect and Information Entropy Approach".
In: *Particles.* Vol. 5, no. 2 (2022), pp. 157–170. DOI: 10.3390/particles5020014.

Contents

Contents

List of Figures

Part I

Introduction

Chapter 1

Information entropy

1.1   Information theory

In 1948, Claude Shannon proposed to consider entropy as a measure of information [Sha48]. Together with Harry Nyquist [Nyq24; Nyq28] and Ralph Hartley [Har28] this allowed to establish information theory. Its development caused the emergence of entire technological industries related to information processing, computing and communication.

The concept of information has been widely accepted in physics. Usually it is used in thermodynamics via both entropy and Landauer's principle. Direct study of the role of information in statistical physics and thermodynamics begins with such works as [Jay57]. In such a relatively new field as quantum thermodynamics [VA16] active research is being conducted on the fusion of quantum mechanics and statistics. Information theory is also widely applied in probability theory, which, in turn, is a must have tool for studying various problems from non-equilibrium phenomena [Bla+20; ZMR96; ZMR97] to particle physics.

As Shannon demonstrated, information is strongly related to entropy; both concepts complement each other. Naively, information may be interpreted as negative entropy. The relation allows to analyze a wide range of physical phenomena going far beyond its common usage as a measure of information lack. It may be used as a useful instrument to analyze different phenomena far beyond information theory.

1.2   Basic concepts

Let us have a message $\mathbb{E}$ and some alphabet $\mathbb{A}_q$ consisting of q symbols. Then $\mathbb{E}$ may be encoded with a word $\mathbb{E}_{\mathbb{A}_q}$ containing

$$n = \mathcal{O}\left(\log_q \mathbb{E}\right), \quad q > 1 \tag{1.1}$$

symbols of the $\mathbb{A}_q$. Quantity n represents amount of information contained in $\mathbb{E}$ which is encoded with $\mathbb{A}_q$.

Expression (1.1) may be transformed as

$$n = \mathcal{O}\left(\log_q \mathbb{E}\right) = \mathcal{O}\left(\log_{q'} q \cdot \log_q \mathbb{E}\right) = \mathcal{O}\left(\log_{q'} \mathbb{E}\right). \tag{1.2}$$

This means that translation to another alphabet $\mathbb{A}_q \to \mathbb{A}_{q'}$ does not influence the amount. In other terms, the size of $\mathbb{E}$ is determined up to some arbitrary constant factor depending on q only. The case $q = 1$ is degenerate and should be omitted: as one can see from (1.1), any unary alphabet $\mathbb{A}_1$ is inefficient for encoding.

So, without any loss of generality the amount of information may be expressed in bits ($q = 2$) or in any other units. The symbol $\mathcal{O}$ absorbs any finite constant, so in what follows, the base of the logarithm in (1.1) will be set equal to e.

Within the formalism, an arbitrary number $N > 1$ may be interpreted as some message (word) $\mathbb{E} \equiv N$. So, N contains $\mathcal{O}(\ln N)$ units of information. This means that N may be encoded with the sequence consisting of $n = \mathcal{O}(\ln N)$ symbols.

Any non-negative number $p < 1$ is mutually and uniquely related to its inverse $\frac{1}{p} > 1$. The problem of finding the inverse reduces to translation from one alphabet to another and, therefore, does not change the amount of information. So, p may be encoded with

$$\ln \frac{1}{p} = -\ln p \tag{1.3}$$

symbols.

1.3 Probability distributions and entropy

Let us have some distribution $\{X\}$ of quantity x with discrete unnormalized probability $d(x)$. For example, one may interpret $\{X\}$ as the set of events where each outcome x is observed with frequency $d(x)$.

Shannon entropy (information entropy) $H(X)$ for the distribution $\{X\}$ is defined as follows

$$\begin{aligned}
H(X) &= -\sum_x \frac{d(x)}{D_X} \ln \frac{d(x)}{D_X} \\
&= \ln D_X - \frac{1}{D_X} \sum_x d(x) \ln d(x),
\end{aligned} \tag{1.4}$$

where

$$D_X = \sum_x d(x) \tag{1.5}$$

is the norm, i.e. the number of all events from $\{X\}$.

As one can see from (1.4), $H(X)$ is invariant with respect to scaling. That is, for any constant $\alpha \neq 0$ it does not change under $d(x) \to \alpha d(x)$. So, frequencies may be normalized in any convenient way, and D_X may be equal to any non-negative number.

From (1.4) it follows that for the uniform distribution Shannon entropy reaches its maximum and equals to

$$\max[H(X)] = \ln \frac{D_X}{d} \quad \Leftrightarrow \quad d(x) = d = \text{const} \neq 0. \tag{1.6}$$

Expression (1.6) is valid only if our knowledge is minimal: all $x \in \{X\}$ are equally likely. We are completely unaware about exact value of x.

Due to the scaling invariance, one can set $d = 1$ in (1.6). Then D_X is simply equal to the number of possible states our system can be found in, and $H(X) = \ln D_X$.

Similarly, one may define information entropy $H(X,Y)$ for a joint distribution $\{X,Y\}$ of two quantities, x and y, with probability $d(x,y)$:

$$
\begin{aligned}
H(X,Y) &= -\sum_{x,y} \frac{d(x,y)}{D_{X,Y}} \ln \frac{d(x,y)}{D_{X,Y}} \\
&= \ln D_{X,Y} - \frac{1}{D_{X,Y}} \sum_{x,y} d(x,y) \ln d(x,y),
\end{aligned}
\tag{1.7}
$$

where

$$
D_{X,Y} = \sum_{x,y} d(x,y)
\tag{1.8}
$$

is the number of events where all possible x and y are being observed.

In case of $\{X,Y\}$ one may define also the conditional distribution $\{X|y\}$ with the corresponding conditional probability $d(x|y)$

$$
d(x|y) = \frac{d(x,y)}{d(y)},
\tag{1.9}
$$

where

$$
d(y) = \sum_x d(x,y).
\tag{1.10}
$$

Here $d(x|y)$ defines the probability to find x if y has been observed.

Shannon entropy $H(X|y)$ for $\{X|y\}$ reads

$$
H(X|y) = -\sum_x d(x|y) \ln d(x|y),
\tag{1.11}
$$

where it has been taken into account that, due to (1.9) and (1.10), $D_{X|y} = 1$.

Substitution of (1.9), (1.10) and (1.11) into (1.7) leads to the well known expression

$$
\begin{aligned}
H(X,Y) &= H(Y) + \langle H(X|y) \rangle_Y \\
&= H(X) + \langle H(Y|x) \rangle_X,
\end{aligned}
\tag{1.12}
$$

where

$$
\langle \zeta \rangle_Z = \frac{1}{D_Z} \sum_z \zeta d(z).
\tag{1.13}
$$

From (1.12) it follows that if $H(Y|x) = H(Y)$ then

$$
H(X,Y) = H(X) + H(Y).
\tag{1.14}
$$

Expression (1.14) is valid if and only if the quantities x and y are independent. So, entropy is additive when $d(x,y) = d(x) d(y)\ \forall x,y$. In that case there is no correlation between x and y: knowledge about one of them has no influence on the other.

If at least some of x and y are correlated, then (1.14) is not valid, and one has to apply (1.12) instead.

All the formulae above are applicable to discrete distributions only. For continuous distribution $\{X_p\}$ with a probability density function $p(x)$ information entropy $H(X_p)$ becomes dimensionally dependent and, therefore, should be re-defined [Jay63; Jay68] as follows:

$$H(X_p) = \ln D_{X_p} - \frac{1}{D_{X_p}} \int p(x) \ln p(x) \, \mathrm{d}x - \langle \ln \mathrm{d}x \rangle_{X_p}, \qquad (1.15)$$

where

$$D_{X_p} = \int p(x) \, \mathrm{d}x$$

$$\langle \zeta \rangle_{X_p} = \frac{1}{D_{X_p}} \int p(x) \, \zeta \mathrm{d}x.$$

The last term in the *rhs* of (1.15) defines the so-called limiting density of discrete points. It estimates information lost under the transition from continuous to discrete distributions. Expression (1.15) is useful when one is working with numerical calculations on continuous distributions.

1.4 Information entropy: interpretation

Entropy (1.4) may be interpreted as a measure of uncertainty. It estimates how much one does not know about the system to determine it completely. If this information were known, the system would have been in some certain state with the probability $d(x) = D_X$. There would be no need in distribution then, and the entropy $H(X)$ itself would have been equal to zero.

As known from information theory, any number $p(x) = \frac{d(x)}{D_X}$ due to (1.3) may be encoded with $-\ln \frac{d(x)}{D_X}$ units of information. Therefore, the distribution $\{X\}$ may be represented by numbers $p(x)$, each requiring a sequence consisting of $-\ln \frac{d(x)}{D_X}$ symbols, with $\langle p(x) \rangle_X \equiv H(X)$ on average (1.13).

Thus, we conclude that Shannon entropy (1.4) is just an average size of the sequence one needs to encode the distribution $\left\{ \frac{d(x)}{D_X} \right\} \equiv \{d(x)\} \equiv \{X\}$. Any correlations inside $\{X\}$ may be used to re-encode the distribution so that the length of the sequence does not exceed $H(X)$. If $\{X\}$ is uniform, i.e. it has no correlations, then, due to (1.6), information entropy reaches its maximum.

One may argue that entropy exhibits behavior depending on which system is under consideration. For example, entanglement entropy seems to differ a lot from its extensive counterpart from thermodynamics. However, information entropy allows to build a bridge between both.

Any information encoded by correlations among subsystems is expected to be determined by their common boundary. Discarding any of these subsystems results in losing this information, that can be quantified by the corresponding entropy. Therefore, entanglement entropy is expected to obey some kind of area law [ECP10].

In thermodynamic equilibrium entropy is an extensive quantity. It exhibits bulk properties thus opposing to the area law. This obvious discrepancy origins from the absence of any correlations in a thermal system. In such case all conditional distributions vanish, and one should apply (1.14) instead of (1.12) thus resulting in additive entropy behavior.

One may argue that entropy calculation with the help of (1.12) is hard. Indeed, the proper use of the expression requires knowledge about all conditional distributions contributing to the process. And this may be computationally costly. Given this, it seems much easier to apply the Zubarev's non-equilibrium statistical operator that has already proved its efficiency [Bla+20].

However, the method is heavily based upon the Jayne's principle of maximum entropy [Jay57]. The last one imposes a strong restriction on the trajectory in N-parametric space, where N is the number of different outcomes for some distribution. Being the consequence of our inability to know all necessary information, the principle seems to be incompatible with a strict mathematical treatment. Moreover, its application to open systems, for which the relevant phase space is ill-defined, may be questioned too. From this one may conclude that, despite its considerable success, the Zubarev's formalism should be applied with great care under certain circumstances.

Contrary to this, conditional distributions may be extracted directly from the measurements. This makes the use of information entropy approach more attractive, especially in case of far-from-equilibrium and open systems.

It should be noted that the discussion above refers only to the Shannon entropy. Other entropy measures, e.g. the Tsallis entropy [Tsa88], might exhibit the properties different from those of (1.4). This may affect (1.12) in such manner that the extensiveness (1.14) is not guaranteed and should be verified separately. In what follows, we will focus on the Shannon entropy and its quantum counterpart, the von Neumann entropy.

Chapter 2

Shear viscosity and entropy in heavy ion collisions

2.1 Quark-gluon plasma as a primordial matter

Since the very beginning humanity has wanted to know what governed our Universe after it appeared to existence. Even now we wonder about the Big Bang and properties of the substance permeating early spacetime. Thanks to atomic and nuclear physics we know a lot about matter, but how did it evolve in times when neither atoms nor even hadrons could exist?

Astronomy is an obvious way to look for the answers. But despite large data supply it cannot provide us with a controllable experiment. To date, high energy physics is the only one to study primordial matter in a laboratory. Ultrarelativistic heavy ion collisions is the unique instrument allowing to recreate the conditions which were typical in the early Universe and orchestrated its evolution at temperatures higher than a few hundred MeV. Being too harsh for hadrons [CP75; Lin79], they imply the presence of a new state of matter, quark-gluon plasma (QGP). Color deconfinement at high energies uncovers new degrees of freedom (DOF) and causes up the emergence of new properties differing a lot from those of common hadron matter.

For a gas of massless non-interacting particles at temperature T one has

$$N_{\mathrm{dof}} = \frac{2\pi^2}{45} \frac{s}{T^3}, \tag{2.1}$$

where N_{dof} is the number of DOF and s is entropy density. So, the ratio s/T^3 should experience a distinct change at some critical temperature, when new degrees of freedom come into play. Similar behavior should be observed for the specific energy density ε/T^4 and pressure p/T^4.

Indeed, lattice quantum chromodynamics (lattice QCD) calculations demonstrate a steep increase of the involved DOF [Baz+14; Bor+14; Kar02]. A direct manifestation of the transition from hadron QCD matter to QGP is shown in Fig. 2.1 depicting the ratios as functions of T. In the vicinity of $T \approx 150$ MeV (yellow region) one meets a continuous crossover, in full accord with cosmological observations and data from accelerators such as RHIC or LHC. The scaled pressure, entropy density and energy density tend to the Stefan-Boltzmann limit. The last one represents the non-interacting regime, which is achievable in the limit of asymptotic freedom only. The ratios reach approximately 80% of the level thus indicating intense coupling among the constituents.

Modern theoretical and experimental knowledge about QCD matter and its dependence on temperature and baryonic chemical potential μ_{B} is summarized
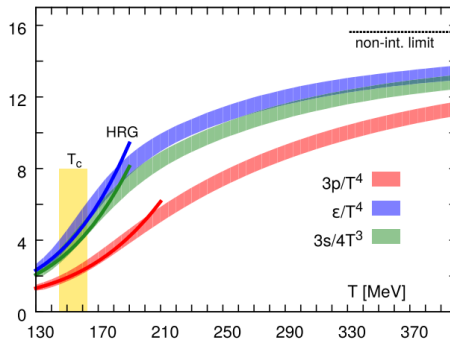
Figure 2.1: Lattice QCD calculations of the scaled pressure $\frac{3p}{T^4}$, energy density $\frac{\varepsilon}{T^4}$ and entropy density $\frac{3s}{4T^3}$ of hot QCD matter. Figure taken from [Baz+14].
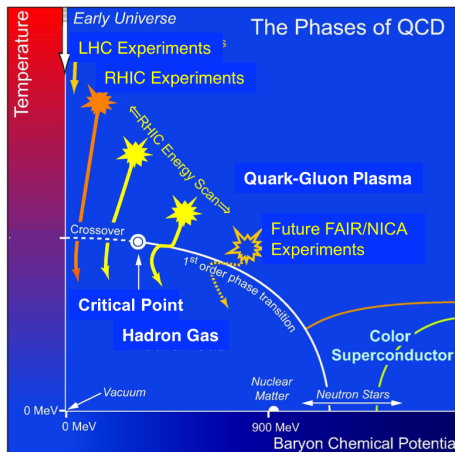
Figure 2.2: (T, μ_{B}) QCD phase diagram. Figure taken from [Nay20].

in Fig. 2.2. Vacuum state is represented by the point $T = 0$, $\mu_{\mathrm{B}} = 0$. The thick dot at $T \approx 0$, $\mu_{\mathrm{B}} \gtrsim 900$ MeV represents common nuclear matter. To the right from it one can see the line rising with temperature and bending to smaller densities. It represents the first order phase transition. The line is expected to end at a critical point, where a phase transition of the first order becomes a phase transition of the second order, and one meets with the smooth crossover familiar from the RHIC and LHC experiments. Hadrons can exist below the line only, whereas quark-gluon DOF are released above it. The lower right corner of the picture represents high baryon densities and low temperatures, at which the matter is believed to be in a color superconductor state. Such extreme conditions might be reproduced inside neutron stars.

2.2 Experimental evidence of QGP

Due to the large amount of processes involved in heavy ion collisions, there is no definite unambiguous evidence of QGP. At the same time, experimental data propose plenty of signals favoring its existence. Below we will get acquainted with some of QGP signs. Comprehensive reviews on the topic can be found in [BRS18; EM22].

2.2.1 Colorless probes

Colorless probes are of great interest for both theoreticians and experimental physicists. The reasons for that are their indifference to strong interactions and low interaction probabilities as compared to hadrons. This means that electromagnetic and lepton probes can almost freely escape the hot QCD medium at any stage of its evolution, including the earliest times. Being undisturbed, they retain information about their production, and that should be of great help while studying thermodynamic properties of the collision fireball.

Fig. 2.3 is a typical example of such signal readout; it depicts temperatures extracted by fitting the direct photon yields at RHIC and LHC energies. Estimates are mostly located within the interval $T \in 174 \div 289$ MeV/c. This clearly indicates that the photons were emitted by the medium too hot for hadrons to exist.
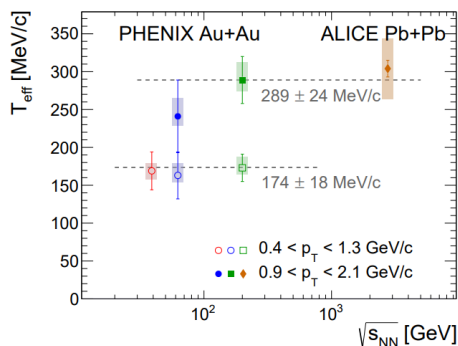
Figure 2.3: Inverse slopes for direct photons from collisions at $\sqrt{s_{NN}} = \{39, 62.4, 200, 2760\}$ GeV. Figure taken from [Abd+23].

From this example one may conclude that the colorless probes are of great advantage to study quark-gluon plasma. Unfortunately, low interaction probability implies small production rates thus making their detection a challenging problem. Moreover, multiple sources (e.g. hadron decays, annihilation, scatterings) contribute to a large background noise, so that any specific signal readout becomes model-dependent. For example, Fig. 2.4 depicts mass distribution for e^+e^- pairs from the PHENIX Collaboration. It clearly demonstrates how a large mixture of dilepton sources may complicate the data

analysis. Therefore, both extraction and interpretation of any signal with the probes require taking into account multiple processes and heavily rely on theoretical description.
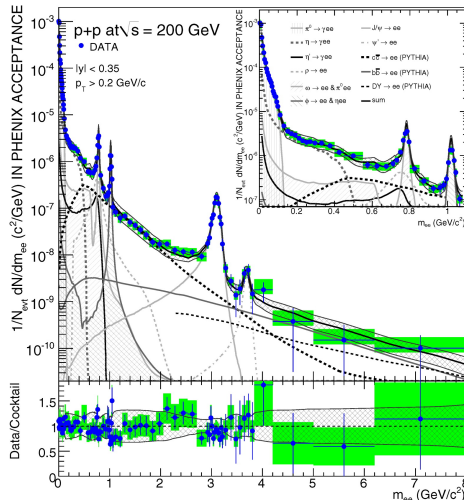
Figure 2.4: e^+e^- yields for $p + p$ collisions as functions of pair mass m_{ee} at $\sqrt{s_{NN}} = 200$ GeV. The inset represents the low mass domain. Figure taken from [Ada+09].

2.2.2 Baryon stopping power

Amount of stopping in heavy ion collisions determines how much of the initial beam energy is being released. Measurements of the net-baryon rapidity distribution dN/dy together with the initial data from the beam allow to estimate the stopping power. Fig. 2.5 depicts dN/dy for AGS, SPS and RHIC central collisions and clearly establishes its dependence on energy. AGS data demonstrate a narrow distribution which is centered around $y = 0$. Therefore, at low collision energies baryons release almost all initial momentum. For SPS one observes a dip with two humps that represent escaping remnants. This shape indicates that at higher energies nuclei become transparent, and their constituents tend to escape from the central region. At top RHIC energies the mid-rapidity net baryon density is small and decreases even more for LHC [Abe+13b].

Having obtained the rapidity loss, one is able to estimate the energy deposited for particle production. It was found that for RHIC about 73% out of initial 100 GeV per participant can be released [Bea+04]. As follows from [Ars+05], total amount of produced particles is about 7000; this estimates the initial energy density to be lower bounded by $\varepsilon \approx 5$ GeV/fm^3. Calculations from the PHENIX Collaboration [Adc+05] indicate even higher values, $\varepsilon \geq 15$ GeV/fm^3. These largely exceed the average energy density inside hadrons or the deconfinement
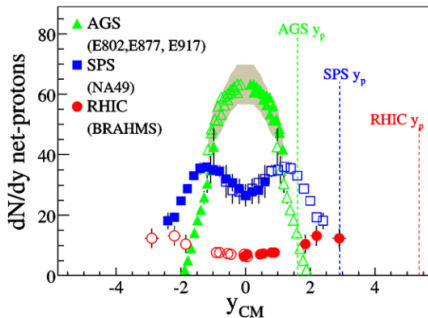
Figure 2.5: Net proton rapidity distribution for central collisions at AGS, SPS and RHIC energies. Figure taken from [Ars+05].

threshold from lattice QCD. Therefore, the data unambiguously hint at the emergence of a new state of matter in collision experiments.

2.2.3 High p_T suppression

High momentum particles are expected to lose a fraction of their own energy while traversing a medium [GP90; WG92]. The loss can be quantified by the nuclear modification factor

$$R_{AB}\left(p_T\right) = \frac{\mathrm{d}^2 N^{AB}/\mathrm{d}p_T\mathrm{d}y}{\langle N_{coll}\rangle\,\mathrm{d}^2 N^{NN}/\mathrm{d}p_T\mathrm{d}y}, \tag{2.2}$$

where $\mathrm{d}^2 N^{AB}/\mathrm{d}p_T\mathrm{d}y$ is the differential yield in the $A+B$ collision, and $\langle N_{coll}\rangle$ is the average number of binary collisions in $A+B$ which is required for normalization reasons.

In heavy ion collisions, particle scattering results in significant changes of their momenta. The effect depends on the coupling; it should be larger for strong interactions, for which one expects $R_{AA} < 1$. On the other hand, photons and other colorless probes interact with the QGP medium much less intensively and thus experience no suppression [Adl+06].

Naive kinematics dictates that momentum loss increases with a path length in the medium. So, the nuclear modification factor should be a function of centrality. Indeed, Fig. 2.6 indicates the presence of a dense medium influencing the high-p_T particles. For central collisions R_{AA} takes the lowest values and rises up with impact parameter exhibiting its path-length dissipation dependence.

2.2.4 Quarkonium probes

Color deconfinement in QGP should prevent heavy quark binding, similarly to the Debye screening [MS86]. Namely, the bound states cannot exist if the screening length is too short as compared to their radius. So, heavy quarkonia,
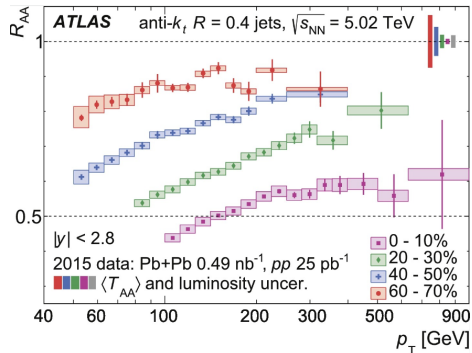
Figure 2.6: Nuclear modification factor for jets at different centralities as a function of p_T. Figure taken from [Aab+19].

once being produced, should experience melting in QGP that results in their suppression. On the other side, for a small number of participants N_{part} the medium cannot emerge and no suppression is expected. The effect may be expressed in terms of a nuclear modification factor and its dependence on N_{part}. Indeed, as follows from [Ada+12], for J/ψ mesons $R_{AA} > 1$ for a small number of participants, but falls below 0.5 for $N_{\mathrm{part}} > 50$.

As shown in Fig. 2.7, the bottomonium $\Upsilon\left(1S\right)$ suppression rate is distinct from that of $\Upsilon\left(2S\right)$ or $\Upsilon\left(3S\right)$. The ground state dissolves at the lowest rate, and the higher excited ones are more suppressed. This phenomenon has much in common with the Mott transition [HKR96] and is known as "sequential melting". The effect manifests itself also during hadronization and may be responsible for the "sequential regeneration" of, e.g., J/ψ and $\psi\left(2S\right)$ mesons [DR15].
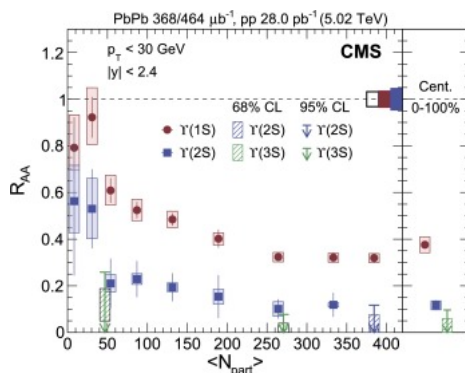
Figure 2.7: Nuclear modification factor as a function of the average number of participants $\langle N_{\mathrm{part}} \rangle$ for different Υ meson states. Figure taken from [Sir+19].

From this one concludes that the emergence of a QGP droplet may be

witnessed via the suppression of quarkonia yields. Naively it can be explained by low coalescence probabilities for heavy quarks in the medium. However, high energy densities induce copious production of heavy quarks, such as $c\bar{c}$ pairs. This increases binding probabilities during hadronization and enhances charmonium production.

2.2.5 Anisotropic flow

The nuclei from a beam are considered to be thin Lorentz-contracted disks of finite radii. For these, geometry requires the introduction of impact parameter b and, consequently, of angular anizotropy of the entire collision. In such case it is reasonable to use Fourier decomposition of particle distributions [VZ96]

$$E\frac{\mathrm{d}^3N}{\mathrm{d}p^3} = \frac{1}{2\pi}\frac{\mathrm{d}^2N}{p_T\mathrm{d}p_T\mathrm{d}y}\left\{1 + 2\sum_{n=1}^{\infty} v_n\cos\left[n\left(\phi - \psi_n\right)\right]\right\}. \tag{2.3}$$

Here ϕ denotes the azimuthal angle, v_n are Fourier coefficients and ψ_n defines the symmetry plane for the nth harmonic.

Coefficients v_n carry useful information about properties of the collision fireball and are of great interest for both theoreticians and experimental physicists.

The first one is known as a directed flow. Being defined as $v_1 = \left\langle\frac{p_x}{p_T}\right\rangle$, it describes the particles' behavior in the reaction plane. The interest to it is stipulated by its sensitivity to a fireball expansion from early times. This allows to deduce information about the equation of state for hybrid model calculations [Ada+14; RR97].

The most studied among the coefficients is v_2, also known as elliptic flow [Oll92]. In non-central collisions the initial almond shape of an overlapping zone induces angular dependence of the pressure gradient in transverse directions. This transforms into momentum anisotropy, which is expressed with v_2. Being dependent on the impact parameter, elliptic flow should vanish for central collisions, and this can be clearly seen from experimental data [Ack+01].

Other harmonics v_n encode information about more detailed scale structure of the fireball. However, being the corrections of higher order, they rapidly decrease with increasing n. Specifying the relevant planes to extract ψ_n makes the problem even more complicated. So, one needs highly sophisticated and computationally costly techniques to estimate the higher order anisotropies. In spite of that, flow coefficients v_n are of great interest due to their sensitivity to the medium properties.

Fig. 2.8 depicts two- and three-particle cumulants for charged hadrons at different centralities for RHIC and LHC energies. Both panels demonstrate minima for central collisions as expected. The flow develops with b, reaches maximum at $35 \div 60\%$ centralities and degrades for peripheral collisions.

Such behavior is explained by collective effects, as can be clearly seen from the good agreement of fluid dynamics with experimental data. For a hadron gas with rare enough scatterings one expects fast momentum randomization.
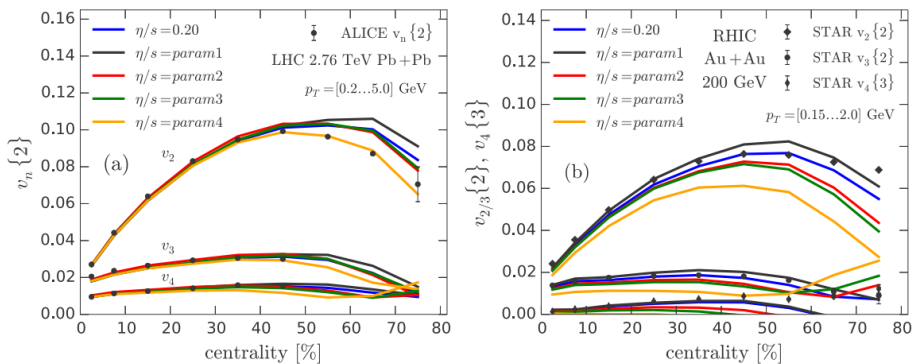
Figure 2.8: Left panel: centrality dependencies of charged hadron anisotropies of the 2nd, the 3rd and the 4th order for $\sqrt{s_{NN}} = 2.76$ TeV Pb+Pb collisions. Right panel: coefficients v_2, v_3, v_4 from two- and three-particle cumulants for $\sqrt{s_{NN}} = 200$ GeV Au+Au collisions as functions of centrality. Hydrodynamic calculations are shown with colored lines. Figure taken from [NEP16].

In this case, any information about the initial spatial distribution rapidly evanesces that results in the reduction of any anisotropies. This makes gas dynamics incompatible with the observed anisotropic flow in heavy ion collisions: coefficients v_n are significant enough to witness intense coupling in the medium. Therefore, one concludes that experimental data clearly pronounce formation of the state with behavior typical for a hydrodynamic system.

2.3   QGP as a liquid

Both theoretical predictions and experimental results confirm the emergence of QGP fluid in ultrarelativistic heavy ion collisions. And its properties differ a lot from those of hadron matter due to new DOF getting into the play.

Surprisingly enough, QGP does not look like an almost free quark-gluon gas, as it was expected at such high energy densities. RHIC data indicate rather the presence of strongly-coupled fluid, with a low transparency for energetic colorful probes [MN06].

Asymptotic freedom allows to expect a bit different picture at higher energies. However, LHC data, despite some quantitative differences, unambiguously confirm the RHIC results: properties of the medium are typical for almost perfect liquid with strong interactions among its constituents [MSW12].

Full relativistic hydrodynamic calculations, with a fluid being close to equilibrium soon after the collision, are required mainly to explain the magnitude of observed anisotropies. Within the linear response approximation, relativistic fluid can be described by its energy momentum tensor $T^{\mu\nu}$ with the following

gradient expansion

$$T^{\mu\nu} = \varepsilon u^\mu u^\nu + p\Delta^{\mu\nu} - \eta\left(\nabla^\mu u^\nu + \nabla^\nu u^\mu - \frac{2}{3}\Delta^{\mu\nu}\nabla_\alpha u^\alpha\right) - \zeta\nabla_\alpha u^\alpha \Delta^{\mu\nu}, \quad (2.4)$$

where ε is the energy density, u^μ is the four-velocity and p is the pressure. Here $\Delta^{\mu\nu} = g^{\mu\nu} + u^\mu u^\nu$, with metric tensor $g^{\mu\nu} = \mathrm{diag}\,(-1, +1, +1, +1)$ and $\nabla^\mu = \Delta^{\mu\nu}\partial_\nu$, where $\partial_\mu u^\nu$ is the covariant derivative. Coefficients η and ζ denote the shear and bulk viscosity correspondingly. Heat transport and the higher order terms have been omitted; these are relevant to large net baryon density and causality [HS13].

Ideal fluid is governed by the first two terms in (2.4), which are of the zeroth order in gradients. Any dissipative processes are completely determined by the remaining two terms in (2.4), which are of the first order in gradients.

Fig. 2.9 depicts coefficients v_n as functions of transverse momentum p_T at both RHIC and LHC energies. The plot clearly establishes the peak at $p_T \in [2.5, 4]$ GeV/c. Ideal fluid dynamics cannot explain the data; it implies a linear growth for v_n without any distinct peaks. In order to explain the data, one should take dissipation into account, which is governed by transport coefficients η and ζ.
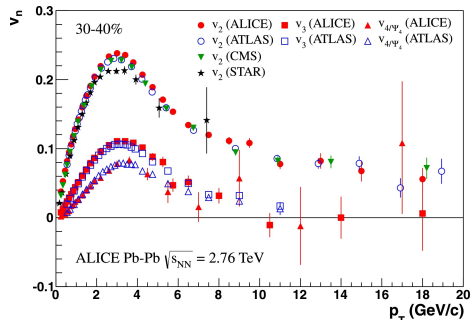
Figure 2.9: Coefficients v_n as functions of p_T at RHIC and LHC energies for $30 - 40\%$ centrality. Figure taken from [Abe+13a].

Having introduced the equation of state $p = p\,(\varepsilon)$, transport coefficients, initial energy and velocity, one can process the evolution of QGP till the hadronization phase. These quantities are the input data; they cannot be specified within hydrodynamics itself and should be extracted from the initial state.

2.3.1 Specific viscosity

It turns out that bulk viscosity becomes essential if the system is not scale invariant [BRS18]. The condition is fulfilled near the deconfinement region, when the number of its DOF varies. Beyond this case ζ can be neglected, and shear viscosity remains the only one to encompass any corrections to $T^{\mu\nu}$ within

the linear approximation (2.4). Physically η describes dissipation in a fluid via momentum transfer and its conversion into heat.

Applicability of hydrodynamics is measured by the Knudsen number

$$\mathrm{Kn} = \frac{\lambda}{L}, \tag{2.5}$$

where λ is the mean free path and L is the characteristic scale on which the liquid properties can change. The standard requirement is $\mathrm{Kn} \ll 1$, which is equivalent to $\lambda \ll L$ due to (2.5). In terms of (2.4) this implies the dominance of ideal fluid contribution over the viscous one.

A fireball is expected to be a highly dynamic system, for which it is hard to expect the gradients to be small. However, the smallness of Kn can be naively fulfilled in other form

$$\frac{\eta}{\varepsilon + p} = \frac{\eta}{Ts} \propto \lambda \ll L, \tag{2.6}$$

where T is the temperature and s is the entropy density of the fluid. A more rigorous analysis requires different sophisticated techniques such as divergent series resummation, hydrodynamics attractors etc. [RR17].

The ratio η/s from (2.6) is known as specific shear viscosity (or specific viscosity for simplicity). It should be noted that for strongly coupled fluids, despite η/s being well-defined, one cannot determine λ as soon as it may be smaller than the de Broglie wavelength $1/T$.

Within the first-order approximation, specific viscosity defines how close our system is to an ideal liquid state. It controls any features of a medium (sound propagation, flow decay, fluctuations etc.) contributing to the heat via dissipation. For heavy ion collisions the ratio is expected to be small, otherwise the information about collective effects will dissipate in the medium before reaching a detector. At the same time, strongly coupled quantum field theories establish a lower limit for η/s to be equal to $1/4\pi$ [Cre11; KSS05].

2.3.2 The critical point

Due to Enskog, the minimum of specific viscosity should be observed at the transition between gaseous and liquid phases. Quite simple explanation of that can be done as follows.

For a fluid the ratio η/s quantifies its momentum transfer properties and is proportional to the mean free path λ. In the gaseous phase λ grows with temperature, that should increase specific viscosity due to (2.6).

On the other side, when the particles are close-packed, $\lambda \propto 1/\rho^{1/3}$, with ρ being a particle density. Lowering the fluid's temperature reduces the chaotic motion in it, thus leading to the increase of ρ and to the decrease of entropy density s simultaneously. Therefore, for a liquid its specific viscosity should rise up when the temperature falls down.

Altogether this leads to the minimum of specific viscosity between the phases, with a cusp at the critical point. Such behavior is typical for the majority of

substances and can be extrapolated to the transition between hadron and QGP phases of the QCD matter [CKM06].

The dependence of η/s on temperature, with $T = T_c$ at the critical point, is depicted in Fig. 2.10. Open symbols represent estimates for the QCD matter, for which $T_c = 170$ MeV is assumed. The red hexagon ($\eta/s = 0.09\pm0.015, T = 165\pm3$ MeV) corresponds to the RHIC elliptic flow measurements for Au+Au collisions at $\sqrt{s_{NN}} = 200$ AGeV [Lac07].
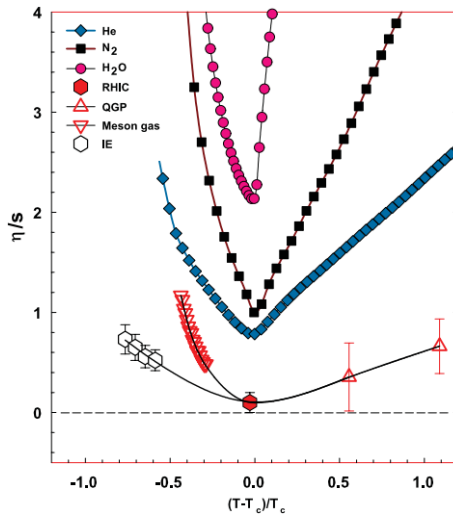
Figure 2.10: Specific viscosity for various substances as a function of temperature T. The critical point is located at $T = T_c$. Figure taken from [Lac+07].

So, one concludes that specific viscosity is an important indicator to pinpoint the critical point of QCD matter. Estimation of η/s and its minimum especially are interesting problems comprising both experimental studies (RHIC BES, FAIR etc.) and theoretical calculations.

2.3.3 Specific viscosity and particle spectra

An elementary analysis dictates the dependence of particle spectra on fluid properties. Dissipation processes wash out any correlations in the system via interactions among its constituents. The corresponding decay rates should depend on specific viscosity. Besides, the effect is expected to depend on the volume of liquid.

Fig. 2.11 depicts pion and proton spectra from the STAR and PHENIX Collaborations at different centralities and compares them to hybrid VISHNU model calculations. The discrepancies between the pion data and theoretical estimations become significant for large impact parameter only. This confirms the applicability of hydrodynamic description to the particle yields. However, the plots demonstrate poor susceptibility to initial conditions. Moreover, varying

η/s within the range $[0, 3/4\pi]$ seems to have almost no effect, thus confirming the earlier results [RR07].
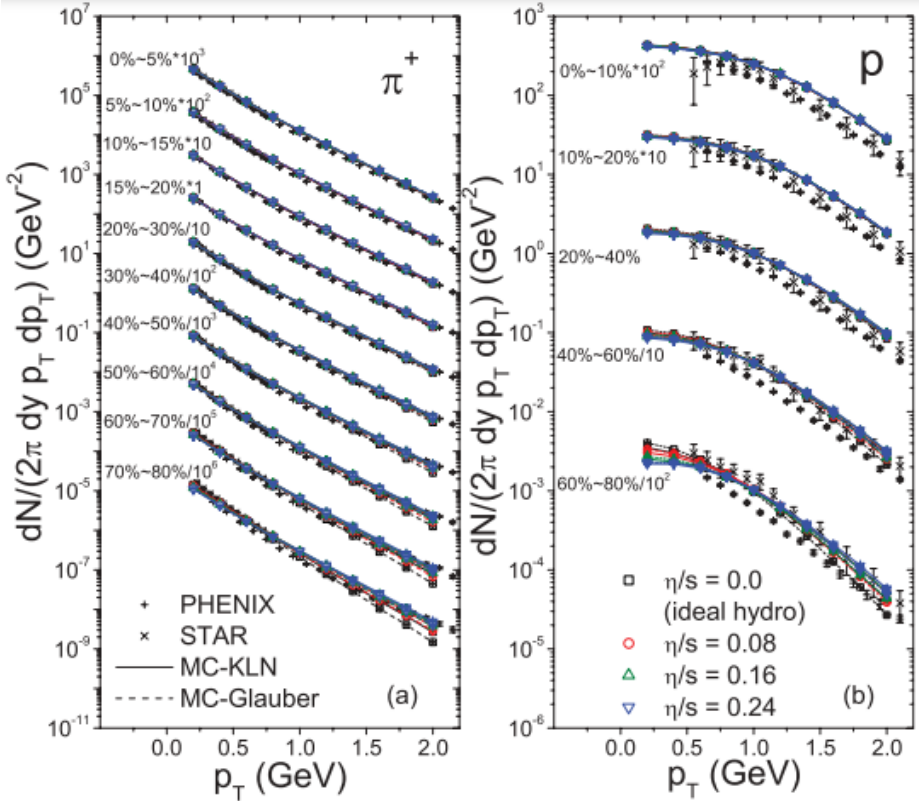
Figure 2.11: Comparison of VISHNU calculations at different initial conditions with transverse momentum spectra for pions (left panel) and protons (right panel) at $\sqrt{s_{NN}} = 200$ AGeV. Different centralities are shifted by multiplicative factors for visibility reasons. Figure taken from [Son+11b].

Particle multiplicities $\frac{\mathrm{d}N}{\mathrm{d}y}$ or mean transverse momenta $\langle p_T \rangle$ were expected to be good indicators for viscous effects. However, data fits at top RHIC energies reveal poor correlation with specific viscosity within the range $\eta/s \in [0, 2/4\pi]$ [RR07]. Fig. 2.12 depicts the dependencies of pion, kaon and proton multiplicities and mean transverse momenta on centrality at LHC energies. Hybrid hydro+transport calculations are presented also. As one may notice, shear viscosity by itself cannot reproduce all the data, even if the switching between the models is involved. The plots clearly indicate the importance of bulk viscosity making the distinction between η and ζ somewhat ambiguous.

This leads to the conclusion that particle spectra are good for general hydrodynamics verification only, while the extraction of QGP fluid properties
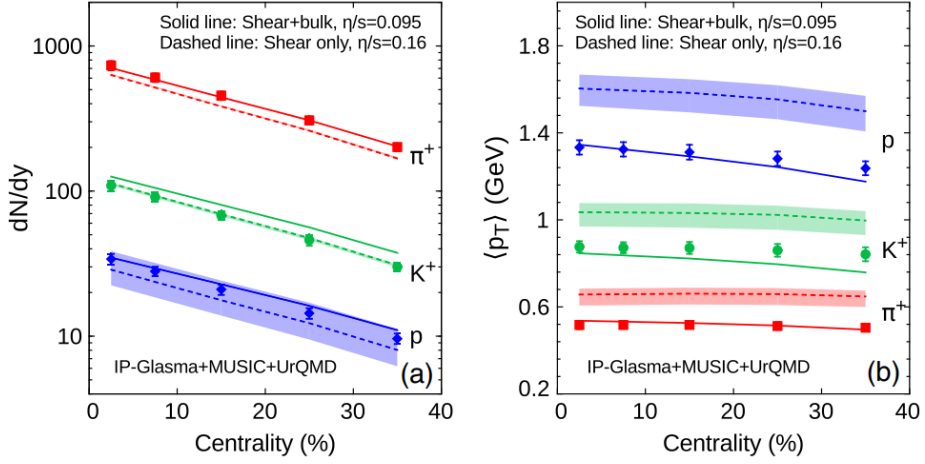
Figure 2.12: Multiplicity (left panel) and mean p_T for pions, kaons and protons from ALICE experiment as functions of centrality. The bands indicate the influence of switching between hydrodynamics and transport calculations. Figure taken from [Ryu+15].

requires more sensitive observables.

It turns out that azimuthal anisotropy is a good tool to extract η/s from data [RR07]. This can be interpreted within a highly non-trivial hydrodynamic response to geometry initial fluctuations [TY12]. As follows from Fig. 2.13, the ratio of elliptic flow v_2 to initial source eccentricity $\varepsilon = \langle y^2 - x^2 \rangle / \langle y^2 + x^2 \rangle$ is highly sensible to specific viscosity and, therefore, may stand for the desired observable.
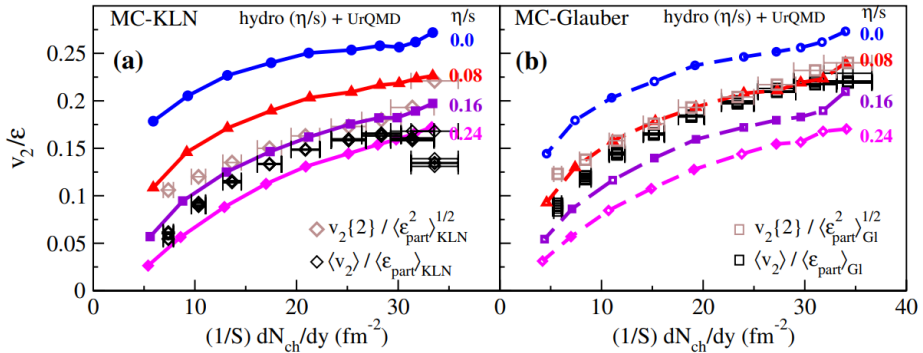
Figure 2.13: Eccentricity-scaled elliptic flow v_2/ε from the STAR Collaboration data and VISHNU calculations as functions of charged hadron rapidity density at MC-KLN (left) and MC-Glauber (right) initial conditions. Figure taken from [Son+11a].

Cumulants from Fig. 2.8 exhibit the susceptibility to η/s too. The largest response is observed for the elliptic flow. At the same time, higher order coefficients are much less sensitive to the specific viscosity. Such behavior is a bit surprising as one would have expected a strong dilution of subtle contributions due to dissipation.

The situation drastically changes for the ratios of anisotropic coefficients at different viscosities $v_n\left(\eta/s\right)/v_n\left(\eta/s=0\right)$, as one can see in Fig. 2.14. The plot clearly heralds the suppression of higher order corrections with n increasing. Here the decay is more pronounced for larger η/s, in full accord with expectations.
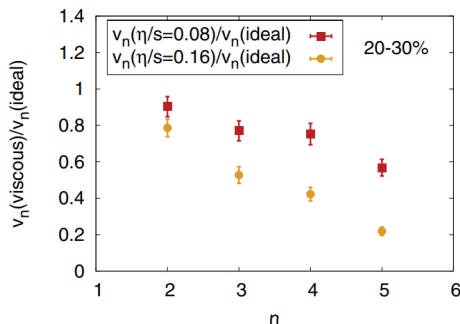
Figure 2.14: Normalized higher flow coefficients v_n for different values of η/s. Figure taken from [SJG12].

The matter created in heavy ion collisions is not a stationary state but rather a highly dynamical open system. For it one would expect rapid evolution of its thermodynamic properties. Therefore, for the QCD matter its specific viscosity should not be constant; it must change as the whole system evolves. This agrees with [SH08] concluding that η/s should be temperature-dependent in order to fit experimental data.

Hybrid approaches incorporating both hydrodynamics and transport models are widely applied to describe the data. Fig. 2.15 depicts the values of η/s used in combined UrQMD and viscous hydrodynamic calculations. These were used to reproduce the observed pseudorapidity and transverse momentum hadron distributions within the range $7.7 < \sqrt{s_{NN}} < 200$ GeV. As one can see, the ratio does not exceed 0.2 at low energies and falls down to the theoretical minimum for $\sqrt{s_{NN}} \gtrsim 40$ GeV.

Instead of evolving parameters, one may suggest to consider the combination of different fluids, each being parameterized in its own way. Following this idea, effective viscosity was extracted within the three-fluid dynamics calculations [IS16]. The model predicts $0.05 \lesssim \eta/s \lesssim 0.5$ for central Au+Au collisions at $\sqrt{s_{NN}} \in [3.3, 39]$ GeV.

There are plenty of other approaches aiming to extract η/s, which incorporate more sophisticated techniques. These encompass correlations of symmetry plane angles Ψ_n [QH12], two-particle p_T correlations [GBM21] etc; comprehensive reviews can be found in [BRS18; EM22; HS13].
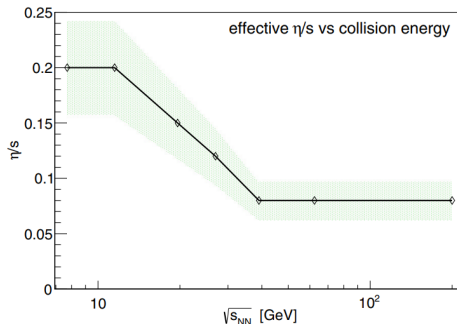
Figure 2.15: Specific viscosity as a function of $\sqrt{s_{NN}}$ from hybrid $3 + 1$-dimensional hydro + UrQMD calculations. The uncertainty arising from variation of model parameters is depicted by the band. Figure taken from [Kar+15].

To summarize, it turns out that specific viscosity should be close to the KSS bound in order to fit the elliptic flow data. The preferred range is $\eta/s \in [1/4\pi \div 3/4\pi]$ and should not exceed 0.4 [TEA10].

2.3.4 Vorticity and spin polarization

Polarization is one more option where viscous hydrodynamics may be of great help. Due to conservation laws, non-central relativistic heavy ion collisions initiate a large angular momentum in the fireball. Dissipation transfers it to fluid vorticity at the rate which depends on its viscous properties. The rotation is distributed among angular momentum DOF of the produced particles. These include particle polarization [BPR08; LW05] and, therefore, can be measured experimentally.

Fig. 2.16 depicts the average polarization of Λ, $\overline{\Lambda}$ as a function of collision energy in Au+Au collisions for $20 \div 50\%$ centrality measured by the STAR Collaboration. Similar measurements were performed by the ALICE Collaboration in Pb+Pb collisions at $\sqrt{s_{NN}} = 2.76$ and 5.02 TeV; experimental data confirm the decreasing trend for polarization at higher energies [Ach+20].

Fitting polarization data with pure and hybrid hydrodynamic calculations allows to extract the ratio η/s [BL20]. It should be noted, however, that the field is still under development. There are some inconsistencies between experiment and theoretical predictions (e.g., the sign problem or transverse polarization azimuthal dependence). These stimulate new proposals and theoretical studies incorporating more subtle effects, such as higher order corrections to the shear and stress-energy tensors [BBP21].

2.3.5 Specific viscosity calculations

Perturbative methods are of great help at high energies, when quarks are almost free. But such conditions are barely fulfilled for liquid QGP in the
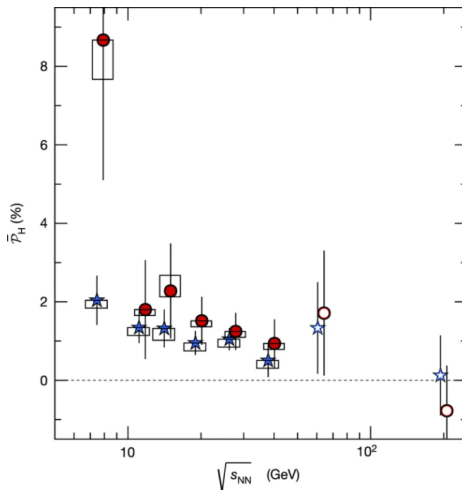
Figure 2.16: Polarization for Λ (stars) and $\overline{\Lambda}$ (circles) from $20 \div 50\%$ central Au+Au collisions as a function of collision energy. Figure taken from [Ada17].

transition region, where the gauge coupling is not small enough. Despite that, the calculation of the ratio η/s at the leading order was performed [AMY03]. More recent results are shown in Fig. 2.17 depicting specific viscosity as a function of temperature for different values of running coupling. The plot clearly demonstrates the smallness of the next-to-leading order correction as compared to the dominating one at high temperatures. The terms seem to overlap in the vicinity of the Hagedorn temperature, which is of great interest for the study. Besides, it is still unclear whether the next terms are small at relevant temperatures too; the convergence verification is a challenging problem that requires highly sophisticated calculations.

Lattice QCD calculations provide reliable insight into the QGP matter and its properties. And it seems reasonable to apply the technique for specific viscosity estimations. The extracted ratio appears to be small [Bor+18], in full accord with anisotropic flow estimations. But the implementation of Euclidean lattice calculations is a challenging task while dealing with time-dependent phenomena. And viscosity is not an exception from the rule: it is responsible for the information dissipation in the medium, so its extraction within the lattice QCD methods should be done with great care. Typical problems one is meeting with can be seen in Fig. 2.18. The plot depicts spectral functions $\rho/\omega \propto \eta$ and the ratio of the corresponding correlators C_1/C_2. As one can notice, even a small correlator deviation (by less than 1%) causes large changes (by up to a factor of 10) for ρ/ω. Therefore, lattice QCD estimations of η/s turn out to be computationally costly and require keeping divergences under the strict control [Mey11].

But lattice QCD calculations are not the only option available. There is a
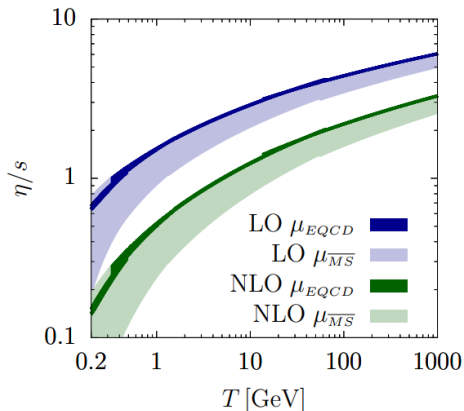
Figure 2.17: Specific viscosity as a function of temperature at leading and next-to-leading orders. Figure taken from [GGD18].
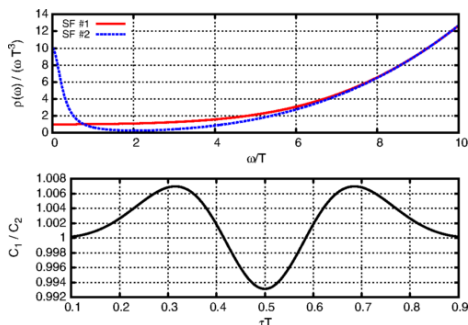
Figure 2.18: Upper panel: spectral function $\rho(\omega)/\omega$ as a function of ω/T. Lower panel: ratio of two different Euclidean correlators specifying the corresponding $\rho(\omega)/\omega$ from the panel above. Figure taken from [Bor+18].

wide variety of numerical models that can be used for the extraction of QGP transport coefficients. Some of the most popular approaches are described in [Wol+22]. Explicit control over system parameters in these models is an advantage allowing to study any region of the phase diagram.

In [Plu+12] shear viscosity and the ratio η/s were calculated from ultrarelativistic Boltzmann transport equation with tree methods: the Green-Kubo formalism, the Chapman-Enskog approach and the relaxation time approximation [Gav85]. Comparing the results authors conclude that the first two are in a good agreement, while the last one underestimates η. However, it does not imply one should exclude the method: the PHSD transport code, which belongs to the same family, shows no significant discrepancies between the Green-Kubo and the relaxation time calculations [Ozv+13b]. Hence, it is not clear which of the formalisms is the best choice for this family of codes.

25

Parton cascade BAMPS calculations demonstrate a significant decrease of dissipative effects for $2 \leftrightarrow 3$ perturbation-QCD gluon bremsstrahlung as compared to elastic scatterings [Wes+11]. At the same time, the ratio η/s exhibits no dependence on temperature if the coupling is kept constant.

Contrary to the BAMPS, GiBUU transport model predicts a rapid drop of specific viscosity at Hagedorn temperature [RGG20].

The approach utilizing quasiparticles and detailed balance can be found in [CK11]. The method may take into account any amount of hadron particle types and predicts the minimum for specific viscosity of relativistic QCD matter.

Thermodynamic parameters of light mesons at zero net baryon density within UrQMD infinite matter calculations were estimated in [Mur04]. Results clearly pronounce the growth of the ratio η/s with temperature, in full accord with expectations.

In [Mot+18] an equilibrated gas of nucleons with no inelastic scattering was studied. Calculations were performed within a wide range of parameters with the help of UrQMD model. Authors conclude that $\eta < 0.17$ fm^{-3}; the result mostly coincides with the one obtained from the Chapman-Enskog approach [CC52].

Specific viscosity calculations within the same model for a relativistic hadron gas are shown in Fig. 2.19. From it one may conclude that the ratio η/s cannot reach the region required by viscous relativistic fluid dynamics (the shaded region) even at large pion and kaon fugacities. Being unable to provide the necessary conditions within the model, this confirms the necessity of introducing QGP with low specific viscosity [DB09].
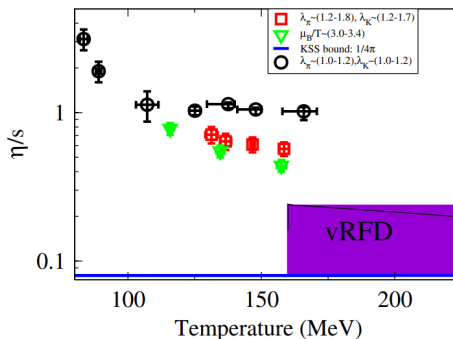
Figure 2.19: UrQMD calculations of specific viscosity for hadron gas as a function of temperature at different values of baryochemical potential μ_B. λ_π and λ_K denote fugacities for pions and kaons correspondingly. Figure taken from [DB09].

The study [GHM08] predicts low specific viscosity. The investigation was performed for hadron resonance gas within the van der Waals excluded volume approach. The ratio η/s exhibits a rapid decline as temperature tends to the critical value. The minimum is reached at $T = 180$ MeV and exceeds the KSS bound approximately by a factor of 3. It should be kept in mind, however,

that dissipative properties of the fluid may be strongly affected by the excluded volume. Particle radius influences both the ability of momentum transfer and entropy density, thus leading to a non-trivial dependence of transport coefficients on the repulsive core size. This can be clearly seen in Fig. 2.20 depicting η/s at various radii: the ratio behaves in a significantly different manner while the core size changes by a factor of 2.5.
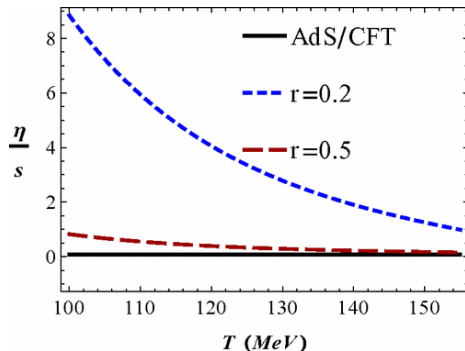
Figure 2.20: Specific viscosity as a function of temperature computed within the hadron resonance gas model. The repulsive radius for hadrons is denoted by r. Figure taken from [NHNG12].

Specific viscosity as a function of temperature and baryochemical potential was calculated in [Ros+18] within the SMASH model. Authors compare results with other approaches and conclude that interactions among particles have a large impact on transport coefficients.

To sum up, there are plenty of approaches which may be applied to calculate viscous properties of the QCD matter. But despite a vast variety of the models, all of them have some common features. Microscopically, any fluid consists of some particles with interactions among them. Viscosity is related to energy dissipation and momentum transfer which are encoded with the corresponding distributions. As shown above, calculations within various approaches predict different behavior for η, thus exhibiting its strong susceptibility to the momentum exchange in the medium. Viscosity extraction requires rigorous analysis of particle re-scattering in the medium.

Chapter 3

Entropy in heavy ion collisions

3.1 Early equilibration problem

As soon as one needs thermodynamic quantities to estimate the ratio η/s, some kind of equilibrium should be assumed. After that one is able to extract temperature T and entropy density s within the statistical model [BL56; Fer50] or any other technique, in order to calculate specific viscosity.

Both experiments on ultrarelativistic high energy collisions and their theoretical interpretations indicate that the produced matter should reach equilibrium quickly enough [NPA19; NPA21]. In particular, to explain the data one expects to start hydrodynamics as early as possible, at times within the interval $t_0 \in [0.2, 1]$ fm/c.

There is no doubt that fluid dynamics successfully describes high energy collisions. But being in a fluid state means that a system is determined by some averaged quantities retaining no memory about its initial state. This one is highly correlated: colliding constituents occupy the domain in a phase space which cannot be described by a spherical momentum distribution. And all this information should be erased at early times, so the justified description of hydrodynamization is required.

The "bottom-up" scenario, which is built upon perturbative QCD, was suggested as a possible solution to the problem [Bai+01]. Within the approach thermalization occurs due to elastic scattering of soft gluons which dominate over the hard ones. Combining this with the linear response to energy-momentum fluctuations allows one to establish hydrodynamization within $t_0 \approx 1$ fm/c [Kur+19].

Another popular approach advocates the solution in terms of the AdS/CFT correspondence. Relaxation rates in a weakly-coupled system are expected to be low because of slow isotropisation of its phase space. Therefore, one may consider the option of rapid QCD matter thermalization due to strong interactions among the particles. Indeed, the study for non-Abelian plasma within the linear response theory [Hel+12] predicts the isotropization to occur at times $t_0 \simeq 1/T$, where T is the temperature. The hydrodynamization rate is depicted in Fig. 3.1 as the deviation of pressure from hydrodynamic predictions. It clearly indicates that plasma exhibits fluid properties at times $\tau \geq 0.35$ fm/c. The similar estimate of the equilibration rate is obtained in [SRP13] and other studies. Basing on these, one may conclude that the transition to hydrodynamic stage occurs at early times after the collision.

As shown in [CY10], for the strongly-coupled $N = 4$ supersymmetric Yang-Mills theory hydrodynamic treatment becomes valid at times $t_0 \geq (1 \div 2)/T$. However, the same paper also concludes that non-hydrodynamic DOF from
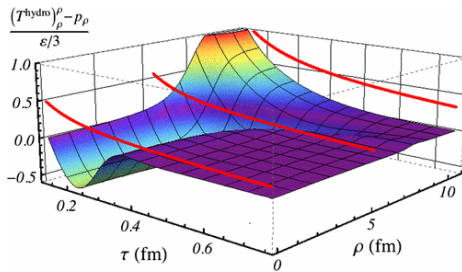
Figure 3.1: Scaled pressure deviation of non-equilibrium state from first-order hydrodynamics as a function of proper time τ and transverse distance ρ. Viscous effects are depicted by red lines. Figure taken from [Sch13].

the initial stage experience an exponential decay. So, despite the fast decline, non-equilibrium effects may contribute even at late times. Even more on that, for the momenta exceeding some threshold value p_c non-hydrodynamic modes dominate, and fluid description becomes questioned [Rom17].

From this one may infer that the fireball is a mixture of both equilibrated and correlated components. As soon as entropy is not maximal for the last one, this implies the presence of correlations in the system. The corresponding information may affect particle spectra analysis, thus attracting much attention to the framework [KTH22].

For the system in a far-from-equilibrium state evolution equations dictate to lose knowledge about its initial conditions before it reaches equilibrium. One may prepare different states at the beginning, but any of them evolves to the same state with high entropy. So, the system ends up in the same behavior irrespective of the starting point. Such observation has drawn much attention to hydrodynamic attractors and their possible role in heavy ion collisions [Sol22].

Many important issues and other approaches to hydrodynamization are discussed in detailed reviews [FHS18; HL14; Str15]. However, despite various approaches to the problem, none of them has been widely accepted yet.

Washing out initial information is a physical process, that cannot be instant; this should take some finite amount of time. At the abstract level, equilibration may be interpreted as the relaxation of charge deviations to their average values. In a given reference frame any such change should obey the diffusion equation and, therefore, cannot violate causality [SS01]. This prohibits a too early start for fluid description, since otherwise equilibration would contradict relativity.

Lattice calculations is a powerful tool that has answered many questions about the QCD matter. Unfortunately, nonperturbative real-time evolution is a hard problem for the method, so QCD hydrodynamization is a challenging task for lattice QCD.

Fireball is an open system, for which it seems incorrect to establish the same conditions anywhere inside. Instead, the notion of locally equilibrated matter may be considered. In this case, the central collision region is expected to fit the

requirements for equilibrium state.

UrQMD calculations for the central cell of the collision system at AGS and SPS energies pronounce isotropization of hadron distributions at times $t \simeq 8$ fm/c only [Bra+06; Bra+99a; Bra+99b]. This demonstrates the inability to reach kinetic equilibrium too early; similar results are obtained for thermal and chemical equilibration times. Particle yields deviate from the statistical model predictions up to 14 fm/c even at the top RHIC energies [Bra+01].

Other models, such as the QGSM, predict similar dynamics. Fig. 3.2 depicts the time dependence of pressure anisotropy in the central cell at top RHIC energies for different centralities. The ratio for hadrons with pseudorapidity $|\eta| \leq 1$ is shown by green symbols. As follows from the plot, the pressure becomes isotropic only at $t \geq 12$ fm/c.
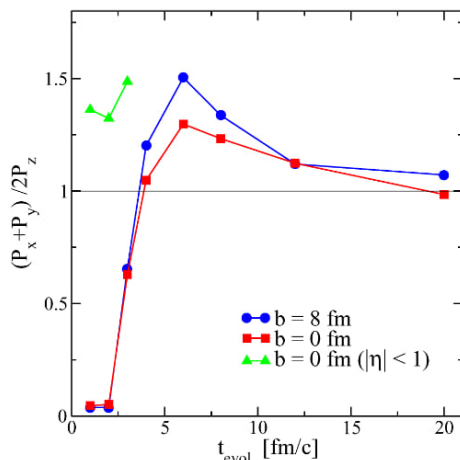
Figure 3.2: QGSM calculations of pressure anisotropy as a function of time in the central cell for Au+Au collisions at $\sqrt{s_{NN}} = 200$ GeV. Figure taken from [Ble+06].

Formation of locally equilibrated matter in the cell within both UrQMD and QGSM models is discussed in [Bra+08]. The study concludes that local equilibrium can be reached only for $t \simeq 10$ fm/c.

So, on one hand, hydrodynamics should be started early in order to explain experimental data. On the other hand, the validity of fluid description should be provided by preliminary thermalization, and this cannot violate causality. Within this context, to define temperature and entropy density of the medium one needs accurate analysis. These are required for the proper extraction of specific viscosity, so the problem seems to be a challenging task.

3.2 Infinite matter simulations

One may argue that any heavy ion collision is an open system evolving all the time since the very beginning and, therefore, cannot be in equilibrium at all. This leads to the following issue: how to determine thermodynamic quantities in the absence of stationary stage?

Infinite matter simulation at charge and energy densities coinciding with those from an open cell seems to be a reasonable ansatz. Such approach omits the boundary conditions problem and allows to expect the system will end up in some stable state close to equilibrium. The concept was studied with various transport models in the box.

UrQMD calculations at fixed baryon density clearly pronounce the isotropization of energy spectra at the same temperature for different hadronic species [Bel+98].

More detailed study within the model was performed in [Bra+00b]. Calculated partial entropy densities as functions of cell time for nucleons and pions are shown in Fig. 3.3. Despite being close enough, the results for central cell and box differ a bit from the statistical model predictions. The manuscript concludes that hadron distributions for both open cell and infinite matter coincide at $t \geq 10$ fm/c. The agreement is observed at different energies. However, this does not mean reaching thermal equilibrium: some discrepancies between the UrQMD and statistical model predictions can still be observed.
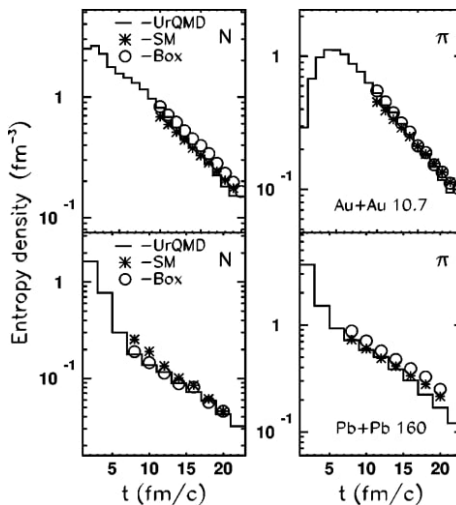
Figure 3.3: Time dependencies of partial entropy densities for nucleons and pions. Histograms denote UrQMD predictions for the central cell; statistical model and UrQMD box calculations are shown by asterisks and circles correspondingly. Figure taken from [Bra+00b].

BUU transport model box calculations show that thermal equilibrium is

achieved at $t \simeq 5$ fm/c [Bra+00a]. This estimate is the lower bound and is observed at SIS energies only; increasing the collision energy leads to larger equilibration times.

Thermal equilibrium is heralded if a system can be described by some constant temperature. Following this definition, the study of equilibration dynamics for infinite matter within the SMASH model was performed [Ros+18]. The results can be found in Fig. 3.4 depicting temperature as a function of box time. As follows from the plot, under some circumstances equilibration time may exceed the lifetime of a fireball.
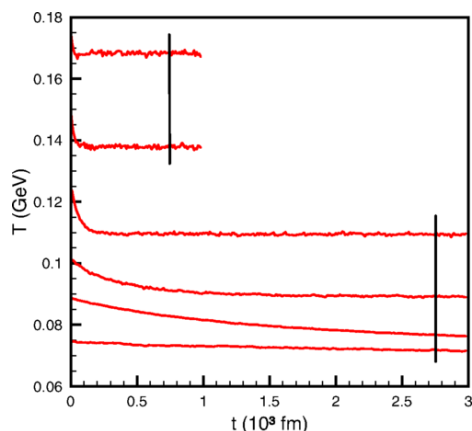
Figure 3.4: Temperature dynamics in the box within the SMASH model for different initial temperatures. Black bars indicate the time at which equilibrium is established. Figure taken from [Ros+18].

However, it would be wrong to conclude that equilibration needs a lot of time and is not achievable in the cell. Highly energetic particles may quickly escape the open system, thus contributing to the rapid cooling of the medium. Such scenario is impossible in the box, where large momenta are forced to be re-scattered among all the constituents, that leads to large equilibration times [Bra+00b]. The box differs a lot from the cell; it cannot help to extract the rate of relaxation to equilibrium in the open system. Reproducing only some stationary state within the chosen model, infinite matter calculations allow us to study its proximity to thermal equilibrium or other properties.

Naive kinetic analysis predicts that equilibration should take a long time for a diluted medium: the probability of momentum re-distribution rapidly falls down at low particle densities. Similar tendency is typical for slow particles. QGP is a system of high energy and particle densities; it does not belong to any of these cases, and one may expect fast thermalization rates for it. Furthermore, for the system with a linear response the relaxation rate is expected to obey exponential time dependence. It means that any deviation of some observable quantity from its average should be proportional to $e^{-t/\tau}$, where τ is relaxation

time. And the decrement rate τ cannot be equal to zero for causality reasons. Indeed, $\tau \geq 2$ fm/c for different components of the QCD matter even in the box regime [Ozv+13a]. This can significantly postpone the equilibrium stage, forcing t_0 to go far beyond the required range.

To sum up, fast equilibration seems to be a challenge for the microscopic treatment of a system possessing some information about its initial state. The problem cannot be completely eradicated even within infinite QCD matter simulations. Therefore, QGP thermodynamic quantities such as temperature and entropy density require careful calculations. Any estimate of equilibration time requires an accurate investigation of correlations among the relevant DOF. The decay rates for these may be extracted from the corresponding conditional distributions. So, one can see that information entropy may be of great help in high energy physics.

3.3 Entropy density in non-equilibrium

An overlapping stage during the collision requires some finite amount of time equal to $\mathcal{O}(1)$ fm/c, so that the projectiles could have passed through each other. Kinematics dictates the nuclei's constituents to scatter at different moments of time. This means that information about their initial (before the scattering) quantum numbers cannot be instantly distributed over all the phase space available. Additional restrictions follow from the conservation laws, which imply correlations among the scattered particles (total momentum, energy, charges). They carry some information, which cannot be dissipated quickly enough. To sum up, kinematics and conservation laws prohibit an instant (or in a too short time) occupation of the maximal phase space volume accessible with any finite-sized system.

Statistical equilibrium means that the probability for a system to occupy some state at energy E is proportional to $e^{-E/T}$, where T is the temperature of the medium. Taking spin statistics into account results in the Bose-Einstein or Fermi-Dirac probability distribution function $f(p, m_i)$. So, in order to describe the equilibrium state of matter, one should apply the statistical model, which is discussed below in Section 4.3, within which entropy density s reaches maximum.

Microscopically an early state (right after the collision) of the particles of the i-th type cannot be described by the distribution $f(p, m_i)$ in the central cell: even at the zero impact parameter the momentum distribution will not be homogeneous. To take this into account, let us define a microscopic distribution function $f(\overrightarrow{p}, m_i)$ as

$$f(\overrightarrow{p}, m_i) = \frac{(2\pi)^3}{V g_i} \frac{\mathrm{d}N_i}{\mathrm{d}^3 p},$$
(3.1)

where the index i defines the type of particles, m_i is their mass, g_i is the corresponding degeneracy factor and $\mathrm{d}N_i$ is the number of particles carrying the momentum from the interval $[\overrightarrow{p}, \overrightarrow{p} + \mathrm{d}\overrightarrow{p}]$. The constant multiplier in the front of distribution guarantees $f(\overrightarrow{p}, m_i)$ to coincide with $f(p, m_i)$, once the equilibrium is achieved.

Entropy density for the particles defined with the distribution (3.1) reads

$$s_i = \frac{g_i}{(2\pi)^3} \int f(\overrightarrow{p}, m_i) \left[1 - \ln f(\overrightarrow{p}, m_i)\right] \mathrm{d}^3 p. \tag{3.2}$$

Let us consider this expression in details. By substituting (3.1) into (3.2) we obtain

$$s_i = \frac{1}{V} \int \left[1 - \ln \frac{(2\pi)^3}{V g_i} - \ln \frac{\mathrm{d}N_i}{\mathrm{d}^3 p}\right] \frac{\mathrm{d}N_i}{\mathrm{d}^3 p} \mathrm{d}^3 p$$

$$= \frac{1}{V} \left[1 - \ln \frac{(2\pi)^3}{V g_i}\right] \int \mathrm{d}N_i + \frac{1}{V} \int \ln\left(\mathrm{d}^3 p\right) \mathrm{d}N_i - \frac{1}{V} \int \ln\left(\mathrm{d}N_i\right) \mathrm{d}N_i.$$

Particle density ρ_i is being defined via (3.1) as

$$\rho_i = \frac{g_i}{(2\pi)^3} \int f(\overrightarrow{p}, m_i) \mathrm{d}^3 p = \frac{N_i}{V}, \tag{3.3}$$

thus resulting in

$$\frac{s_i}{\rho_i} = 1 - 3\ln(2\pi) - \ln \rho_i + \ln g_i + H\left(\frac{\mathrm{d}N_i}{\mathrm{d}^3 p}\right), \tag{3.4}$$

where

$$H\left(\frac{\mathrm{d}N_i}{\mathrm{d}^3 p}\right) = \ln N_i - \frac{1}{N_i} \int \ln\left(\mathrm{d}N_i\right) \mathrm{d}N_i + \left\langle \ln \mathrm{d}^3 p \right\rangle_{\mathrm{d}N_i/\mathrm{d}^3 p} \tag{3.5}$$

is the Shannon entropy for the momentum distribution $\left\{\frac{\mathrm{d}N_i}{\mathrm{d}^3 p}\right\}$ generalized to the continuous distributions (Jayson entropy), see (1.15). The last term in (3.5), which is equal to

$$\left\langle \ln \mathrm{d}^3 p \right\rangle_{\mathrm{d}N_i/\mathrm{d}^3 p} = \frac{1}{N_i} \int \frac{\mathrm{d}N_i}{\mathrm{d}^3 p} \ln\left(\mathrm{d}^3 p\right) \mathrm{d}^3 p = \frac{1}{N_i} \int \ln\left(\mathrm{d}^3 p\right) \mathrm{d}N_i, \tag{3.6}$$

takes into account information encoding the transition from discrete to continuous quantities [Jay63; Jay68], in full accord with (1.15).

Total entropy density may be defined as

$$s = \sum_i s_i. \tag{3.7}$$

It should be mentioned that (3.7) is governed by the set of general distributions (3.1). One extracts these straight from the experimental data. In general case the observed system is not required to be in equilibrium, so $f(\overrightarrow{p}, m_i) \neq f(p, m_i)$.

Total particle density of the system is simply

$$\rho = \sum_i \rho_i. \tag{3.8}$$

Let us introduce an averaging over types of the particles involved

$$\langle \zeta \rangle_\rho = \frac{1}{\rho} \sum_i \zeta \rho_i \equiv \frac{1}{N} \sum_i \zeta N_i.$$

Then, after multiplying (3.4) with (3.3) and substituting the result into (3.7) one gets

$$\frac{s}{\rho} = 1 - 3\ln(2\pi) - \ln\rho + \langle \ln g_i \rangle_\rho + H\left(\frac{\mathrm{d}N_i}{\mathrm{d}^3 p}, \rho_i\right). \tag{3.9}$$

Here the term $\langle \ln g_i \rangle_\rho$ takes into account entropy related to the degeneracy factor, and $H\left(\frac{\mathrm{d}N_i}{\mathrm{d}^3 p}, \rho_i\right)$ equals to

$$\begin{aligned} H\left(\frac{\mathrm{d}N_i}{\mathrm{d}^3 p}, \rho_i\right) &= \ln\rho - \sum_i \rho_i \ln\rho_i + \frac{1}{\rho}\sum_i \rho_i H\left(\frac{\mathrm{d}N_i}{\mathrm{d}^3 p}\right) \\ &\equiv H(\rho) + \left\langle H\left(\frac{\mathrm{d}N_i}{\mathrm{d}^3 p}\middle| \rho_i\right)\right\rangle_\rho, \end{aligned} \tag{3.10}$$

i.e. stands for the Shannon entropy of joint distribution $\left\{\frac{\mathrm{d}N_i}{\mathrm{d}^3 p}, \rho_i\right\}$ over both momentum and particle species and, therefore, should be expressed in the form of (1.12).

Thereby we see that in spite of additive behavior of s_i in (3.7), see (1.14), the detailed analysis of the components of total entropy density does not prohibit the presence of correlations among different components of the system: conditional distributions are taken into account due to (1.12).

It is worth paying attention to the dependence of entropy per particle on the system parameters in (3.9). In particular, let us consider the situation when the system is close to equilibrium, and momentum re-distribution has finished almost. This corresponds to the case when the amount of re-distributions in the system is small. Consequently, the last term in (3.9) is expected to be approximately constant, thus making particle density ρ the only one to be responsible for any changes of s/ρ. This dependence is determined with the term $-\ln\rho$ that weakly depends on particle density. In such case s/ρ is expected to be almost constant at the final phase of the momentum re-distribution [Bra+01].

Therefore, the moment when s/ρ reaches a plateau may indicate the emergence of (quasi)equilibrium. It should be emphasized that in spite of thermodynamic approach and phenomenological models, which are based on equations of state, the presented result origins from the microscopic analysis and uses techniques of information theory only. This method justifies the so-called isentropic expansion of excited matter without imposing equilibrium conditions of any kind.

Obviously, an arbitrary state of the system should obey the inequality

$$s \leq s_{\mathrm{SM}}, \tag{3.11}$$

where s_{SM} is the Boltzmann entropy density. Both sides of (3.11) are equal if and only if one deals with equilibrium. It means that entropy reaches its

maximum when partial microscopic distributions coincide with their equilibrium counterparts, $f\left(\overrightarrow{p}, m_i\right) \to f\left(p, m_i\right)$.

Chapter 4

Used models and formalisms

4.1   UrQMD model

UrQMD [Bas+98; Ble+99] model is an event generator for computer calculations of elementary particles and heavy ion collisions. It is designed to process the collision of two hadrons, nuclei or their combination at different energies, covering the range from Bevalac and SIS up to RHIC. One can extend this up to LHC energies with some restrictions, and in case a hydrodynamic phase is introduced.

The model contains 55 different baryon types including a long list of resonances, and 39 meson types. The catalog is supplemented by the corresponding anti-particle states. Any of the enlisted particles may be produced during collisions. To allow for subsequent re-scatterings without causality violation, they can interact with the other participants only after some certain time interval (formation time).

In addition to isospin DOF, baryonic and electrical charges, UrQMD takes into account strangeness and charm as well.

Within the UrQMD model particle production is realized via the color string mechanism, as some excitation or decay process. The strings themselves are being produced through the momentum exchange among the participants in every single event. The strings are being initialized among quarks and may be stretched with the tension factor of about 1 GeV/fm. When the critical energy level is reached, the color tube experiences the Schwinger decay thus producing quark-antiquark pairs and, consequently, particles.

Within the model elementary particles obey classical equations of motion. An interaction among participating hadrons occurs only at the distances not exceeding the range $r \leq \sqrt{\sigma/\pi}$, where σ is the total cross section of the process. It depends on such DOF of colliding particles as isospin, flavor and energy. To ensure the calculations are correct, the relevant values of σ and decay widths are taken from experiments. In case the data are incomplete, the model applies various approaches, such as detailed balance conditions, single boson exchange, spin and isospin symmetries, Pauli principle etc. In total, this allows UrQMD to implement $\mathcal{O}\left(10^4\right)$ different elementary particle-particle interactions.

UrQMD can be run in two different regimes. The first one is the "open regime" implementing open boundary conditions: elementary particles and ions can freely leave the interaction volume and pass to infinity. The situation corresponds to real scattering processes which one may detect in reality.

The second regime is know as "box" [Bel+98; Bra+00b]. It is designed to calculate particle interactions in a cubic-shaped domain of space. To increase the precision, one may vary the linear size parameter of the cube. In this regime, the constituents cannot freely escape the interaction volume. Depending

on the initial conditions, once any of them reaches the volume boundary, it can be reflected (mirror mode) or injected (transparent mode) at the opposite border with the same momentum. The regime allows to implement infinite matter calculations. Interpreting microscopic perturbations inside the box as thermodynamic fluctuations, one may investigate stationary quasi-equilibrium states of infinite QCD matter.

4.2 Green-Kubo formalism and viscosity

The study of system's response to external forces is a common problem in physics. This may be done with the help of Green-Kubo formalism [Gre54; Kub57]. It is applicable for the states close to equilibrium, thus implying that the disturbances caused by the forces are small. This allows to develop a linear response approximation; in a more general case, the differentiability of distribution functions in equilibrium should be fulfilled. The method interconnects the microscopic background of to macroscopic properties of a medium so that transport coefficients can be calculated via the corresponding correlation functions.

Viscosity is being understood as the dissipation of momentum that causes a fluid to turn back into its equilibrium state. This may be interpreted also as the decay of information about momentum correlations. Within the Green-Kubo formalism this establishes that shear viscosity η can be calculated as follows:

$$\eta = \frac{V}{T} \int_{t_0}^{\infty} \langle \pi(t) \pi(t_0) \rangle_t \, \mathrm{d}t, \tag{4.1}$$

where V is the volume of the liquid, T is its temperature, t_0 denotes initial time to start estimation of the correlator $\langle \pi(t) \pi(t_0) \rangle_t$. The last one reads:

$$\langle \pi(t) \pi(0) \rangle_t = \frac{1}{3} \sum_{\substack{i,j=1 \\ i \neq j}}^{3} \left[\lim_{t_{\max} \to \infty} \frac{1}{t_{\max} - t_0} \int_{t_0}^{t_{\max}} \pi^{ij}(t + t') \pi^{ij}(t') \, \mathrm{d}t' \right]. \tag{4.2}$$

Here quantities $\pi^{ij}(t)$ represent off-diagonal components of the stress-energy tensor. One can express them via averaged momenta $p^i(t), p^j(t)$ and energy $E(t)$ of the particles calculated at time t:

$$\pi^{ij}(t) = \frac{1}{V} \sum_{k=1}^{N} \frac{p_k^i(t) \, p_k^j(t)}{E_k(t)}, \tag{4.3}$$

where the sum takes into account all particles in V.

From the Abel theorem it follows that in equilibrium arbitrary fluctuations decrease exponentially with time [Kub57]. So, the correlator (4.2) undergoes the following evolution

$$\langle \pi(t) \pi(t_0) \rangle_t = \langle \pi(t_0) \pi(t_0) \rangle \, e^{-(t-t_0)/\tau}, \tag{4.4}$$

where τ is the relaxation time determining a decrement in the medium. Expression (4.4) implies the evanescence of any information, which is encoded by the correlator, with time. For example, one may transfer information to the fluid in a form of induced current or a wave. Gradually, multiple interactions will redistribute (re-code) this collective initial momentum among all the constituents. Equation (4.4) allows to estimate the rate of this decay.

Substituting (4.4) into (4.1) one gets

$$\eta = \frac{V}{T}\tau\left\langle \pi\left(t_0\right)\pi\left(t_0\right)\right\rangle. \tag{4.5}$$

Equation (4.5) reduces the problem of viscosity estimation to the calculation of τ assuming the fluctuation experiences an exponential decay.

A more rigorous analysis requires to use (4.1). This one is more general due to taking into account the contribution of stochastic deviations.

4.3   Statistical model of an ideal hadron gas

Statistical model of an ideal hadron gas (SM) has been established in [BL56; Fer50]. A detailed description and general protocol of calculations can be found in [Bel+98; Bra+99b].

The model describes an equilibrium state of a system consisting of non-interacting particles (ideal gas) at temperature T. Some certain type of the particles is being defined by their mass m_i, baryon and strangeness charges B_i and S_i correspondingly. The system may be a mixture of different types. The particles themselves obey the distribution function $f\left(p, m_i\right)$

$$f\left(p, m_i\right) = \left[\exp\left(\frac{\sqrt{p^2 + m_i^2} - B_i\mu_{\mathrm{B}} - S_i\mu_{\mathrm{S}}}{T}\right) \pm 1\right]^{-1}, \tag{4.6}$$

where p is the momentum, μ_{B} and μ_{S} stand for baryon and strangeness chemical potentials correspondingly. Electrical chemical potential is small compared to the first two and, therefore, usually is excluded from the analysis. The sign $\pm$ takes spin statistics into account.

Partial density ρ_i of the i-th particle specie reads

$$\rho_i\left(T, \mu_{\mathrm{B}}, \mu_{\mathrm{S}}\right) = \frac{g_i}{\left(2\pi\right)^3}\int_0^\infty f\left(p, m_i\right)\mathrm{d}^3p, \tag{4.7}$$

where g_i is the spin-isospin degeneracy factor.

Having obtained the distribution $f\left(p, m_i\right)$ from (4.6), one may define the partial energy density ϵ_i as

$$\epsilon_i = \frac{g_i}{\left(2\pi\right)^3}\int_0^\infty \sqrt{p^2 + m_i^2}f\left(p, m_i\right)\mathrm{d}^3p. \tag{4.8}$$

From (4.7) and (4.8) one may construct the system of non-linear equations

$$\begin{cases} \epsilon = \sum_{i=1}^{n} \epsilon_i \left(T, \mu_B, \mu_S\right) \\ \rho_B = \sum_{i=1}^{n} B_i \rho_i \left(T, \mu_B, \mu_S\right) \\ \rho_S = \sum_{i=1}^{n} S_i \rho_i \left(T, \mu_B, \mu_S\right), \end{cases} \tag{4.9}$$

where the total quantities such as the energy density ϵ, baryon density ρ_B and strangeness density ρ_S are the onset data.

A numerical solution of (4.9) allows to find thermodynamic parameters of the system in equilibrium. In particular, one may obtain temperature T, baryon chemical potential μ_B and strangeness chemical potential μ_S.

So, SM describes the equilibrium state of matter with ϵ, ρ_B, ρ_S being fixed. Its entropy density s_{SM} may be estimated from the thermodynamic identity

$$\epsilon = T s_{SM} + \mu_B \rho_B + \mu_S \rho_S - P$$

and reaches the maximum value possible. Here P stands for the pressure

$$P = \sum_{i=1}^{n} P_i = \sum_{i=1}^{n} \frac{g_i}{(2\pi)^3} \frac{1}{3} \int_0^{\infty} \frac{p^2}{\sqrt{p^2 + m_i^2}} f\left(p, m_i\right) \mathrm{d}^3 p.$$

On the other hand, s_{SM} can be calculated via the partial distribution functions $f\left(p, m_i\right)$ as

$$s_{SM} = \sum_{i=1}^{n} s_i = \sum_{i=1}^{n} \frac{g_i}{(2\pi)^3} \int_0^{\infty} f\left(p, m_i\right) \left[1 - \ln f\left(p, m_i\right)\right] \mathrm{d}^3 p, \tag{4.10}$$

where $f\left(p, m_i\right)$ is given by (4.6).

As one can see from (4.10), total entropy density s_{SM} is a simple sum of partial entropy densities s_i. Such a behavior consequences from the absence of any correlations among the species: all partial distribution functions $f\left(p, m_i\right)$ are statistically independent.

Chapter 5

Specific viscosity: main results

The results of specific viscosity calculations are published in [Paper I; Paper II; Paper III; Paper IV; Paper V].

At first, central Au+Au collisions were calculated within the UrQMD model. Any scattering event describes an open system with no specified boundary; its parameters experience a highly dynamical evolution with time. One expects to meet the most close to equilibrium state in the central region of a fireball only. So, a cubic cell from the center was chosen to extract the energy density ε and densities of the net baryon ρ_B and the net strangeness ρ_S charges. Data analysis was performed on the set consisting of 80 points. This includes:

- the bombarding energy range $E_{lab} = \{10, 20, 30, 40\}$ AGeV in the laboratory frame, with the ensemble of 51200 generated Au+Au collisions per each E_{lab};

- time slices from the interval $t_{cell} = 1 \div 20$ fm/c, with the step $\delta t_{cell} = 1$ fm/c.

Next, temperature T, entropy density s_{SM} and other thermodynamics characteristics of the central cell were calculated within the statistical model of the ideal hadron gas; the corresponding protocol can be found in Section 4.3.

Typical dependencies for the quantities can be found in Fig. 5.1 depicting their time dynamics. The upper panel represents the values extracted from the central cell; calculations within the SM model are shown on the lower panel. It should be noted that the cell temperature is the same for all beam energies at late times, when $t_{cell} \geq 7$ fm/c. But, they can be distinguished with the help of chemical potentials μ_B and μ_S.

A highly dynamical evolution in the central cell prohibits the straight application of the Green-Kubo formalism, as mentioned in Section 4.2. Microscopic treatment for viscosity calculations requires the knowledge of relaxation rates in the medium. The required correlator dynamics was derived by using of UrQMD model calculations in the box regime for the time range $t_{box} = 1 \div 1000$ fm/c, with the temporal resolution $\delta t_{box} = 1$ fm/c. Conditions from the central cell were reproduced by initializing the infinite matter regime with the previously extracted densities $\varepsilon, \rho_B, \rho_S$.

Correlator temporal decrements τ_{int} in the box were extracted with the help of (4.1). Fig. 5.2 depicts relaxation times τ_{int} as functions of initial time $t_0 = 1 \div 1000$ fm/c for each of 80 points from the cell. For visibility reasons, only every tenth value of t_0 is displayed. As one can see, the decrements saturate in the range $t_0 \in [200, 800]$ fm/c. Smaller values of t_0 refer to the initializing state of the box, when the medium is still out of steady state. For $t_0 \geq 800$ fm/c
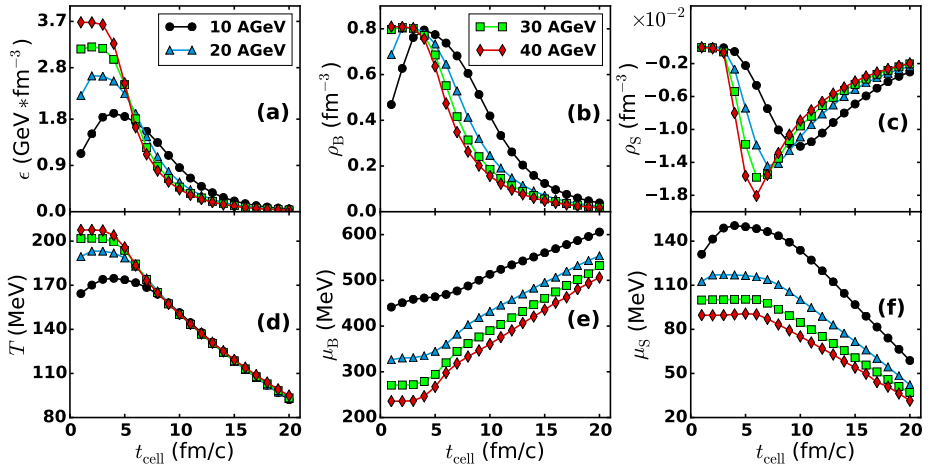
Figure 5.1: Upper panel: energy density ε (a), net baryon density ρ_B (b) and net strangeness density ρ_S (c) from the cell. Lower panel: temperature T (d), baryon chemical potential μ_B (e) and strangeness chemical potential μ_S (f) from the SM. Quantities are depicted as functions of the cell time t_{cell}. Figure taken from [Paper II].

the averaging temporal range is not large enough, and here an analog of the Brownian motion may be observed.
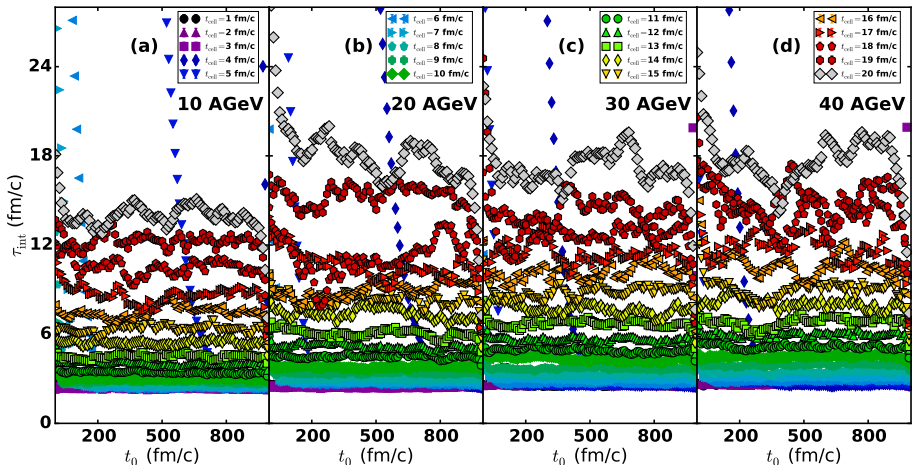
Figure 5.2: Correlator relaxation times τ_{int} as functions of initial time t_0 at different bombarding energies and cell times. Figure taken from [Paper I].

The plot definitely pronounces the impact of stochastic fluctuations on the medium properties. To study the effect, similar calculations were performed by

fitting (4.4) to extract τ_{fit}. The ratios of averaged over the plateau $t_0 = [200, 800]$ fm/c temporal decrements are shown in Fig. 5.3. The dashed lines depict the overlapping stage, when the whole system is in the non-equilibrium state. Data manifest the rise of relaxation rates due to stochastic processes in the medium.
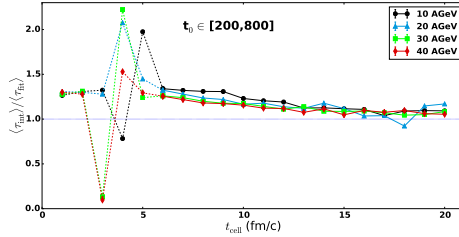
Figure 5.3: Ratio $\langle \tau_{\text{int}} \rangle / \langle \tau_{\text{fit}} \rangle$ as a function of the cell time. Figure taken from [Paper I].

This suggests to take τ_{int} as the upper bound for shear viscosity calculations. The corresponding results can be seen in Fig. 5.4. Similar to temperature, η weakly depends on the collision energy at times $t_{\text{cell}} = 7 \div 20$ fm/c.
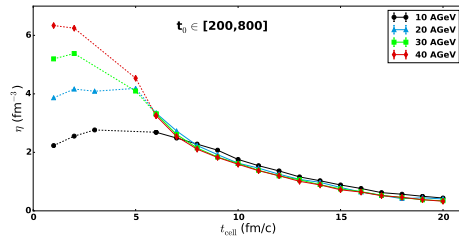
Figure 5.4: Shear viscosity η for hadron matter in Au+Au collisions as a function of the cell time. Figure taken from [Paper I].

Finally, specific viscosity as the ratio η / s_{SM} was extracted. Fig. 5.5 represents the results for each of 80 points from the set. The statistics per point consists of 12800 box calculations that requires approximately $5 \div 8$ Tbytes of data on average. Statistical errors are smaller than the size of symbols. Panels depict specific viscosity as a function of time t_{cell} and thermodynamic quantities derived within the SM model T, μ_{B} and μ_{S}. The blue dashed line at the bottom stands for the KSS bound.

Results indicate the minima of specific viscosity at $t_{\text{cell}} = 4 \div 5$ fm/c for all beam energies. The lowest value reaches about 0.3 for $E_{\text{lab}} = 10$ AGeV, i.e. for the baryon-dominated medium. After that it starts rising up with time as expected.

As one can notice, the minimum is not sharp but exhibits a smooth U-shaped behavior. The lowest values are observed in the dashed region, when nuclei overlap and the cell experiences the most dynamic evolution.

Figure 5.5: The ratio η/s_{SM} for hadron matter in the central cell as a function of: (a) cell time t_{cell}, (b) temperature T, (c) baryon chemical potential μ_{B} and (d) strangeness chemical potential μ_{S}. Figure taken from [Paper II].

In general, the method to study the evolution of shear viscosity and its ratio to entropy density has been developed. The approach allows to extract the quantities at every point of the fireball. As discussed in Section 2.3, usually these quantities are being extracted as functions of either temperature or chemical potential, with the other one to be constant. Such situation seems to differ from what is expected for colliding nuclei, when all thermodynamic characteristics evolve with time. Compared to previous studies, the presented self-consistent protocol allows to investigate shear viscosity and its ratio as functions of time, temperature, baryon chemical potential and strangeness chemical potential for a dynamical medium simultaneously.

Both viscosity η and entropy density s_{SM} decrease with time t_{cell}. This correlates with the rise of baryon chemical potential and the drop of both strangeness chemical potential and temperature. For the ratio η/s_{SM} smooth minima are observed for all bombarding energies.

The obtained U-shaped pattern may originate from the assumption about equilibrium in the central cell. One may argue that such treatment is not valid, especially at early times when the nuclei overlap. To study the hypothesis, microscopic entropy density s was extracted with the help of the technique discussed in Section 3.3. Both entropy densities, s_{SM} and s, should coincide in thermal equilibrium. However, they differ for a system carrying correlations among any of its DOF. The discrepancy may affect the ratio's behavior at the critical point of QCD matter. This was the main motivation to compare both the microscopic and the statistical model predictions. The corresponding calculations were performed in [Paper II; Paper IV].

Fig. 5.6 presents the ratio of shear viscosity to microscopic entropy density

s. The extremes are higher as compared to $\eta/s_{\rm SM}$ due to the lower entropy density. However, the minima become more pronounced: the V-shaped pattern is observed at $t_{\rm cell} \approx 5 \div 6$ fm/c. Compared to $\eta/s_{\rm SM}$, the non-equilibrium ratio manifests larger discrepancies with respect to the bombarding energy.

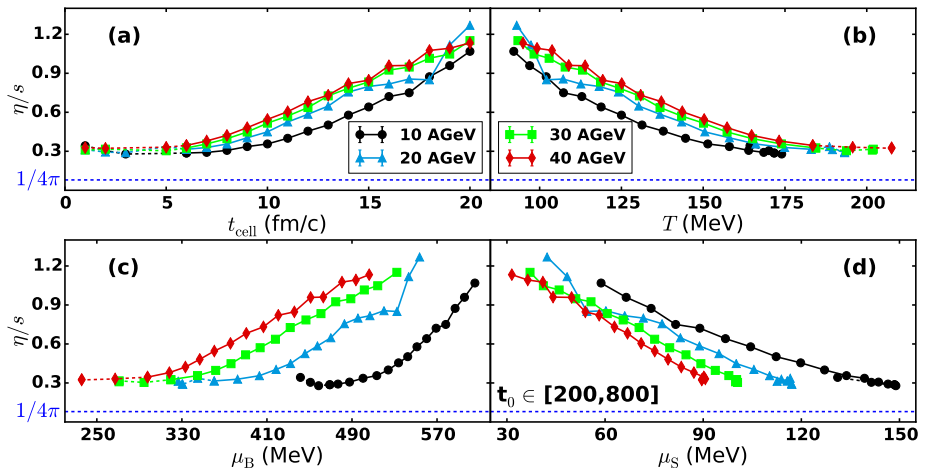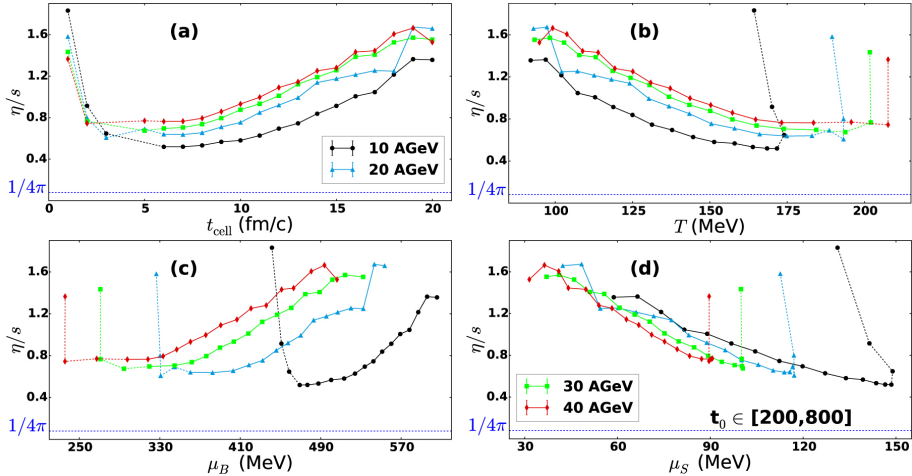Figure 5.6: The ratio of shear viscosity to microscopic entropy density η/s for hadron matter in the central cell as a function of: (a) cell time $t_{\rm cell}$, (b) temperature T, (c) baryon chemical potential $\mu_{\rm B}$ and (d) strangeness chemical potential $\mu_{\rm S}$. Figure taken from [Paper II].

So, the microscopic analysis recovers the expected behavior and makes the extremes more distinct. This allows to pinpoint the critical point with much higher accuracy.

The procedure above estimates specific viscosity for the whole medium. But the fireball consists of different particle species. One may consider this as a mixture of pure components, each contributing separately to dissipative processes in the substance. To study the case, partial viscosities for nucleons and pions were analyzed separately in [Paper III]; the extension to a larger list of particle types one can find in [Paper V].

For example, Fig. 5.7 shows the partial shear viscosity for all baryons from the cocktail. Its dependence on $t_{\rm cell}$ and thermodynamic quantities is similar to the one observed for the medium as a whole.

The same behavior was observed for all mesons and separate particle species. For example, Fig. 5.8 and Fig. 5.9 depict partial viscosities η_N for nucleons and $\eta_{\Lambda+\Sigma}$ for $\Lambda + \Sigma$ baryons respectively.

As one can notice from Fig. 5.8, $\eta_{\rm bar}$ manifests the uprising trend with the bombarding energy. Similar dependence, however not so distinct, is observed for $\Lambda + \Sigma$ hyperons, while meson and pion components recover the typical energy trend of the cocktail [Paper V].
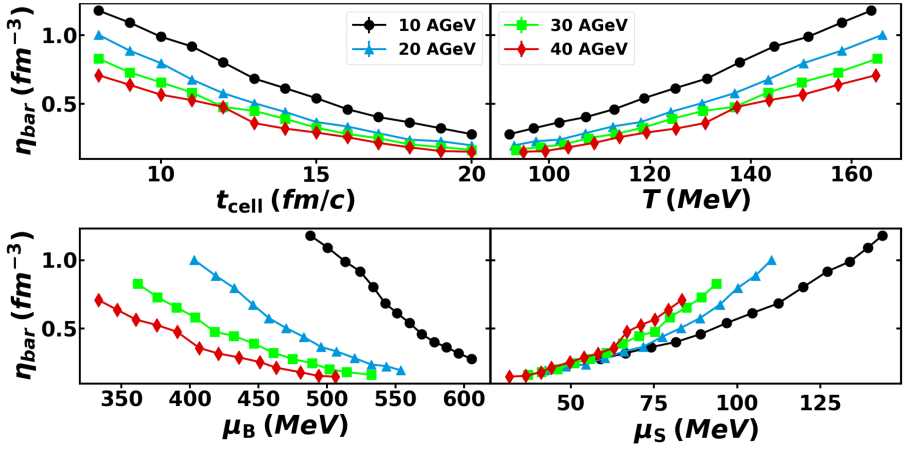
Figure 5.7: Partial shear viscosity η_{bar} for baryons. Figure taken from [Paper V].
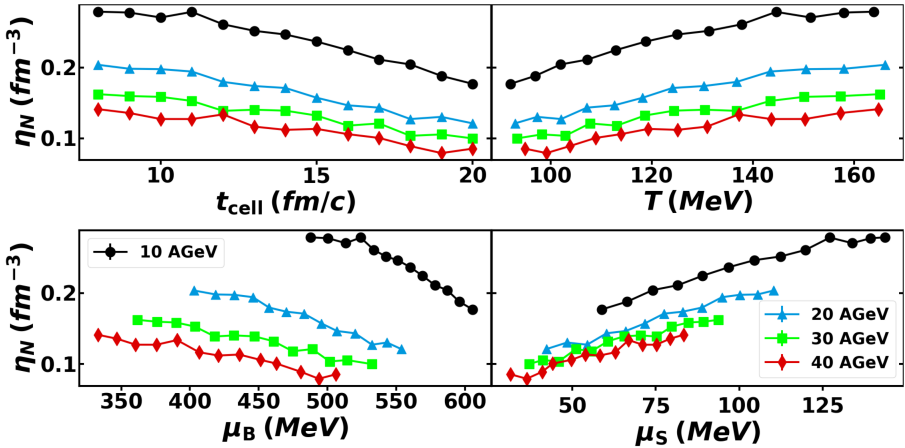
Figure 5.8: Partial shear viscosity η_N for the nucleon component. Figure taken from [Paper V].
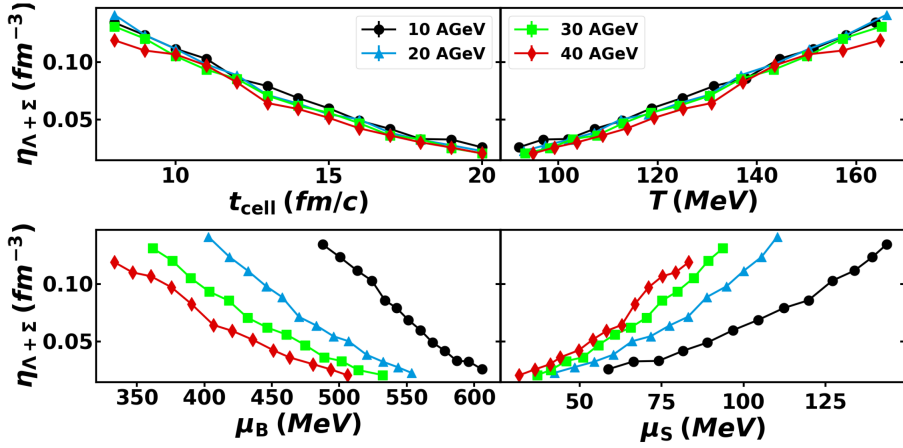
Figure 5.9: Partial shear viscosity $\eta_{\Lambda+\Sigma}$ for $\Lambda + \Sigma$ baryons. Figure taken from [Paper V].

Partial specific viscosities η_{bar}/s_{SM} for baryon and η_{mes}/s_{SM} for meson components are depicted in Fig. 5.10 and Fig. 5.11 respectively. Baryon sector seems to be mostly indifferent to the beam energy, while mesons indicate a much higher sensitivity. Both plots manifest the uprising dynamics with time, similarly to the whole cocktail. At the same time, partial ratios go beyond the minima observed for the substance.
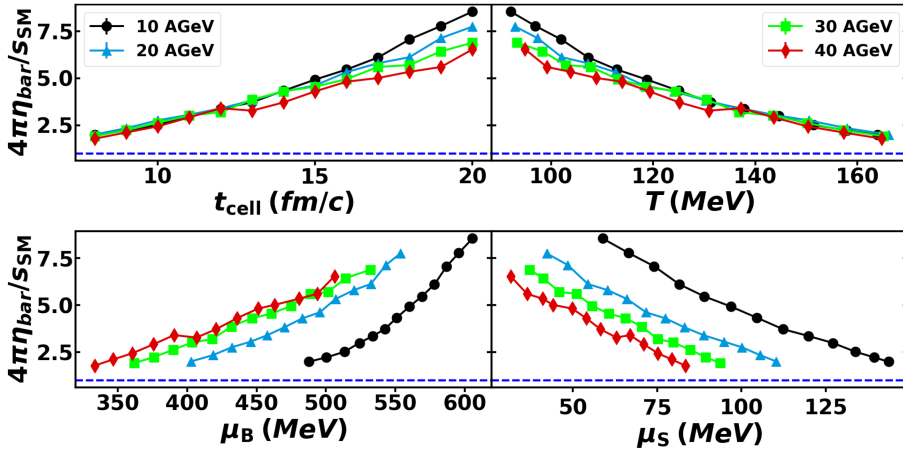
Figure 5.10: Partial specific viscosity η_{bar}/s_{SM} for baryons. The blue dashed line shows the KSS bound. Figure taken from [Paper V].

The results indicate that the uprising trend with energy for the hadron
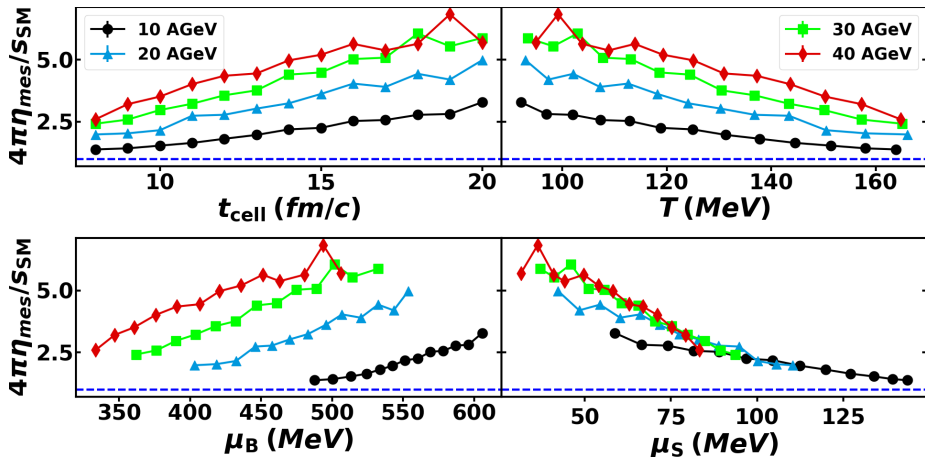
Figure 5.11: Partial specific viscosity $\eta_{\mathrm{mes}}/s_{\mathrm{SM}}$ for mesons. The blue dashed line shows the KSS bound. Figure taken from [Paper V].

specific viscosity should be ascribed to its meson component. This conclusion might be useful for hydrodynamic calculations in the considered energy range.

Also, the following common tendency may be drawn out from the pictures above: partial viscosities tend to be much lower compared to the combined quantity. The most significant drop is observed for $\eta_{\Lambda+\Sigma}$. This may lead to dramatic results: specific viscosity for this component is expected to break the KSS bound.

Such behavior is explained as follows. Partial microscopic correlator $\langle \pi(t)\pi(t_0) \rangle_t$ takes into account momentum re-distribution over some certain particle specie only. All other information, being encoded with mutual interactions among the constituents of different types, is left behind. This results in much smaller temporal decrements τ and may break the theoretical minimum for the specific viscosity in a strongly coupled medium.

So, the hadron substance consists of different particles which cannot be considered separately. Information dynamics is of great importance in heavy ion collisions and requires the proper microscopic analysis of all involved correlations.

Chapter 6

Black hole radiation

6.1 Black hole thermodynamics

Both general relativity and quantum mechanics claim to be the most verified theories in physics. They provide a strong basement for any field of modern science. The application range encompasses our reality at any level, from the Big Bang theory and particle accelerators to pharmacy industry and GPS navigation in our cell phones. But, despite a prominent success, merging both of them into the single theory of quantum gravity is still a challenge for modern science [Add+22; Sch14].

At the fundamental level both theories seem to differ so much that they result in opposite conclusions. Black holes may serve as an evidence of discrepancies between general relativity and quantum physics.

In general relativity, a black hole is the object with such strong gravity force that even light cannot escape it after reaching its event horizon. It may be interpreted as a one-way sink of spacetime. Being unable to emit anything from the inside, black hole cannot decrease; it is really black.

Despite that, it turned out to have much in common with thermodynamics. In 1973 Bekenstein [Bek73] revealed that entropy H_{BH} of a spherically symmetric Schwarzschild black hole equals to the area A of its event horizon multiplied by some unknown coefficient. The laws similar to those from thermodynamics have been formulated in [BCH73]:

- The 0th law: the black hole's surface gravity κ is constant over its event horizon.

- The 1st law: close to the horizon, the rate of mass change δM equals to the same of its surface area δA times $\frac{\kappa}{8\pi}$, plus some other terms defining the work.

- The 2nd law: the area of the event horizon is either constant or increasing; it cannot shrink, $\delta A \geq 0$.

- The 3rd law: the surface gravity cannot be decreased to zero by any process consisting of finite amount of steps.

So, the properties of a black hole resemble the properties of any thermal system. The laws do look like those from thermodynamics. However, any thermal system should exchange energy with its surrounding in both directions, via absorption and emission. Processes of the first type are typical for gravitational collapse, but how about the second? Is this just the similarity leading to no new effects? Can gravity induce emission at the presence of horizon?

Quantum physics answers affirmatively: black holes should emit particles [Haw75]. Loosely speaking, due to quantum fluctuations a pair of virtual particles may pop out of the vacuum at different spacetime domains with respect to the event horizon. Then, the outer particle is allowed to escape to infinity, while its partner is doomed to be trapped under the horizon. For an outside observer the process looks like an outgoing flux of particles, which is generated at the cost of black hole's energy. So, due to quantum effects, any black hole should eventually evaporate.

Therefore, for the infalling matter a black hole is not a one-way trip as the general relativity dictates. Quantum laws establish that it is not absolutely black: there should be particle emission from its event horizon.

6.2 Information loss problem

General relativity states that a black hole has no hair: one can derive no information about it but except its mass, angular momentum and electric charge. Any other data about an object falling down inside cannot be extracted; once it crosses the event horizon, it is lost forever for the outer world.

Quantum evaporation at the event horizon is not of great help here because the outgoing radiation is completely thermal [Haw75]. Therefore, it should be described by a mixed state rather than by a pure one [Haw76], with no useful information inside.

At the same time, any object or particle falling down the horizon carries some information about its structure and properties. It is encoded by the correlations among the relevant degrees of freedom. And all this information is expected to be lost completely, as soon as the black hole evaporates away. This is the essence of the famous information loss problem, which was formulated by Hawking [Haw05].

The situation becomes even more dramatic if one considers a collapsing set of particles as some scattering process. Quantum mechanics dictates that any closed system obeys unitary evolution. However, if the collapse results in the formation of a black hole then the detected radiation will be in a mixed state. Therefore, one may conclude that gravity violates unitarity.

6.3 Black hole entropy

In 1975 S. Hawking revealed the famous area law [Haw75]. In Planck units it reads

$$H_{\mathrm{BH}} = A/4, \tag{6.1}$$

where H_{BH} is the entropy of a black hole and A is the area of its event horizon.

The law seems to be strange for several reasons.

At first, for any system, once it is in equilibrium, its entropy should be an extensive quantity. Therefore, if black holes obey thermodynamics then their entropy is expected to exhibit bulk properties, but not the area law.

The second problem origins from the black hole evaporation itself. Quantum particle emission from the hole is supplied at the cost of its own mass M. Therefore, the black hole's radius $r = 2M$ decreases with time thus resulting in entropy reduction. But this contradicts the second law of thermodynamics. One may argue that taking an environment into account will cause the entropy to change in the right direction. Unfortunately, some estimates indicate this might not work in the case of black holes [Sto18].

One more important issue is the magnitude of H_{BH}. One can easily figure out that for an ordinary black hole of stellar mass its entropy is large. For example, even for the Sun $H_{\mathrm{BH}\odot} \sim 10^{77}$. And it is a challenging task to explain physical phenomena generating so large amount of entropy.

Thermodynamics asserts that for any system its entropy is bounded from above with the logarithm of the number of possible states. So, for a black hole the number should be of order $e^{H_{\mathrm{BH}}}$. This leads to the related but even a more dramatic challenge: where should the corresponding degrees of freedom originate from?

6.4 Main approaches to solve the problems

Attempts to solve the aforementioned problems have caused the development of different approaches and investigations. It should be kept in mind that it is hard to encompass such a vast topic, so only some typical trends suggesting the solutions are discussed below. In addition, the classification is rather blurred due to multiple interconnections among the techniques.

6.4.1 Counting microstates

Entropy is determined by the occupied volume in the system's phase space. Thus, counting over all available microstates allows to calculate its entropy.

Loop quantum gravity is one of such approaches that offers a solution to the entropy problem. Due to it, the area law (6.1) is obtained through the introduction of the black hole's phase space with its consequent quantization [Ash+98]. Within the approach, the area spectrum of a spherical shape can be quantized [Khr02]; in Planck units it reads

$$A = 8\pi\gamma \sum_{i=1}^{n} \sqrt{j_i\,(j_i + 1)}, \qquad (6.2)$$

where γ is the Barbero-Immirzi parameter and $j_i\,(j_i + 1)$ is the eigenvalue of an operator $\overrightarrow{j}_i^{\,2}$, which is governed by the algebra of angular momentum. Quantum numbers j_i may take either integer of half-integer positive values. They are associated with the set of n edges determining the geometry. Having the area from (6.2) and taking the degeneracy factor $g_i = 2j_i + 1 \,\forall j_i$ into account, one can calculate the amount of possible surface states N and derive the entropy

as its logarithm. The method implies that the contribution of $j_i = 0$ should be discarded, otherwise the entropy cannot be determined unambiguously.

From (6.2) it follows that the quantized surface is governed by $\overrightarrow{j}$. This allows to represent the system in the form of a closed chain, as can be seen in Fig. 6.1.
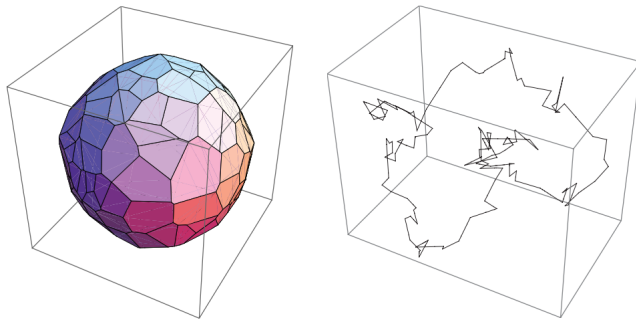
Figure 6.1: Left panel: tessellated quantized surface representing the horizon. Right panel: polymer chain, which is isomorphic to the surface. Figure taken from [Bia11].

Therefore, counting of black hole's microstates can be mapped to the problem of conformal configurations for a polymer chain [Bia11; LT12]. Within the analogy statistical physics bridges to gravity and its possible entropic origin [Ver11].

Black hole area quantization also leads to another important issue. The procedure influences its radiation spectrum and establishes its dependence on black hole's angular momentum and charge [Khr08]. As the author states, this provides the opportunities for verification of the whole framework with the help of existing gamma-ray telescopes.

As known, by varying the potential one may influence the spectrum of a quantum system. The changes might results in significant differences of the system's radiation entropy from that of a black body. Similarly, the emission spectrum of a black hole might exhibit time dependence once its area is quantized, as shown in Fig. 6.2. The spectrum is expected to become less entropic as the black hole evaporates away [SL11]. This implies the possibility of information extraction thus suggesting a solution to the information loss problem.

The resulting entropy (6.2) depends on the Barbero-Immirzi parameter corresponding to a set of different quantum theories. The study [Khr04] concludes that the exact value of γ is crucial for the whole black hole entropy estimate. On the other hand, its influence may be argued in case of a specific renormalization [Jac07]. So, the role of the parameter needs clarification.

One more candidate to explain the puzzles is string theory. For a highly excited string state its entropy is proportional to $\sqrt{N}$, where N is the corresponding excitation level [Hor07]. Recalling that the amount of possible states in equilibrium is just e^H, where H is entropy, one reduces the problem
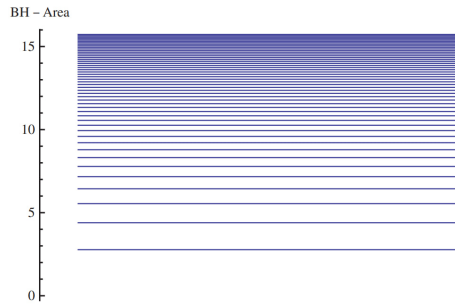
Figure 6.2: The area spectrum of a black hole within the topology change model. Figure taken from [SL11].

to the estimation of available string configurations. From this perspective, the approach has much in common with the loop quantum gravity.

At first, the area law was recovered at the leading order for a charged five-dimensional black hole [SV96]. Calculations within the M-theory framework recover the area law (6.1) for the Kaluza-Klein black hole [EH06]. The result turns out to depend on the mutual orientation of branes and their rotational DOF, which contribute via the tensor product of relevant Hilbert spaces. The extension to extremal Kerr black holes was also fruitful [EM07; HR07]. These and other successful entropy calculations for a variety of black hole types have inspired further investigations in different directions [Gom11; Pre08] and revealed that there is still much to be investigated. In addition, a whole concept still lacks of unambiguous experimental verification [LMT07].

6.4.2   Event horizon contribution

For a system in thermal equilibrium, one expects all its volume to contribute to entropy. But in the case of a black hole one has the area law (6.1), which indicates that the event horizon is responsible for its entropy. Therefore, it seems reasonable to study the DOF located in the vicinity of the horizon.

In 1985 't Hooft proposed an efficient method known as the brick wall model ['t 85]. It assumes that wave functions should vanish at the horizon's nearby. So, the black hole's boundary behaves much like an ideal mirror. Estimating the total number of available modes via the well-known WKB approximation in the vicinity of the horizon, one arrives at the area law for entropy. However, vanishing field implies the impenetrable horizon. This makes it detectable in the infalling frame and, therefore, seems to contradict the equivalence principle.

Despite seemingly naive simplicity and coordinate non-invariance, the model predicts that quantum properties of the black hole are caused by its horizon. The approximation allows even to find the higher order corrections [WS13].

The brick wall model suggests the presence of sharp boundary. From the Heisenberg's uncertainty principle it follows then that momentum can take an

value, so the density of states becomes infinite at the horizon. This results in the divergence of total energy and entropy, which can be treated by smoothing the edge [BK11].

In relativity, particles cannot escape a black hole after crossing its surface. So, one may consider it as a potential barrier for the inside quanta and calculate the tunneling probability p of its emission. Within the WKB approximation it reads [VAC11]

$$p \propto e^{\Delta H}, \tag{6.3}$$

where $\Delta H = -8\pi M E \left(1 - \frac{E}{2M}\right)$ is the entropy change induced by the tunneling of a particle at energy E, and M is the black hole's mass. Calculations for different masses and spins [Li11] show that the corresponding entropy contains both area and logarithmic correction terms. The last ones are suggested to be responsible for back-reaction effects, thus indicating the possible impact of emitted particles on the background metric. In such case, one is expected to analyze the relevant conditional distributions, which might go beyond the imposed approximations.

6.4.3 Entanglement entropy

As follows from general relativity, there is no access to information about the intrinsic region of a black hole from the outside. Its event horizon separates a whole spacetime into observable and non-observable domains. Therefore, any remote observer has access to some part of a state only, which, in turn, cannot be represented by a single vector. The relevant density matrix ρ is derived by partial tracing over all the inaccessible quantum DOF. But projecting the state onto the corresponding Hilbert subspace implies neglecting any data encoded with quantum correlations at the horizon. Being measured by the von Neumann entropy

$$H_{\text{ent}}(\rho) = -\text{Tr}\rho \ln \rho, \tag{6.4}$$

this information depends on the size of boundary among the domains, as discussed in Section 1.4. So, the entanglement at the event horizon should be responsible for the area dependence of the black hole entropy [Sre93].

The problem may be analyzed at an abstract algebraic level. For example, one may consider a tensor product of two subspaces for a $D = 1 + 1$ spacetime, with bosonic modes in each of them. Then, algebraic deformation, which can be associated with some Bogoljubov transformation [ILV02], recasts the vacuum state as a Schmidt decomposition of coupled modes. The corresponding entanglement entropy H_{ent} is extracted by tracing out the "non-accessible" subspace.

Specific calculations for a spherical shell in the vicinity of black hole horizon clearly indicate the area-like behavior for the upper bound for H_{ent} [ILV04], in case total entropy is extensive. The method proposes a qualitative estimate for the entanglement entropy and clearly exhibits its surface dependence, as one would expect for an entangled system. However, the exact value $1/4$ for the

coefficient still requires clarification. The approach has much in common with the Unruh effect [Unr76], which will be discussed later.

Similar results were derived within lattice calculations [DS07b]. Namely, for a massless scalar field its Hamiltonian may be discretized and transformed to the one of a set of N coupled harmonic oscillators in the form

$$ H = \frac{1}{2} \sum_{i=1}^{N} p_i^2 + \frac{1}{2} \sum_{i,j=1}^{N} x_i K_{ij} x_j, \tag{6.5} $$

where K_{ij} is the operator determining pairwise interactions. Event horizon is introduced by partial tracing over $n < N$ modes of the total density matrix. Due to the entanglement caused by the coupling among the oscillators, one results in the non-zeroth entropy for the accessible modes. The area law is recovered for the ground state of the field, as shown in Fig. 6.3.
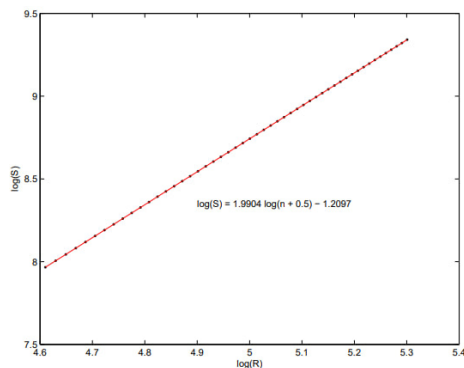
Figure 6.3: Dependence of entropy S on the radius R of the horizon. Figure taken from [DS07a].

Excited field states modify the entropy dependence due to the contribution of DOF far from the event horizon. This concludes that the area law (6.1) origins from DOF at the horizon. The extension to a massive fields modifies the interaction matrix K_{ij} and also exhibits deviations from the area law [DSS08]. These corrections indicate some underground correlations, which might origin from conservation laws, even in the case of oscillator potentials.

As mentioned above, quantum fluctuations are responsible for the black hole evaporation. However, only a tiny fraction of produced particles can escape to infinity. The major part is doomed to fall back into the black hole thus forming some kind of atmosphere close to its event horizon. Conservation laws entangle these particles to their counterparts, which cannot be observed from the outside, and produce an equilibrated medium. Entropy H_{atm} of the emerging thermal atmosphere becomes extensive, in full accord with Section 1.4, and can

be represented as [JP07]

$$H_{\text{atm}} = \int dE \sum_l (2l+1) \, n_{E,l} H_E. \tag{6.6}$$

Here E is the mode energy, l is the angular momentum, $n_{E,l}$ is the density of outer modes, and H_E stands for the entropy per mode. The area dependence is recovered because $\sum_l (2l+1) \propto r^2$, where r is the horizon radius. Due to its additive behavior, H_{atm} suffers spectrum divergences, so a careful regularization analysis ir required. In order to analyze all possible momenta, one needs a rigorous quantum description.

6.4.4 Information depository

As known, quantum entanglement represents non-classical correlations among subsystems. It is a quantum resource which may be quantified in different ways, and entanglement entropy is the one estimating amount of information between the partitions. It takes into account correlations only among the subsystems. Any information encoded entirely inside any of them has no effect on the entanglement entropy. Even more on that, in case the boundary is removed it vanishes completely.

Within the context, it seems natural to suggest an event horizon as a depository of this information. The key essence of this approach is depicted in Fig. 6.4. Here the arrow of time t is directed upwards, so that any horizontal slice represents some certain moment of time, and the red-shaded boundary represents an enclosed system. The red domain obeys unitary evolution due to the absence of outer environment and, therefore, its information is a conserved quantity. This means that any data from the inside should be available at any moment of time, otherwise one would be able to detect its fluctuations and this violate the unitary dynamics of the boundary.

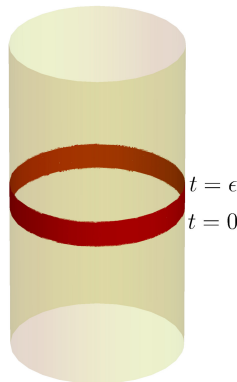Figure 6.4: The red-shaded boundary as an information depository. Figure taken from [Raj22].

As soon as the boundary area A is finite, it should encode some certain amount of information only, with the upper bound suggested to be $A/4$ [Bou99]. This allows to interpret entanglement and the corresponding entropy within the AdS/CFT correspondence and to study extensions of black hole entropy [RT06a; RT06b].

Mapping this to black hole unambiguously binds together its inner dynamics and surface area. In other words, any information about its interior is encoded by the event horizon acting as some kind of a screen.

The approach implies an elegant solution to the black hole's information and entropy problems. Unfortunately, this does not mean one is able to extract any data about the interior domain: being the smallest screen possible, horizon packs any information at the most efficient way and makes it look highly encrypted. Black hole evaporation might suggest the way to decipher the data, providing more room at the screen so that one could find some repeatable patterns. Unfortunately, any such particle emission is processed at the cost of the black hole's energy and the corresponding shrinkage of its horizon.

So, despite the whole concept suggests various fruitful and intriguing insights [Sus95], there is still much to be understood [NRT09; Raj22].

6.4.5   Information outflow

Existence of an unobservable domain is equivalent to a restricted data access. Having no possibility to read all information implies averaging over states of the inaccessible partition. The state of the available domain becomes uncertain due to its dependence on the hidden one. Entropy of the corresponding distribution serves as the measure of such uncertainty. In general case, this entropy vanishes if and only if one gains full access to the data. In such case, all information about the system is known, so the probability distribution reduces to the only state available.

This is exactly what one observes for any finite entangled system. Having no access to some subsystem implies partial tracing over it, thus neglecting any correlations between it and the rest. In general case, the observed partition will be in some mixed state with non-zeroth entropy. Gradual gain of access means one is able to read more data so that the amount of unobservable correlations shrinks down. In short, available information increases due to the uncertainty reduction. But this does not mean that additional information can be generated: the capacity of the whole system is bounded. So, moving the boundary between its subsystems just induces information flow from one partition to another [Pag93b].

From this perspective, the black hole entropy is a bit virtual quantity in the sense that it might reduce with time. Indeed, as the black hole's mass becomes smaller, its radius diminishes. Due to the area law, its entropy shrinks which equals to gaining more access as the black hole evaporates away. From this one concludes that gravity must not cause the loss of information, and there should be some mechanism allowing it to escape.

Information I_{out}, which is carried out by radiation during the evaporation process, reads [Pag93a]

$$I_{\text{out}} = \ln N_{\text{out}} - H_{\text{ent}}, \tag{6.7}$$

where N_{out} stands for the amount of microstates of the emitted particles, and H_{ent} is entanglement entropy between the black hole and outgoing quanta. H_{ent} is defined by its density matrix ρ_{out} and can be quantified with (6.4).

Fig. 6.5 depicts both I_{out} and H_{ent} as functions of thermodynamic entropy $\ln N_{\text{out}}$. It can be clearly seen that information encoded by the outgoing states increases, while entanglement between the black hole and its radiation goes down. Thermodynamic entropy can never decrease and depicts the arrow of time.
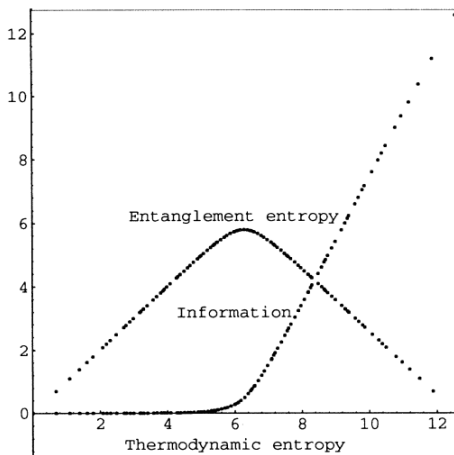
Figure 6.5: Entanglement entropy H_{ent} and information I_{out} as functions of thermodynamic entropy $\ln N_{\text{out}}$. Figure taken from [Pag93a].

Therefore, the Bekenstein-Hawking radiation, despite its thermal-like behavior, favors non-zeroth data flow from the black hole. The analysis above estimates information but does not prescribe the recipe for its escape. Obviously, this should be encoded in some correlations of the outgoing radiation, but what are these DOF?

The answer may be the energy of the radiation itself [Zha+09]. In brief, the idea exploits information theory methods as follows.

Let us consider consequent emission of particles with probabilities $d(E_i)$ at energies E_i, where the i-th quantum is being emitted after the i'-th one if $i > i'$. For the first particle from the sequence one has

$$d(E_1) = e^{-8\pi E_1(M - E_1/2)}, \tag{6.8}$$

with M being the black hole's mass. Energy conservation dictates that any other probability should be correlated with the previous one

$$d(E_{i+1}, E_i) = d(E_i)\, d(E_{i+1}|E_i), \quad i = \overline{1, n-1}. \tag{6.9}$$

Here $d\left(E_{i+1}|E_i\right)$ is the conditional probability (1.9). Suggesting the logarithm of these probabilities with negative sign as the corresponding entropy allows to reproduce the area law (6.1) exactly. The method relies on the tunneling mechanism that specifies conditional distributions in (6.9). Unfortunately, one cannot be sure these are correct until the exact evolution of the black hole since the very beginning is known.

Besides, the analysis above exploits energy conservation only within the context of correlations among the quanta. Similar treatment may be built upon conditional distributions over other DOF. So, conservation laws seem to be of great importance for unitary evolution of gravity, and entanglement may play here a crucial role [Sol11].

Summing up, attempts to connect quantum mechanics and relativity have inspired various studies of the black hole physics, fabric of spacetime and unitarity of gravity [Har16; Pol16; Sto18; UW17; Wal18]. Despite endeavors, both the entropy and the information loss problems are still unsolved. The key issue here is the poor understanding of black hole physics at the microscopic level [Car09; Pag05]. To date, there is no agreement about which of the approaches is correct if any. The only point everyone agrees on is that we need quantum gravity to be able to find the solutions. Such a theory requires merging of quantum mechanics and physics of curved spacetimes, which is a highly non-trivial task, as can be seen from Fig. 6.6.

Figure 6.6: Logical structure of thermodynamics in the spacetimes with horizons. Figure taken from [Pad05].

Chapter 7

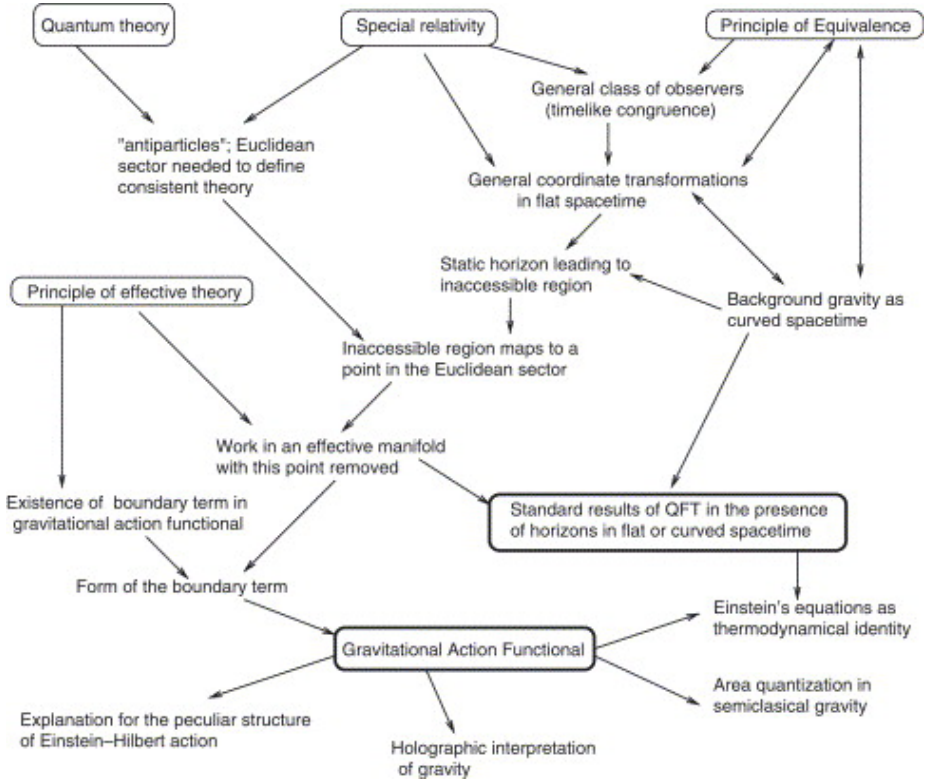# Unruh effect

7.1 Unruh radiation and its temperature

Considering a system embedded into a spacetime implies merging together both quantum physics and relativity. Usually this is done within the relativistic quantum mechanics and thus does not seem to be a problem at all. Unfortunately, a rigorous quantum-mechanical treatment is not an easy problem: the number of particles turns out to be non-invariant. In 1976 Unruh demonstrated that the definition of vacuum state depends on the observer's reference frame [Unr76]. In brief, it may be described as follows.

Let us consider an inertial reference frame in empty space. The observer who is at rest in this frame does not detect any particles and concludes a field to be in its vacuum state $|0\rangle$ at any point in space. She or he is located at the center of Fig. 7.1; the corresponding light cones are depicted by straight diagonal lines. The conclusion about the vacuum state $|0\rangle$ will be shared among all inertial observers moving at constant speeds with respect to each other.

Now, let us introduce an accelerated observer moving at some constant acceleration a, who is depicted by the red curve in Fig. 7.1. It can be clearly seen that the accelerated observer has no access to events from the future light cone of the first one. Similarly, she or he cannot (at any past moment of time) send a signal into the corresponding past light cone: any message may reach the inertial one in the future light cone only, with no chance to read the reply. Therefore, the accelerated observer will have restricted access to any event inside the cones. Due to the finitude of the speed of light, the corresponding spacetime domain will be hidden behind some kind of an event horizon, which is marked with blue dashed lines.

But having no access means inability to take into account any correlations crossing the horizon. So, the accelerated observer will detect some other state differing a lot from the vacuum $|0\rangle$. Indeed, he or she will detect thermal radiation at (Davies-Unruh) temperature T, which in Planck units reads [Dav75; Ful73; Unr76]

$$T = \frac{a}{2\pi}, \tag{7.1}$$

while any inertial observer will see no particles at all. Today this is known as the Fulling-Davies-Unruh effect, or shortly the Unruh effect.

So, the number of particles and temperature appear to be functions of acceleration. Consequently, thermodynamic properties of any system become non-invariant: they depend on a reference frame.

At first, the Unruh effect was derived for spinless particles. From this one may conclude that it refers to bosons only, since fermions have different statistics. However, the effect may be obtained from exact solutions of the Klein-Gordon
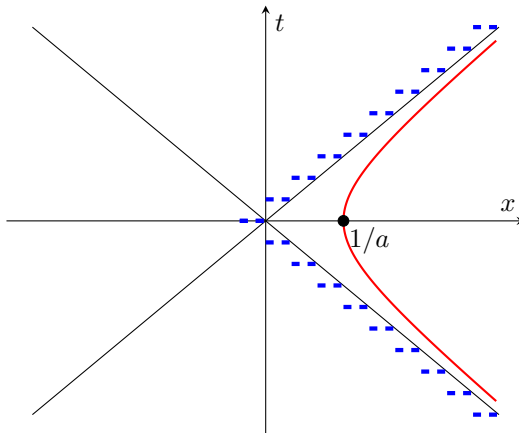
Figure 7.1: Unruh horizon

and Dirac equations as the consequence of quantum tunneling through the horizon. It was shown that the treatment is valid for both bosons and fermions [BM09; Roy09].

Moreover, even the tunneling is not required: path integral formalism provides similar results [UW84] for various statistics and interacting fields.

From this one concludes that Unruh radiation is not a specific issue which is valid in some certain cases only. It is a general phenomenon emerging from the fusion of relativity and quantum mechanics.

One may argue that the effect relies upon an everlasting constant acceleration, with no dependence on time. But this is a somewhat artificial situation: the eternal acceleration requires an infinite energy supply. More realistic scenarios should consider observers being accelerated during finite time. In such case, when the acceleration is limited in time, the situation looks a bit different because of switching dynamics coming into the play. Proper calculations of the probability to detect the Unruh radiation predict logarithmic ultraviolet divergences [HMP93]; the extension to a wider class of switching functions can be found in [LS08; SP96]. The studies clearly show that the Unruh effect cannot be eradicated for realistic finite non-zeroth accelerations.

Time duration is not the only option available. In its simplest form the Unruh effect utilizes a $D = 1 + 1$ spacetime. This is valid till other spatial dimensions contribute via a tensor product and, therefore, may be excluded with no consequences for the final result. However, the statistics inversion of the power spectrum is reported for odd dimensions [Tak86], so the situation is not as simple as it seems.

Imposing additional spatial dimensions extends the phenomena to arbitrary trajectories. The corresponding analytical and numerical calculations of the Unruh particle's detection probability can be found in [OM07]. If a rotation is taken into account, the vacuum non-invariance resembles a typical behavior of

rotating black holes [KL04].

At the first glance, the concept of non-invariant vacuum seems to be tricky a bit. One expects that thermodynamic properties of any system should not depend on the reference frame in such a dramatic manner. This favors to consider the Davies-Unruh temperature as a virtual quantity. However, any particle emission can be measured by a detector. This, in turn, may be interpreted as some two-level quantum system, and Unruh particles should cause its transition from one state (ground) to another (excited). This is a real process taking some finite amount of time. Therefore, the detector's excitation probability should depend on its acceleration [SS92] and influence the measurement results, as has been already discussed above.

But, as follows from (7.1), it may be hard to notice any changes: the impact is small until one reaches the Planck scale. A large acceleration is required in order to make the effect detectable, otherwise any changes to the thermal bath's temperature will be too tiny. Estimates reveal that the signal-to-noise ratio does not exceed unity even for electrons accelerated by $\mathcal{O}\left(10^{15}\right)$W power laser [CT99]. So, how can one measure so tiny effect? As shown in [BL83], polarization measurements for the accelerated fermions may be of great help here. This suggests an implementation of the Unruh effect for thermometry, with spin DOF serving as temperature probes.

Even more on that, the effect was suggested to be responsible for thermalization in high energy collisions [KT05]. In such case, the vacuum non-invariance may be tested with the help of existing particle accelerator facilities. Fig. 7.2 depicts some color string fragmentation process. The world lines of initial quarks are shown by red curves. String formation causes their deceleration, so the quarks are associated with non-inertial reference frames. Emitted hadrons are being formed at the blue hypersurface and are interpreted as the Unruh radiation.
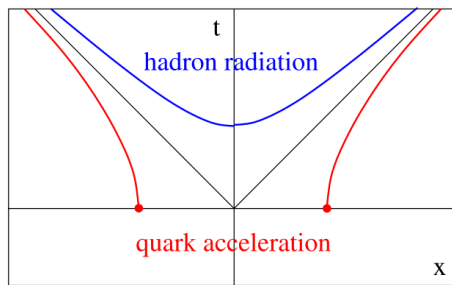
Figure 7.2: Hadronization as the Unruh radiation. Figure taken from [CKS07].

Estimating the momentum rate loss via the string tension σ, one arrives at $a = \sqrt{2\pi\sigma}$ [Sat07]. Together with (7.1) this recovers the Hagedorn temperature of QCD matter. Strong interaction among the quarks induces large acceleration rates thus making the whole concept very perspective for solving the early equilibration problem, which is discussed in Section 3.1. Unfortunately, the

suggested analysis turns out to be phenomenological mostly, so a rigorous description is still underway. Besides, an unambiguous test for the Unruh radiation requires dealing with the mixed states in the relevant basis, which seems to be out of scope for existing elementary particle detector facilities.

Due to the Unruh effect, a system seen by accelerated and inertial observers exhibits different properties. Once one is dealing with acceleration, the phenomenon will cause an impact on thermodynamic properties of the system. But, how to interpret the effect exhibiting dependence on a reference frame?

The answer was suggested in [Bec18]. Basing on the Zubarev's nonequilibrium density operator [ZPS79], it was shown that relativistic fluid cannot have temperature lower than $a/2\pi$, with a being the local acceleration. So, (7.1) specifies the lower bound for any temperature measurements, as can be seen from Fig. 7.3.
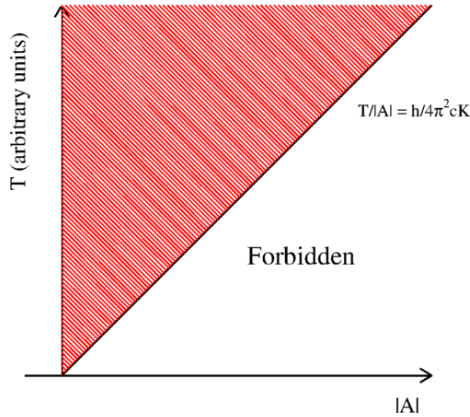
Figure 7.3: Fluid temperature as a function of acceleration A. Allowed values are shaded with red. Figure taken from [Bec18].

Determining entropy via the logarithm of partition function, one arrives at its extensiveness for the non-degenerate lower-bounded spectrum of non-equilibrium operator [BR19]. The study reveals that under such circumstances, an accelerated medium thermalizes due to the Unruh effect. This allows to extract entanglement entropy at the horizon and other thermodynamic properties in non-inertial frames. It should be noted that the approach is built upon the Jayne's principle [Jay63], so it should be used with care for unbounded systems, as discussed in Section 1.4.

Interconnecting quantum physics and relativity, the Unruh effect has induced a broad study of quantum gravity and related topics [CHM08].

Substituting the surface gravity κ to (7.1), one easily obtains the temperature of a Schwarzschild black hole. At the same time, at the absence of acceleration an inertial observer will detect no particles in vacuum, as it should be for a free-falling observer crossing the event horizon. Therefore, one may conclude that the Unruh effect is responsible for the black hole thermodynamics. But, in

such case one should be able to reproduce the area law from the Unruh radiation. Moreover, the information loss problem is expected to be solved as well.

In order to do this one should properly estimate the relevant DOF. Non-invariant number of particles means that the phase space is seen in a different manner by inertial and accelerated observers. Consequently, one concludes that entropy is a subtle quantity, which is observer-dependent [MMR04]. But even knowing the number of particles and their energy does not mean one is able to calculate the entropy. Any change of a reference frame causes re-distribution of entanglement among the modes due to the change of the preferred basis in Hilbert space [AFSE07], thus contributing to the total entropy. The situation is complicated by the dependence on spin statistics effecting multiplicity [Als+06; FSM05] and requires a delicate study.

To sum up, the quantum physics of curved spacetimes is within the scope of thermodynamics. And the Unruh effect may serve as a useful tool to look into the origin of black hole entropy and the information loss problem. However, the framework requires correct estimate for all the DOF involved, and information theory methods can help a lot here.

7.2   Density matrix of Unruh radiation

As one can see from Fig. 7.1, the observers from inertial and accelerated reference frames have access to different spacetime domains. From quantum physics it follows then that Hermitian operators for each of them may differ and are not required to commute. In other terms, any observer defines her or his own complete sets of basis vectors to describe common Hilbert space.

In particular, the accelerated observer feels comfortable with the basis of states which are separated to the accessible (above the horizon) and inaccessible (below the horizon) domains. The inertial one will detect no event horizon, therefore having no need in such distinction among the states. For example, bosonic creation and annihilation operators from different reference frames are connected via the Bogoliubov transformation [Unr76]

$$
\begin{aligned}
\hat{a}^{\dagger} &= \frac{1}{\sqrt{1 - e^{-E/T}}} \hat{b}^{\dagger}_{\text{out}} - \frac{e^{-E/2T}}{\sqrt{1 - e^{-E/T}}} \hat{b}_{\text{in}} \\
\hat{a} &= \frac{1}{\sqrt{1 - e^{-E/T}}} \hat{b}_{\text{out}} - \frac{e^{-E/2T}}{\sqrt{1 - e^{-E/T}}} \hat{b}^{\dagger}_{\text{in}},
\end{aligned}
\tag{7.2}
$$

where $\hat{a}^{\dagger}$ and $\hat{a}$ are responsible for mode excitation and annihilation in the inertial frame; $\hat{b}^{\dagger}_{\text{in(out)}}$ and $\hat{b}_{\text{in(out)}}$ are the creation and annihilation operators for the accelerated observer, E is the energy of the quanta generated at the horizon at Unruh temperature T. Here the subscripts in(out) denote quanta generated inside and outside with respect to the horizon (Rindler modes).

Then the Minkowski vacuum state $|0\rangle$ reads [CHM08]

$$
|0\rangle = \sqrt{\frac{1 - e^{-E/T}}{1 - e^{-NE/T}}} \sum_{n=0}^{N-1} e^{-nE/(2T)} |n\rangle_{\text{in}} |n\rangle_{\text{out}},
\tag{7.3}
$$

for which $\hat{a} \,|0\rangle = 0$. Here $N - 1$ is the maximum number of particles at energy E. Expression (7.3) is valid for both bosons and fermions [BM09; Roy09]. The last case is obtained by formal setting $N = 2$.

In case of bosons the common assumption is $N \to \infty$. This ensures the completeness of the chosen basis. But such choice describes a bit idealized situation, which cannot happen in reality. The non-inertial observer is able to detect only finite number of particles, thus implying the finitude of N in any realistic physical situation. As follows from conservation laws, the energy of Unruh radiation cannot exceed the energy supply necessary to provide the observer's acceleration.

It should be mentioned that (7.3) implies no influence of the states $|n\rangle_{\text{in}}$, $|n\rangle_{\text{out}}$ on the background metric (the so-called quasiclassical approach). In other words, Rindler modes do not affect the temperature T.

Obviously, the state (7.3) is pure in both reference frames. In the chosen basis it is exactly the Schmidt decomposition, for which the Rindler number equals to $N - 1$. For any $N > 1$ the inside and outside modes are entangled. But the accelerated observer cannot measure the inside modes. Having access to the outside domain only, she or he should take the partial trace of $\rho = |0\rangle \langle 0|$ over the DOF below the horizon. Doing so, the observer loses all information about correlations among the modes from different domains. The resulting state is represented by density matrix ρ_{out}

$$\rho_{\text{out}} = \text{Tr}_{\text{in}} \,|0\rangle \langle 0| = \frac{1 - e^{-E/T}}{1 - e^{-NE/T}} \sum_{n=0}^{N-1} e^{-nE/T} \,|n\rangle_{\text{out}} \langle n|_{\text{out}} \qquad (7.4)$$

and describes particles emitted at the horizon. The source of radiation is the horizon itself. Therefore, the Minkowski vacuum state $|0\rangle$, which is pure in the inertial reference frame, is seen as the mixed one in the accelerated frame.

The density matrix ρ_{out} is diagonal in the chosen basis. Its eigenvalues determine the probability to emit n particles at some fixed N, energy E and temperature T. In other terms, ρ_{out} describes the conditional multiplicity distribution $\{n|N, E, T\}$.

7.3 Entropy of Unruh radiation

For any density matrix ρ one can estimate its von Neumann entropy with the help of (6.4).

For any pure state ρ has only one non-zeroth eigenvalue. In this case one knows everything about a system, and $H(\rho) = 0$ as it should be.

In case of a mixed state density matrix contains more than one non-zeroth eigenvalue. This means that one has no access to complete information about the state. Therefore, it should be described by some distribution consisting of the non-zeroth eigenvalues of ρ in its own basis. Consequently, the von Neumann entropy for the mixed state is non-zeroth and estimates the amount of unavailable information.

Substituting (7.4) and

$$\sum_{n=0}^{N-1} n e^{-nE/T} = -\frac{1}{E/T} \frac{\partial}{\partial \alpha} \sum_{n=0}^{N-1} e^{-\alpha E/T} \bigg|_{\alpha=1}$$

$$= \frac{\left(1 - e^{-NE/T}\right) e^{-E/T} - N \left(1 - e^{-E/T}\right) e^{-NE/T}}{\left(1 - e^{-E/T}\right)^2}$$

to (6.4) one obtains that for Unruh radiation its von Neumann entropy reads

$$H\left(\rho_{\text{out}}\right) = H\left(n|N, E, T\right) = \frac{E/T}{e^{E/T} - 1} - \frac{NE/T}{e^{NE/T} - 1} - \ln \frac{1 - e^{-E/T}}{1 - e^{-NE/T}}. \quad (7.5)$$

As it should be, $H\left(\rho_{\text{out}}\right)$ depends on three parameters: the maximum number of particles $N - 1$, their energy E and the temperature T of the source.

Quantities N, E and T serve as external parameters of the multiplicity distribution. The first of them can be estimated via statistical measurements. The horizon's temperature T is completely determined with the observer's acceleration due to (7.1). As for E, here the situation is not so simple. The Unruh effect cannot produce more energy than provided by the source generating the acceleration itself. So, there should be some correlation between parameters N and E. Any exact value of E is defined by some distribution $\{E\}$ governed by conservation laws.

As one can see, entropy $H\left(\rho_{\text{out}}\right)$ is an even function with respect to the energy E and temperature T:

$$H\left(n|N, E, T\right) = H\left(n|N, \pm E, T\right) = H\left(n|N, E, \pm T\right). \quad (7.6)$$

Asymptotics of $H\left(n|N, E, T\right)$:

$$\lim_{E/T \to 0} H\left(n|N, E, T\right) = \ln N = \max\left[H\left(\rho_{\text{out}}\right)\right],$$
$$\lim_{E/T \to \infty} H\left(n|N, E, T\right) = 0. \quad (7.7)$$

To sum up, the von Neumann entropy of Unruh radiation will go to its maximum value $\ln N$ for large temperatures T of the Unruh source or for small energies E of the emitted particles. This means that in the case of $E/T \to 0$ the Unruh radiation is described with the uniform distribution over the Fock states. Decomposing the eigenvalues of ρ_{out} from (7.4) into Taylor series with respect to $E/T \to 0$, one may easily notice that the emission probability at small energies (as compared to the temperature T of the source) approaches constant value. Such a behavior originates from the system's indifference to the amount of emitted particles until conservation laws are fulfilled.

In the case of large energies E or small temperatures T Unruh entropy tends to zero. It can be explained as follows. As one can see from (7.4), for any number of emitted particles the corresponding eigenvalues decline exponentially due to the factor $e^{-E/T}$. The state $|0\rangle_{\text{out}} \langle 0|_{\text{out}}$ is the only exception from this

general rule. So, for $E/T \to \infty$ all the eigenvalues tend to zero, but except the one for which $n = 0$, i.e. describing the absence of radiation at all. Such a case determines the pure state, for which the von Neumann entropy is zero. The situation is a consequence of energy conservation law: the probability to emit a particle at energy E by the source at the temperature $T \ll E$ diminishes to zero.

Also one should keep in mind that for any finite T total entropy of radiation is governed by a joint distribution $\{n, E|T\}$. Due to (1.12), it reads

$$H(n, E|T) = H(E|T) + \langle H(n|E, T) \rangle_E \qquad (7.8)$$

and may be large even if some of $H(n|E, T)$ are small.

Chapter 8

Unruh entropy of a black hole: main results

The results regarding the Unruh entropy calculations are published in [Paper VI; Paper VII; Paper VIII].

The case of a Schwarzschild black hole, which is embedded into $D = 3 + 1$ spacetime, was considered in [Paper VI; Paper VII].

Unruh entropy (7.5) does not take into account the amount of spatial dimensions: the corresponding Schmidt decomposition (7.3) is valid even for a $D = 1 + 1$ spacetime. Other two spatial dimensions contribute via the tensor product and can be traced out with no impact on the eigenvalues of density matrix $\hat{\rho}_{\text{out}}$. To estimate how the effect contributes to the entropy of an object having two additional dimensions, angular DOF were taken into account.

The analysis suggested homogeneous distribution $\{l, \mu\}$ over angular momentum l and its projection μ. For a spherically symmetric black hole its emission spectrum should not contain any correlations induced by angular momentum conservation. So, the total radiation entropy H becomes additive with respect to quantum numbers l and μ:

$$H = \sum_{l,\mu} H\left(\rho_{\text{out}}\right) = \left(l_{\max} + 1\right)^2 H\left(\rho_{\text{out}}\right), \tag{8.1}$$

where $l_{\max}$ is the maximum value of l.

Neglect of backreaction on the background metric within the quasiclassical approach implies the radiation entropy to be additive with respect to the energy of outgoing quanta. In such case, the probability of particle emission is constant and obeys the energy conservation only. This imposes the upper bound of the emission spectrum equal to the black hole's mass M_{BH}.

Within the aforementioned assumptions, total Unruh entropy was estimated for the spinless quanta of mass m covering the range of all known elementary particles. The analysis for Schwarzschild black holes of mass $M_{\text{BH}} > 1$ in Planck units can be found in [Paper VI].

For $mM_{\text{BH}} \ll 1$ it was found that the Unruh entropy exhibits the following dependence

$$\frac{H}{H_{\text{BH}}} \approx 1.452 \times 10^{-3} \left(1 - 4.348 m^2 M_{\text{BH}}^2\right), \tag{8.2}$$

thus reproducing the area law (6.1) in the case $m = 0$ only.

The asymptotic analysis for the case $mM_{\text{BH}} \gg 1$ predicts that

$$-\frac{2\pi - 1}{3\pi^4} m^2 M_{\text{BH}}^2 e^{-8\pi m M_{\text{BH}}} \lesssim \frac{H}{H_{\text{BH}}} \lesssim \frac{m^2 M_{\text{BH}}^2}{3\pi^4} e^{-8\pi m M_{\text{BH}}}. \tag{8.3}$$

So, the Unruh contribution to the entropy of a heavy black hole is exponentially suppressed.

Both estimates include the negative terms for massive particles. This reduces the total Unruh entropy, thus favoring the information outflow from the horizon, in full accord with the discussion in Section 6.4.5. On the other hand, the observed tendency may originate from the applied restrictions.

The study of small black holes, for which $M_{\mathrm{BH}} \leq 1$, was reported in [Paper VII]. In addition to the previous assumptions, the multiplicity of emitted particles was assumed to be upper bounded with $N - 1$. It was shown that in this case the Unruh entropy approximately reads

$$
\frac{H}{H_{\mathrm{BH}}} \propto - \left(\sum_{n=1}^{N} \frac{e^{-8\pi M_{\mathrm{BH}} E n}}{n} - e^{-8\pi M_{\mathrm{BH}} E N} \right) \Bigg|_{E=m}^{E=M_{\mathrm{BH}}} , \tag{8.4}
$$

where the following notation is used:

$$
f(x) \Big|_{x=a}^{x=b} = f(a) - f(b) . \tag{8.5}
$$

Together with the subleading terms the ratio H/H_{BH} transforms to the sum of polylogarithms of different orders and cannot reproduce the area law dependence.

Similarly to the black holes with $M_{\mathrm{BH}} > 1$, here massive particles reduce the total entropy.

In both cases, $M_{\mathrm{BH}} > 1$ and $M_{\mathrm{BH}} < 1$, the contribution of the Unruh radiation to H_{BH} does not exceed 0.15%.

A more subtle analysis should include energy correlations and, therefore, must be governed by (7.8). This requires the knowledge of probability emission at some fixed value of energy E. Such information seems to be hardly available: there is no access to DOF under the horizon. So, one should make some assumptions about the energy distribution $\{E\}$ instead. The corresponding ansatz with the emission probability $p(E) \propto e^{-E/T}$, where T is the temperature of the source, was considered in [Paper VIII] for the case of $D = 1 + 1$ dimensions.

Fig. 8.1 depicts the total entropy $H(n, E | N = 2, T)$ of Unruh radiation as a function of m/T and M/T. Here m is the mass of particles, M it their maximum energy, and T is the temperature of the Unruh horizon. Parameter $N = 2$ describes the fermion case, when maximum one particle can be emitted at energy E.

As one can notice, $H(n, E | N = 2, T)$ is large if m/T is small. The entropy vanishes for $m \to M$, in full accord with the energy conservation.

From Fig. 8.2 one concludes that the same tendency is observed for larger N. The increasing particle multiplicity leads to the expected rise of total entropy and makes the maximum for small m/T more pronounced.

Asymptotic estimates reveal different behavior of the total Unruh entropy for cold and hot horizons. As shown in Fig. 8.3, for $T \to 0$ the quantity exhibits indifference to spin statistics: the entropy is independent of N. It has a maximum at $m/T \approx 1/2$ and exponentially decreases to unity for large m/T.
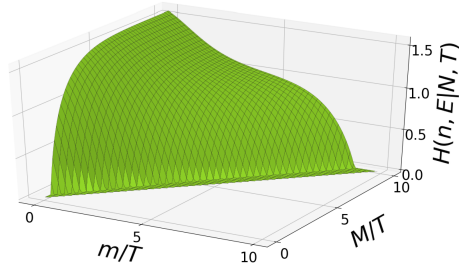
Figure 8.1: Total entropy of Unruh radiation for $N = 2$ as a function of m/T and M/T in the 2-dimensional case. Figure taken from [Paper VIII].
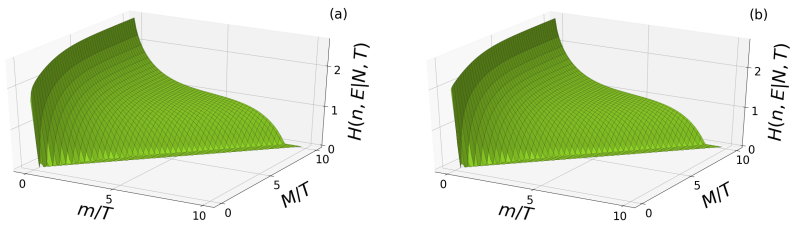
Figure 8.2: Total entropy of Unruh radiation for bosons as a function of m/T and M/T in the 2-dimensional case. Left panel: $N = 100$; right panel: $N = 1000$. Figure taken from [Paper VIII].
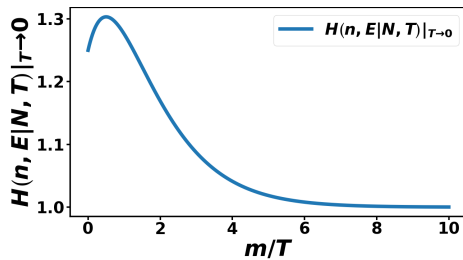
Figure 8.3: $H(n, E|N, T)$ as a function of m/T at low temperatures of the horizon. Figure taken from [Paper VIII].

For hot horizons, when $T \to \infty$, the dependence on particle multiplicity is retained. As one can see from Fig. 8.4, $H\left(n, E|N, T\right)$ weakly depends on the mass of emitted quanta, but rapidly rises up with the increase of their maximum energy. The slope demonstrates a steeper trend at large N due to the growth of available phase space.

Figure 8.4: Total entropy of Unruh radiation for $T \to \infty$ as a function of m and M in the 2-dimensional case. Left panel: fermion case, $N = 2$; right panel: boson case, $N = 100$. Figure taken from [Paper VIII].
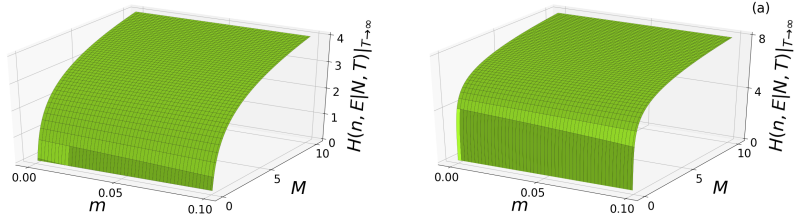
Chapter 9

Conclusion and outlook

The present study is focused on ultrarelativistic heavy ion collisions and astrophysics. So, the conclusion consists of two separate sections for each of them and is accompanied with the outlook of forthcoming research.

9.1 Specific viscosity

Specific viscosity of QCD matter is calculated within microscopic transport calculations. The method consists of three major blocks:

1. UrQMD model calculations for nuclear collisions were performed at collision energies from the range $E_{\text{lab}} = \{10, 20, 30, 40\}$ AGeV. To eliminate any effects from the boundary, the central cell of a fireball is selected for data extraction at different stages of its evolution. The obtained values of energy density, net baryon and net strangeness densities serve as input for the next two blocks.

2. Calculations within the statistical model of an ideal hadron gas. This allows to determine thermodynamic properties of QCD matter at equilibrium, namely its temperature, entropy density s_{SM} and chemical potentials.

3. UrQMD model box calculations at the same densities as in the open regime. The approach is designed to extract relaxation rates for the infinite nuclear matter, which is reproduced via periodic boundary conditions.

It is shown that momentum fluctuations increase relaxation rates approximately by 20%. However, the noise contribution falls below 10% for late stages of the fireball evolution.

The ratio of shear viscosity to entropy density η/s_{SM} for hadron matter is calculated in the vicinity of the expected critical point. Specific viscosity exhibits a smooth minimum at times when the colliding nuclei experience an overlap or right after that [Paper I]. The minimum is slightly deeper at lower collision energies. The smallest value of specific viscosity is reached at the bombarding energy $E_{\text{lab}} = 10$ AGeV, when the matter is baryon-rich and the contribution of quark-gluon DOF is expected to be small. The ratio η/s_{SM} exceeds the KSS bound approximately by a factor of 3.5.

Taking into account microscopic momentum distributions slightly increases the ratio [Paper II; Paper IV]. The maximum of microscopic entropy density s is achievable in thermal equilibrium only. In any other state the calculated values of s are lower and tend to rise with the cell time, in full accord with expectations. This indicates the presence of correlations in the fireball at early

times: the microscopic transport approach cannot provide an instant emergence of equilibrated matter without causality violation.

The extreme of the ratio η/s itself is sharper (closer to the V-shaped pattern) as compared to η/s_{SM} (U-shaped). Therefore, highly dynamical evolution in the cell makes the minimum more pronounced. Taking correlations into account via the microscopic entropy density s allows to pinpoint the critical point with higher precision.

Similar calculations were performed separately for different particle species from the fireball. The results are presented in [Paper III; Paper V]. Partial viscosities demonstrate the similar behavior to the total one. However, the values are small for baryon or meson matter; their contribution to η slightly exceeds 50%. For Λ and Σ baryons the situation becomes even more dramatic: they exhibit almost ideal fluid behavior.

Low partial viscosity does not mean that the corresponding constituents give no contribution to momentum transfer in the medium. Conversely, the observed behavior is explained by multiple interactions among the particles of different species. As a result, momentum correlations cannot be traced back within some certain particle type. Representing the QCD matter as a mixture of separate fluids may violate the KSS bound as soon as this does not take into account relevant conditional distributions.

9.2 Unruh entropy

The contribution of the Unruh effect to the Bekenstein-Hawking radiation entropy H_{BH} of the Schwarzchild black hole is calculated. General assumptions for the study included additive entropy behavior with respect to angular momentum DOF.

Entropy dependence on various combinations of the relevant parameters has been investigated. This includes:

1. The maximum number of emitted particles $N - 1$.

2. The black hole's mass M_{BH} within a wide range, from the stellar to the sub-Plank scale.

3. The mass of emitted particles m covering the mass spectrum of the known particle species.

Asymptotic behavior of the calculated Unruh entropy with respect to M_{BH} and m was analyzed in details. Any other DOF of the particles, such as spin or charges of outgoing quanta, have not been taken into account.

Within the aforementioned assumptions, the obtained results pronounce the presence of negative terms in the expression for entropy. Despite being small, they reduce total entropy of emitted quanta. So, the outgoing radiation might encode information about the internals of the black hole, as one would expect for an entangled system within the Page formalism.

Negative entropy terms vanish for massless particles. This might witness that the law of energy conservation causes correlations among different spacetime domains. On the other hand, the terms may origin from the absence of radiation back-reaction on the background metric. Therefore, the situation is not clear and a more sophisticated analysis is required.

The results indicate the inability to reproduce the Bekenstein-Hawking entropy with the Unruh effect only. In the case of $M_{\mathrm{BH}}m < 1$ the Unruh contribution is upper bounded by 0.15% [Paper VI; Paper VII]. Moreover, the radiation entropy is exponentially suppressed by the factor $e^{-8\pi M_{\mathrm{BH}}m}$ for $M_{\mathrm{BH}}m \gg 1$ even for an infinite particle multiplicity [Paper VI].

The smallness of the contribution is caused by the neglect of conditional distributions during entropy estimates. Within the considered approximation, the Unruh entropy is additive with respect to energy. This means that all field modes contribute independently to the total entropy; they are disentangled with the background. In other words, the assumption implies that emitted particles are not correlated. However, this is valid for the massive black holes only; a more strict analysis requires the presence of correlations among the field modes due to energy conservation at least.

Due to (1.12), these correlations lead to the non-additivity of entropy for different modes and require knowledge about the emission probability at given energy. The exponential energy distribution was studied in [Paper VIII] for the $D = 1+1$ spacetime. Even in the such relatively simple case the entropy exhibits a highly non-trivial dependence of its parameters.

The exact energy distribution $\{E\}$ can be extracted only from the black hole's Hamiltonian that encompasses its internal dynamics. Unfortunately, such information is inaccessible according to the general relativity.

The analysis does not take into account the influence of quantum effects on the background metric. Such restriction origins from specific assumptions while obtaining the density matrix (7.4), namely the quasiclassical approach. Neglect of any back-reaction on the black hole excludes the impact on the Unruh temperature as well. However, imposing the metric dependence on the Unruh radiation is a non-trivial problem and requires gravity quantization.

9.3   Outlook

Extracting viscosity within the Green-Kubo formalism implies small deviations from thermal equilibrium. The protocol requires the temperature of a fluid to be known. A common procedure of its extraction in ultrarelativistic heavy-ion experiments utilizes spectra of produced particles. But strictly speaking, temperature is a well-defined quantity only in equilibrium. Contrary to this, collision experiments generate a state which is governed by a dynamical evolution. To solve the problem, one may suggest to use the Zubarev non-equilibrium statistical operator formalism. Unfortunately, its applicability may be questioned for far-from-equilibrium open systems, such as a collision fireball.

Moreover, it is unclear whether the amount of produced particles suffices for an ensemble. If multiplicity is not large enough, one should deal rather with a density matrix. In such case, a temperature extraction becomes ambiguous: matrix eigenvalues may be governed by different distributions for each Hermitian operator from a pairwise commuting set. The problem has much in common with the one from mesoscopic physics, where one has to deal with a set of temperatures within the same system [Gia+06].

So, it seems interesting to construct some function, which is well-defined at any stage of the fireball's evolution and reaches the conventional temperature for a stationary state.

One more important issue is the entropy density of the fireball itself. Section 3.3 describes how it can be extracted from microscopic momentum distributions even if the medium is out of equilibrium. However, the technique implies the homogeneity of spatial particle distribution. The calculated entropy density s is just the upper bound for the real one at early times: neither spatial nor momentum DOF provide spherically symmetric phase space volume for the emerging fireball. Therefore, the analysis of spatial-momentum correlations since the very beginning is a challenging problem for further study. And the information entropy may become of great utility here.

As known, the amount of possible microstates depends on intrinsic DOF contributing to the available phase space of a system. Regarding to the Unruh radiation, additional quantum numbers (charges, spin etc.) might significantly increase its contribution to the black hole entropy. This is one more interesting item for investigation.

Intrinsic quantum numbers impose additional conservation laws of angular momentum and charges. These affect relevant conditional distributions and, consequently, the total entropy of Unruh radiation. A side effect of such correlations is their impact on the background metric, that cannot be eradicated by the aforementioned quasiclassical approach. For example, particles with spin or non-zeroth electrical charge might change the black hole's type and the metric as well. All this significantly complicates the problem. On the other hand, such correlations may be responsible for the information outflow from the black hole [CHS23].

Therefore, intrinsic DOF of Unruh particles and their possible impact on the metric are intriguing issues to study within information entropy techniques.

Bibliography

[Aab+19]   Aaboud, M. et al. "Measurement of the nuclear modification factor for inclusive jets in Pb+Pb collisions at sNN=5.02TeV with the ATLAS detector". In: *Physics Letters B* vol. 790 (2019), pp. 108–128.

[Abd+23]   Abdulameer, N. J. et al. "Low-p_T direct-photon production in $Au + Au$ collisions at $\sqrt{s_{NN}} = 39$ and 62.4 GeV". In: *Phys. Rev. C* vol. 107 (2 2023), p. 024914.

[Abe+13a] Abelev, B. et al. "Anisotropic flow of charged hadrons, pions and (anti-)protons measured at high transverse momentum in Pb?Pb collisions at sNN=2.76 TeV". In: *Physics Letters B* vol. 719, no. 1 (2013), pp. 18–28.

[Abe+13b] Abelev, B. et al. "Centrality dependence of π, K, and p production in Pb-Pb collisions at $\sqrt{s_{NN}} = 2.76$ TeV". In: *Phys. Rev. C* vol. 88 (4 2013), p. 044910.

[Ach+20]   Acharya, S. et al. "Global polarization of Λ and $\overline{\Lambda}$ hyperons in Pb-Pb collisions at $\sqrt{s_{NN}} = 2.76$ and 5.02 TeV". In: *Phys. Rev. C* vol. 101 (4 2020), p. 044611.

[Ack+01]   Ackermann, K. H. et al. "Elliptic Flow in $Au + Au$ Collisions at $\sqrt{s}_{NN} = 130$GeV". In: *Phys. Rev. Lett.* vol. 86 (3 2001), pp. 402–407.

[Ada+09]   Adare, A. et al. "Dilepton mass spectra in p+p collisions at s=200 GeV and the contribution from open charm". In: *Physics Letters B* vol. 670, no. 4 (2009), pp. 313–320.

[Ada+12]   Adare, A. et al. "J/ψ suppression at forward rapidity in Au + Au collisions at $\sqrt{s_{NN}} = 39$ and 62.4 GeV". In: *Phys. Rev. C* vol. 86 (6 2012), p. 064901.

[Ada+14]   Adamczyk, L. et al. "Beam-Energy Dependence of the Directed Flow of Protons, Antiprotons, and Pions in Au+Au Collisions". In: *Phys. Rev. Lett.* vol. 112 (16 2014), p. 162301.

[Ada17]   Adamczyk, L. e. a. S. C. "Global Λ hyperon polarization in nuclear collisions". In: *Nature* vol. 548 (2017), pp. 62–65.

[Adc+05]   Adcox, K. et al. "Formation of dense partonic matter in relativistic nucleus-nucleus collisions at RHIC: Experimental evaluation by the PHENIX Collaboration". In: *Nuclear Physics A* vol. 757, no. 1 (2005). First Three Years of Operation of RHIC, pp. 184–283.

[Add+22]   Addazi, A. et al. "Quantum gravity phenomenology at the dawn of the multi-messenger era?A review". In: *Progress in Particle and Nuclear Physics* vol. 125 (2022), p. 103948.

[Adl+06]   Adler, S. S. et al. "Common Suppression Pattern of η and π^0 Mesons at High Transverse Momentum in Au + Au Collisions at $\sqrt{s_{NN}} = 200$ GeV". In: *Phys. Rev. Lett.* vol. 96 (20 2006), p. 202301.

[AFSE07]   Adesso, G., Fuentes-Schuller, I., and Ericsson, M. "Continuous-variable entanglement sharing in noninertial frames". In: *Phys. Rev. A* vol. 76 (6 2007), p. 062112.

[Als+06]   Alsing, P. M. et al. "Entanglement of Dirac fields in noninertial frames". In: *Phys. Rev. A* vol. 74 (3 2006), p. 032326.

[AMY03]   Arnold, P., Moore, G. D., and Yaffe, L. G. "Transport coefficients in high temperature gauge theories, 2. Beyond leading log". In: *Journal of High Energy Physics* vol. 2003, no. 05 (2003), p. 051.

[Ars+05]   Arsene, I. et al. "Quark-gluon plasma and color glass condensate at RHIC? The perspective from the BRAHMS experiment". In: *Nuclear Physics A* vol. 757, no. 1 (2005). First Three Years of Operation of RHIC, pp. 1–27.

[Ash+98]   Ashtekar, A. et al. "Quantum Geometry and Black Hole Entropy". In: *Phys. Rev. Lett.* vol. 80 (5 1998), pp. 904–907.

[Bai+01]   Baier, R. et al. "?Bottom-up? thermalization in heavy ion collisions". In: *Physics Letters B* vol. 502, no. 1 (2001), pp. 51–58.

[Bas+98]   Bass, S. A. et al. "Microscopic models for ultrarelativistic heavy ion collisions". In: *Progr. Part. Nucl. Phys.* vol. 41 (1998), pp. 255–369.

[Baz+14]   Bazavov, A. et al. "Equation of state in $(2 + 1)$-flavor QCD". In: *Phys. Rev. D* vol. 90 (9 2014), p. 094503.

[BBP21]   Becattini, F., Buzzegoli, M., and Palermo, A. "Spin-thermal shear coupling in a relativistic fluid". In: *Physics Letters B* vol. 820 (2021), p. 136519.

[BCH73]   Bardeen, J. M., Carter, B, and Hawking, S. W. "The Four Laws of Black Hole Mechanics". In: *Commun. Math. Phys.* vol. 31 (1973), pp. 161–170.

[Bea+04]   Bearden, I. G. et al. "Nuclear Stopping in Au + Au Collisions at $\sqrt{s_{NN}} = 200$ GeV". In: *Phys. Rev. Lett.* vol. 93 (10 2004), p. 102301.

[Bec18]   Becattini, F. "Thermodynamic equilibrium with acceleration and the Unruh effect". In: *Phys. Rev. D* vol. 97 (8 2018), p. 085013.

[Bek73]   Bekenstein, J. D. "Black Holes and Entropy". In: *Phys. Rev. D* vol. 7 (8 1973), pp. 2333–2346.

[Bel+98] Belkacem, M et al. "Equation of state, spectra, and composition of hot and dense infinite hadronic matter in a microscopic transport model". In: *Phys. Rev. C* vol. 58 (3 1998), pp. 1727–1733.

[Bia11] Bianchi, E. "Black hole entropy, loop gravity, and polymer physics". In: *Classical and Quantum Gravity* vol. 28, no. 11 (2011), p. 114006.

[BK11] Brustein, R. and Kupferman, J. "Black hole entropy divergence and the uncertainty principle". In: *Phys. Rev. D* vol. 83 (12 2011), p. 124014.

[BL20] Becattini, F. and Lisa, M. A. "Polarization and Vorticity in the Quark?Gluon Plasma". In: *Annual Review of Nuclear and Particle Science* vol. 70, no. 1 (2020), pp. 395–423. eprint: https://doi.org/10.1146/annurev-nucl-021920-095245.

[BL56] Belenkij, S. Z. and Landau, L. D. "Hydrodynamic theory of multiple production of particles". In: *Nuovo Cimento Suppl.* vol. 3 (1956), pp. 15–31.

[BL83] Bell, J. and Leinaas, J. "Electrons as accelerated thermometers". In: *Nuclear Physics B* vol. 212, no. 1 (1983), pp. 131–150.

[Bla+20] Blaschke, D. et al. *Nonequilibrium Phenomena in Strongly Correlated Systems.* MDPI, 2020.

[Ble+06] Bleibel, J. et al. "Energy densities and equilibration in heavy ion collisions at sNN=200GeV with the quark?gluon string model". In: *Nuclear Physics A* vol. 767 (2006), pp. 218–232.

[Ble+99] Bleicher, M et al. "Relativistic hadron-hadron collisions in the ultrarelativistic quantum molecular dynamics model". In: *J. Phys. G* vol. 25 (1999), p. 1859.

[BM09] Banerjee, R. and Majhi, B. R. "Hawking black body spectrum from tunneling mechanism". In: *Physics Letters B* vol. 675, no. 2 (2009), pp. 243–245.

[Bor+14] Borsányi, S. et al. "Full result for the QCD equation of state with 2+1 flavors". In: *Physics Letters B* vol. 730 (2014), pp. 99–104.

[Bor+18] Borsányi, S. et al. "High statistics lattice study of stress tensor correlators in pure $SU(3)$ gauge theory". In: *Phys. Rev. D* vol. 98 (1 2018), p. 014512.

[Bou99] Bousso, R. "Holography in general space-times". In: *Journal of High Energy Physics* vol. 1999, no. 06 (1999), pp. 028–028.

[BPR08] Becattini, F., Piccinini, F., and Rizzo, J. "Angular momentum conservation in heavy ion collisions at very high energy". In: *Phys. Rev. C* vol. 77 (2 2008), p. 024906.

[BR19] Becattini, F. and Rindori, D. "Extensivity, entropy current, area law, and Unruh effect". In: *Phys. Rev. D* vol. 99 (12 2019), p. 125011.

[Bra+00a]   Bratkovskaya, E. L. et al. "Aspects of thermal and chemical equilibration of hadronic matter". In: *Nuclear Physics A* vol. 675, no. 3 (2000), pp. 661 –691.

[Bra+00b]   Bravina, L. V. et al. "Local equilibrium in heavy-ion collisions: Microscopic analysis of a central cell versus infinite matter". In: *Phys. Rev. C* vol. 62 (6 2000), p. 064906.

[Bra+01]   Bravina, L. V. et al. "Equation of state of resonance-rich matter in the central cell in heavy-ion collisions at $\sqrt{s} = 200$ AGeV". In: *Phys. Rev. C* vol. 63 (6 2001), p. 064902.

[Bra+06]   Bravina, L. V. et al. "Equilibration of matter near the QCD critical point". In: *Journal of Physics G: Nuclear and Particle Physics* vol. 32, no. 12 (2006), S213.

[Bra+08]   Bravina, L. V. et al. "Microscopic models and effective equation of state in nuclear collisions in the vicinity of $E_{\text{lab}} = 30$ AGeV at the GSI Facility for Antiproton and Ion Research (FAIR) and beyond". In: *Phys. Rev. C* vol. 78 (1 2008), p. 014907.

[Bra+99a]   Bravina, L. V. et al. "Equilibrium and non-equilibrium effects in relativistic heavy ion collisions." In: *Nuclear Physics A* vol. 661, no. 1 (1999), pp. 600 –603.

[Bra+99b]   Bravina, L. V. et al. "Local equilibrium in heavy ion collisions: Microscopic model versus statistical model analysis". In: *Phys. Rev. C* vol. 60 (2 1999), p. 024904.

[BRS18]   Busza, W., Rajagopal, K., and Schee, W. van der. "Heavy Ion Collisions: The Big Picture and the Big Questions". In: *Annual Review of Nuclear and Particle Science* vol. 68, no. 1 (2018), pp. 339–376. eprint: https://doi.org/10.1146/annurev-nucl-101917-020852.

[Car09]   Carlip, S. "Black Hole Thermodynamics and Statistical Mechanics". In: *Physics of Black Holes: A Guided Tour.* Ed. by Papantonopoulos, E. Berlin, Heidelberg: Springer Berlin Heidelberg, 2009, pp. 89–123.

[CC52]   Chapman, S. and Cowling, T. G. *The Mathematical Theory of Non-uniform Gases. An account of the kinetic theory of viscosity, thermal conduction, and diffusion in gases.* Cambridge: Cambridge University Press, 1952.

[CHM08]   Crispino, L. C. B., Higuchi, A., and Matsas, G. E. A. "The Unruh effect and its applications". In: *Rev. Mod. Phys.* vol. 80 (3 2008), pp. 787–838.

[CHS23]   Calmet, X., Hsu, S. D., and Sebastianutti, M. "Quantum gravitational corrections to particle creation by black holes". In: *Physics Letters B* vol. 841 (2023), p. 137820.

[CK11]   Chakraborty, P and Kapusta, J. I. "Quasiparticle theory of shear and bulk viscosities of hadronic matter". In: *Phys. Rev. C* vol. 83 (1 2011), p. 014906.

[CKM06]   Csernai, L. P., Kapusta, J. I., and McLerran, L. D. "Strongly Interacting Low-Viscosity Matter Created in Relativistic Nuclear Collisions". In: *Phys. Rev. Lett.* vol. 97 (15 2006), p. 152303.

[CKS07]   Castorina, P, Kharzeev, D, and Satz, H. "Thermal hadronization and Hawking-Unruh radiation in QCD". In: *Eur. Phys. J. C* vol. 52 (2007), pp. 187–201.

[CP75]   Collins, J. C. and Perry, M. J. "Superdense Matter: Neutrons or Asymptotically Free Quarks?" In: *Phys. Rev. Lett.* vol. 34 (21 1975), pp. 1353–1356.

[Cre11]   Cremonini, S. "The Shear Viscosity to Entropy Ratio: A Status Report". In: *Mod.Phys.Lett.B* vol. 25 (23 2011), pp. 1867–1888.

[CT99]   Chen, P and Tajima, T. "Testing Unruh Radiation with Ultraintense Lasers". In: *Phys. Rev. Lett.* vol. 83 (2 1999), pp. 256–259.

[CY10]   Chesler, P. M. and Yaffe, L. G. "Boost invariant flow, black hole formation, and far-from-equilibrium dynamics in $\mathcal{N} = 4$ supersymmetric Yang-Mills theory". In: *Phys. Rev. D* vol. 82 (2 2010), p. 026006.

[Dav75]   Davies, P. C. W. "Scalar production in Schwarzschild and Rindler metrics". In: *Journal of Physics A: Mathematical and General* vol. 8, no. 4 (1975), p. 609.

[DB09]   Demir, N and Bass, S. A. "Shear-Viscosity to Entropy-Density Ratio of a Relativistic Hadron Gas". In: *Phys. Rev. Lett.* vol. 102 (17 2009), p. 172302.

[DR15]   Du, X. and Rapp, R. "Sequential regeneration of charmonia in heavy-ion collisions". In: *Nuclear Physics A* vol. 943 (2015), pp. 147–158.

[DS07a]   Das, S. and Shankaranarayanan, S. "Entanglement as a source of black hole entropy". In: *Journal of Physics: Conference Series* vol. 68, no. 1 (2007), p. 012015.

[DS07b]   Das, S. and Shankaranarayanan, S. "Where are the black-hole entropy degrees of freedom?" In: *Classical and Quantum Gravity* vol. 24, no. 20 (2007), p. 5299.

[DSS08]   Das, S., Shankaranarayanan, S., and Sur, S. "Black hole entropy from entanglement: A review". In: (2008).

[ECP10]   Eisert, J., Cramer, M., and Plenio, M. B. "Colloquium: Area laws for the entanglement entropy". In: *Rev. Mod. Phys.* vol. 82 (1 2010), pp. 277–306.

[EH06]   Emparan, R and Horowitz, G. T. "Microstates of a Neutral Black Hole in M Theory". In: *Phys. Rev. Lett.* vol. 97 (2006), p. 141601.

[EM07]   Emparan, R. and Maccarrone, A. "Statistical description of rotating Kaluza-Klein black holes". In: *Phys. Rev. D* vol. 75 (8 2007), p. 084006.

[EM22]   Elfner, H. and Mller, B. *The exploration of hot and dense nuclear matter: Introduction to relativistic heavy-ion physics*. 2022.

[Fer50]   Fermi, E. "High Energy Nuclear Events". In: *Progress of Theoretical Physics* vol. 5, no. 4 (July 1950), pp. 570–583. eprint: https://academic.oup.com/ptp/article-pdf/5/4/570/5430247/5-4-570.pdf.

[FHS18]   Florkowski, W., Heller, M. P., and Spali?ski, M. "New theories of relativistic hydrodynamics in the LHC era". In: *Reports on Progress in Physics* vol. 81, no. 4 (2018), p. 046001.

[FSM05]   Fuentes-Schuller, I. and Mann, R. B. "Alice Falls into a Black Hole: Entanglement in Noninertial Frames". In: *Phys. Rev. Lett.* vol. 95 (12 2005), p. 120404.

[Ful73]   Fulling, S. A. "Nonuniqueness of Canonical Field Quantization in Riemannian Space-Time". In: *Phys. Rev. D* vol. 7 (10 1973), pp. 2850–2862.

[Gav85]   Gavin, S. "Transport coefficients in ultra-relativistic heavy-ion collisions". In: *Nuclear Physics A* vol. 435, no. 3 (1985), pp. 826–843.

[GBM21]   Gonzalez, V., Basu, S., and Marin, A. e. a. "Extraction of the specific shear viscosity of quark-gluon plasma from two-particle transverse momentum correlations". In: *Eur. Phys. J. C* vol. 81 (2021), p. 465.

[GGD18]   Ghiglieri, J, G.D., M., and D., T. "QCD shear viscosity at (almost) NLO". In: *Journal of High Energy Physics* vol. 03 (2018), p. 179.

[GHM08]   Gorenstein, M. I., Hauer, M., and Moroz, O. N. "Viscosity in the excluded volume hadron gas model". In: *Phys. Rev. C* vol. 77 (2 2008), p. 024911.

[Gia+06]   Giazotto, F. et al. "Opportunities for mesoscopics in thermometry and refrigeration: Physics and applications". In: *Rev. Mod. Phys.* vol. 78 (1 2006), pp. 217–274.

[Gom11]   Gomes, J. "Quantum entropy of supersymmetric black holes". In: *arXiv:1111.2025 [hep-th]* (2011). eprint: arXiv:1111.2025 [hep-th].

[GP90]   Gyulassy, M. and Plmer, M. "Jet quenching in dense matter". In: *Physics Letters B* vol. 243, no. 4 (1990), pp. 432–438.

[Gre54]   Green, M. S. "Markoff Random Processes and the Statistical Mechanics of Time-Dependent Phenomena. II. Irreversible Processes in Fluids". In: *The Journal of Chemical Physics* vol. 22 (1954), pp. 398–413.

[Har16]   Harlow, D. "Jerusalem lectures on black holes and quantum information". In: *Rev. Mod. Phys.* vol. 88 (1 2016), p. 015002.

[Har28]   Hartley, R. V. L. "Transmission of information". In: *The Bell System Technical Journal* vol. 7, no. 3 (1928), pp. 535–563.

[Haw05]   Hawking, S. W. "Information Loss in Black Holes". In: *Phys. Rev. D* vol. 72 (2005), p. 084013.

[Haw75]   Hawking, S. W. "Particle Creation by Black Holes". In: *Commun. Math. Phys.* vol. 43 (1975), pp. 199–220.

[Haw76]   Hawking, S. W. "Breakdown of predictability in gravitational collapse". In: *Phys. Rev. D* vol. 14 (10 1976), pp. 2460–2473.

[Hel+12]   Heller, M. P. et al. "Strong Coupling Isotropization of Non-Abelian Plasmas Simplified". In: *Phys. Rev. Lett.* vol. 108 (19 2012), p. 191601.

[HKR96]   Hfner, J., Klevansky, S., and Rehberg, P. "Soft deconfinement ? critical phenomena at the Mott transition in a field theory for quarks and mesons". In: *Nuclear Physics A* vol. 606, no. 1 (1996), pp. 260–282.

[HL14]   Huang, X.-G. and Liao, J. "Kinetic evolution of the glasma and thermalization in heavy ion collisions". In: *Int. J. Mod. Phys. E* vol. 23 (2014), p. 1430003.

[HMP93]   Higuchi, A., Matsas, G. E. A., and Peres, C. B. "Uniformly accelerated finite-time detectors". In: *Phys. Rev. D* vol. 48 (8 1993), pp. 3731–3734.

[Hor07]   Horowitz, G. T. "Black Holes, Entropy, and Information". In: *arXiv:0708.3680 [astro-ph]* (2007).

[HR07]   Horowitz, G. T. and Roberts, M. M. "Counting the Microstates of a Kerr Black Hole". In: *Phys. Rev. Lett.* vol. 99 (2007), p. 221601.

[HS13]   Heinz, U. and Snellings, R. "Collective Flow and Viscosity in Relativistic Heavy-Ion Collisions". In: *Annual Review of Nuclear and Particle Science* vol. 63, no. 1 (2013), pp. 123–151. eprint: https://doi.org/10.1146/annurev-nucl-102212-170540.

[ILV02]   Iorio, A, Lambiase, G, and Vitiello, G. "Quantization of scalar fields in curved background, deformed Hopf algebra and entanglement". In: *arXiv:quant-ph/0207173* (2002).

[ILV04]   Iorio, A., Lambiase, G., and Vitiello, G. "Entangled quantum fields near the event horizon and entropy". In: *Annals of Physics* vol. 309, no. 1 (2004), pp. 151–165.

[IS16]   Ivanov, Y. B. and Soldatov, A. A. "Estimation of the shear viscosity from 3FD simulations of Au + Au collisions at $\sqrt{s_{NN}} = 3.3 - 39$ GeV". In: *EPJA* vol. 52 (2016), p. 117.

[Jac07]   Jacobson, T. "A note on renormalization and black hole entropy in loop quantum gravity". In: *Classical and Quantum Gravity* vol. 24, no. 18 (2007), p. 4875.

[Jay57]   Jaynes, E. T. "Information Theory and Statistical Mechanics". In: *Phys. Rev.* vol. 106 (4 1957), pp. 620–630.

[Jay63]   Jaynes, E. T. "Information Theory and Statistical Mechanics". In: *Lecture in Theoretical Physics. Statistical Physics*. Ed. by Ford, K. W. Vol. 3. New York: W. A. Benjamin, Inc., 1963, pp. 181–218.

[Jay68]   Jaynes, E. T. "Prior Probabilities". In: *IEEE Transactions On Systems Science and Cybernetics* vol. sec-4 (1968), pp. 227–241.

[JP07]   Jacobson, T and Parentani, R. "Black hole entanglement entropy regularized in a freely falling frame". In: *Phys. Rev. D* vol. 76 (2007), p. 024006.

[Kar02]   Karsch, F. "Lattice results on QCD thermodynamics". In: *Nuclear Physics A* vol. 698, no. 1 (2002). 15th Int. Conf. on Ultra-Relativistic Nucleus-Nucleus Collisions (Quark Matter 2001), pp. 199–208.

[Kar+15]   Karpenko, I. A. et al. "Estimation of the shear viscosity at finite net-baryon density from A+A collision data at $\sqrt{s_{NN}} = 7.7 - 200$ GeV". In: *Phys. Rev. C* vol. 91 (6 2015), p. 064901.

[Khr02]   Khriplovich, I. "Entropy and area of black holes in loop quantum gravity". In: *Physics Letters B* vol. 537, no. 1 (2002), pp. 125–129.

[Khr04]   Khriplovich, I. B. *Holographic bound and spectrum of quantized black hole.* 2004.

[Khr08]   Khriplovich, I. "Quantized black holes, their spectrum and radiation". In: *Physics of Atomic Nuclei* vol. 71, no. 4 (2008), pp. 671–680.

[KL04]   Korsbakken, J. I. and Leinaas, J. M. "Fulling-Unruh effect in general stationary accelerated frames". In: *Phys. Rev. D* vol. 70 (8 2004), p. 084016.

[KSS05]   Kovtun, P. K., Son, D. T., and Starinets, A. O. "Viscosity in Strongly Interacting Quantum Field Theories from Black Hole Physics". In: *Phys. Rev. Lett.* vol. 94 (11 2005), p. 111601.

[KT05]   Kharzeev, D. and Tuchin, K. "From color glass condensate to quark?gluon plasma through the event horizon". In: *Nuclear Physics A* vol. 753, no. 3 (2005), pp. 316–334.

[KTH22]   Kanakubo, Y., Tachibana, Y., and Hirano, T. "Nonequilibrium components in the region of very low transverse momentum in high-energy nuclear collisions". In: *Phys. Rev. C* vol. 106 (5 2022), p. 054908.

[Kub57]   Kubo, R. "Statistical-Mechanical Theory of Irreversible Processes. I. General Theory and Simple Applications to Magnetic and Conduction Problems". In: *J Phys Soc Jpn* vol. 12 (1957), pp. 570–586.

[Kur+19]   Kurkela, A. et al. "Effective kinetic description of event-by-event pre-equilibrium dynamics in high-energy heavy-ion collisions". In: *Phys. Rev. C* vol. 99 (3 2019), p. 034910.

[Lac07]   Lacey, R. A. "Is there a Sonic Boom in the Little Bang at RHIC?"
            In: *Nuclear Physics A* vol. 785, no. 1 (2007). Proceedings of the 7th
            International Conference on Strong and Electroweak Matter 2006,
            pp. 122–127.

[Lac+07]   Lacey, R. A. et al. "Has the QCD Critical Point Been Signaled
            by Observations at the BNL Relativistic Heavy Ion Collider?" In:
            Phys. Rev. Lett. vol. 98 (9 2007), p. 092301.

[Li11]   Li, R. "Logarithmic entropy of black hole in gravity with conformal
            anomaly from quantum tunneling approach". In: *Europhysics
            Letters* vol. 96, no. 6 (2011), p. 60014.

[Lin79]   Linde, A. D. "Phase transitions in gauge theories and cosmology".
            In: *Reports on Progress in Physics* vol. 42, no. 3 (1979), p. 389.

[LMT07]   Louis, J., Mohaupt, T., and Theisen, S. "String Theory: An
            Overview". In: *Approaches to Fundamental Physics: An Assessment
            of Current Theoretical Ideas.* Ed. by Stamatescu, I.-O. and Seiler, E.
            Berlin, Heidelberg: Springer Berlin Heidelberg, 2007, pp. 289–323.

[LS08]   Louko, J and Satz, A. "Transition rate of the Unruh–DeWitt
            detector in curved spacetime". In: *Classical and Quantum Gravity*
            vol. 25, no. 5 (2008), p. 055012.

[LT12]   Livine, E. R. and Terno, D. R. "Entropy in the classical and quantum
            polymer black hole models". In: *Classical and Quantum Gravity*
            vol. 29, no. 22 (2012), p. 224012.

[LW05]   Liang, Z.-T. and Wang, X.-N. "Globally Polarized Quark-Gluon
            Plasma in Noncentral $A + A$ Collisions". In: *Phys. Rev. Lett.* vol. 94
            (10 2005), p. 102301.

[Mey11]   Meyer, H. B. "Transport properties of the quark-gluon plasma". In:
            Eur. Phys. J. A vol. 47 (2011), p. 86.

[MMR04]   Marolf, D., Minic, D., and Ross, S. F. "Notes on spacetime
            thermodynamics and the observer dependence of entropy". In: *Phys.
            Rev. D* vol. 69 (6 2004), p. 064006.

[MN06]   Müller, B. and Nagle, J. L. "Results from the Relativistic Heavy
            Ion Collider". In: *Annual Review of Nuclear and Particle Science*
            vol. 56, no. 1 (2006), pp. 93–135. eprint: https://doi.org/10.1146/
            annurev.nucl.56.080805.140556.

[Mot+18]   Motornenko, A et al. "Nucleon matter equation of state, particle
            number fluctuations, and shear viscosity within UrQMD box
            calculations". In: *Journal of Physics G: Nuclear and Particle
            Physics* vol. 45, no. 3 (2018), p. 035101.

[MS86]   Matsui, T. and Satz, H. "J/? suppression by quark-gluon plasma
            formation". In: *Physics Letters B* vol. 178, no. 4 (1986), pp. 416–
            422.

[MSW12]   Müller, B., Schukraft, J., and Wysłouch, B. "First Results from Pb+Pb Collisions at the LHC". In: *Annual Review of Nuclear and Particle Science* vol. 62, no. 1 (2012), pp. 361–386. eprint: https://doi.org/10.1146/annurev-nucl-102711-094910.

[Mur04]   Muronga, A. "Shear viscosity coefficient from microscopic models". In: *Phys. Rev. C* vol. 69 (4 2004), p. 044901.

[Nay20]   Nayak, T. K. "Probing the QCD phase structure using event-by-event fluctuations". In: *Journal of Physics: Conference Series* vol. 1602, no. 1 (2020), p. 012003.

[NEP16]   Niemi, H., Eskola, K. J., and Paatelainen, R. "Event-by-event fluctuations in a perturbative QCD + saturation + hydrodynamics model: Determining QCD matter shear viscosity in ultrarelativistic heavy-ion collisions". In: *Phys. Rev. C* vol. 93 (2 2016), p. 024907.

[NHNG12] Noronha-Hostler, J, Noronha, J, and Greiner, C. "Hadron mass spectrum and the shear viscosity to entropy density ratio of hot hadronic matter". In: *Phys. Rev. C* vol. 86 (2 2012), p. 024913.

[NPA19]   NPAQM2018. In: *Nuclear Physics A* vol. 982 (2019). The 27th International Conference on Ultrarelativistic Nucleus-Nucleus Collisions: Quark Matter 2018, pp. 1–1066.

[NPA21]   NPAQM2019. In: *Nuclear Physics A* vol. 1005 (2021). The 28th International Conference on Ultra-relativistic Nucleus-Nucleus Collisions: Quark Matter 2019, p. 122104.

[NRT09]   Nishioka, T., Ryu, S., and Takayanagi, T. "Holographic entanglement entropy: an overview". In: *Journal of Physics A: Mathematical and Theoretical* vol. 42, no. 50 (2009), p. 504008.

[Nyq24]   Nyquist, H. "Certain factors affecting telegraph speed". In: *The Bell System Technical Journal* vol. 3, no. 2 (1924), pp. 324–346.

[Nyq28]   Nyquist, H. "Certain Topics in Telegraph Transmission Theory". In: *Transactions of the American Institute of Electrical Engineers* vol. 47, no. 2 (1928), pp. 617–644.

[Oll92]   Ollitrault, J.-Y. "Anisotropy as a signature of transverse collective flow". In: *Phys. Rev. D* vol. 46 (1 1992), pp. 229–245.

[OM07]   Obadia, N. and Milgrom, M. "Unruh effect for general trajectories". In: *Phys. Rev. D* vol. 75 (6 2007), p. 065006.

[Ozv+13a] Ozvenchuk, V. et al. "Dynamical equilibration of strongly interacting "infinite" parton matter within the parton-hadron-string dynamics transport approach". In: *Phys. Rev. C* vol. 87 (2 2013), p. 024901.

[Ozv+13b] Ozvenchuk, V et al. "Shear and bulk viscosities of strongly interacting "infinite" parton-hadron matter within the parton-hadron-string dynamics transport approach". In: *Phys. Rev. C* vol. 87 (6 2013), p. 064903.

[Pad05]   Padmanabhan, T. "Gravity and the thermodynamics of horizons". In: *Physics Reports* vol. 406, no. 2 (2005), pp. 49–125.

[Pag05]   Page, D. N. "Hawking radiation and black hole thermodynamics*". In: *New Journal of Physics* vol. 7, no. 1 (2005), p. 203.

[Pag93a]   Page, D. N. "Information in black hole radiation". In: *Phys. Rev. Lett.* vol. 71 (23 1993), pp. 3743–3746.

[Pag93b]   Page, D. N. "Average entropy of a subsystem". In: *Phys. Rev. Lett.* vol. 71 (9 1993), pp. 1291–1294.

[Plu+12]   Plumari, S et al. "Shear viscosity of a strongly interacting system: Green-Kubo correlator versus Chapman-Enskog and relaxation-time approximations". In: *Phys. Rev. C* vol. 86 (5 2012), p. 054902.

[Pol16]   Polchinski, J. "The Black Hole Information Problem". In: *New Frontiers in Fields and Strings*. WORLD SCIENTIFIC, 2016.

[Pre08]   Prester, P. "α'-corrections and heterotic black holes". In: *Proceedings of Workshop "Black Holes in General Relativity and String Theory"*. 2008.

[QH12]   Qiu, Z. and Heinz, U. "Hydrodynamic event-plane correlations in Pb+Pb collisions at s=2.76A TeV". In: *Physics Letters B* vol. 717, no. 1 (2012), pp. 261–265.

[Raj22]   Raju, S. "Lessons from the information paradox". In: *Physics Reports* vol. 943 (2022). Lessons from the information paradox, pp. 1–80.

[RGG20]   Rais, J, Gallmeister, K, and Greiner, C. "Shear viscosity to entropy density ratio of Hagedorn states". In: *Phys. Rev. D* vol. 102 (3 2020), p. 036009.

[Rom17]   Romatschke, P. "Do nuclear collisions create a locally equilibrated quark-gluon plasma?" In: *Eur. Phys. J. C* vol. 77 (2017), p. 21.

[Ros+18]   Rose, J.-B. et al. "Shear viscosity of a hadron gas and influence of resonance lifetimes on relaxation time". In: *Phys. Rev. C* vol. 97 (5 2018), p. 055204.

[Roy09]   Roy, D. "The Unruh thermal spectrum through scalar and fermion tunneling". In: *Physics Letters B* vol. 681, no. 2 (2009), pp. 185–189.

[RR07]   Romatschke, P and Romatschke, U. "Viscosity Information from Relativistic Nuclear Collisions: How Perfect is the Fluid Observed at RHIC?" In: *Phys. Rev. Lett.* vol. 99 (17 2007), p. 172301.

[RR17]   Romatschke, P. and Romatschke, U. *Relativistic Fluid Dynamics In and Out of Equilibrium – Ten Years of Progress in Theory and Numerical Simulations of Nuclear Collisions*. 2017.

[RR97]   Reisdorf, W. and Ritter, H. G. "COLLECTIVE FLOW IN HEAVY-ION COLLISIONS". In: *Annual Review of Nuclear and Particle Science* vol. 47, no. 1 (1997), pp. 663–709. eprint: https://doi.org/10.1146/annurev.nucl.47.1.663.

[RT06a]   Ryu, S. and Takayanagi, T. "Aspects of holographic entanglement entropy". In: *Journal of High Energy Physics* vol. 2006, no. 08 (2006), p. 045.

[RT06b]   Ryu, S. and Takayanagi, T. "Holographic Derivation of Entanglement Entropy from the anti–de Sitter Space/Conformal Field Theory Correspondence". In: *Phys. Rev. Lett.* vol. 96 (18 2006), p. 181602.

[Ryu+15]   Ryu, S. et al. "Importance of the Bulk Viscosity of QCD in Ultrarelativistic Heavy-Ion Collisions". In: *Phys. Rev. Lett.* vol. 115 (13 2015), p. 132301.

[Sat07]   Satz, H. "Thermal Hadron Production by QCD Hawking Radiation". In: *Progress of Theoretical Physics Supplement* vol. 168 (Mar. 2007), pp. 338–346. eprint: https://academic.oup.com/ptps/article-pdf/doi/10.1143/PTPS.168.338/5178265/168-338.pdf.

[Sch13]   Schee, W. van der. "Holographic thermalization with radial flow". In: *Phys. Rev. D* vol. 87 (6 2013), p. 061901.

[Sch14]   Schulz, B. *Review on the quantization of gravity*. 2014. eprint: arXiv: 1409.7977 [gr-qc].

[SH08]   Song, H and Heinz, U. "Multiplicity scaling in ideal and viscous hydrodynamics". In: *Phys. Rev. C* vol. 78 (2 2008), p. 024902.

[Sha48]   Shannon, C. E. "A Mathematical Theory of Communication". In: *The Bell System Technical Journal* vol. 27 (1948), pp. 379–423, 623–656.

[Sir+19]   Sirunyan, A. et al. "Measurement of nuclear modification factors of $\Upsilon(1S)$, $\Upsilon(2S)$, and $\Upsilon(3S)$ mesons in PbPb collisions at sNN=5.02 TeV". In: *Physics Letters B* vol. 790 (2019), pp. 270–293.

[SJG12]   Schenke, B., Jeon, S., and Gale, C. "Higher flow harmonics from $(3+1)$D event-by-event viscous hydrodynamics". In: *Phys. Rev. C* vol. 85 (2 2012), p. 024901.

[SL11]   Silva, C. A. S. and Landim, R. R. "A note on black hole entropy, area spectrum, and evaporation". In: *Europhys. Lett.* vol. 96 (2011), p. 10007.

[Sol11]   Solodukhin, S. N. "Entanglement Entropy of Black Holes". In: *Living Reviews in Relativity* vol. 14, no. 1 (2011).

[Sol22]   Soloviev, A. "Hydrodynamic attractors in heavy ion collisions: a review". In: *Eur. Phys. J. C* vol. 82 (2022), p. 319.

[Son+11a]   Song, H. et al. "200 *A* GeV Au + Au Collisions Serve a Nearly Perfect Quark-Gluon Liquid". In: *Phys. Rev. Lett.* vol. 106 (19 2011), p. 192301.

[Son+11b]   Song, H. et al. "Hadron spectra and elliptic flow for 200 *A* GeV Au + Au collisions from viscous hydrodynamics coupled to a Boltzmann cascade". In: *Phys. Rev. C* vol. 83 (5 2011), p. 054910.

[SP96]   Sriramkumar, L and Padmanabhan, T. "Finite-time response of inertial and uniformly accelerated Unruh - DeWitt detectors". In: *Classical and Quantum Gravity* vol. 13, no. 8 (1996), p. 2061.

[Sre93]   Srednicki, M. "Entropy and area". In: *Phys. Rev. Lett.* vol. 71, no. 5 (1993), pp. 666–669.

[SRP13]   Schee, W. van der, Romatschke, P., and Pratt, S. "Fully Dynamical Simulation of Central Nuclear Collisions". In: *Phys. Rev. Lett.* vol. 111 (22 2013), p. 222302.

[SS01]   Shuryak, E. V. and Stephanov, M. A. "Long-range charge fluctuations and search for a quark-gluon plasma signal". In: *Phys. Rev. C* vol. 63 (6 2001), p. 064903.

[SS92]   Svaiter, B. F. and Svaiter, N. F. "Inertial and noninertial particle detectors and vacuum fluctuations". In: *Phys. Rev. D* vol. 46 (12 1992), pp. 5267–5277.

[Sto18]   Stoica, O. C. "Revisiting the Black Hole Entropy and the Information Paradox". In: *Advances in High Energy Physics* vol. 2018 (2018), p. 4130417.

[Str15]   Strickland, M. "Thermalization and isotropization in heavy-ion collisions". In: *Pramana – J. Phys.* vol. 84, no. 5 (2015), pp. 671–684.

[Sus95]   Susskind, L. "The world as a hologram". In: *Journal of Mathematical Physics* vol. 36, no. 11 (1995), pp. 6377–6396.

[SV96]   Strominger, A. and Vafa, C. "Microscopic origin of the Bekenstein-Hawking entropy". In: *Physics Letters B* vol. 379, no. 1 (1996), pp. 99–104.

['t 85]   't Hooft, G. "On the quantum structure of a black hole". In: *Nuclear Physics B* vol. 256 (1985), pp. 727–745.

[Tak86]   Takagi, S. "Vacuum Noise and Stress Induced by Uniform Acceleration: Hawking-Unruh Effect in Rindler Manifold of Arbitrary Dimension". In: *Progress of Theoretical Physics Supplement* vol. 88 (Mar. 1986), pp. 1–142. eprint: https://academic.oup.com/ptps/article-pdf/doi/10.1143/PTP.88.1/5461184/88-1.pdf.

[TEA10]   TEANEY, D. A. "VISCOUS HYDRODYNAMICS AND THE QUARK GLUON PLASMA". In: *Quark-Gluon Plasma 4*. WORLD SCIENTIFIC, 2010, pp. 207–266.

[Tsa88]   Tsallis, C. "Possible generalization of Boltzmann-Gibbs statistics". In: *J. Stat. Phys.* vol. 52 (1988), pp. 479–487.

[TY12]   Teaney, D. and Yan, L. "Nonlinearities in the harmonic spectrum of heavy ion collisions with ideal and viscous hydrodynamics". In: *Phys. Rev. C* vol. 86 (4 2012), p. 044908.

[Unr76]   Unruh, W. G. "Notes on black-hole evaporation". In: *Phys. Rev. D* vol. 14 (4 1976), pp. 870–892.

[UW17]   Unruh, W. G. and Wald, R. M. "Information loss". In: *Reports on Progress in Physics* vol. 80, no. 9 (2017), p. 092002.

[UW84]   Unruh, W. G. and Weiss, N. "Acceleration radiation in interacting field theories". In: *Phys. Rev. D* vol. 29 (8 1984), pp. 1656–1662.

[VA16]   Vinjanampathy, S and Anders, J. "Quantum thermodynamics". In: *Contemporary Physics* vol. 57, no. 4 (2016), pp. 545–579. eprint: https://doi.org/10.1080/00107514.2016.1201896.

[VAC11]   Vanzo, L, Acquaviva, G, and Criscienzo, R. D. "Tunnelling methods and Hawking's radiation: achievements and prospects". In: *Classical and Quantum Gravity* vol. 28, no. 18 (2011), p. 183001.

[Ver11]   Verlinde, E. "On the origin of gravity and the laws of Newton". In: *Journal of High Energy Physics* vol. 2011, no. 4 (2011).

[VZ96]   Voloshin, S. and Zhang, Y. "Flow study in relativistic nuclear collisions by Fourier expansion of azimuthal particle distributions". In: *Z Phys C – Particles and Fields* vol. 70 (1996), pp. 665–671.

[Wal18]   Wall, A. C. "A Survey of Black Hole Thermodynamics". Version v2. In: *arXiv:1804.10610* (2018). eprint: arXiv:1804.10610.

[Wes+11]   Wesp, C et al. "Calculation of shear viscosity using Green-Kubo relations within a parton cascade". In: *Phys. Rev. C* vol. 84 (5 2011), p. 054911.

[WG92]   Wang, X.-N. and Gyulassy, M. "Gluon shadowing and jet quenching in A+A collisions at $\sqrt{s}$ =200A GeV". In: *Phys. Rev. Lett.* vol. 68 (10 1992), pp. 1480–1483.

[Wol+22]   Wolter, H. et al. "Transport model comparison studies of intermediate-energy heavy-ion collisions". In: *Progress in Particle and Nuclear Physics* vol. 125 (2022), p. 103962.

[WS13]   Wontae, K and Shailesh, K. "Higher order WKB corrections to black hole entropy in brick wall formalism". In: *Eur. Phys. J. C* vol. 73 (2013), p. 2398. eprint: arXiv:1205.4586 [hep-th] (hep-th).

[Zha+09]   Zhang, B. et al. "Hidden messenger revealed in Hawking radiation: A resolution to the paradox of black hole information loss". In: *Physics Letters B* vol. 675, no. 1 (2009), pp. 98–101.

[ZMR96]   Zubarev, D., Morozov, V., and Ropke, G. *Statistical Mechanics of Nonequilibrium Processes, Volume 1 (See 3527400834): Basic Concepts, Kinetic Theory.* Statistical Mechanics of Nonequilibrium Processes. Wiley, 1996.

[ZMR97]   Zubarev, D., Morozov, V., and Röpke, G. *Statistical Mechanics of Nonequilibrium Processes, Statistical Mechanics of Nonequilibrium Processes. Volume 2: Relaxation and Hydrodynamic Processes.* Statistical Mechanics of Nonequilibrium Processes. Wiley, 1997.

[ZPS79]   Zubarev, D. N., Prozorkevich, A. V., and Smolyanskii, S. A. "Deriva-
            tion of nonlinear generalized equations of quantum relativistic hy-
            drodynamics". In: *Theor. Math. Phys.* vol. 40 (1979), pp. 821–831.

Part II

Papers

Shear viscosity in microscopic calculations of $A + A$ collisions at energies available at the Nuclotron-based Ion Collider fAcility (NICA)

M. Teslyk ●,[*] L. Bravina, O. Panova ●,[*] O. Vitiuk ●,[*] and E. Zabrodin ●[†]
Department of Physics, University of Oslo, PB 1048 Blindern, N-0316 Oslo, Norway

Time evolution of shear viscosity η, entropy density s, and their ratio η/s in the central area of central gold-gold collisions at energies available at the Nuclotron-based Ion Collider fAcility (NICA) are studied within the ultrarelativistic quantum molecular dynamics (UrQMD) transport model. The extracted values of energy density, net baryon density, and net strangeness density are used as input to (i) the statistical model of an ideal hadron gas to define temperature, baryochemical potential, and strangeness chemical potential, and to (ii) a UrQMD box with periodic boundary conditions to study the relaxation process of highly excited matter. During the relaxation stage, the shear viscosity is determined in the framework of the Green-Kubo approach. The procedure is performed for each of 20 time slices, corresponding to conditions in the central area of the fireball at times from 1 to 20 fm/c. For all tested energies the ratio η/s reaches its minimum, $(\eta/s)_{min} \approx 0.3$ at $t \approx 5$ fm/c. Then it increases up to the late stages of the system evolution. This rise is accompanied by the drop of both temperature and strangeness chemical potential and by the increase of baryochemical potential.

I. INTRODUCTION

Relativistic heavy-ion collisions have been intensively studied both theoretically and experimentally to obtain information about the properties of highly excited nuclear matter. To date, these collisions are the only means to study the conditions of early Universe in the laboratory, thus leading to the term "little big bang" [1]. According to the theoretical estimates and lattice quantum chromodynamics (lQCD) calculations, nuclear matter under certain extreme conditions should experience a deconfinement phase transition into a new phase of matter, a quark-gluon plasma (QGP). The expanding hot fireball should, however, rapidly cool off, and the plasma will undergo hadronization. Experiments show that in heavy-ion collisions at the ultrarelativistic energies of the Relativistic Heavy Ion Collider (RHIC), $\sqrt{s} = 200$ GeV, and of the Large Hadron Collider (LHC), $\sqrt{s} = 2.76$ and 5.02 TeV, there is a crossover type of the phase transition. In contrast, at much lower energies the transition might be of the first order. In this case the line of the first-order phase transition in the nuclear phase diagram ends up in the tricritical point, where the transition becomes of second order. The search for the tricritical point is in the agenda of experiments with heavy-ion beams at the forthcoming Nuclotron-based Ion Collider fAcility (NICA) and the Facility for Antiproton and Ion Research (FAIR), and within the beam energy scan (BES) program at RHIC. Therefore, one has to look for the observable most

sensitive to the QGP-hadrons transition. One such observable is the ratio of shear viscosity η to entropy density s, η/s. This ratio drops to a minimum at critical temperatures for all known substances [2], and in relativistic heavy-ion collisions it is expected to be of order of its theoretical lower bound, $1/4\pi$ [3]; for details see, e.g., [4] and references therein.

Despite the interest in this topic, it is still difficult to estimate the value of the ratio exactly due to the high calculation complexity required by QCD simulations. Therefore, various works in the field have explored different approaches and approximations for the conditions expected to prevail near the phase transition; see e.g., [5–14]. For example, in [5] thermodynamic quantities of hadronic matter are studied for a system of light mesons embedded in a box with periodic boundary conditions generated by the ultrarelativistic quantum molecular dynamics (UrQMD) model. A relativistic hadron gas in thermal and chemical equilibrium and with zero baryon and strangeness chemical potentials was considered in [6]. In [11] the authors obtain viscosity η by solving the ultrarelativistic Boltzmann transport equation and compare it to the one obtained via the Chapman-Enskog approximation. Recently, the shear viscosity and its ratio to entropy density were calculated for a gas of Hagedorn states [15] with masses up to 10 GeV/c^2. It was found that, because of the rapid growth of s in the vicinity of Hagedorn limiting temperature $T_H = 165$ MeV, the ratio η/s came close to and was even below the bounding $1/4\pi$ given by anti–de Sitter and conformal field theory (AdS-CFT) [3]. Among the other papers on the topic are [16], where viscosity is extracted within the SMASH transport model, and [17], where the UrQMD model was employed for system of nucleons at intermediate temperatures between 10 and 50 MeV. In the latter case the nucleons were allowed to experience only elastic collisions.

---

[*]Also at Taras Shevchenko National University of Kyiv, UA-01033 Kyiv, Ukraine.
[†]Also at Skobeltsyn Institute of Nuclear Physics, Moscow State University, RU-119991 Moscow, Russia.

Definitely, heavy-ion collisions at energies of NICA and higher are more complex. As mentioned in [18], the ratio η/s cannot be constant during the evolution of the fireball. To provide better fits to the experimental data, this ratio should depend on both temperature and chemical potentials. Consequently, it is essential to explore the time dynamics of the ratio η/s from the very beginning of a relativistic heavy-ion collision.

In the present paper we investigate fluctuation relaxation time τ and shear viscosity η, as well as its ratio to entropy density, η/s, for central Au + Au collisions calculated in the UrQMD model [19,20] within the NICA energy range. Compared to the previous researches, we study the evolution of η, s, and η/s in heavy-ion collisions, where all characteristics are quickly changing, and not, e.g., the temperature dependence of the η/s ratio at constant chemical potentials. Investigation of dynamics of the relaxation process in a box with periodic boundary conditions allows us to estimate both the lower and upper bounds of the time interval at different energies, where it is possible to extract τ.

The paper is organized as follows. Section II describes briefly the features of the UrQMD model and the UrQMD box calculations. To extract the thermodynamic quantities, such as temperature T, baryochemical potential μ_B and strangeness chemical potential μ_S, one has to compare microscopic model calculations with the results provided by the statistical model (SM) of an ideal hadron gas with essentially the same degrees of freedom. This model is also explained in Sec. II. The formalism employed to determine the shear viscosity of hot and dense nuclear matter is presented in Sec. III. Section IV contains results of our study, including the time evolution of η and η/s in the central area of heavy-ion collisions, and dependencies of η/s on T, μ_B, and μ_S. Finally, conclusions are drawn in Sec. V.

II. MODELS EMPLOYED FOR THE ANALYSIS

In our study of shear viscosity we employ three computational models. The first one is the microscopic transport model UrQMD to calculate $A + A$ collisions at a given energy and get the bulk characteristics of hot and dense nuclear matter, namely, energy density ε, net baryon density ρ_B, and net strangeness density ρ_S. The second model is the UrQMD box with periodic boundary conditions to study the relaxation process and find the relaxation time τ. Finally, to determine thermodynamic parameters of the equilibrated system, i.e., temperature T, baryon chemical potential μ_B, and strangeness chemical potential μ_S, we apply the statistical model of an ideal hadron gas. The main features of all three models are as follows.

A. UrQMD model

This is a well-known model [19,20] widely used for the analysis of heavy-ion collisions in a broad energy range. UrQMD is based on covariant propagation of hadrons on classical trajectories, stochastic binary interactions of these hadrons if the distance between them is less than $d \leqslant d_0 = \sqrt{\sigma^{tot}/\pi}$, where σ^{tot} is the total cross section, formation and

decay of resonances, and, when a certain collision energy limit is exceeded, formation and subsequent fragmentation of specific colored objects, strings. For the treatment of strings UrQMD employs classical Lund model [21]. As independent degrees of freedom the model considers 55 different baryon states with masses up to $m_B^{max} \leqslant 2.25$ GeV/c^2 and 39 different meson states, including the charmed ones. The list of particles is supplemented by corresponding antiparticles and isospin-projected states. Cross sections of hadron-hadron (hh) interactions are taken from the available experimental data [22]. If this information is missing, the model relies on the unitarity, the additive quark model, and detailed balance considerations.

B. Calculation of nuclear infinite matter: UrQMD box

The box with finite volume and periodic boundary conditions serves to simulate the properties of infinite nuclear matter [23,24]. All particle interactions assumed in UrQMD are allowed in the box as well. However, if any particle leaves the box, another particle with absolutely identical parameters enters it, thus ensuring the preservation of initial energy density, net baryon density, and net strangeness density in the box. The initial state in the box can be generated as mixture of baryons and antibaryons, or a baryon-free gas of mesons, or even a system of strings and resonances. In the case of nonzero net baryon charge and zero net strangeness it is convenient to initialize the box containing neutrons and protons only. All nucleons can be uniformly distributed in the space, whereas their momenta are randomly distributed in a Fermi sphere and then rescaled to ensure the required energy density. Note also that relaxation to equilibrium in the box proceeds much longer compared to, e.g., that in the central cell in heavy-ion collisions [24]. In an open-system-like cell, the most energetic particles leave it earlier, and the whole system is cooling down. In a closed-system-like box, one has to wait until the kinetic energy of the most "hot" particles will be redistributed among other particles and also converted to the mass of newly produced hadrons.

Finally, we have to determine temperature and chemical potentials in the system. This is done by multiple fits of hadron abundances and energy spectra in UrQMD to those calculated within the statistical model.

C. Statistical model of ideal hadron gas

If the system of hadrons containing $1 \leqslant i \leqslant n$ different species is in equilibrium at temperature T, all many-particle correlations in it are reduced to a set of distribution functions (in system of natural units $c = \hbar = k_B = 1$)

$$f(p, m_i) = \left[\exp\left(\frac{\epsilon_i - \mu_i}{T}\right) + C\right]^{-1}. \qquad (1)$$

Here $C = +1$ for fermions and $C = -1$ for baryons, and p, m_i, ϵ_i, and μ_i are hadron momentum, mass, energy, and chemical potential, respectively. The last depends on chemical potentials assigned to baryon charge B_i, strangeness content

S_i, and electric charge Q_i of ith hadron. However, the chemical potential μ_Q of electric charge is usually much smaller compared to baryochemical potential μ_B and strangeness chemical potential μ_S. Therefore, we will consider the linear combination of two terms for the full chemical potential of a hadron:

$$\mu_i = B_i \mu_B + S_i \mu_S. \tag{2}$$

The partial number density n_i, the energy density ε_i, and the entropy density s_i read

$$n_i = \frac{g_i}{2\pi^2} \int_0^\infty f(p, m_i) p^2 \, dp, \tag{3}$$

$$\varepsilon_i = \frac{g_i}{2\pi^2} \int_0^\infty \sqrt{p^2 + m_i^2} f(p, m_i) p^2 \, dp, \tag{4}$$

$$s_i = -\frac{g_i}{2\pi^2} \int_0^\infty f(p, m_i)[\ln f(p, m_i) - 1] p^2 \, dp, \tag{5}$$

where g_i is the spin-isospin degeneracy factor. The values of T, μ_B, and μ_S should satisfy the set of nonlinear equations

$$\varepsilon = \sum_i \varepsilon_i(T, \mu_B, \mu_S), \tag{6}$$

$$\rho_B = \sum_i B_i n_i(T, \mu_B, \mu_S), \tag{7}$$

$$\rho_S = \sum_i S_i n_i(T, \mu_B, \mu_S), \tag{8}$$

where ε, ρ_B, and ρ_S are taken as input from microscopic model calculations.

III. SHEAR VISCOSITY DETERMINATION PROCEDURE

We calculate central Au + Au collisions in the laboratory frame at energies $E_{lab} = 10A$, $20A$, $30A$, and $40A$ GeV, corresponding to $\sqrt{s}$ from 4.5 to 8.8 GeV in the center-of-mass frame. From the whole system the central cell with volume $5 \times 5 \times 5 = 125$ fm^3 is selected. Then, the energy density ε, the net baryon density ρ_B, and the net strangeness density ρ_S in the cell are extracted at times $t_{cell} = 1$–20 fm/c with the time step of 1 fm/c. In order to minimize statistical errors an ensemble of 51 200 Au + Au central collisions at each energy has been generated.

The extracted data are inserted in the statistical model of the ideal hadron gas to obtain temperature T, entropy density s_{sm}, baryon chemical potential μ_B, and strangeness chemical potential μ_s. After that we start UrQMD box calculations. The box with volume $V = 10 \times 10 \times 10 = 1000$ fm^3 is initialized with the same values of ε, ρ_B, and ρ_S as extracted from the cell analysis. Baryon density is provided by protons and neutrons taken in equal proportion, $N_p : N_n = 1 : 1$. Nonzero strangeness density is generated by the admixture of kaons. The box data are analyzed for times $t_{box} = 1$–1000 fm/c with the time step 1 fm/c. The box ensemble consists of 12 800 box simulations for each of 80 points.

To extract η the Green-Kubo [25,26] formalism was used. The formalism requires the existence of an equilibrated state in the medium in order to provide exponential damping of deviations from the equilibrium with time. Thus, the verification

of equilibrium or of exponential damping of fluctuations is the necessary condition to be checked.

From the Green-Kubo formalism it follows that shear viscosity η may be defined as

$$\eta(t_0) = \frac{V}{T} \int_{t_0}^\infty dt \langle \pi(t)\pi(t_0)\rangle_t, \tag{9}$$

where t_0 and t denote moments of time in the box, and correlator $\langle \pi(t)\pi(t_0)\rangle_t$ can be cast in the form

$$\langle \pi(t)\pi(t_0)\rangle_t = \sum_{\substack{i,j=1 \\ i \neq j}}^3 \frac{1}{3}\Bigg[\lim_{t_{max} \to \infty} \frac{1}{t_{max}}$$
$$\times \int_{t_0}^{t_{max}} dt' \pi^{ij}(t+t')\pi^{ij}(t') \Bigg] \tag{10}$$

with π^{ij} being nondiagonal part of the stress-energy tensor T^{ij}

$$\pi^{ij}(t) = \frac{1}{V} \sum_{i \neq j} \frac{p^i(t)p^j(t)}{E(t)}. \tag{11}$$

Here $p^{i(j)}$ and E are the $i(j)$th components of momentum and energy of the particle, respectively. t_0 is the initial cutoff time indicating the beginning of the extraction of quantities from the box. The coefficient $1/3$ in the sum $\sum_{i,j}$ means averaging over the directions, which allows one to reduce the statistical errors. Usually the cutoff time t_0 is set to zero. We have left it here on purpose to explore the influence of the onset of data extraction from box calculations on the extracted value of shear viscosity.

If the system is in equilibrium, the correlator (10) is expected to experience an exponential drop with time, i.e.,

$$\langle \pi(t)\pi(t_0)\rangle_t = \langle \pi(t_0)\pi(t_0)\rangle \exp\left(-\frac{t-t_0}{\tau}\right), \tag{12}$$

with τ being an effective relaxation time of the system.

Inserting Eq. (12) in Eq. (9), one gets

$$\eta(t_0) = \frac{\tau V}{T} \langle \pi(t_0)\pi(t_0)\rangle. \tag{13}$$

As follows from Eq. (13), the problem of evaluation of η is reduced to estimation of τ. Shear viscosity may be obtained then in two different ways: (i) by direct calculation of integral from Eq. (9), which is equivalent to taking into account all time contributions to the correlator, or (ii) by fitting the correlator to Eq. (12) in some selected time interval and applying Eq. (13). The key difference here is the influence of fluctuations. The first case takes them into account and assumes that they are mostly mutually extinguished, whereas the second one cuts off fluctuations at times $t \gg \tau$ when the correlator is too small compared to the fluctuations (white noise) [11]. In what follows we compare the relaxation times τ for both cases.

IV. RESULTS

First, we study the time evolution of the bulk characteristics in central cell of Au + Au collisions at four energies in
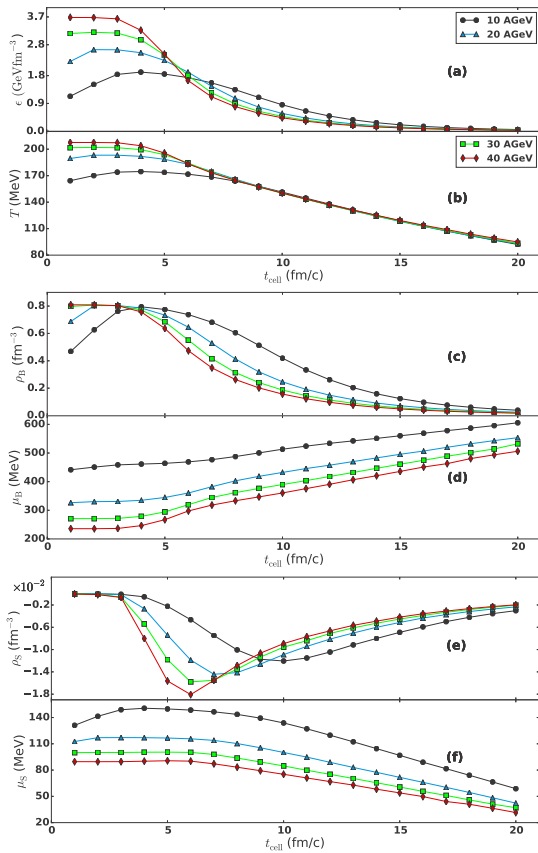
FIG. 1. Time evolution of (a) energy density ε, (c) net baryon density $\rho_{\mathrm{B}}^{\mathrm{net}}$, (e) net strangeness density $\rho_{\mathrm{S}}^{\mathrm{net}}$, (b) temperature T_{SM}, (d) baryon chemical potential μ_{B}, and (f) strangeness chemical potential μ_{S} in the central cell with $V = 125$ fm^3 in central Au + Au collisions calculated within UrQMD at energies $E_{\mathrm{lab}} = 10A$ GeV (circles), $20A$ GeV (triangles), $30A$ GeV (squares), and $40A$ GeV (diamonds). Lines are drawn to guide the eye.

question. Entropy density, net baryon density, and net strangeness density obtained in the cell from the microscopic calculations at time $1 \leqslant t \leqslant 20$ fm/c are displayed in Figs. 1(a), 1(c), and 1(e). At lowest bombarding energy $E_{\mathrm{lab}} = 10A$ GeV the maximum values of ε and ρ_{B} are reached at $t \approx 5$ fm/c, corresponding to complete overlap of two colliding nuclei. With rising bombarding energy, the nuclei overlap occurs earlier, thus the maxima of the distributions are shifted to times $t \approx 1$–3 fm/c. With the net strangeness in the cell the situation is more peculiar. Copious production of strange particles takes place between 4 fm/c and 8–10 fm/c when the matter in the cell is baryon rich. As mentioned in [27–30], K^+'s can leave the selected volume a bit earlier compared to the K^-'s because of the smaller interaction cross sections. Therefore, the net strangeness in the cell is always negative, though small. Applying the procedure explained in Sec. III
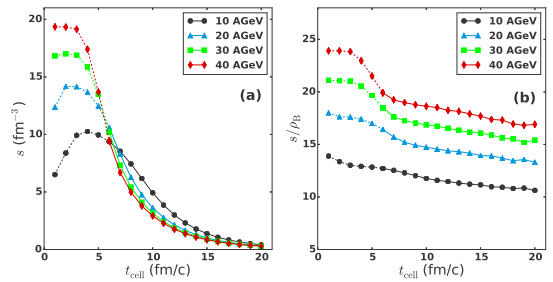
FIG. 2. (a) Entropy density s_{sm} and (b) its ratio to net baryon density $s_{\mathrm{sm}}/\rho_{\mathrm{b,net}}$ for different collision energies E in UrQMD central cell calculations. Lines are drawn to guide the eye.

we insert the values of $\{\varepsilon, \rho_{\mathrm{B}}, \rho_{\mathrm{S}}\}$ as an input in the SM to get $\{T, \mu_{\mathrm{B}}, \mu_{\mathrm{S}}\}$ corresponding to an ideal hadron gas in chemical and thermal equilibrium. Evolutions of these parameters are shown in Figs. 1(b), 1(d), and 1(f). It is worth noting that the local equilibrium in the cell at energies between $10A$ and $40A$ GeV is reached not earlier than $t \approx 6$–8 fm/c. Therefore, one should treat the SM parameters obtained for earlier times with great care. Large baryon and energy densities observed at $t \leqslant 6$ fm/c are caused by interpenetration of two Lorentz-contracted nuclei. This leads to extra-high temperatures of the ideal hadron gas, seen in Fig. 1(b). For the extraction of more reliable values of T and μ_{B} we have to wait until the remnants of colliding nuclei will pass through each other and leave the tested volume. From here, we will indicate the thermodynamic results related to the early phase of the matter evolution in the cell by dashed lines in the figures.

Despite the differences in the cell initial conditions, all four temperature curves sit on the top of each other after $t = 7$ fm/c. Both baryon and strangeness chemical potentials drop with increasing bombarding energy, in full accord with the SM analysis of experimental data. However, μ_{B} increases whereas μ_{S} decreases, while the temperature in the cell drops and the matter becomes more dilute.

Figure 2(a) presents the evolution of the entropy density in the central cell in the studied reactions. This behavior is qualitatively similar to that of $\varepsilon(t)$ seen in Fig. 1(a). Note, however, that the entropy density here is calculated within the SM implying the maximum values for s. For the nonequilibrium state at $t \leqslant 6$ fm/c the entropy density is lower than the s^{SM}. The ratio of entropy density to baryon density, s/ρ_{B}, shown in Fig. 2(b), also should be lower during the stage of relaxation to equilibrium. It drops slightly, about 15% between 6 and 20 fm/c, indicating that the expansion proceeds nearly isentropically.

We are switching now to the box calculations. Figure 3 shows correlators defined by Eq. (10) calculated for all four collision energies. The input data $\varepsilon, \rho_{\mathrm{B}}, \rho_{\mathrm{S}}$ were extracted from the central cell of Au + Au central collisions at times from 1 fm/c up to 20 fm/c after the beginning of the collision. To see the differences between the distributions more distinctly, each correlator was multiplied by the factor $10^{t_{cell}-1}$. Recall, that the results of the box calculations are shown for
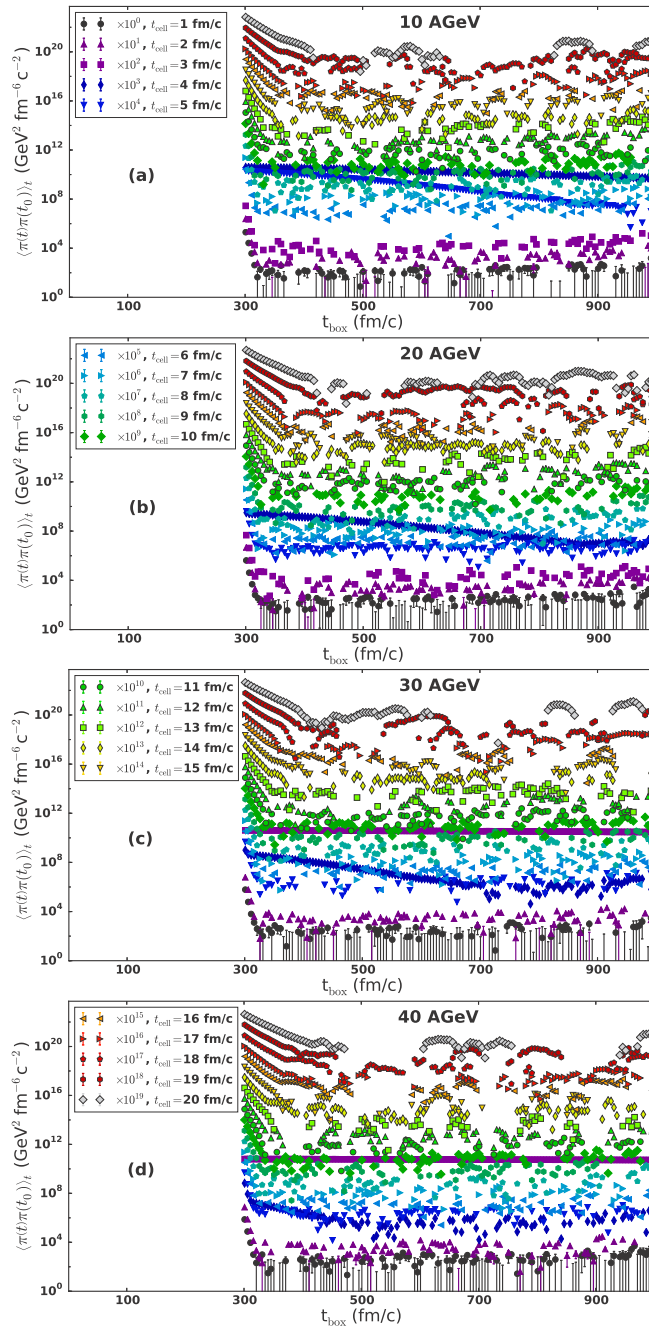
FIG. 3. Correlators $\langle \pi(t)\pi(t_0)\rangle_t$ for initial cutoff time $t_0 = 300$ fm/c in the UrQMD box calculations. Initial conditions for the boxes are taken from the central cell with $V = 125$ fm^3 of Au + Au collisions at (a) $E_{\mathrm{lab}} = 10A$ GeV, (b) $20A$ GeV, (c) $30A$ GeV, and (d) $40A$ GeV at times $t = 1$–20 fm/c. Each distribution is multiplied by factor $10^{t_{\mathrm{cell}}-1}$.
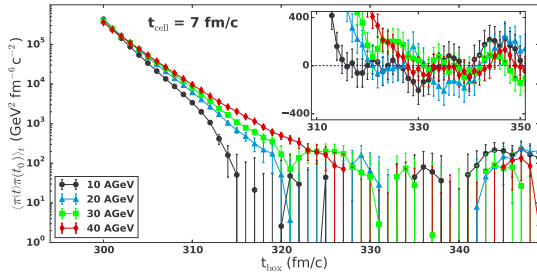
FIG. 4. UrQMD box calculations of the correlators $\langle \pi(t)\pi(t_0)\rangle_t$. Initial conditions in the box correspond to those in the central cell of Au + Au collisions at $E_{lab} = 10A$ GeV (circles), $20A$ GeV (triangles), $30A$ GeV (squares), and $40A$ GeV (diamonds) taken at time $t_{cell} = 7$ fm/c. Lines are drawn to guide the eye.

times $t_{box} \geqslant 300$ fm/c. This timescale has nothing to do with the typical relaxation times of hot and dense matter in heavy-ion collisions [24]. One can see that all correlators reveal exponential falloff with time in accordance with Eq. (12). However, for the conditions corresponding to early cell times, the relaxation rates are several orders of magnitude slower compared to those corresponding to late times. This cannot be explained entirely by large baryon and energy densities in the central cell at early t_{cell}, when nuclei overlap. Here one has to initialize the box with one or two very ultrarelativistic kaons that cannot redistribute their energy and momenta quickly enough. This circumstance results in a slow relaxation of the appropriate correlators. In order to extract the correct data corresponding to the overlap of nuclei, one has to process the box calculations for longer periods of time; see, e.g., [16]. Note also that microscopic transport models usually lack the inverse reactions to multiparticle processes $2 \to N$ ($N \geqslant 3$).

In this case the matter in the box will relax to the steady state rather than to the pure equilibrium; see, e.g., [23,24,31,32]. However, the matter in the central cell at $t \geqslant 6$ fm/c in heavy-ion collisions at energies below $E_{lab} = 40A$ GeV becomes dilute very quickly. Its energy density drops, and the many-particle inelastic reactions in the box with similar ε, ρ_B, and ρ_S rapidly cease, thus leading to equilibrium similar to that of the SM.

At late times of the box calculations it appears that the correlations are rising. This is a technical effect. Namely, at the end of the UrQMD box calculations the program forces decay of all strongly decaying resonances, which may lead to some momentum correlations.

Typical behavior of the correlator dynamics on shorter timescales is demonstrated in Fig. 4, where the correlators for different collision energies are depicted. Again, as in Fig. 3, the initial cutoff time in the box is $t_0 = 300$ fm/c. The initial conditions in the box correspond to that in the cell at $t_{cell} = 7$ fm/c. The exponential falloff with time occurs within $t \lesssim t_0 + 30$ fm/c. After that time the correlators become too weak, and fluctuations start to dominate the system. Domination of the fluctuations leads to the necessity of cutting off the dataset while fitting the correlator $\langle \pi(t)\pi(t_0)\rangle_t$ to Eq. (12), as was proposed in [11,16].

The necessity for dataset cutoff raises the question of direct applicability of Eq. (9) in numerical calculations. In order to investigate the problem, we compare next the relaxation times extracted from the integral in Eq. (9), $\tau_{int}(t_0)$, and by fitting the correlator to Eq. (12) within the time interval cutoff $t_0 \leqslant t \leqslant (t_0 + 30)$ fm/c, $\tau_{fit}(t_0)$.

Figure 5 depicts the dependence of relaxation time τ_{int}, extracted from the integral in Eq. (9), on the initial cutoff time t_0, with every tenth point being shown. As one can see, the relaxation usually takes a longer period for t_0 shorter than 200 fm/c and vanishes for $t_0 \geqslant 900$ fm/c. For the initial times between these two limits the relaxation time
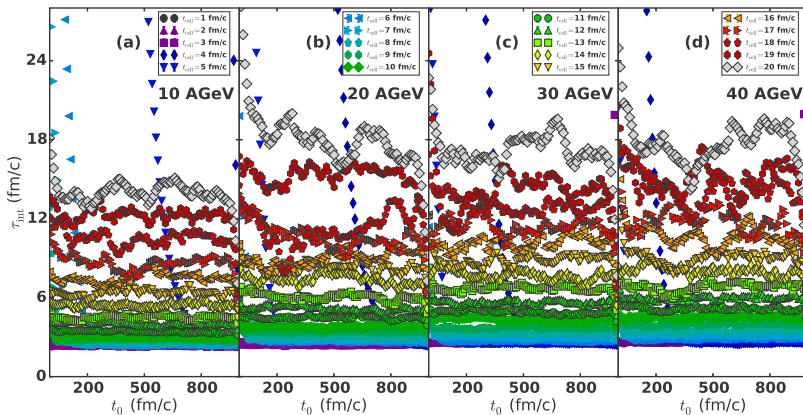

FIG. 5. Relaxation time $\tau_{int}(t_0)$ for the collision energies (a) $E_{lab} = 10A$ GeV, (b) $20A$ GeV, (c) $30A$ GeV, and (d) $40A$ GeV and for all cell times $1 \leqslant t_{cell} \leqslant 20$ fm/c in the UrQMD box calculations.
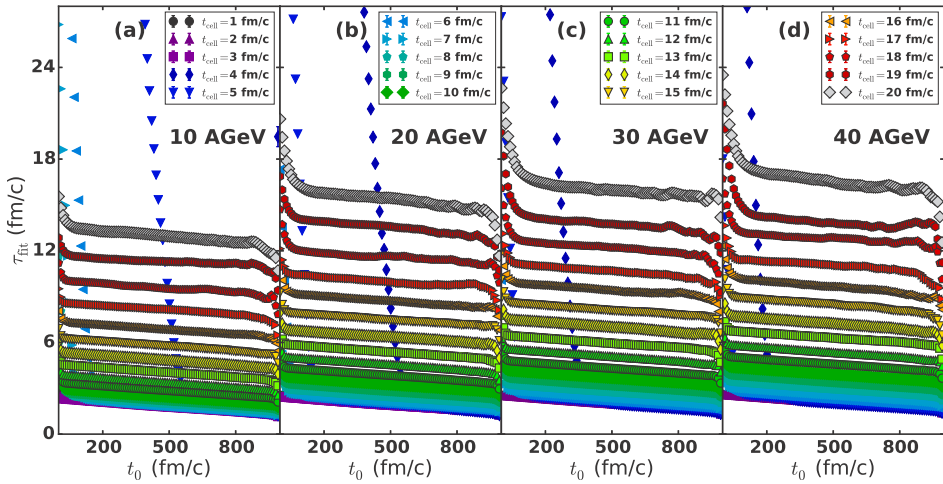
FIG. 6. The same as Fig. 5 but for relaxation time $\tau_{\text{fit}}(t_0)$.

is rather constant. The only exceptions are at the early cell times.

Figure 6 displays the dependence of relaxation time τ_{fit} extracted by fitting over the time interval $t_{\text{box}} \in [t_0, t_0 + 30]$. The behavior of τ_{fit} is pretty similar to that of τ_{int}. However, the results presented in Fig. 6 have no stochastic oscillations, in contrast to those shown in Fig. 5. This can be explained by the influence of fluctuations on τ_{int}. It is worth mentioning that, as one can notice, the plateau demonstrates some slope in Fig. 6 at $t_0 \geqslant 200$ fm/c as compared to the results shown in Fig. 5. The slope may significantly influence the determination of η values, because for early cell times with minimum values of τ_{fit} it may vary approximately by 40% for $200 \leqslant t_0 \leqslant 800$ fm/c. Small values of $\tau_{\text{int(fit)}}$ at large t_0 are dealing with the small averaging interval; see Eq. (10). Namely, the time resolution at large t_0 is too high to observe the correlator falloff, and one finds a kind of Brownian motion instead.

For the midrange of the initial cutoff time t_0 at the plateau—see Figs. 5 and 6—the falloff rate does not change significantly. Thus, the values of t_0 from this range are well suited for our task. In the following we average the value of $\tau_{\text{int(fit)}}$ over the plateau in order to reduce statistical errors. Large values of the relaxation time $\tau_{\text{int/fit}}$ for some early cell times t_{cell} are explained by the copious production of new hadrons and their subsequent rescatterings in very hot and dense baryon-rich matter at the very beginning of the collision. Additional time delay is caused by energetic single negative kaons. Combination of these factors forces the extension of the box calculations up to 2000 (sometimes 3000) fm/c.

Figure 7 shows ratio of the relaxation times determined by Eqs. (9) and (12), $\langle\tau_{\text{int}}\rangle/\langle\tau_{\text{fit}}\rangle$. As we see, τ_{int} exceeds τ_{fit} by 25% at $t = 6$ fm/c. For the cell conditions at later stages the relaxation times converge and agree with each other within

10% accuracy at $t \geqslant 15$ fm/c. Thus, taking the fluctuations into account results in increase of τ, as well as in its noise-like oscillations. The only difference, except for the general slope of τ_{fit}, is observed at the early cell times, when the nuclei overlap.

Shear viscosity $\eta(t_0)$, calculated with τ_{int}, is presented in Fig. 8. Since η is proportional to τ_{int} due to exponential falloff behavior of the correlator, distributions in Figs. 5 and 8 have many similar features. Shear viscosity shows larger values for the initial box fluctuations at small times t_0. It is reduced significantly at large t_0, and has a plateau at intermediate times.

After averaging over the plateau, which we define as $t_0 \in [200, 800]$ fm/c, one may obtain shear viscosity for different cell times at all the collision energies considered. Results are shown in Fig. 9. The statistical errors are smaller than the symbol sizes. We see that shear viscosity reaches its maximum
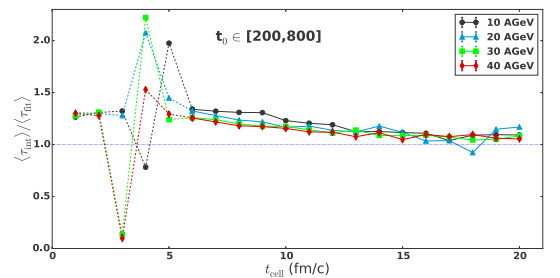

FIG. 7. Ratio $\langle\tau_{\text{int}}\rangle/\langle\tau_{\text{fit}}\rangle$ for the collision energies $10A$ GeV (circles), $20A$ GeV (triangles), $30A$ GeV (squares), and $40A$ GeV (diamonds) for all cell times t_{cell}. Errors are smaller than the symbol sizes.
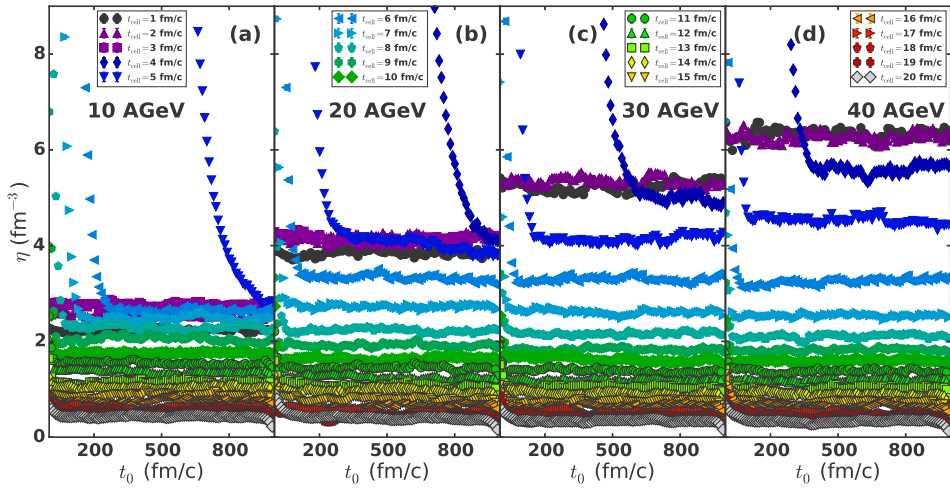
FIG. 8. Shear viscosity $\eta(t_0)$ for the collision energies (a) $E_{lab} = 10A$ GeV, (b) $20A$ GeV, (c) $30A$ GeV, and (d) $40A$ GeV for all cell times $1 \leqslant t_{cell} \leqslant 20$ fm/c within the UrQMD box calculations.

at the very beginning of the heavy-ion collision. Then it gradually drops almost to zero at the late cell times. Decrease of η with time is explained by the fact that at the late stages of the evolution of nuclear matter in the central cell there are only (quasi)elastic processes, i.e., soft scattering modes, remaining [29]. All energetic hadrons with large momenta have already left the cell. This circumstance results in the fast redistribution of momentum and energy of soft hadrons over the system, and, consequently, in small relaxation rate τ of the correlator.

At early times the shear viscosity is larger for heavy-ion collisions at larger energies. But after $t \approx 6$ fm/c all curves representing four different energies quickly converge. This behavior is very similar to the drop of the cell temperatures shown in Fig. 1(d). Both effects are caused by the faster loss of energy and baryon density in the central cell of central collisions with increasing bombarding energies.
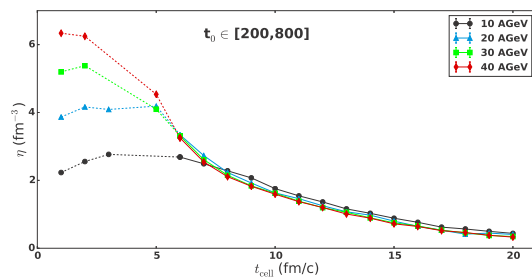
FIG. 9. Shear viscosity $\eta(t_{cell})$ of hadrons in the central cell of central Au + Au collisions at (a) $E_{lab} = 10A$ GeV, (b) $20A$ GeV, (c) $30A$ GeV, and (d) $40A$ GeV within the UrQMD box calculations. Lines are drawn to guide the eye.

Finally, Fig. 10 displays η/s dependencies on the evolution of the cell parameters, i.e., time [Fig. 10(a)], SM temperature [Fig. 10(b)], baryon chemical potential [Fig. 10(c)], and strangeness chemical potential [Fig. 10(d)]. The statistical errors are smaller than the symbol sizes. For all energies the ratio η/s reaches its minimum at $t \approx 5$ fm/c, when the nuclei are expected to overlap. Despite being small enough, the minima are about four times larger than the theoretical minimum value $1/4\pi$. After that the ratio η/s in the cell increases with time. The lower the collision energy, the smaller the ratio. It is also increasing with the drop of temperature and strangeness chemical potential, as shown in Figs. 10(b) and 10(d), and with the rise of baryochemical potential; see Fig. 10(c). It is worth noting that at $t \leqslant 5$ fm/c the matter in the cell is still out of equilibrium, whereas the estimates of T, μ_B, and μ_S are done for fully a equilibrated system of hadrons. Therefore, all distributions at early times are indicated by the dashed curves.

Comparing our results to those calculated within the SMASH model in [16], one can notice a qualitatively different dependence of η/s^{SM} on the temperature. In contrast to the rise of η/s with the temperature drop in the UrQMD cell calculations, SMASH demonstrates almost constant behavior of this ratio within the same temperature range. However, in the latter case the calculations were performed for a fixed baryon chemical potential, whereas in the UrQMD calculations it increases with the cell time t_{cell}. Another reason for deviations is the nonzero strangeness chemical potential in our calculations. Nevertheless, as shown in [16], the ratio η/s increases in SMASH calculations with rise of baryon chemical potential, in accord with our results. Both UrQMD and SMASH indicate that shear viscosity decreases with decreasing temperature. This agreement is not accidental because of the conceptual similarity between UrQMD and SMASH. Further analysis concerning the influence of details of the system's internal dynamics,
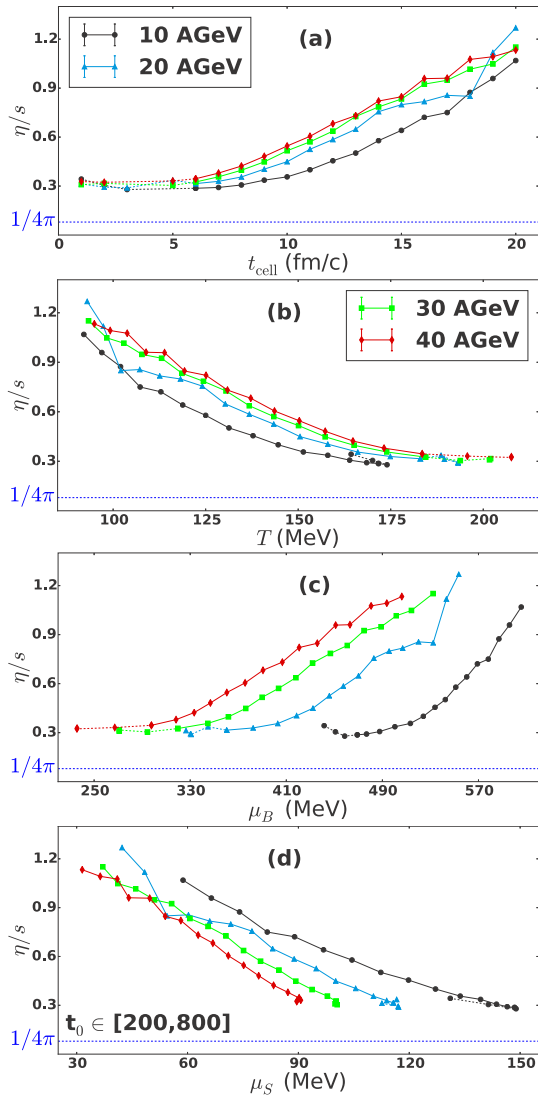
FIG. 10. Shear viscosity to SM entropy ratio η/s_{sm} as functions of (a) time, (b) temperature, (c) baryon chemical potential, and (d) strangeness chemical potential in the UrQMD calculations of central cell of central Au + Au collisions at $E_{lab} = 10A$ GeV (circles), $20A$ GeV (triangles), $30A$ GeV (squares), and $40A$ GeV (diamonds). Lines are drawn to guide the eye.

particularly, the role of lifetimes of resonances, on the η/s ratio can be found in [16].

V. CONCLUSIONS

We have studied the shear viscosity of highly excited nuclear matter produced in the central area of central Au + Au collisions at energies $E_{lab} = 10A$, $20A$, $30A$, and $40A$ GeV. Calculations are done within the UrQMD model. At the first stage, the energy density, the net baryon density, and the net strangeness density are determined for a cubic central cell with volume $V = 125$ fm^3. After that, the obtained values are used as input to the statistical model of an ideal hadron gas to calculate temperature, baryon chemical potential and strangeness chemical potential, as well as entropy density. The extracted values of ε, ρ_B, and ρ_S are used also for initialization of the UrQMD box with periodic boundary conditions to study the relaxation of hot and dense nuclear matter to equilibrium. The Green-Kubo formalism is explored to calculate the shear viscosity.

It is shown that equilibrium in the box is achieved approximately after $t \geqslant 200$ fm/c for all but very high baryon and energy densities, corresponding to the overlap of the nuclei. The influence of initial cutoff time t_0 on momentum correlators is studied. Finally, the shear viscosity and its ratio to entropy density are calculated. We found that, for all four tested energies, η and s in the cell drop with time. Their ratios η/s, however, reach minima about 0.3 at $t \approx 5$ fm/c, irrespective of the bombarding energy. Then the ratios rise to $\eta/s = 1.0$–1.2 at $t = 20$ fm/c. This increase is accompanied by the simultaneous rise of baryon chemical potential and drop of both temperature and strangeness chemical potential in the cell.

[1] E. V. Shuryak, *The QCD Vacuum, Hadrons and Superdense Matter*, Lecture Notes in Physics, Vol. 71 (World Scientific, Singapore, 2004).

[2] L. P. Csernai, J. I. Kapusta, and L. D. McLerran, Phys. Rev. Lett. **97**, 152303 (2006).

[3] P. K. Kovtun, D. T. Son, and A. O. Starinets, Phys. Rev. Lett. **94**, 111601 (2005).

[4] P. Romatschke and U. Romatschke, Phys. Rev. Lett. **99**, 172301 (2007).

[5] A. Muronga, Phys. Rev. C **69**, 044901 (2004).

[6] N. Demir and S. A. Bass, Phys. Rev. Lett. **102**, 172302 (2009).

[7] P. Chakraborty and J. I. Kapusta, Phys. Rev. C **83**, 014906 (2011).

[8] C. Wesp, A. El, F. Reining, Z. Xu, I. Bouras, and C. Greiner, Phys. Rev. C **84**, 054911 (2011).

[9] S. Cremonini, Mod. Phys. Lett. B **25**, 1867 (2011).

[10] J. Noronha-Hostler, J. Noronha, and C. Greiner, Phys. Rev. C **86**, 024913 (2012).

[11] S. Plumari, A. Puglisi, F. Scardina, and V. Greco, Phys. Rev. C **86**, 054902 (2012).

[12] V. Ozvenchuk, O. Linnyk, M. I. Gorenstein, E. L. Bratkovskaya, and W. Cassing, Phys. Rev. C **87**, 064903 (2013).

[13] Iu. A. Karpenko, P. Huovinen, H. Petersen, and M. Bleicher, Phys. Rev. C **91**, 064901 (2015).

[14] Yu.B. Ivanov and A. A. Soldatov, Eur. Phys. J. A **52**, 117 (2016).

[15] J. Rais, K. Gallmeister, and C. Greiner, arXiv:1909.04522.

[16] J. B. Rose, J. M. Torres-Rincon, A. Schäfer, D. R. Oliinychenko, and H. Petersen, Phys. Rev. C **97**, 055204 (2018).

[17] A. Motornenko, L. Bravina, M. I. Gorenstein, A. G. Magner, and E. Zabrodin, J. Phys. G **45**, 035101 (2018).

[18] H. Song and U. Heinz, Phys. Rev. C **78**, 024902 (2008).

[19] S. A. Bass *et al.*, Prog. Part. Nucl. Phys. **41**, 255 (1998).

[20] M. Bleicher *et al.*, J. Phys. G **25**, 1859 (1999).

[21] B. Andersson, G. Gustafson, and B. Nilsson-Almqvist, Nucl. Phys. B **281**, 289 (1987).

[22] M. Tanabashi *et al.* (Particle Data Group), Phys. Rev. D **98**, 030001 (2018).

[23] M. Belkacem *et al.*, Phys. Rev. C **58**, 1727 (1998).

[24] L. V. Bravina, E. E. Zabrodin, S. A. Bass, M. Bleicher, M. Brandstetter, S. Soff, H. Stöcker, and W. Greiner, Phys. Rev. C **62**, 064906 (2000).

[25] M. S. Green, J. Chem. Phys. **22**, 398 (1954).

[26] R. Kubo, J. Phys. Soc. Jpn. **12**, 570 (1957).

[27] L. V. Bravina *et al.*, Phys. Lett. B **434**, 379 (1998).

[28] L. V. Bravina *et al.*, J. Phys. G **25**, 351 (1999).

[29] L. V. Bravina *et al.*, Phys. Rev. C **60**, 024904 (1999).

[30] L. V. Bravina *et al.*, Phys. Rev. C **78**, 014907 (2008).

[31] L. V. Bravina *et al.*, Nucl. Phys. A **661**, 600 (1999).

[32] E. L. Bratkovskaya, W. Cassing, C. Greiner, M. Effenberger, U. Mosel, and A. Sibirtsev, Nucl. Phys. A **675**, 661 (2000).

Calculation of shear viscosity in Au+Au collisions at NICA energies

E Zabrodin[1,2], **M Teslyk**[1,3] ⓘ, **O Vitiuk**[1,3] **and L Bravina**[1,2]

[1] Department of Physics, University of Oslo, PB 1048 Blindern, N-0316 Oslo, Norway
[2] Skobeltsyn Institute of Nuclear Physics, Moscow State University, RU-119991 Moscow, Russia
[3] Taras Shevchenko National University of Kyiv, UA-01033 Kyiv, Ukraine

E-mail: zabrodin@fys.uio.no

Abstract

Shear viscosity of hot and dense nuclear matter, produced in the central zone of central gold-gold collisions at energies of NICA, is calculated within the UrQMD model. Besides the microscopic simulations of heavy ion collisions, the procedure assumes the application of statistical model to determine the temperature and chemical potentials in the system, and study of the relaxation process within the UrQMD box with periodic boundary conditions. The latter is used for calculation of the correlator which enters the Green-Kubo formula for shear viscosity. The fluctuations at early and late stages of the system evolution are studied. Results are compared to predictions of other models.

Keywords: relativistic heavy-ion collisions, microscopic transport model, box calculations, shear viscosity, Green-Kubo formalism

(Some figures may appear in colour only in the online journal)

1. Introduction

Experiments on heavy-ion collisions at relativistic and ultra-relativistic energies are the only means to study the properties of hot and dense nuclear matter in the laboratory. Analyzing the data obtained at RHIC (BNL) physicists came to the conclusion that the created substance possessed the properties of perfect fluid [1–4]. However, it became clear soon that one had to employ the nonzero shear viscosity η for the correct description of differential elliptic flow v_2 of hadrons as function of transverse momentum p_T within the framework of hydrodynamics. Recall, that the absolute minimum for the ratio of η to the entropy density s, η/s, estimated in the AdS-CFT formalism, equals $1/4\pi$ [5] in system of natural units, $c = \hbar = k_B = 1$. Hydrodynamic calculations use a bit higher values to describe the experimental data, i.e. $\eta/s = 0.12$ at

RHIC for Au+Au collisions at $\sqrt{s} = 200\,\text{GeV}$, and 0.20 at LHC (CERN) for Pb+Pb collisions at $\sqrt{s} = 2.76$ TeV [6].

As was pointed out in [7], the ratio η/s reaches minimum in the vicinity of tricritical point for all known substances. It appears that at energies of LHC the phase transition between the quark-gluon plasma (QGP) and hadrons is a smooth crossover. The phase transition QGP−hadrons is expected to be of the first order at much lower energies accessible for beam energy scan (BES) at RHIC and future facilities NICA (JINR) and FAIR (GSI). The search for the tricritical point, where the first order phase transition becomes the second order one, is in the agenda of all experiments planned at the aforementioned accelerators. In the present work we would like to study the shear viscosity and its ratio to entropy density in the midrapidity range of central heavy-ion collisions at energies between $E_{lab} = 10$ and 40 AGeV generated by the microscopic transport model UrQMD [8, 9]. Note, that except of [10], η/s ratio was studied in various models for closed systems with fixed values of energy density and baryon density [11–22]. We are going to extend the results of [10], obtained within the equilibrium approach for calculation

of the entropy density, to the nonequilibrium case. The paper is organized as follows. Determination of shear viscosity by means of Green-Kubo approach is described in section 2. Section 3 presents the basic ingredients of model calculations including the UrQMD model, statistical model (SM) of an ideal hadron gas, and UrQMD box, which is a closed system. Results of our study obtained both with equilibrium and nonequilibrium entropy are discussed in section 4. Conclusions are drawn in section 5.

2. Determination of shear viscosity. Green-Kubo formalism

To determine the shear viscosity one usually employs the Green-Kubo method [23, 24]. It assumes the exponential damping of fluctuations whereas the closed system relaxes to equilibrium. The shear viscosity for the system with volume V and temperature T reads

$$\eta(t_0) = \frac{V}{T} \int_{t_0}^{\infty} dt \, \langle \pi^{ij}(t) \pi^{ij}(t_0) \rangle_t, \qquad (1)$$

where t_0 and t is the initial time and final time, respectively. The correlator in the integrand is

$$\langle \pi^{ij}(t) \pi^{ij}(t_0) \rangle_t = \lim_{t_{\max} \to \infty} \left[\frac{1}{t_{\max}} \int_{t_0}^{t_{\max}} dt' \pi^{ij}(t + t') \pi^{ij}(t') \right]. \qquad (2)$$

It contains the traceless parts of the energy-momentum tensor T^{ij}

$$\pi^{ij}(t) = \frac{1}{V} \sum_{k=1}^{N_{part}} \frac{p_k^i(t) p_k^j(t)}{E_k(t)}. \qquad (3)$$

Here $p_k^{i(j)}(t)$ and $E_k(t)$ denote the $i(j)$-th components of momentum and energy of k-th particle. The sum in Eq.(3) runs over all particles. The correlator (2) should drop exponentially with time in the vicinity of equilibrium, therefore, it can be approximated by the exponential

$$\langle \pi^{ij}(t) \pi^{ij}(t_0) \rangle_t = \langle \pi^{ij}(t_0) \pi^{ij}(t_0) \rangle \exp\left(-\frac{t - t_0}{\tau} \right), \qquad (4)$$

containing the effective relaxation time τ. Thus, to find the shear viscosity one has to determine both T and τ, because Eq.(1) is reduced to

$$\eta(t_0) = \tau \frac{V}{T} \langle \pi^{ij}(t_0) \pi^{ij}(t_0) \rangle. \qquad (5)$$

Calculation of these parameters is explained in the next section.

3. Model setup

From the description of the method of shear viscosity extraction it becomes clear that we have to organize several steps to complete our task. First, while running the transport string model for heavy-ion collisions at given energy, we should determine the volume to search for local equilibrium.

Previous studies reveal [25–28] that central cubic cell with volume $V = 5 \times 5 \times 5 = 125$ fm^3 is well suited for our analysis. But the cell is an open system and particles can leave it freely. The initially hot and dense fireball quickly expands, and its bulk characteristics are promptly changing. In order to investigate how far is the matter in the cell from local equilibrium one has to extract three basic parameters, namely, energy density ε, net baryon density ρ_B, and net strangeness density ρ_S, and insert it as an input to the statistical model of an ideal hadron gas. If the abundances of hadronic species and their energy spectra in the microscopic model calculations are close to those given by the SM, we can conclude that the matter is in the vicinity of chemical and thermal equilibrium. This procedure enables us to determine the temperature T, baryochemical potential μ_B, and the strangeness chemical potential μ_S. Finally, the behavior of the correlator $\langle \pi^{ij}(t) \pi^{ij}(t_0) \rangle_t$ in a system with fixed parameters ε, ρ_B, ρ_S should be studied. This can be done with the help of box with periodic boundary conditions to keep key system parameters constant. At this stage we get the value of shear viscosity at given T, μ_B, μ_S. The basic principles of the three stages are presented below.

3.1. Microscopic transport model

The UrQMD is formulated as Monte-Carlo event generator allowing to perform various analyzes of the measurable quantities by introducing all necessary experimental cuts. The model is designed to describe hadronic, hadron-nucleus, and nucleus-nucleus collisions in a broad energy range. In the hadronic sector UrQMD treats the production of new particles via formation and fragmentation of specific colored objects, strings. Strings are uniformly stretched, with constant string tension $\kappa \approx 1$ GeV/fm, between the quarks, diquarks and their antistates. The excited string is fragmenting into pieces via the Schwinger-like mechanism of $q\bar{q}$-pair production, and the produced hadrons are uniformly distributed in the rapidity space.

In contrast to models which rely on the color exchange mechanism of string excitation, like QGSM [29, 30] or NEXUS [31], the UrQMD model employs the longitudinal excitation of strings. Here the string masses arise from the momentum transfer. Tables of the experimentally available information, like hadron cross sections, resonance widths, their decay modes, and so forth are implemented. In case of lacking the information, the model employs the detailed balance considerations, the one-boson exchange model, and isospin symmetry conditions. The propagation of particles is governed by Hamilton equation of motion. Newly produced hadrons can interact further only after a certain formation time. The Pauli principle is taken into account via the blocking of the final state, if the outgoing phase space is occupied.

3.2. Statistical model of an ideal hadron gas

If the system is in thermal and chemical equilibrium, its macroscopic characteristics are fully determined by particle

distribution functions

$$f(p, m_i) = \left[\exp\left(\frac{\sqrt{p^2 + m_i^2} - \mu_B B_i - \mu_S S_i}{T} \right) \pm 1 \right]^{-1},$$

(6)

where p and m_i is the momentum and the mass of the hadron species i, respectively. Sign $-$ stands for bosons and $+$ for fermions. One has to know just three parameters, namely, temperature T and chemical potentials assigned to the conserved charges, i.e. baryon chemical potential μ_B and strangeness chemical potential μ_S. Chemical potential of i-th hadron depends on its baryon and strangeness content, $\mu_i = B_i \mu_B + S_i \mu_S$. The dependence on chemical potential μ_Q associated with electric charge is disregarded here, because μ_Q is usually an order of magnitude weaker compared to μ_B and μ_S. Then, the expressions for particle number density n_i, energy density ε_i and pressure P read

$$n_i = \frac{g_i}{2\pi^2} \int_0^\infty p^2 f(p, m_i) dp$$

(7)

$$\varepsilon_i = \frac{g_i}{2\pi^2} \int_0^\infty p^2 \sqrt{p^2 + m_i^2} \, f(p, m_i) dp$$

(8)

$$P = \frac{g_i}{2\pi^2} \int_0^\infty p^2 dp \; \frac{p^2}{3(p^2 + m_i^2)^{1/2}} f(p, m_i).$$

(9)

with g_i being the spin-isospin degeneracy factor. The entropy density s_i can be calculated either from the Gibbs thermodynamic identity

$$T s_i = \varepsilon_i + P_i - \mu_B \rho_{B_i} - \mu_S \rho_{S_i},$$

(10)

or via the distribution function

$$s_i = -\frac{g_i}{2\pi^2} \int_0^\infty f(p, m_i)[\ln f(p, m_i) - 1] \, p^2 dp,$$

(11)

The total energy density ε, baryon density ρ_B and strangeness density ρ_S calculated microscopically within the cell at time t are inserted into the set of nonlinear equations

$$\varepsilon = \sum_i \varepsilon_i^{SM}(T, \mu_B, \mu_S),$$

(12)

$$\rho_B = \sum_i B_i \cdot n_i^{SM}(T, \mu_B, \mu_S),$$

(13)

$$\rho_S = \sum_i S_i \cdot n_i^{SM}(T, \mu_B, \mu_S).$$

(14)

to determine temperature T, baryon chemical potential μ_B and strangeness chemical potential μ_S. After that all characteristics of the system in equilibrium are known and particle spectra can be compared with those obtained from microscopic model calculations.

### 3.3. Box for simulation of infinite nuclear matter

The standard choice for such a simulation is a cubic box with periodic boundary conditions [32–34] to ensure the energy and momentum conservation. If one particle leaves the box, another particle, fully identical to the first one, enters the box from the opposite side. The box should be neither too big nor too small, e.g. $V = 10 \times 10 \times 10 = 1000$ fm^3 [32] or

$V = 5 \times 5 \times 5 = 125$ fm^3 [33]. The energy density ε, the net baryon density ρ_B, and the net strangeness density ρ_S are fixed at the initial stage. Recall, that for the infinite nuclear matter the net strangeness is zero, but for the central cell in relativistic heavy-ion collisions, which is an open system, ρ_S can differ from zero [25, 27]. In case of $\rho_S = 0$ the initial configuration in the box consists of protons and neutrons uniformly distributed in the configuration space. Their momenta are then rescaled to get the required energy density. If $\rho_S \neq 0$ certain admixture of kaons can be added. When the system is prepared, hadrons start to interact, and one can follow the microscopic model calculations to trace the system evolution and study the relaxation of hadron-string matter in the box to equilibrium.

4. Results

A bit more than 50.000 Au+Au collisions were generated at each of four bombarding energies. Figures 1(a)–(c) shows energy density, net baryon density, and net strangeness density obtained from the microscopic calculations in the central cell at times between 1 and 20 fm/c. Within first few fermiseconds the colliding nuclei fully overlap. This moment corresponds to highest energy density and baryon density in the fireball. The fireball expands, and both characteristics drop. Strangeness demonstrates another behavior. It is negative for all four energies. After reaching minimum, ρ_S is relaxing to zero at late times. This behavior is explained by domination of baryons over antibaryons in the cell. Therefore, according to [25–28], positive kaons can leave the cell earlier than negative kaons because of the smaller interaction cross sections, thus maintaining the negative though small net strangeness. Inserting the values of $\{\varepsilon, \rho_B, \rho_S\}$ as an input in the SM we obtain $\{T, \mu_B, \mu_S\}$ corresponding to equilibrated ideal hadron gas. Evolutions of these parameters are shown in figures 1(d)–(f). Since the matter in the cell at the very beginning is far from the equilibrium, one should treat the SM parameters obtained for earlier times with great care. Large baryon and energy densities observed at $t \leqslant 5$ fm/c are caused by interpenetration of two Lorentz-contracted nuclei, thus leading to very high temperatures of the hadron gas. Chemical and thermal equilibrium of nuclear matter in microscopic calculations in this energy range takes about 6-8 fm/c. After this time, as seen in figure 1(d), the temperature obtained at all four energies sit on the top of each other. Both chemical potentials tend to rise with decreasing energy of the collisions. However, μ_B in all cells increases with time, whereas μ_S decreases.

We are ready now to start the box calculations. Figure 2 shows correlators defined by equation (1) calculated for all four collision energies. The input data again are $\varepsilon, \rho_B, \rho_S$ extracted from the central cell of Au+Au central collisions at times 1, 3, 6, 9, 12, 15, 18, and 20 fm/c after the beginning of the collision. The results of the box calculations are shown for times $t_{box} \geqslant 300$ fm/c, which are typical relaxation times of hot and dense nuclear matter in the box [33]. All correlators
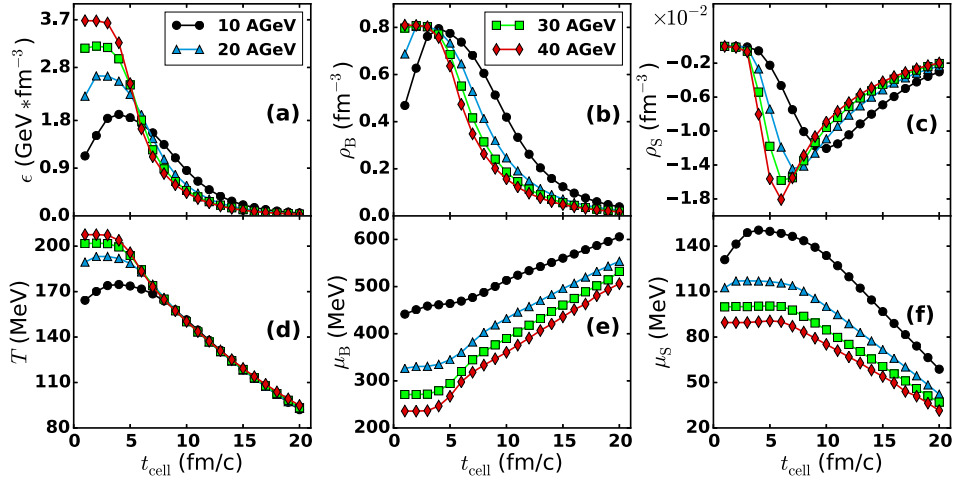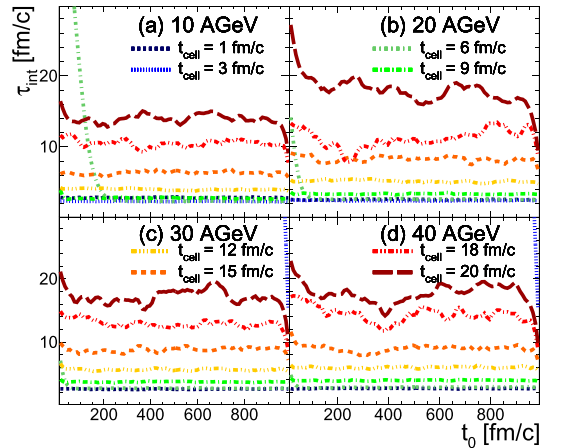
Figure 1. Time evolution of (a) energy density ε, (b) net baryon density ρ_B^{net}, (c) net strangeness density ρ_S^{net}, (d) temperature T_{SM}, (e) baryon chemical potential μ_B, and (f) strangeness chemical potential μ_S in the central cell with $V = 125$ fm^3 in central Au+Au collision calculated within UrQMD at energies $E_{lab} = 10$ AGeV (circles), 20 AGeV (triangles), 30 AGeV (squares), and 40 AGeV (diamonds). Lines are drawn to guide the eye.
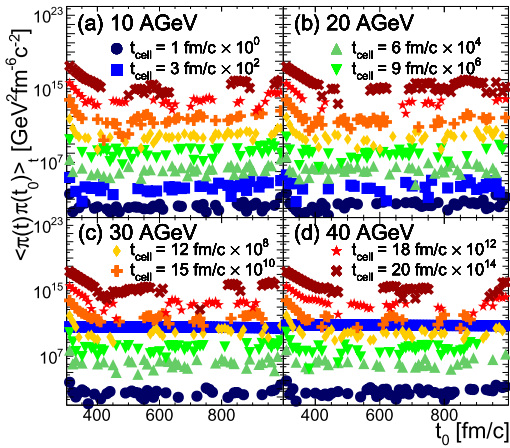
Figure 2. Correlators $\langle \pi(t)\pi(t_0)\rangle_t$ for initial cutoff time $t_0 = 300$ fm/c in the UrQMD box calculations. Initial conditions for the boxes are taken from the central cell with $V = 125$ fm^3 of Au+Au collisions at (a) $E_{lab} = 10$ AGeV, (b) 20 AGeV, (c) 30 AGeV and (d) 40 AGeV at times $t = 1, 3, 6, 9, 12, 15, 18, 20$ fm/c. Each distribution is multiplied by its own factor 10^n.

Figure 3. Relaxation time $\tau_{int}(t_0)$ for the collision energies (a) $E_{lab} = 10$ AGeV, (b) 20 AGeV, (c) 30 AGeV, and (d) 40 AGeV for the cell times $t_{cell} = 1, 3, 6, 9, 12, 15, 18, 20$ fm/c in the UrQMD box calculations.

reveal exponential falloff with time in accordance with equation (5). For few of them, corresponding to early cell times, the relaxation rates are significantly slower compared to those corresponding to late times. One can see such behavior in figure 2(c) and (d) for calculations with initial conditions similar to those at $t = 3$ fm/c in the central cell of central Au+Au collisions at $E_{lab} = 30$ and 40 AGeV. This occurs because of initialization of one (or two) very ultra-relativistic kaons. It takes quite long time to redistribute their

energy and momenta among other particles in the box. The correlators appear to rise at late times. These momentum correlations arise because the UrQMD forces decay of all strongly decaying resonances at the end of the box calculations. Figure 3 displays the relaxation time τ_{int}, determined by means of equation (2), as function of the initial cutoff time t_0. The relaxation takes a longer period for t_0 shorter than 200 fm/c and vanishes for $t_0 \geqslant 900$ fm/c. For the initial times within the interval $200 \leqslant t_0 \leqslant 900$ fm/c the relaxation time is constant, except for very early cell times.
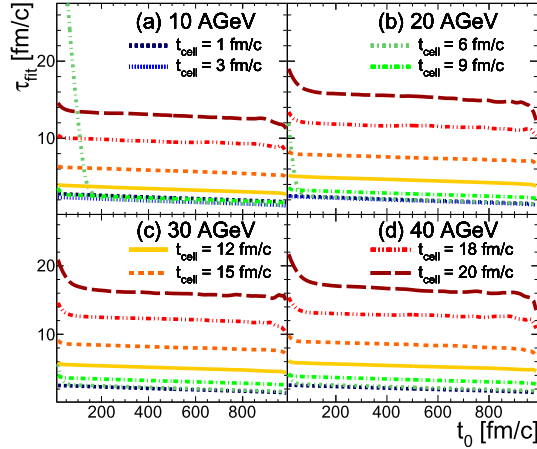
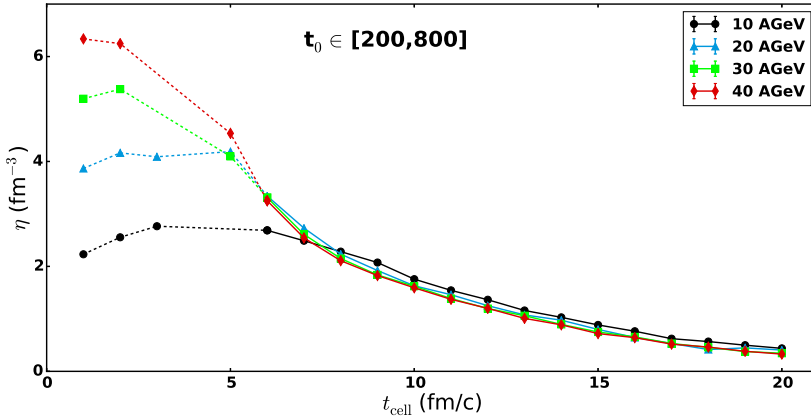**Figure 4.** The same as figure 3 but for relaxation time $\tau_{\mathrm{Fit}}(t_0)$.

Figure 5. Shear viscosity $\eta(t_{\mathrm{cell}})$ of hadrons in the central cell of central Au+Au collisions at (a) $E_{lab} = 10$ AGeV, (b) 20 AGeV, (c) 30 AGeV, and (d) 40 AGeV within the UrQMD box calculations. Lines are drawn to guide the eye.

The behavior of τ_{fit}, obtained after fitting our results to equation (3), is presented in figure 4. It is very similar to that of τ_{int}, but it has no stochastic oscillations. Note that the distributions demonstrates some slope in the plateau region at $t_0 \geqslant 200$ fm/c as compared to the results shown in figure 3. This slope may somehow influence the determination of η values. Therefore, we average the value of $\tau_{\mathrm{int\,(fit)}}$ over the plateau in order to reduce statistical errors. Large values of the relaxation time $\tau_{\mathrm{int(fit)}}$ for some early cell times t_{cell} are explained by the abundant production of new particles and their rescattering in very hot and dense baryon-rich matter at the very beginning of the collision. Additional time delay is caused by the aforementioned single negative kaons. Combination of these factors leads to the extension of the box calculations up to 2000-2500 fm/c.

Results, obtained after averaging over the plateau, are displayed in figure 5. Note that the statistical errors are smaller than the symbol sizes. One can see that shear viscosity distributions for all four energies converge to each other at $t \approx 6$ fm/c. The matter in the cell becomes very dilute at the late times, and η drops almost to zero. This behavior is almost identical to the decrease of the cell temperatures seen in figure 1(d). Recall that the chemical potentials of net baryon charge and net strangeness are different, as shown in figure 1(e)-(f). It means that shear viscosity is predominantly determined by the temperature and not by μ_B and μ_S. The entropy density, however, does depend on both temperature and chemical potentials.

To show this we present in figure 6 the dependencies of ratio η/s on (a) time, (b) temperature, (c) baryon chemical potential, and (d) strangeness chemical potential for all four reactions in question.

The nonequilibrium stages of the system evolution are shown by dashed lines. We see that this ratio decreases with
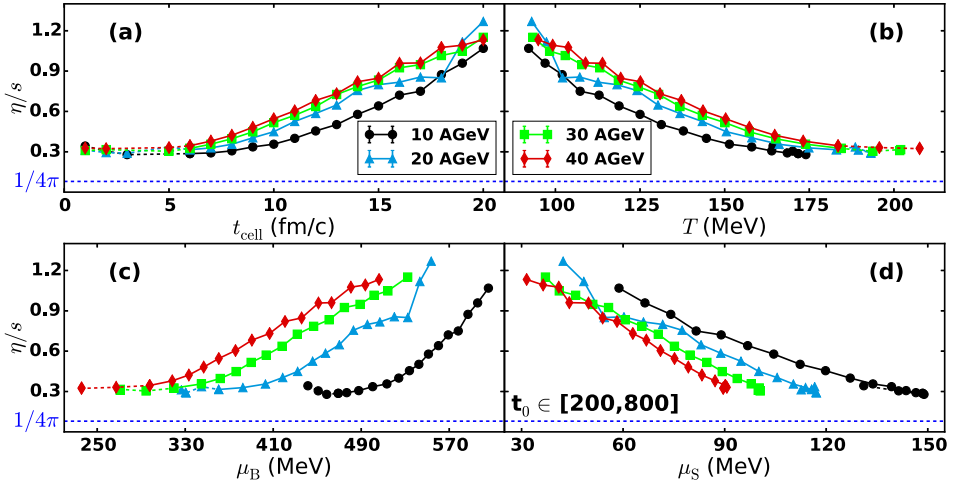
Figure 6. Shear viscosity to entropy ratio η/s^{sm} as function of (a) time t, (b) temperature T, (c) baryon chemical potential μ_B, and (d) strangeness chemical potential μ_S in the UrQMD calculations of central cell of central Au+Au collisions at $E_{lab} = 10$ AGeV (circles), 20 AGeV (triangles), 30 AGeV (squares), and 40 AGeV (diamonds). Lines are drawn to guide the eye.
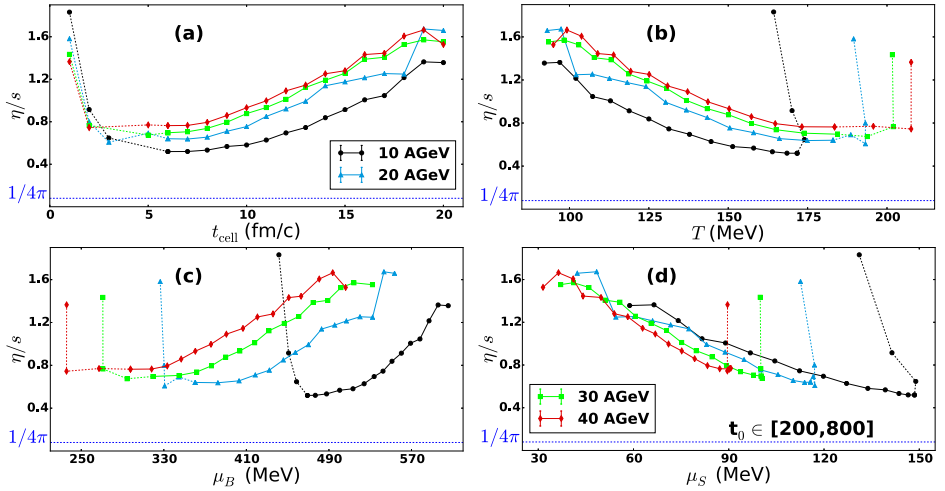
Figure 7. The same as figure 6 but for ratio of shear viscosity to nonequilibrium entropy density, η/s^{noneq}.

increase of the bombarding energy. Since the shear viscosity is almost the same, this circumstance implies the drop of entropy density with rising E_{lab}. It can be explained by faster loss of energy density in the central cell in case of more energetic collisions. Also, no distinct minima are observed. Recall, however, that we used the entropy density, calculated for the hadron gas in thermal and chemical equilibrium, even for the early stages of the collision when the matter in the cell was far from equilibrium. Obviously, the entropy density of nonequilibrated system should be lower than that of the equilibrated one. To estimate the nonequilibrium entropy, we insert in Eq. (11) instead of the equilibrium distribution functions (6)

another ones provided by the hadron momentum distributions

$$f_i(p) = \frac{(2\pi)^3}{V g_i} \frac{dN_i}{d^3 p} \qquad (15)$$

It is worth noting that the temperature at nonequilibrium stage is determined as average of partial temperatures of hadron species. Time evolution of η/s^{noneq} in the cell together with its dependencies on temperature, on baryon chemical potential, and on strangeness chemical potential are shown in figure 7. Here the minima for all four energies are clearly seen. This occurs at time $t \approx 5 - 6$ fm/c corresponding to maximum baryon density in the system. The lower the

bombarding energy, the deeper the minimum in of η/s distribution. The study should be extended to lower energies in order to see where the ratio of shear viscosity to entropy density will stop to decrease. We are in the energy region where the equation of state (EOS) is expected to be changed because of the formation of non-hadronic objects, quark-gluon strings.

5. Conclusions

The self-consistent procedure for determination of shear viscosity and its ratio to entropy density within the microscopic model calculations is developed. It includes three steps. First, we define the volume in A + A collisions to look for the local equilibrium. This is a very important condition, because the Green-Kubo formalism employed for determination of shear viscosity implies the relaxation of out-of-equilibrium matter to the equilibrated state. The central cubic cell with volume $V = 125$ fm^3 is well suited for our analysis. Second, we extract the energy density, net baryon density, and net strangeness density out of the tested volume. The procedure is repeated with the time step $\Delta t = 1$ fm/c. The extracted values are inserted into a system of non-linear equations of the statistical model of an ideal hadron gas with essentially the same number of degrees of freedom, as in the microscopic model. This allows one to determine temperature, baryon chemical potential, and strangeness chemical potential in the tested volume in case the hadron yields and energy spectra, calculated micro- and macroscopically, are close to each other. Finally, the values of T, μ_B, μ_S are used to initialize the box with periodic boundary conditions in the framework of the same microscopic transport model. Here the Green-Kubo formalism is applied to determine η, ratio η/s, and so forth.

The developed procedure was used to study the shear viscosity of hot and dense nuclear matter in the central zone of central gold-gold collisions at energies $E_{lab} = 10$, 20, 30 and 40 AGeV, accessible for BES, NICA, and FAIR facilities. For calculations we employ the UrQMD model. We found that, for all four tested energies, the temperatures and shear viscosities are very close to each other after 5-6 fm/c. Both T, η and s in the cell drop with time, whereas the ratios η/s, however, reach minima at $t \approx 5$ fm/c, irrespective of the bombarding energy. Then the ratios rise until the very late stages of the system evolution. The minima in η/s become more pronounced if the nonequilibrium entropy density is used. The rise of η/s is accompanied by the simultaneous increase of baryon chemical potential and decrease of both temperature and strangeness chemical potential in the cell.

Acknowledgments

ORCID iDs

M Teslyk ⦿ https://orcid.org/0000-0001-6311-4679

References

[1] BRAHMS Collaboration, Arsene I *et al* 2005 *Nucl. Phys.* A **757** 1
[2] PHOBOS Collaboration, Back B B *et al* 2005 *Nucl. Phys.* A **757** 28
[3] STAR Collaboration, Adams J *et al* 2005 *Nucl. Phys.* A **757** 102
[4] PHENIX Collaboration, Adcox K *et al* 2005 *Nucl. Phys.* A **757** 184
[5] Kovtun P, Son D T and Starinets A O 2005 *Phys. Rev. Lett.* **94** 111601
[6] Schenke B, Tribedy P and Venugopalan R 2012 *Phys. Rev. Lett.* **108** 252301
    Schenke B, Tribedy P and Venugopalan R 2012 *Phys. Rev.* C **86** 034908
[7] Csernai L P, Kapusta J I and McLerran L D 2006 *Phys. Rev. Lett.* **97** 152303
[8] Bass S A *et al* 1998 *Prog. Part. Nucl. Phys.* **41** 255
[9] Bleicher M *et al* 1999 *J. Phys. G: Nucl. Part. Phys.* **25** 1859
[10] Teslyk M *et al* 2020 *Phys. Rev.* C **101** 014904
[11] Muronga A 2004 *Phys. Rev.* C **69** 044901
[12] Demir N and Bass S A 2009 *Phys. Rev. Lett.* **102** 172302
[13] Chakraborty P and Kapusta J I 2011 *Phys. Rev.* C **83** 014906
[14] Wesp C *et al* 2011 *Phys. Rev.* C **84** 054911
[15] Cremonini S 2011 *Mod. Phys. Lett.* B **25** 1867
[16] Noronha-Hostler J *et al* 2012 *Phys. Rev.* C **86** 054902
[17] Ozvenchuk V *et al* 2013 *Phys. Rev.* C **87** 064903
[18] Karpenko Iu A *et al* 2015 *Phys. Rev.* C **91** 064901
[19] Ivanov Yu B and Soldatov A A 2016 *Eur. Phys. J.* A **52** 117
[20] Rais J, Gallmeister K and Greiner C 2019 *The shear viscosity to entropy density ratio in Hagedorn states* arXiv:1909.04522 [hep-ph]
[21] Rose J B *et al* 2018 *Phys. Rev.* C **97** 055204
[22] Motornenko A *et al* 2018 *J. Phys. G: Nucl. Part. Phys.* **45** 035101
[23] Green M S 1954 *J. Chem. Phys.* **22** 398
[24] Kubo R 1957 *J. Phys. Soc. Japan* **12** 1957
[25] Bravina L V *et al* 1998 *Phys. Lett.* B **434** 379
[26] Bravina L V *et al* 1999 *J. Phys. G: Nucl. Part. Phys.* **25** 351
[27] Bravina L V *et al* 1999 *Phys. Rev.* C **60** 024904
[28] Bravina L V *et al* 2008 *Phys. Rev.* C **78** 014907
[29] Amelin N S and Bravina L V 1990 *Sov. J. Nucl. Phys* **51** 133
[30] Bleibel J, Bravina L V and Zabrodin E E 2016 *Phys. Rev.* D **93** 114012
[31] Drescher H J *et al* 2001 *Phys. Rept* **350** 93
[32] Belkacem M *et al* 1998 *Phys. Rev.* C **58** 1727
[33] Bravina L V *et al* 2000 *Phys. Rev.* C **62** 064906
[34] Bratkovskaya E L *et al* 2000 *Nucl. Phys.* A **675** 661

III

Shear viscosity of nucleons and pions in heavy-ion collisions at energies of NICA

E Zabrodin[1,2]**, M Teslyk**[1,3]**, O Vitiuk**[1,3] **and L Bravina**[1,2]

[1] Department of Physics, University of Oslo, PB 1048 Blindern, N-0316 Oslo, Norway
[2] Skobeltsyn Institute of Nuclear Physics, Moscow State University, RU-119991 Moscow, Russia
[3] Taras Shevchenko National University of Kyiv, UA-01033 Kyiv, Ukraine

E-mail: `zabrodin@fys.uio.no`

Abstract. The shear viscosity is calculated microscopically via the Green-Kubo relation for the series of snapshots in the central region in an ongoing relativistic collision simulated via the UrQMD framework for various bombarding energies in the anticipated NICA experiments. In previous works the shear viscosity was calculated as function of temperature, while the chemical potential of baryon charge was kept constant. In present work we extract, in various time windows, the average energy density, the net baryon density and the small though nonzero net strangeness density. By fitting these parameters to statistical model, one can get temperature and both chemical potentials of baryon charge and strangeness. Simultaneously, these parameters are used as input to simulations in a box, again within the UrQMD transport model. The autocorrelations in time of the energy stress tensor are extracted, and subsequently via the Green-Kubo identities the shear viscosity coefficient of that equilibrium hadronic system is obtained. Then we calculate partial viscosity both for nucleons and pions for five collision energies from $E_{lab} = 5$ to 40 AGeV. It appears that substantial part of the contribution to total shear viscosity of the system comes out from pion-nucleon and other correlators.

1. Introduction

The main aim of experiments on heavy-ion collisions at ultrarelativistic energies is the study of properties of a new state of matter called quark-gluon plasma (QGP). - For present status of the field see, e.g., [1] and references therein. - Nowadays the QGP is considered as an almost perfect strongly interacting fluid rather than ideal gas of non-interacting partons. When the hot fireball with QGP expands it experiences phase transition to hadronic matter at a certain transition temperature. The order of this transition depends on the energy of the collision. Analysis of experimental data on Au+Au and Pb+Pb collisions at energies of $\sqrt{s_{NN}} = 200$ GeV at RHIC and $\sqrt{s_{NN}} = 2.76$ and 5.02 TeV at LHC indicates that the matter experiences a smooth crossover. In contrast, at intermediate energies, say, above few GeV, the deconfinement phase transition should be of first order. The curve of the first order phase transition on the QCD phase diagram ends up at the tricritical point, where the phase transition becomes of the second order. Exact position of the tricritical point should be determined experimentally. Its search for is among the primary goals of experiments at beam energy scan (BES) at RHIC, SPS at CERN, and at coming in a nearest future FAIR and NICA facilities.

Shear viscosity, η, is a promising signal to probe the tricritical point on the phase diagram because its ratio to entropy density, η/s, reaches there minimum for all known substances [2].

It is interesting to study also how close is this ratio for hot and dense nuclear matter to the absolute limit, estimated within the AdS/CFT correspondence as $1/(4\pi)$ [3]. These issues were studied by means of microscopic models in, e.g., [4–15]. Usually, the temperature dependence of η/s was investigated at fixed baryochemical potential and zero chemical potential. In our analysis we will use technique developed in [16–18] which permits us to study the evolution of the η/s ratio during the course of heavy-ion collision as a function of temperature T, baryon chemical potential μ_B, and strangeness chemical potential μ_S simultaneously.

2. Technique and method

The Green-Kubo formalism [19, 20] is employed to determine the shear viscosity in the system. Its important assumption is that the closed system, which is initially out of equilibrium, should evolve towards the equilibrated state. Then, in system of natural units $c = \hbar = k_B$ the shear viscosity reads

$$\eta\left(t_0\right) = \frac{V}{T} \int_{t_0}^{\infty} \langle \pi\left(t\right) \pi\left(t_0\right) \rangle_t \mathrm{d}t \tag{1}$$

Here V and T is the volume and the temperature of the system, respectively, t_0 is initial time and t is the final time. The correlator in equation (1) can be calculated as

$$\langle \pi\left(t\right) \pi\left(t_0\right) \rangle_t = \lim_{t_{\max} \to \infty} \frac{1}{t_{\max} - t_0} \int_{t_0}^{t_{\max}} \pi^{ij}\left(t + t'\right) \pi^{ij}\left(t'\right) \mathrm{d}t' \tag{2}$$

$$\approx \langle \pi\left(t_0\right) \pi\left(t_0\right) \rangle \exp\left(-\frac{t - t_0}{\tau}\right) , \tag{3}$$

with τ being the effective relaxation time. Finally, the tensor $\pi^{ij}(t)$ is the non-diagonal part of the stress energy tensor T^{ij}

$$\pi^{ij}\left(t\right) = \frac{1}{V} \sum_{k=1}^{particles} \frac{p_k^i\left(t\right) p_k^j\left(t\right)}{E_k\left(t\right)} , \tag{4}$$

where E_k and $p_k^{i(j)}$ is the energy and $i(j)$ components of momentum of particle k. Inserting equation (3) into equation (1) we get

$$\eta\left(t_0\right) = \frac{V\tau}{T} \langle \pi\left(t_0\right) \pi\left(t_0\right) \rangle , \tag{5}$$

indicating that one needs to determine the correlator $\langle \pi(t_0)\pi(t_0) \rangle$, the relaxation time, and the temperature to find the shear viscosity.

We employ the well-known UrQMD model [21, 22] for our calculations. The model successfully describes various features of hadronic and nuclear interactions in a broad energy range. The bombarding energy of central Au+Au collisions studied in our paper varies from $E_{lab} = 5$ to 40 GeV, accessible for NICA. Because even in most central heavy-ion collisions the net baryon charge is not distributed uniformly within the whole volume, we opted for the central cubic cell with volume $V = 5 \times 5 \times 5 = 125$ fm^3. Previous studies [23–28] revealed that such cell is well suited for the investigation of the relaxation process in hot and dense nuclear matter. - Recall, that we have to determine temperature of the (sub)system, and there is no rigorous definition of the temperature for the out-of-equilibrium systems. - To do this, we employ the formalism developed in [23, 25]. Namely, one has to extract values of the energy density, the net baryon density, and the net strangeness out of the microscopic calculations and insert it then to system

of nonlinear equations provided by the statistical model (SM) of ideal hadron gas

$$\varepsilon^{mic} = \sum_i \epsilon_i^{SM}(T, \mu_B, \mu_S) \tag{6}$$

$$\rho_B^{mic} = \sum_i B_i\, n_i^{SM}(T, \mu_B, \mu_S) \tag{7}$$

$$\rho_S^{mic} = \sum_i S_i\, n_i^{SM}(T, \mu_B, \mu_S)\ , \tag{8}$$

where both partial number density n_i^{SM} and energy density ϵ_i^{SM} of hadron specie "i" are just functions of temperature T and both chemical potentials, μ_B and μ_S. Total chemical potential of specie "i" depends on its baryon B_i and strangeness S_i content

$$\mu_i = B_i\mu_B + S_i\mu_S\ . \tag{9}$$

In the statistical model of ideal hadron gas the values of ϵ_i^{SM}, n_i^{SM}, and partial pressure P_i^{SM} are derived via the distribution function $f(p, m_i)$ as

$$n_i^{SM} = \frac{g_i}{(2\pi)^3}\int_0^\infty f(p, m_i) d^3p \tag{10}$$

$$\epsilon_i^{SM} = \frac{g_i}{(2\pi)^3}\int_0^\infty \epsilon_i f(p, m_i) d^3p \tag{11}$$

$$P_i^{SM} = \frac{g_i}{(2\pi)^3}\int_0^\infty \frac{p^2}{3\epsilon_i} f(p, m_i) d^3p \tag{12}$$

$$f(p, m_i) = \left[\exp\left(\frac{\epsilon_i - \mu_i}{T}\right) \pm 1\right]^{-1}\ . \tag{13}$$

Here g_i is the spin-isospin degeneracy factor, p is the hadron momentum, $\epsilon_i = \sqrt{p^2 + m^2}$ is the hadron energy, and m is its mass. Sign $+$ in equation (13) stands for fermions, and sign $-$ is for bosons. Comparing the particle yields and energy spectra, obtained in microscopic model calculations, to those given by the SM we can find the beginning of equilibrium and determine, therefore, values of T, μ_B, and μ_S. Then, we have to determine (i) the effective relaxation time τ and (ii) the correlator $\langle \pi(t_0)\pi(t_0)\rangle$. This can be done by studying the relaxation process in the UrQMD box with periodic boundary conditions [29, 30], which preserve the energy density and the net quark content in the box. To initialize the box with volume $10 \times 10 \times 10 = 1000$ fm^3 we use again the values of $\varepsilon, \rho_B, \rho_S$ extracted from the cell. Net baryon density is provided by neutrons and protons, taken in equal proportion, whereas the nonzero strangeness density can be generated by admixture of Lambdas or kaons. Relaxation process in the box takes much longer times compared to the cell calculations [29, 30], therefore we run the calculations until $t_{box} = 1000$ fm/c.

3. Results
Results of our calculations of the shear viscosity and the ratio η/s in the central cell of central gold-gold collisions at $E_{lab} = 5, 10, 20, 30$ and 40 AGeV can be found elsewhere [16–18]. In present paper we would like to study partial contributions of nucleons and pions to the total shear viscosity. To do this we replace the summation over all particles in equation (4) to the

summation over either all nucleons or all pions in the system. For each of 5 bombarding energies, the central cell parameters were extracted at times from $t = 1$ fm/c up to $t = 20$ fm/c with the time step $\Delta t = 1$ fm/c.

Figure 1 displays the partial shear viscosity of nucleons η_N as a function of initial time t_0. For small values of t_0 and for early times in the cell corresponding to the overlap of colliding nuclei, the values of η_N are large. They quickly drop to an approximately constant value for $200 \leq t_0 \leq 800$ fm/c. In order to reduce statistical errors, therefore, we averaged the values of η_N over the plateau $t_0 \in [200, 800]$ fm/c. Another interesting feature is the decrease of η_N for all times with increasing bombarding energy, whereas pions demonstrate the opposite trend.
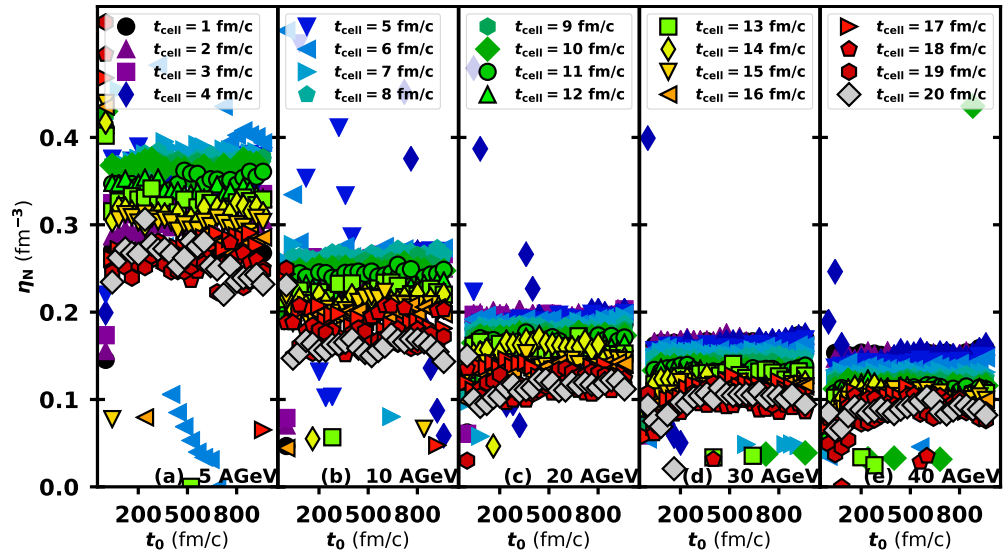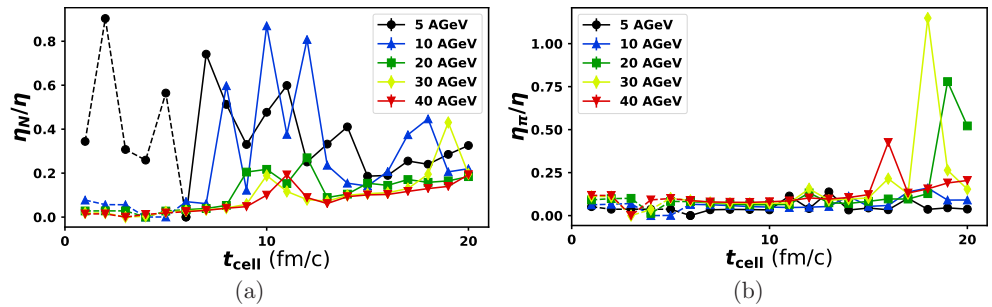

Figure 1. Shear viscosity of nucleons $\eta_N(t_0)$ for five collision energies from 5 AGeV to 40 AGeV and for the cell times $t \in [1, 20]$ fm/c.

The total shear viscosity of nuclear matter calculated within the aforementioned initial time interval is shown in figure 2. For early cell conditions the total η seems to increase with rising energy. - Note, however, that the matter is out-of-equilibrium here. Therefore, results for the very beginning of nuclear collisions should be treated with great care. - At $t \geq 6$ fm/c, when the matter approaches equilibrium, all curves $\eta(t_{cell})$ sit on the top of each other.

Figure 3 depicts the partial contributions of nucleons and pions to the total shear viscosity. Results concerning the non-equilibrium stages are shown by dashed lines. The ratios of η_N/η and η_π/η are quite peculiar. At lower bombarding energies, $E_{lab} = 5$ and 10 AGeV, the contribution of nucleons, which dominate the particle spectrum, is more than 50% for early times of the collision. It drops to 15-25% at the late stages. For higher energies, the nucleon contribution to η does not exceed 10-15%. Pions, as seen in figure 3, make rather modest though stable contribution at any times for all considered energies. Their part does not exceed 10-15% of total η. Where is the missing 60%? It would be interesting, therefore, to study the role of $\pi - N$ correlators, as well as resonances, in the formation of shear viscosity of hadrons.
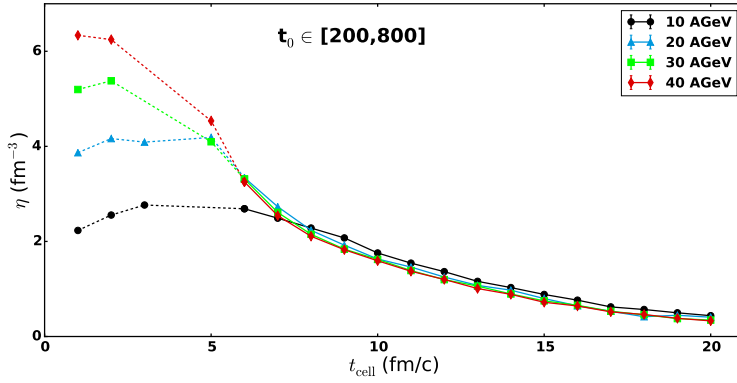
Figure 2. Shear viscosity of hadrons as function of time in the central cell in gold-gold collisions at energies from 10 AGeV to 40 AGeV.

Figure 3. Time evolution of the ratio of shear viscosity of nucleons (a) and pions (b) to total shear viscosity in the cell for Au+Au collisions at energies from 5 AGeV to 40 AGeV.

4. Conclusions

The UrQMD model is employed to study the partial shear viscosity of nucleons and pions in the central zone of central Au+Au collisions at energies between $E_{lab} = 5$ and 40 AGeV accessible for NICA. The self-consistent procedure to determine η at temperatures and chemical potentials corresponding to those in heavy-ion collisions is developed. It is based on (i) application of the statistical model to determine temperature T, baryon chemical potential μ_B, and strangeness chemical potential μ_S, and (ii) UrQMD box calculations to determine the relaxation rates and correlators, employed further within the Green-Kubo formalism to calculate η.

The developed procedure was used to calculate partial shear viscosity of nucleons and pions based on nucleon-nucleon and pion-pion correlators. At lower energies the shear viscosity of nucleons is about 50-70% of total η right after beginning of the equilibrium. At late stages of the matter evolution it drops to 15-25%. For higher bombarding energies η_N is below 20% regardless of time. Pion contribution does not practically depend on collision energy or evolution time. However, pions contribute just 10-15% to the total shear viscosity. It means that substantial part of η comes out from other correlators. This question deserves further investigations.

Acknowledgments

References

[1] Antinori A *et al.* 2019 *Nucl. Phys.* A **9**82 1-1066
[2] Csernai L P, Kapusta J I and McLerran L D 2006 *Phys. Rev. Lett.* **97** 152303
[3] Kovtun P, Son D T and Starinets A O 2005 *Phys. Rev. Lett.* **9**4 111601
[4] Muronga A 2004 *Phys. Rev.* C **69** 044901
[5] Demir N and Bass S A 2009 *Phys. Rev. Lett.* **1**02 172302
[6] Chakraborty P and Kapusta J I 2011 *Phys. Rev.* C **83** 014906
[7] Wesp C *et al.* 2011 *Phys. Rev.* C **8**4 054911
[8] Cremonini S 2011 *Mod. Phys. Lett.* B **25** 1867
[9] Noronha-Hostler J *et al.* 2012 *Phys. Rev.* C **86** 054902
[10] Plumari S *et al.* 2012 *Phys. Rev.* C **86** 054902
[11] Ozvenchuk V *et al.* 2013 *Phys. Rev.* C **87** 064903
[12] Karpenko Iu A *et al.* 2015 *Phys. Rev.* C **9**1 064901
[13] Ivanov Yu B and Soldatov A A 2016 *Eur. Phys. J.* A **52** 117
[14] Rose J B *et al.* 2018 *Phys. Rev.* C **97** 055204
[15] Motornenko A *et al.* 2018 *J. Phys.* G **45** 035101
[16] Teslyk M *et al.* 2020 *Phys. Rev.* C **1**01 014904
[17] Zabrodin E *et al.* 2020 *Phys. Scr.* **9**5 074009
[18] Zabrodin E *et al.* 2020 *Preprint* 2002.05181
[19] Green M S 1954 *J. Chem. Phys.* **22** 398
[20] Kubo R 1957 *J. Phys. Sos. Jpn.* **12** 570
[21] Bass S A *et al.* 1998 *Prog. Part. Nucl. Phys.* **4**1 255
[22] Bleicher M *et al.* 1999 *J. Phys.* G **2**5 1859
[23] Bravina L V *et al.* 1998 *Phys. Lett.* B **4**34 379
[24] Bravina L V *et al.* 1999 *J. Phys.* G **2**5 351
[25] Bravina L V *et al.* 1999 *Phys. Rev.* C **6**0 024904
[26] Bravina L V *et al.* 2002 *Nucl. Phys.* A **6**98 383
[27] Bravina L V *et al.* 2001 *Phys. Rev.* C **63** 064902
[28] Bravina L V *et al.* 2008 *Phys. Rev.* C **78** 014907
[29] Belkacem M *et al.* 1998 *Phys. Rev.* C **5**8 1727
[30] Bravina L V *et al.* 2000 *Phys. Rev.* C **62** 064906

IV

XXVIIIth International Conference on Ultrarelativistic Nucleus-Nucleus Collisions
(Quark Matter 2019)

Early thermalization and shear viscosity to entropy ratio in heavy-ion collisions at energies of BES, FAIR and NICA

E. Zabrodin,[a,b] L. Bravina,[a,b] M. Teslyk,[a,c] O. Vitiuk[a,c]

[a]*Department of Physics, University of Oslo, PB 1048 Blindern, N-0316 Oslo, Norway*
[b]*Scobeltzyn Institute of Nuclear Physics, Moscow State University, RU-119991 Moscow, Russia*
[c]*Taras Shevchenko National University of Kyiv, UA-01033 Kyiv, Ukraine*

Abstract

Equilibration of highly excited baryon-rich matter is studied within the microscopic model calculations in A+A collisions at energies of BES, FAIR and NICA. It is shown that the system evolution from the very beginning of the collision can be approximated by relativistic hydrodynamics, although the hot and dense nuclear matter is not in local equilibrium yet. During the evolution of the fireball the extracted values of energy density, net baryon and net strangeness densities are used as an input to Statistical Model (SM) in order to calculate temperature T, chemical potentials μ_B and μ_S, and entropy density s of the system. Also, they are used as an input for the box with periodic boundary conditions to investigate the momentum correlators in the infinite nuclear matter. Shear viscosity η is calculated according to the Green-Kubo formalism. At all energies, shear viscosity to entropy density ratio shows minimum at time corresponding to maximum baryon density. The ratio dependence on T, μ_B, μ_S is investigated for both in- and out of equilibrium cases.

Keywords: transport models, heavy-ion collisions at BES/FAIR/NICA energies, Green-Kubo formalism, η/s ratio

1. Introduction

One of the goals of experiments on heavy-ion collisions at intermediate energies below $\sqrt{s} = 20$ GeV is the search for the predicted tricritical point of the QCD phase diagram. At this point the first-order deconfinement phase transition between the quark-gluon plasma (QGP) and hadronic matter should become of the second-order. Various signals of such a phenomenon were predicted. The ratio of shear viscosity to entropy density, η/s, looks very prominent, because for all known substances this ratio reaches minimum value in the vicinity of critical point [1]. The absolute limit for η/s estimated within the AdS/CFT correspondence is $1/(4\pi)$ [2]. Except of Ref. [3], this ratio was usually studied in microscopic models as function of temperature T taken at fixed baryochemical potential and zero chemical potential of strangeness [4, 5, 6, 7, 8].

The standard procedure of η determination by means of a transport model relies on the Green-Kubo formalism. The system of hadrons is inserted into a box with periodic boundary conditions. The shear

viscosity is calculated in system of natural units $c = \hbar = k_B = 1$ as

$$\eta(t_0) = \frac{V}{T} \int_{t_0}^{\infty} dt \langle \pi^{ij}(t)\, \pi^{ij}(t_0) \rangle_t \tag{1}$$

Here V and T is the box volume and temperature, and t_0 and t denote moments of time, respectively. The correlator $\langle \ldots \rangle_t$ reads

$$\langle \pi^{ij}(t)\, \pi^{ij}(t_0) \rangle_t = \lim_{t_{max} \to \infty} \left[\frac{1}{t_{max}} \int_{t_0}^{t_{max}} dt'\, \pi^{ij}(t+t')\, \pi^{ij}(t') \right] \tag{2}$$

containing the nondiagonal parts π^{ij} of the energy-momentum tensor

$$\pi^{ij}(t) = \frac{1}{V} \sum_{k=1}^{N_{part}} \frac{p_k^i(t)\, p_k^j(t)}{E_k(t)} \ . \tag{3}$$

The formalism requires that the initially out-of-equilibrium system is relaxed to the equilibrium state. The developed procedure and the results of our study are presented below.

2. The method

First, we have to define the area in heavy-ion collision most appropriate for studying the relaxation process. Previous studies show that the central cell with volume $V = 125$ fm^3 is most suitable for our research [9, 10]. To determine whether or not the equilibration takes place, one has to employ the statistical model (SM) of an ideal hadron gas with essentially the same number of degrees of freedom as in the transport model. In equilibrium, all characteristics of the system are determined via a set of distribution functions

$$f(p, m_i) = \left[\exp\left(\frac{\epsilon_i - \mu_i}{T} \right) \pm 1 \right]^{-1} \tag{4}$$

Here p is momentum of a hadron specie i, m_i is its mass, ϵ_i and μ_i is energy density and chemical potential, respectively. The last depends on the particle's baryon charge B_i and strange charge S_i, $\mu_i = B_i \mu_B + S_i \mu_S$. Due to its smallness, we consider zero electric chemical potential. Plus and minus signs stand for Fermi-Dirac and Bose-Einstein statistics. The number density and the energy density can be found as the first and the second moments of $f(p, m_i)$, and the entropy density is

$$s_i = -\frac{g_i}{2\pi^2} \int\limits_0^\infty f(p, m_i) \left[\ln f(p, m_i) - 1 \right] p^2 dp \tag{5}$$

where g_i is the degeneracy factor. In the vicinity of equilibrium the particle yields and energy spectra in the cell should be close to those provided by the SM. To find the shear viscosity the extracted cell parameters $\varepsilon, \rho_B,$ and ρ_S should be used as an input to initialize the box with periodic boundary conditions [11, 12]. The UrQMD model [13, 14] is employed for both the cell and the box calculations. The cubic box with volume $V = 1000$ fm^3 was initialized. At this stage the correlator given by Eq. (2) is calculated. Because of the ceaseless change of the energy density, net-baryon density, and net-strangeness density in the tested volume, one has to perform a series of snapshots of the system bulk conditions. We opted for 20 time slices, from $t = 1$ to 20 fm/c, with the time step $\Delta t = 1$ fm/c.

3. Results

About 50 000 central Au+Au collisions were generated at each of four energies, $E_{lab} = 10, 20, 30,$ and 40 AGeV. The calculations show that the matter in the cell expands with almost constant entropy-per-baryon
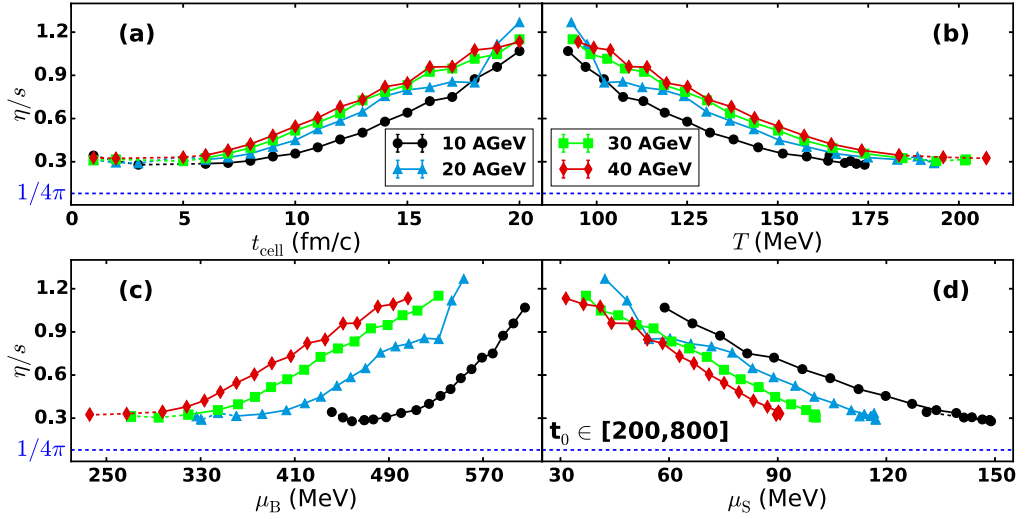
Fig. 1. Shear viscosity to SM entropy ratio η/s_{sm} as function of (a) time t, (b) temperature T, (c) baryochemical potential μ_B, and (d) strangeness chemical potential μ_S in the UrQMD calculations of central cell of central Au+Au collisions at E_{lab} = 10 AGeV (circles), 20 AGeV (triangles), 30 AGeV (squares), and 40 AGeV (diamonds). Lines are drawn to guide the eye.

ratio already after $t = 1$ fm/c. Pressure in the cell also appears to be very close to the pressure calculated within the SM for the hadronic gas in equilibrium. Both observations strongly support application of hydrodynamics to very early stages of nuclear collisions [15]. Relaxation to equilibrium in the box, however, takes much longer times compared to the cell case. The results of the calculations were averaged over the time period between 200 and 800 fm/c, where the correlator has a plateau. Figure 1 shows the dependencies of η/s on (a) time, (b) temperature, (c) baryochemical potential, and (d) strangeness chemical potential. The statistical errors are smaller than the symbol sizes. The parts of the spectra related to nonequilibrium stages of the evolution are shown by the dashed lines. We see that the ratio η/s decreases with decreasing bombarding energy from 40 to 10 AGeV. Also, it increases with the drop of temperature in the cell, accompanied by increasing μ_B and decreasing μ_S. The smaller the bombarding energy, the lower the η/s ratio. No distinct minima are observed. However, the entropy density and other macroscopic characteristics were calculated for the ideal hadron gas *in equilibrium*, whereas the system was *out of equilibrium* within the first few fm/c after beginning of the collision. The entropy density in the equilibrated system is larger than that in the non-equilibrated one. To account for this circumstance, we replace the distribution functions given by Eq. (1) to those provided by the momentum distributions of hadrons

$$f_i(p) = \frac{(2\pi)^3}{V g_i} \frac{dN_i}{d^3 p} \tag{6}$$

In equilibrium, results obtained by both methods should coincide. Time evolution of η/s in the cell and temperature dependence of this ratio, where the entropy density is calculated via Eq. (6), is shown in Fig. 2(a,b). Here all distributions reveal clear minima at $t \approx 5 - 6$ fm/c corresponding to maximum baryon density in the system. The minima become deeper with the decreasing energy of the collision. It would be important to study this effect at lower energies, say, up to $\sqrt{s} = 2 - 3$ GeV. If the dip in the ratio η/s will stop to drop further, it could be taken as indication of change of the equation of state due to formation of non-hadronic objects, i.e., quark-gluon strings. These strings can be considered as a precursor of the QGP formation. Also, the larger entropy density in the QGP phase could change the temperature dependence of η/s at $T \geq 155$ MeV.
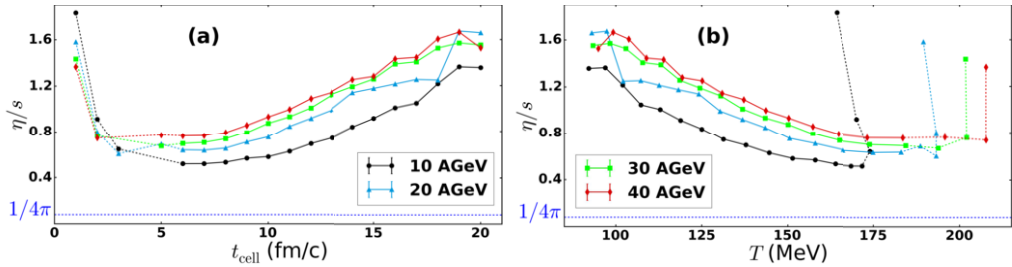
Fig. 2. Shear viscosity to nonequilibrium entropy ratio $\eta/s_{noneq.}$ as function of (a) time t and (b) temperature T in the UrQMD calculations of central cell of central Au+Au collisions at $E_{lab} = 10, 20, 30$ and 40 AGeV. Lines are drawn to guide the eye.

4. Conclusions

The following conclusions can be drawn from our study. We calculated the shear viscosity, the entropy density, and their ratio in the central cell with volume $V = 125$ fm^3 of central Au+Au collisions at energies from $E_{lab} = 10$ to 40 AGeV within the UrQMD model. First, the entropy density was estimated for an ideal hadron gas in equilibrium. Then, the entropy density of nonequilibrium state was calculated via the momentum distribution functions. For both cases shear viscosity and entropy density in the cell drop with time, whereas their ratio η/s reaches minimum at $t \approx 5 - 6$ fm/c regardless of the collision energy. At later times this ratio increases. The lower the energy, the smaller the ratio. Further studies at lower energies are needed to check where η/s will stop to decrease.

References

[1] L.P. Csernai, J.I. Kapusta, L.D. McLerran, On the Strongly-Interacting Low-Viscosity Matter Created in Relativistic Nuclear Collisions, Phys. Rev. Lett. 97 (2006) 152303. arXiv:nucl-th/0604032.

[2] P. Kovtun, D.T. Son, A.O. Starinets, Viscosity in strongly interacting quantum field theories from black hole physics, Phys. Rev. Lett. 94 (2005) 111601. arXiv:hep-th/0405231.

[3] M. Teslyk *et al.,* Shear viscosity in microscopic calculations of $A + A$ collisions at energies of Nuclotron-based Ion Collider fAcility (NICA), Phys. Rev. C 101 (2020) 014904. arXiv:1910.06293.

[4] A. Muronga, Shear viscosity coefficient from microscopic models, Phys. Rev. C 69 (2004) 044901. arXiv:nucl-th/0309055.

[5] N. Demir, S.A. Bass, Shear-Viscosity to Entropy-Density Ratio of a Relativistic Hadron Gas, Phys. Rev. Lett. 102 (2009) 172302.

[6] V. Ozvenchuk *et al.*, Shear and bulk viscosities of strongly interacting "infinite" parton-hadron matter within the parton-hadron-string dynamics transport approach, Phys. Rev. C 87 (2013) 064903. arXiv:1212.5393.

[7] Iu.A. Karpenko, P. Huovinen, H. Petersen, M. Bleicher, Estimation of the shear viscosity at finite net-baryon density from $A + A$ collision data at $\sqrt{s_{NN}} = 7.7 - 200$ GeV, Phys. Rev. C 91 (2015) 064901. arXiv:1502.01978.

[8] J.B. Rose *et al.*, Shear viscosity of a hadron gas and influence of resonance lifetimes on relaxation time, Phys. Rev. C 97 (2018) 055204. arXiv:1709.03826.

[9] L.V. Bravina *et al.*, Local equilibrium in heavy ion collisions: Microscopic model versus statistical model analysis, Phys. Rev. C 60 (1999) 024904. arXiv:hep-ph/9906548.

[10] L.V. Bravina *et al.*, Microscopic models and effective equation of state in nuclear collisions at FAIR energies, Phys. Rev. C 78 (2008) 014907. arXiv:0804.1484.

[11] M. Belkacem *et al.*, Equation of state, spectra and composition of hot and dense infinite hadronic matter in a microscopic transport model, Phys. Rev. C 58 (1998) 1727. arXiv:nucl-th/9804058.

[12] L.V. Bravina *et al.*, Local equilibrium in heavy ion collisions: Microscopic analysis of a central cell versus infinite matter, Phys. Rev. C 62 (2000) 064906. arXiv:nucl-th/0011011.

[13] S.A. Bass *et al.*, Microscopic models for ultrarelativistic heavy ion collisions, Prog. Part. Nucl. Phys. 41 (1998) 255.

[14] M. Bleicher *et al.*, Relativistic hadron-hadron collisions in the ultrarelativistic quantum molecular dynamics model, J. Phys. G 25 (1999) 1859. arXiv:hep-ph/9909407.

[15] E.E. Zabrodin, L.V. Bravina, Why the hydrodynamics is valid at early stage of heavy-ion collisions? J. Phys. Conf. Ser. 1390 (2019) 012019.

Article

Total and Partial Shear Viscosity in Heavy-Ion Collisions at Energies of BES, FAIR and NICA

Maksym Teslyk [1,2,†], Larisa Bravina [1,†] and Evgeny Zabrodin [1,3,*,†]

[1] Department of Physics, University of Oslo, PB 1048 Blindern, N-0316 Oslo, Norway; machur@ukr.net (M.T.); larissa.bravina@fys.uio.no (L.B.)

[2] Faculty of Physics, Taras Shevchenko National University of Kyiv, UA-03022 Kyiv, Ukraine

[3] Skobeltsyn Institute of Nuclear Physics, Moscow State University, RU-119991 Moscow, Russia

*   Correspondence: zabrodin@fys.uio.no

† These authors contributed equally to this work.

Abstract: We calculated the shear viscosity of hot and dense nuclear matter produced in a symmetric system of central gold–gold collisions at energies of BES RHIC, FAIR and NICA. For calculations of the collisions, the transport model UrQMD was employed. The shear viscosity was obtained within the Green–Kubo formalism. The hadron resonance gas model was used to determine temperature and chemical potentials of baryon charge and strangeness out of microscopic model calculations. In contrast to our previous works, we determined the partial viscosity of the main hadron species, such as nucleons, pions, kaons and Lambdas, via the nucleon–nucleon, pion–pion and so forth, correlators. A decrease in the beam energy from $E_{lab} = 40$ to 10 AGeV leads a to rise in baryon shear viscosity accompanied by a drop in the shear viscosity of mesons. The ratio of total shear viscosity to entropy density also decreases.

Keywords: relativistic heavy-ion collisions; transport models; HRG model; shear viscosity; η/s ratio

1. Introduction

The interest in this topic is due to several reasons. The theory of strong interactions, quantum chromodynamics (QCD), predicts the transition of nuclear matter to a new state, called quark–gluon plasma QGP, at extremely high density and temperature; see, e.g., [1,2] and references therein. Such transition may take place in, e.g., neutron stars; however, the only means to get the nuclear matter under extreme conditions in the laboratory are heavy-ion collisions at (ultra)relativistic energies. Although the first hydrodynamic model of multiparticle production was proposed almost 70 years ago [3], its further modifications have become very popular nowadays because of the successful description of experimental results obtained for heavy-ion collisions at energies of RHIC BNL (up to $\sqrt{s} = 200$ GeV) and LHC CERN (up to $\sqrt{s} = 5.02$ TeV). After analysis of RHIC data, it was announced by all four RHIC collaborations, BRAHMS, PHENIX, PHOBOS and STAR, that the created hot and dense nuclear substance behaved similarly to a perfect fluid [4–7]. At the same time, theoretical calculations of the shear viscosity to entropy density, made within strongly coupled conformal gauge theory by means of the anti-de Sitter/conformal field theory (AdS/CFT) correspondence [8], set the lower limit for this ratio, $\eta/s \geq 1/(4\pi)$, for all physical systems. Additionally, more thorough study of differential elliptic flow v_2 [9,10] of charged particles, produced in A+A collisions at energies of RHIC and LHC, as a function of transverse momentum p_T, has revealed that a small but nonzero value of the ratio η/s is needed for the correct description of the signal at $p_T \geq 2.5$ GeV/c. Recall that for all known substances the shear viscosity over entropy density should reach minimum if the system is in the tricritical point [11].

Since then, the values of η/s began to be intensively estimated. Hydrodynamic models are macroscopic ones; therefore, a dissipative term such as shear viscosity enters the equations of viscous hydrodynamics as an external parameter, which should be

obtained somehow. One way to do so is fitting the calculations performed within the viscous hydrodynamic model, or hybrid model, to the experimental data [12–18]. For the sake of simplicity, these calculations imply the constant ratio of η/s, although several works have tried to take the temperature dependence of this ratio into account [19,20]. The computation of transport coefficients of hadronic systems, consisting of mixture of hadron species, is possible within the microscopic kinetic theory. However, this is a non-trivial task from an analytic point of view [21,22] because one has to know cross-sections of various hadronic collisions and mean fields. Therefore, lattice QCD calculations of η/s are usually done for gluons at zero net baryon density and at temperatures around 160 MeV [23,24]. Microscopic transport models are better suited for such study. In the past, the shear viscosity and its ratio over entropy density were studied in, e.g., the ultra-relativistic quantum molecular dynamics (UrQMD) model [25–29], the parton-hadron-string dynamics (PHSD) model [30], the simulating many accelerated strongly interacting hadrons (SMASH) model [31] and the parton cascade (PC) models to solve various types of Boltzmann collision processes [32–35]. Many of these calculations were performed at conditions corresponding to those of heavy-ion collisions at energies of RHIC and LHC. In this domain, the transition between QGP and hadronic matter is just a smooth crossover.

The modern trend in high-energy physics nowadays is to search for the critical point, at which the deconfinement first-order phase transition becomes a second-order one, at much lower collision energies accessible to the Beam Energy Scan (BES) program at RHIC and at soon-to-open facilities NICA at JINR and FAIR at GSI. Our study is devoted to the beam energies between $E_{lab} = 10$ AGeV and $E_{lab} = 40$ AGeV. In this energy range, the temperature of deconfinement phase transition is expected to be lower compared to that at higher energies, but the baryon chemical potential is quite significant and cannot be neglected. The transition from meson-dominated to baryon-dominated hadronic matter with decreasing beam energy takes place here as well. The main aim of the present paper is to the evolution of partial shear viscosities of the most abundant hadronic species in an expanding and cooling hadronic mixture formed in a symmetric system of centrally colliding gold nuclei. We used the UrQMD model [36,37] and employed the technique developed in [28,29,38]. Section 2 describes the Green–Kubo formalism for determination of the shear viscosity. Within this approach, one has to know the correlator, the relaxation time and the temperature of the system. Determination of these parameters, and baryon chemical potential and strangeness chemical potential, is explained in Section 3. Section 4 presents the calculations of evolution of partial shear viscosity and its ratio over entropy density for nucleons, pions, kaons and $\Lambda + \Sigma$ in the central area of central Au+Au collisions at four different beam energies, $E_{lab} = 10, 20, 30$ and 40 AGeV. Finally, conclusions are drawn in Section 5.

2. Calculation of Shear Viscosity within Green–Kubo Formalism

In classical thermodynamics, one can determine the shear viscosity by means of Chapman–Enskog method [39]. Microscopic transport models, however, allow calculation of the shear viscosity by using the Green–Kubo formalism [40,41] during the study of relaxation process in the disturbed system. Note that the formalism relies on assumption of existence of the equilibrated state. Therefore, one has to study the relaxation of the system to equilibrium before calculation of shear viscosity. The whole formalism is quite straightforward. It is convenient to use Planck, or natural, units: $\hbar = k_B = c = 1$. The shear viscosity in these units is

$$\eta(t_0) = \frac{V}{T} \int_{t_0}^{\infty} \langle \pi(t)\pi(t_0) \rangle_t \mathrm{d}t \tag{1}$$

containing the volume V and temperature T of the system, and initial (t_0) and final (t) time of the calculation. The correlator in the integrand reads

$$\langle \pi(t)\pi(t_0) \rangle_t = \lim_{t_{\max} \to \infty} \frac{1}{t_{\max} - t_0} \int_{t_0}^{t_{\max}} \pi^{ij}(t + t')\pi^{ij}(t')\mathrm{d}t' \tag{2}$$

where $\pi^{ij}(t)$ is the non-diagonal part of the energy-momentum tensor T^{ij}.

$$\pi^{ij}(t) = \frac{1}{V} \sum_{k=1}^{particles} \frac{p_k^i(t) p_k^j(t)}{E_k(t)} . \tag{3}$$

Here $p_k^{i(j)}$ is the $i(j)$th components of momentum of particle k and E_k is its energy, respectively. The correlator (2) can be approximated by [40,41]

$$\langle \pi(t) \pi(t_0) \rangle_t \approx \langle \pi(t_0) \pi(t_0) \rangle \exp\left(-\frac{t - t_0}{\tau} \right) , \tag{4}$$

where τ is the effective relaxation time. By combining Equation (4) with Equation (1), we get the final expression to calculate the shear viscosity:

$$\eta(t_0) = \frac{V\tau}{T} \langle \pi(t_0) \pi(t_0) \rangle . \tag{5}$$

By looking at Equation (5), it becomes clear that, besides of calculation of the correlator, one has to determine simultaneously temperature of the substance T and the relaxation time τ. Since the procedure to define unambiguously temperature of out-of-equilibrium media is absent, it is necessary to check that the hot and dense nuclear matter in an expanding fireball is in the vicinity of the local equilibrium. After that, temperature, relaxation time and the correlator itself should be determined somehow. The algorithm describing all steps in detail is presented in next section.

3. The Three-Component Method

First of all, one has to choose one of the event generators designed for description of nucleus–nucleus interactions in the investigated energy range. For this purpose, we employ the UrQMD model [36,37]. Some very useful data for our study came from a rich table of particles, antiparticles and resonances from the Particle Data Group (PDG) [42] with masses up to 2.25 GeV/c. The UrQMD describes both hadronic and nuclear collisions at energies ranging from one hundred MeV (Bevalac) to several hundred GeV (RHIC) [36,37] and a few TeV (LHC) [43]. Compared to energies of RHIC and LHC, the energy range selected for the present study is rather modest. We studied very central gold–gold collisions, with impact parameter $b = 0$ fm, within the energy interval from $E_{lab} = 10$ to 40 AGeV. This energy range is accessible for the Beam Energy Scan (BES) at RHIC and for planned facilities, such as FAIR and NICA. As was shown in previous studies within the UrQMD [44–47], there is no global equilibrium within the whole volume of the fireball, even in very central heavy-ion collisions because, for instance, the net baryon charge and net strangeness are not uniformly distributed. A local equilibrium, however, is very likely [46,48–51] at least in the central zone of a rapidly expanding fireball. The investigations revealed that the central cubic cell with volume $V = 5 \times 5 \times 5 = 125$ fm^3 is appropriate for investigating the process of relaxation to equilibrium of hot and dense nuclear matter produced in relativistic heavy-ion collisions. It is worth mentioning that the picked-up volume should be neither too large to provide uniform distribution of energy density and conserved charges nor too small to contain enough particles. However, the cell is an open system, and hadrons can leave it freely, thereby decreasing its energy density and particle densities. Therefore, to prove that the matter in the cell is in the vicinity of equilibrium, the following procedure was developed; see, e.g., [44,46,49]. Three main parameters characterizing the cell—namely, the energy density, ε^{mic}; the net baryon density, ρ_B^{mic}; and the net strangeness density, ρ_S^{mic}—were extracted from the microscopic calculations of the fireball evolution. The time step was just $\Delta t = 1$ fm/c. These parameters were inserted into the statistical model (SM) of an ideal hadron gas containing precisely the same set of degrees of freedom as the microscopic model. The set of nonlinear equations reads

$$\varepsilon^{mic} = \sum_i \epsilon_i^{SM} \tag{6}$$

$$\rho_B^{mic} = \sum_i B_i \, n_i^{SM} \tag{7}$$

$$\rho_S^{mic} = \sum_i S_i \, n_i^{SM} \, , \tag{8}$$

containing partial energy density ϵ_i^{SM} and partial number density n_i^{SM} of hadron specie "i," and its baryon B_i and strangeness S_i content. Both n_i^{SM} and ϵ_i^{SM} are just first and second moments of the distribution function

$$f(p, m_i) = \left\{ \exp\left(\frac{\epsilon_i - \mu_i}{T} \right) \pm 1 \right\}^{-1} , \tag{9}$$

namely,

$$n_i^{SM} = \frac{g_i}{(2\pi)^3} \int_0^\infty f(p, m_i) d^3 p \tag{10}$$

$$\epsilon_i^{SM} = \frac{g_i}{(2\pi)^3} \int_0^\infty \epsilon_i f(p, m_i) d^3 p \tag{11}$$

where m_i is particle mass and p is its momentum, and g_i is the spin-isospin degeneracy factor. Sign "$-$" in Equation (9) stands for bosons and sign "$+$" stands for fermions. The total chemical potential of the hadron is a linear combination of chemical potentials, related to conserved charges in strong interactions, μ_B and μ_S, respectively. It depends on particle's baryon B_i and strangeness S_i content:

$$\mu_i = B_i \mu_B + S_i \mu_S \, . \tag{12}$$

As follows in Equations (9)–(12), the ideal gas of hadrons in the statistical model is fully determined by three parameters, temperature, baryon chemical potential and strangeness chemical potential. If partial particle abundances and energy spectra given by the SM are close (within 10% accuracy) to those of the cell in microscopic model's calculations, one can conclude that the matter in the cell is in the vicinity of local equilibrium. Then, we are able to determine temperature of the system which enters the expression for calculation of shear viscosity.

However, this is not a full story yet, because we have to determine both the correlator $\langle \pi(t_0) \pi(t_0) \rangle$ and the effective relaxation time τ. This study cannot be done within the analysis of an open system, such as our cell, because of permanently changing conditions in the cell. These conditions must be fixed somehow. Therefore, the third component of the scheme is the box with periodic boundary conditions [52–54] preserving both the total energy and the net baryon and net strangeness composition. Namely, the particles are free to leave the box; however, other particles with the same characteristics (masses, momenta, quantum numbers) enter the box immediately. Elastic and inelastic interactions of hadrons in the box proceed similarly to those in model generated hadronic or nuclear collisions.

The volume of the box can be $V_{box} = 5 \times 5 \times 5 = 125$ fm^3, similar to that of the central cell, or larger—e.g., $V_{box} = 10 \times 10 \times 10 = 1000$ fm^3—to reduce the fluctuation effects. The box is initialized with the values of energy density, net baryon density and net strangeness density, which are extracted from the cell at a certain moment. Its initial hadron composition consists usually of protons and neutrons with the admixture (in case of nonzero strangeness density) of kaons or Lambdas. It is worth noting that the relaxation process to a stationary state in the box is quite long; see [52,53]. The typical time scale for the box calculations is about 1000–2000 fm/c. One can study the relaxation process and determine both the correlator(s) and relaxation time τ.

The method developed for determination of shear viscosity in microscopic calculations consists of three steps. The first step includes the generation of heavy ion collisions within the microscopic transport model; determination of volume, in which the occurrence of a local equilibrium is expected; and extraction of three key parameters, i.e., energy density, net baryon density and net strangeness density, out of it. These three parameters are used as an input for the statistical model of ideal hadron gas. This is the second step of the proposed scheme. If the partial yields of hadrons and their energy spectra in the selected volume are close to those given by the SM, one can conclude that the matter is in the vicinity of a local equilibrium. The SM provides us with the values of thermodynamic characteristics, such as temperature, baryon chemical potential and strangeness chemical potential. At the third step we use the extracted values of ε, ρ_B and ρ_S to initialize the box with periodic boundary conditions. The correlators and the relaxation times are determined during the study of the matter evolution in the box towards equilibrium.

4. Results: Total and Partial Shear Viscosity of Hadrons

Version 3.4 of the UrQMD model in default cascade mode was employed. Calculations were performed for central gold–gold collisions at four beam energies, $E_{lab} = 10, 20, 30$ and 40 AGeV. At each energy, ca. 50 thousand collisions were generated. Figure 1 displays the evolution of energy density (a), net baryon density (b) and net strangeness density (c) in the central cubic cell of the collision with volume $V = 125$ fm^3.
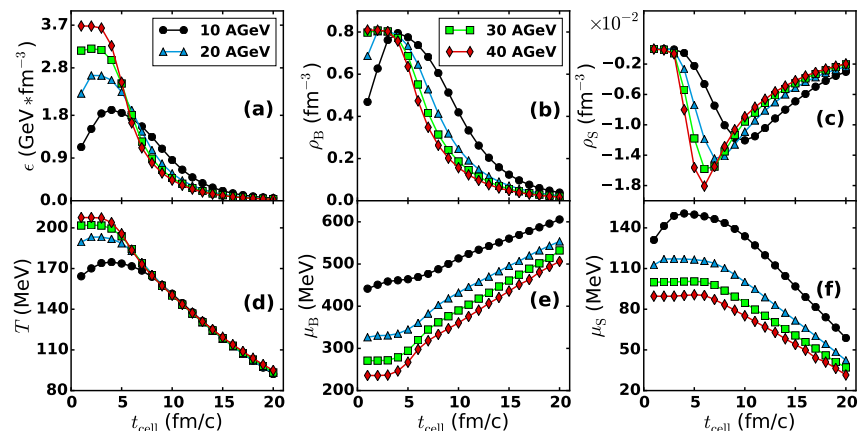

Figure 1. Distributions of (**a**) energy density, ε; (**b**) net baryon density, ρ_B; and (**c**) net strangeness density, ρ_S, of central Au+Au collisions generated within UrQMD model at $E_{lab} = 10$ AGeV (black circles), 20 AGeV (blue triangles), 30 AGeV (green squares) and 40 AGeV (red diamonds) in the central cell, 125 fm^3 in size. The values of (**d**) temperature, T; (**e**) baryochemical potential, μ_B; and (**f**) strangeness chemical potential, μ_S were calculated from the fit to SM of ideal hadron gas. Lines were drawn to guide the eye (From [29]).

We can see that at early times, $t \leq 5$ fm/c, the energy density in the cell is larger for collisions with larger bombarding energies. However, both remnants of colliding nuclei and very energetic particles leave the central area quickly. After $t \approx 6$ fm/c, the drop of energy density proceeds with similar rates for all four energies. Net baryon density drops with time also, but here one can observe the clear energy dependence: the lower the beam energy, the higher the net baryon density. The net strangeness density in the cell is small, though negative, at $1 \leq t \leq 20$ fm/c, as shown in Figure 1c, in line with the previous results; see, e.g., [38,46,49]. This fact can be explained by different cross-sections of positive and negative kaons in baryon-dominated medium. After that, we acquired the temperatures (Figure 1d), baryon chemical potential (Figure 1e) and strangeness chemical potential (Figure 1f) of an ideal hadron gas by inserting the extracted values of ε, ρ_B and ρ_S into the

SM equations. Note that matter in the cell reaches chemical and thermal equilibrium in the investigated energy range not earlier than after $t = 6$–8 fm/c. Therefore, parameters T, μ_B, μ_S obtained at earlier times should be treated with great care. It is interesting that at $t \geq 7$ fm/c and until $t = 20$ fm/c, temperatures in the cell shown in Figure 1d coincide for the studied beam energies. Baryon chemical potentials, shown in Figure 1e, increase with time, whereas chemical potentials of strangeness decrease, as displayed in Figure 1f.

As was shown in [28], shear viscosity in the box calculations reveals a remarkable plateau for initial times (see Equation (2), 200 fm/$c \leq t_0 \leq 800$ fm/c). The extracted values of η averaged over the plateau are shown in Figure 2. It is worth mentioning that, because of the high number of events used for the box generation at each timestep and averaging over the plateau, the statistical errors in this figure and in the subsequent ones are less than the symbol sizes. Data points corresponding to early times in the cell, $\tau_{cell} \leq 6$ fm/c, are connected by the dashed lines. At these times the energy density in the cell is not distributed evenly throughout the cell volume, and hadron abundances and energy spectra, compared to these of the SM of ideal hadron gas, indicate that the matter in the cell is still out of equilibrium [46,49]. Determination of shear viscosity in the cell at $t \leq 6$ fm/c is, therefore, ambiguous. However, when remnants of colliding nuclei and most energetic particles leave the cell, the chemical and thermal equilibrium sets in quickly. One can see that all four distributions $\eta(t_{cell})$ sit practically on the top of each other at 7 fm/$c \leq t \leq 20$ fm/c, fully resembling the temperature drop shown in Figure 1d. The explanation of the decrease in η is as follows. After $t = 6$ fm/c, inelastic collisions in the cell rapidly cease, and (quasi)elastic interactions start to dominate. The soft scattering modes quickly redistribute the energy and momentum of hadrons, which leads to a decrease in the relaxation time τ, and consequently, the shear viscosity in the cell.
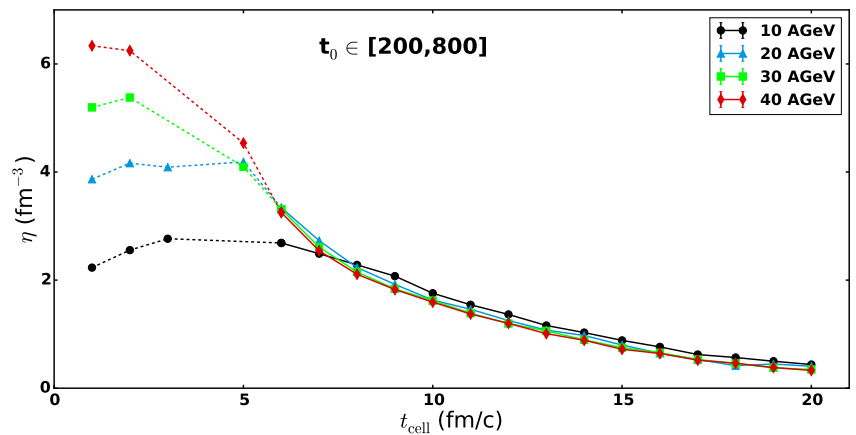
Figure 2. Shear viscosity of hadrons in the UrQMD box with initial conditions corresponding to those of the central cell of UrQMD-generated central Au+Au collisions at $E_{lab} = 40$ AGeV (red diamonds), 30 AGeV (green squares), 20 AGeV (blue triangles) and 10 AGeV (black circles). Dashed lines indicate the out-of-equilibrium stage, whereas solid lines correspond to the (nearly) equilibrium stage. See text for details.

In what follows, we study the partial shear viscosities of the main hadron species in the central cell, namely, nucleons, pions, kaons and $\Lambda + \Sigma$, and the combined viscosities of baryons and mesons. This means that only the correlators for the appropriate type of hadrons, e.g., $\langle \pi^N \pi^N \rangle$, are considered. The analysis of the thermodynamic conditions in the cell starts from time $t = 8$ fm/c when the hadronic matter is close to thermal and chemical equilibrium. Shear viscosity of nucleons in Au+Au collisions at all four beam energies is shown in Figure 3. It smoothly decreases with time, and therefore, with temperature for all

reactions. Additionally, the lower the energy of nuclear collision, the higher the nucleon's shear viscosity. Since temperatures in the cell after $t = 8\,\text{fm}/c$ are practically the same at different timesteps for all four beam energies, the difference in η values can be attributed to different values of baryon chemical potential and to dominance of baryon fraction in the particle spectrum.
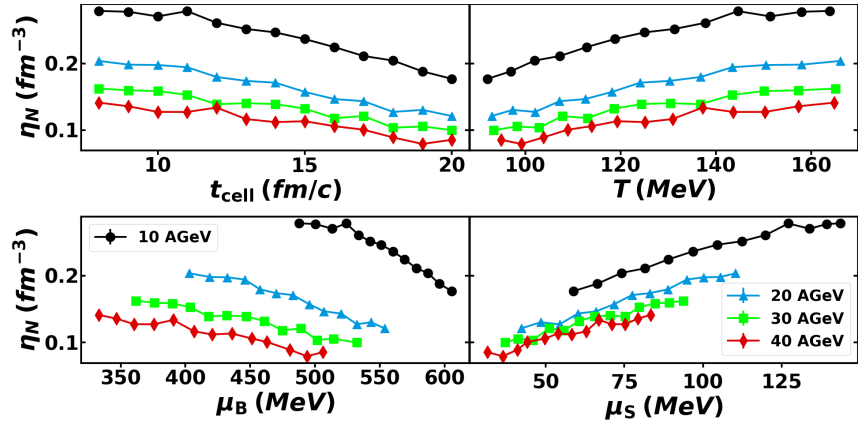
Figure 3. Upper row: Shear viscosity of nucleons, η^N, calculated in the central cell as function of time t_{cell} after the beginning of nuclear collision (**left**), and temperature T of the cell (**right**). **Bottom row**: The same as the upper one but for baryon chemical potential, μ_B, (**left**) and for strangeness chemical potential, μ_S, (**right**). Beam energies and labeling of the curves are the same as in Figure 1.

The partial shear viscosity of the combined spectrum of Lambdas and Sigmas, displayed in Figure 4, also demonstrates this tendency, although very weak. The calculated distributions $\eta^{\Lambda+\Sigma}(t_{cell})$ and $\eta^{\Lambda+\Sigma}(T)$ are close to each other within the studied energy range. One can see also that the values of shear viscosity of $\Lambda + \Sigma$ hyperons are almost two times lower compared to those of nucleons. The plausible explanation is that the yield of hyperons in Au+Au collisions at $10\,\text{AGeV} \leq E_{lab} \leq 40\,\text{AGeV}$ is relatively low. Therefore, hyperons interact mainly with other hadrons and the genuine correlation between them is lost quite early.
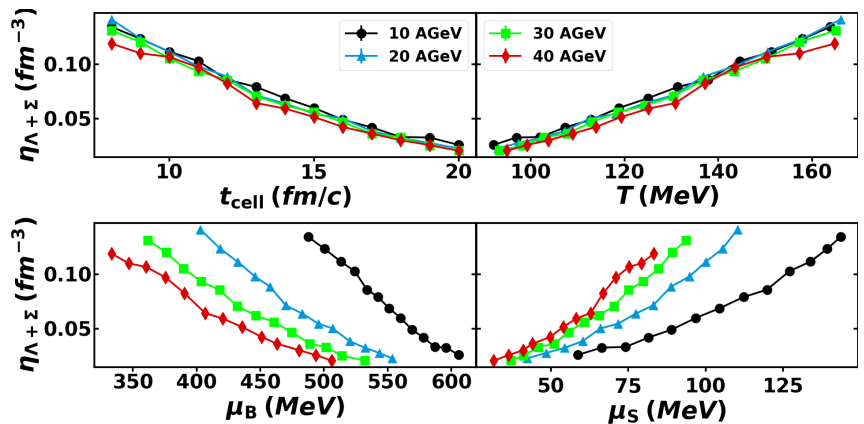
Figure 4. The same as Figure 3 but for shear viscosity of $\Lambda + \Sigma$.

Pions are the most abundant mesons among the produced particles. In contrast to nucleons, the partial shear viscosity of pions drops with decreasing beam energy for the

distributions $\eta^{\pi}(t_{cell})$ and $\eta^{\pi}(T)$, as shown in Figure 5. Recall that temperatures in the cell at all four energies are almost the same within the time interval $8 \leq t_{cell} \leq 20$ fm/c, and that pions are not affected by chemical potentials of the baryon charge and strangeness. The spectrum of hadrons in heavy-ion collisions at low and intermediate energies is dominated by baryons, and less pions are produced at lower energies. The decrease in pion shear viscosity with time in the cell proceeds faster compared to that of the nucleon one.
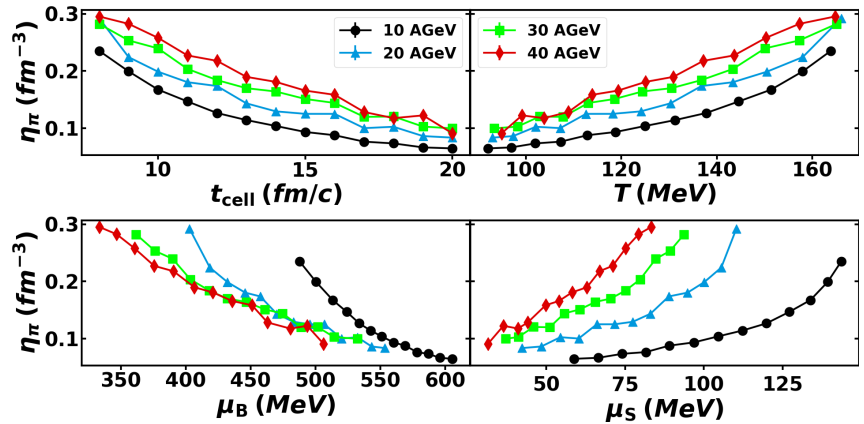

Figure 5. The same as Figure 3 but for shear viscosity of pions.

The next group of mesons in particle spectrum is kaons. Figure 6 displays their shear viscosity in the central cell. Here. one can see no difference between $\eta^{K}(t_{cell})$ and $\eta^{K}(T)$ for beam energies between 10 and 40 AGeV despite the different strangeness chemical potentials. It seems that chemical potentials play a minor role in the (partial) shear viscosity of hadrons. The latter is mainly determined by temperature of the system and particle abundances.
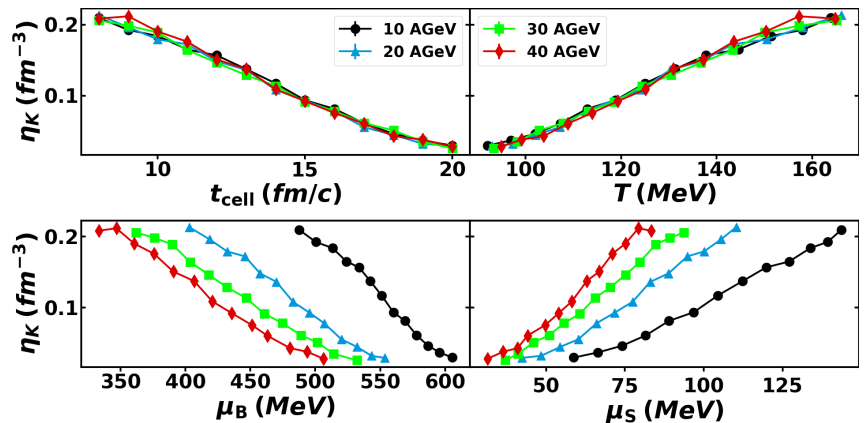

Figure 6. The same as Figure 3 but for shear viscosity of kaons.

The combined shear viscosity of baryons in the central cell is presented in Figure 7, and Figure 8 shows that of mesons. Both figures reveal the same trends observed earlier for individual hadron distributions. Namely, the shear viscosities of both baryons and mesons, in the central cell drop with time, and therefore, with decreasing energy density and temperature of the cell. However, for baryons the shear viscosity increases with decreasing beam energy, whereas shear viscosity of mesons demonstrates the opposite tendency. When the beam energy goes down from $E_{lab} = 40$ to 20 AGeV, the difference in meson or baryon shear viscosities for neighbor beam energies is about 10% or less. Note also that at $E_{lab} \approx 30$ AGeV the partial shear viscosities of baryons and mesons are about the same. Significant rise of $\eta^{baryons}$ is observed at $E_{lab} = 10$ AGeV; see Figure 7. Here the total spectrum of hadrons is heavily dominated by baryons.
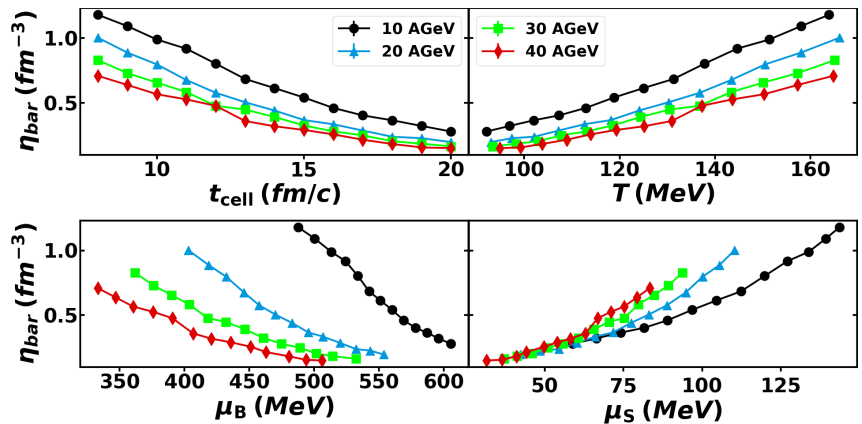

Figure 7. The same as Figure 3 but for combined shear viscosity of baryons.
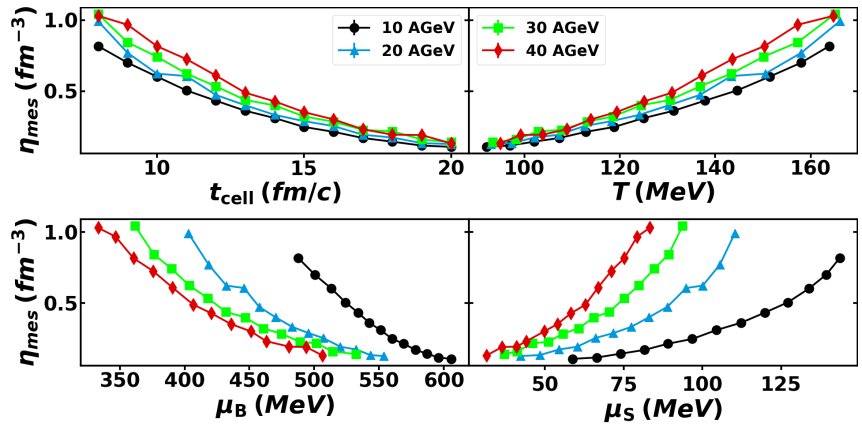

Figure 8. The same as Figure 7 but for combined shear viscosity of mesons.

This energy range is very interesting. If heavy ions are colliding with the beam energies of hundred MeV, one deals merely with hadrons and their excited states, resonances. When the energy of nuclear collisions increases to several GeV, new objects, called strings, come into play. Strings are not hadrons and can be considered as precursors of quark–gluon plasma. With a further increase in bombarding energy, mesons (mainly, pions) become the most abundant part of the hadronic spectrum, and therefore, a transition from baryon-dominated to meson-dominated matter takes place. Thus, it is important to check the

possible fingerprints of these transitions on the ratio of shear viscosity to entropy density. The latter is determined in the SM for a hadronic specie "i" as

$$s_i = -\frac{g_i}{2\pi^2} \int_0^\infty f(p, m_i) \left[\ln f(p, m_i) - 1\right] p^2 dp \,, \qquad (13)$$

Bearing in mind the ratio limit $\eta/s \geq 1/4\pi$ [8], we plotted the ratio $4\pi\eta/s$ for all hadrons as a function of t_{cell}, T, μ_B and μ_S in Figure 9. One can see that this ratio for all hadrons in the system decreases with decreasing beam energy of Au+Au collisions. However, even for the collisions with $E_{lab} = 10$ AGeV the minimum of $4\pi\eta/s$ is four times larger than unity. It is worth mentioning that open symbols in Figure 9 indicate the results obtained at early times for out-of-equilibrium stage. These results, therefore, are ambiguous and should be treated with great care, and the indications on shallow minima of η/s around $t_{cell} \sim 5$ fm/c.
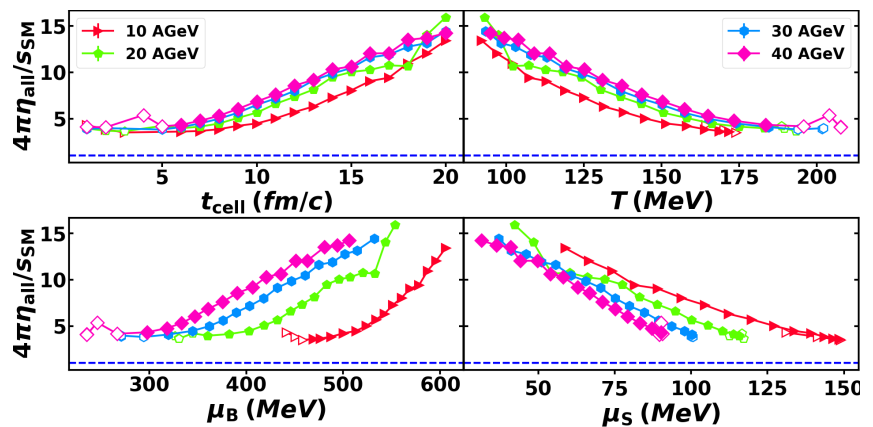

Figure 9. The same as Figure 8 but for ratio of total shear viscosity of hadrons to their entropy density, $4\pi\eta/s$.

A direct comparison of the obtained results with the results of other models is difficult, since the latter were obtained at a constant (most often, zero) value of the baryon chemical potential. The general trend, however, is qualitatively correct. The ratio of the shear viscosity over the entropy density increases (i) with decreasing temperature and (ii) with increasing baryon chemical potential. A more detailed comparison of the predictions of different models can be found in [31].

The last step is to study the partial contributions of baryons and mesons to η/s ratio. Figures 10 and 11 display the ratios $4\pi\eta^{baryons}/s$ and $4\pi\eta^{mesons}/s$, respectively. Figure 10 indicates that the evolution of partial ratio η/s for baryons in the cell at 8 fm/$c \leq t_{cell} \leq 20$ fm/c proceeds similarly for all four beam energies. However, a very weak rise in this ratio with dropping beam energy seems to take place. The reduction in the ratio of total shear viscosity to entropy density in the medium is caused by the decreased contribution of mesons, as shown in Figure 11. In stark contrast to baryons, the mesonic ratio η^{mesons}/s demonstrates distinct separation in terms of temperature and chemical potentials. Note also that this ratio varies slightly in the cell within the considered time interval.
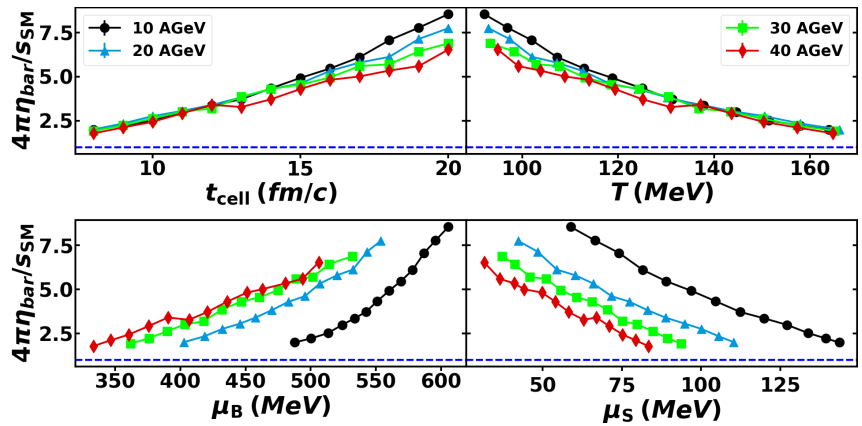
Figure 10. The same as Figure 9 but for shear viscosity of baryons to the entropy density ratio.
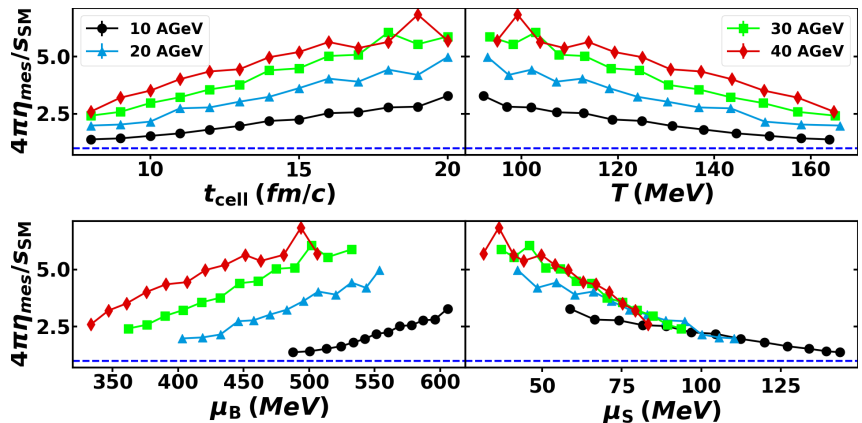

Figure 11. The same as Figure 10 but for shear viscosity of mesons to the entropy density ratio.

5. Discussion and Conclusions

We studied evolution of shear viscosity η of hot and dense nuclear matter produced in the central area of gold–gold collisions at beam energies ranging from $E_{lab} = 10$ to 40 AGeV. The main goal was to study the partial contributions to η of main hadron species, such as nucleons, pions, kaons and lambdas/sigmas. The general procedure for determination of the shear viscosity in microscopic transport calculations consists of three main parts; see, e.g., [28,29]. Firstly, a central cubic cell 125 fm^3 in size was selected. Then, energy density, net baryon density and net strangeness density in the cell were determined. Secondly, our statistical model of ideal hadron gas employed the extracted values of $\varepsilon, \rho_B, \rho_S$ to determine temperature T, baryon chemical potential μ_B and strangeness chemical potential μ_S of hadron resonance gas in thermal and chemical equilibrium. If the yields and energy spectra of hadronic species in microscopic calculations are close to those given by the SM, the matter in the cell can be considered to be in the vicinity of local equilibrium. Thus, one gets T, μ_B and μ_S of the system. Third, we determined the shear viscosity of the system with the Green–Kubo approach. To do this, one has to initialize the box with periodic boundary conditions with essentially the same values of $\varepsilon, \rho_B, \rho_S$ as given by the cell calculations at each time snapshot.

The obtained physical results can be summarized as follows. Temperatures in the central cell at each time step between $t = 8$ fm/c and $t = 20$ fm/c are similar for all four

energies. The total shear viscosities in the central areas of the four different reactions are also similar within this time interval. Partial shear viscosities, however, demonstrate different tendencies. The lower the beam energy, the higher the nucleon shear viscosity. Hyperons $\Lambda + \Sigma$ also reveal this trend, but to a much lesser extent. In contrast, shear viscosity of pions decreases with decreasing beam energy, whereas kaon shear viscosity is almost independent on the beam energy within the investigated interval. The contributions of baryons and mesons to the total shear viscosity are approximately the same at beam energy 30 AGeV. At higher and lower beam energies, this symmetry between the baryon and the meson sectors is broken. The ratio of shear viscosity of hadrons to their entropy density also declines with decreasing collision energy. This drop is attributed to mesons. For baryons, the distributions of $\eta^{baryons}/s(t_{cell})$ increase slightly, though remaining very close to each other, with dropping E_{lab}. Our results might be useful also for the development of sophisticated hydrodynamic models for heavy-ion collisions at intermediate energies.

Author Contributions: Investigation, methodology, software and visualization, M.T.; conceptualization, methodology and supervision, L.B.; conceptualization, investigation, methodology and writing—original draft, E.Z. All authors have read and agreed to the published version of the manuscript.

Institutional Review Board Statement: Not applicable.

Informed Consent Statement: Not applicable.

Data Availability Statement: Not applicable.

Conflicts of Interest: The authors declare no conflict of interest.

References

1. Sarkar, S.; Satz, H.; Sinha, B. *The Physics of the Quark-Gluon Plasma: Introductory Lectures*; Lecture Notes in Physics; Springer: Berlin/Heidelberg, Germany, 2010; Volume 785, pp. 1–369. [CrossRef]
2. *Proceedings of Quark Matter 2019*; Liu, F., Wang, E., Wang, X.-N., Xu, N., Zhang, B.-W., Eds.; Nuclear Physics A; Elsevier: Amsterdam, The Netherlands, 2021; Volume 1005.
3. Landau, L.D. On the multiparticle production in high-energy collisions. *Izv. Akad. Nauk. Ser. Fiz.* **1953**, *17*, 51–64.
4. Arsene, I.; Bearden, I.; Beavis, D.; Besliu, C.; Budick, B.; Bøggild, H.; Chasman, C.; Christensen, C.; Christiansen, P.; Cibor, J.; et al. Quark gluon plasma and color glass condensate at RHIC? The Perspective from the BRAHMS experiment. *Nucl. Phys. A* **2005**, *757*, 1–27. [CrossRef]
5. Back, B.; Baker, M.; Ballintijn, M.; Barton, D.; Becker, B.; Betts, R.; Bickley, A.; Bindel, R.; Budzanowski, A.; Busza, W.; et al. The PHOBOS perspective on discoveries at RHIC. *Nucl. Phys. A* **2005**, *757*, 28–101. [CrossRef]
6. Adams, J.; Aggarwal, M.; Ahammed, Z.; Amonett, J.; Anderson, B.; Arkhipkin, D.; Averichev, G.; Badyal, S.; Bai, Y.; Balewski, J.; et al. Experimental and theoretical challenges in the search for the quark gluon plasma: The STAR Collaboration's critical assessment of the evidence from RHIC collisions. *Nucl. Phys. A* **2005**, *757*, 102–183. [CrossRef]
7. Adcox, K.; Adler, S.; Afanasiev, S.; Aidala, C.; Ajitanand, N.; Akiba, Y.; Al-Jamel, A.; Alexander, J.; Amirikas, R.; Aoki, K.; et al. Formation of dense partonic matter in relativistic nucleus-nucleus collisions at RHIC: Experimental evaluation by the PHENIX collaboration. *Nucl. Phys. A* **2005**, *757*, 184–283. [CrossRef]
8. Kovtun, P.; Son, D.T.; Starinets, A.O. Viscosity in strongly interacting quantum field theories from black hole physics. *Phys. Rev. Lett.* **2005**, *94*, 111601. [PubMed]
9. Ollitrault, J.-Y. Anisotropy as a signature of transverse collective flow. *Phys. Rev. D* **1992**, *46*, 229–245. [PubMed]
10. Poskanzer, A.M.; Voloshin, S.A. Methods for analyzing anisotropic flow in relativistic nuclear collisions. *Phys. Rev. C* **1998**, *58*, 1671–1678. [CrossRef]

11. Csernai, L.P.; Kapusta, J.I.; McLerran, L.D. On the Strongly-Interacting Low-Viscosity Matter Created in Relativistic Nuclear Collisions. *Phys. Rev. Lett.* **2006**, *97*, 152303. [CrossRef]
12. Romatschke, P.; Romatschke, U. Viscosity Information from Relativistic Nuclear Collisions: How Perfect is the Fluid Observed at RHIC? *Phys. Rev. Lett.* **2007**, *99*, 172301. [CrossRef]
13. Dusling, K.; Teaney, D. Simulating elliptic flow with viscous hydrodynamics. *Phys. Rev. C* **2008**, *77*, 034905. [CrossRef]
14. Schenke, B.; Tribedy, P.; Venugopalan, R. Fluctuating Glasma initial conditions and flow in heavy ion collisions. *Phys. Rev. Lett.* **2012**, *108*, 252301. [CrossRef] [PubMed]
15. Schenke, B.; Tribedy, P.; Venugopalan, R. Event-by-event gluon multiplicity, energy density, and eccentricities in ultrarelativistic heavy-ion collisions. *Phys. Rev. C* **2012**, *86*, 034908. [CrossRef]
16. Karpenko, I.A.; Huovinen, P.; Petersen, H.; Bleicher, M. Estimation of the shear viscosity at finite net-baryon density from A+A collision data at $\sqrt{s_{NN}} = 7.7 - 200$ GeV. *Phys. Rev. C* **2015**, *91*, 064901. [CrossRef]
17. Ivanov, Y.B.; Soldatov, A.A. Entropy Production and Effective Viscosity in Heavy-Ion Collisions. *Eur. Phys. J. A* **2016**, *52*, 367. [CrossRef]
18. Ivanov, Y.B.; Soldatov, A.A. Estimation of the shear viscosity from 3FD simulations of Au + Au collisions at $\sqrt{s_{NN}} = 3.3 - 39$ GeV. *Eur. Phys. J. A* **2016**, *52*, 117. [CrossRef]
19. Song, H.; Bass, S.A.; Heinz, U. Viscous QCD matter in a hybrid hydrodynamic+Boltzmann approach. *Phys. Rev. C* **2011**, *83*, 024912. [CrossRef]
20. Niemi, H.; Denicol, G.S.; Huovinen, P.; Molnar, E.; Rischke, D.H. Influence of a temperature-dependent shear viscosity on the azimuthal asymmetries of transverse momentum spectra in ultrarelativistic heavy-ion collisions. *Phys. Rev. C* **2012**, *86*, 014909. [CrossRef]
21. Chakraborty, P.; Kapusta, J.I. Quasi-Particle Theory of Shear and Bulk Viscosities of Hadronic Matter. *Phys. Rev. C* **2011**, *83*, 014906. [CrossRef]
22. Noronha-Hostler, J.; Noronha, J.; Greiner, C. Hadron Mass Spectrum and the Shear Viscosity to Entropy Density Ratio of Hot Hadronic Matter. *Phys. Rev. C* **2012**, *86*, 024913. [CrossRef]
23. Meyer, H.B. A Calculation of the shear viscosity in SU(3) gluodynamics. *Phys. Rev. D* **2007**, *76*, 101701. [CrossRef]
24. Astrakhantsev, N.; Braguta, V.; Kotov, A. Temperature dependence of shear viscosity of SU(3)–gluodynamics within lattice simulation. *J. High Energy Phys.* **2017**, *4*, 101. [CrossRef]
25. Muronga, A. Shear viscosity coefficient from microscopic models. *Phys. Rev. C* **2004**, *69*, 044901. [CrossRef]
26. Demir, N.; Bass, S.A. Shear-Viscosity to Entropy-Density Ratio of a Relativistic Hadron Gas. *Phys. Rev. Lett.* **2009**, *102*, 172302. [CrossRef] [PubMed]
27. Motornenko, A.; Bravina, L.; Gorenstein, M.I.; Mager, A.G.; Zabrodin, E. Nucleon matter equation of state, particle number fluctuations, and shear viscosity within UrQMD box calculations. *J. Phys. G* **2018**, *45*, 035101. [CrossRef]
28. Teslyk, M.; Bravina, L.; Panova, O.; Vitiuk, O.; Zabrodin, E. Shear viscosity in microscopic calculations of A+A collisions at energies available at the Nuclotron-based Ion Collider fAcility (NICA). *Phys. Rev. C* **2020**, *101*, 014904. [CrossRef]
29. Zabrodin, E.; Teslyk, M.; Vitiuk, O.; Bravina, L. Calculation of shear viscosity in Au+Au collisions at NICA energies. *Phys. Scr.* **2020**, *85*, 074009. [CrossRef]
30. Ozvenchuk, V.; Linnyk, O.; Gorenstein, M.I.; Bratkovskaya, E.L.; Cassing, W. Shear and bulk viscosities of strongly interacting "infinite" parton-hadron matter within the parton-hadron-string dynamics transport approach. *Phys. Rev. C* **2013**, *87*, 064903. [CrossRef]
31. Rose, J.B.; Torres-Rincon, J.M.; Schäfer, A.; Oliinychenko, D.R.; Petersen, H. Shear viscosity of a hadron gas and influence of resonance lifetimes on relaxation time. *Phys. Rev. C* **2018**, *97*, 055204. [CrossRef]
32. Xu, Z.; Greiner, C.; Stoecker, H. PQCD calculations of elliptic flow and shear viscosity at RHIC. *Phys. Rev. Lett.* **2008**, *100*, 172301. [CrossRef]
33. Plumari, S.; Puglisi, A.; Scardina, F.; Greco, V. Shear viscosity of a strongly interacting system: Green-Kubo correlator versus Chapman-Enskog and relaxation-time approximations. *Phys. Rev. C* **2012**, *86*, 054902. [CrossRef]
34. Wesp, C.; El, A.; Reining, F.; Xu, Z.; Bouras, I.; Greiner, C. Calculation of shear viscosity using Green-Kubo relations within a parton cascade. *Phys. Rev. C* **2011**, *84*, 054911. [CrossRef]
35. Rais, J.; Gallmeister, K.; Greiner, C. The shear viscosity to entropy density ratio in Hagedorn states. *Phys. Rev. D* **2020**, *102*, 036009. [CrossRef]
36. Bass, S.A. Microscopic models for ultrarelativistic heavy ion collisions. *Prog. Part. Nucl. Phys.* **1998**, *41*, 255–369. [CrossRef]
37. Bleicher, M.; Zabrodin, E.; Spieles, C.; Bass, S.; Ernst, C.; Soff, S.; Bravina, L.; Belkacem, M.; Weber, H.; Stöcker, H.; et al. Relativistic hadron hadron collisions in the ultrarelativistic quantum molecular dynamics model. *J. Phys. G* **1999**, *25*, 1859–1896. [CrossRef]
38. Zabrodin, E.; Bravina, L.; Teslyk, M.; Vitiuk, O. Early thermalization and shear viscosity to entropy ratio in heavy-ion collisions at energies of BES, FAIR and NICA. *Nucl. Phys. A* **2021**, *1005*, 121861. [CrossRef]
39. De Groot, S.R.; van Leeuwen, W.A.; Weert, C. *Relativistic Kinetic Theory, Principles and Applications*; North-Holland Publishing Company: Amsterdam, The Netherlands, 1980.
40. Green, M.S. Markoff Random Processes and the Statistical Mechanics of Time-Dependent Phenomena. II. Irreversible Processes in Fluids. *J. Chem. Phys.* **1954**, *22*, 398. [CrossRef]

41. Kubo, R. Statistical-Mechanical Theory of Irreversible Processes. I. General Theory and Simple Applications to Magnetic and Conduction Problems. *J. Phys. Soc. Jpn.* **1957**, *12*, 570–586. [CrossRef]

42. Tanabashi, M.; Hagiwara, K.; Hikasa, K.; Nakamura, K.; Sumino, Y.; Takahashi, F.; Tanaka, J.; Agashe, K.; Aielli, G.; Amsler, C.; et al. Review of Particle Physics. *Phys. Rev. D* **2018**, *98*, 030001. [CrossRef]

43. Mitrovski, M.; Schuster, T.; Gräf, G.; Petersen, H.; Bleicher, M. Charged particle (pseudo-)rapidity distributions in $p + \bar{p}/p + p$ and Pb+Pb/Au+Au collisions from UrQMD calculations at energies available at the CERN Super Proton Synchrotron to the Large Hadron Collider. *Phys. Rev. C* **2009**, *79*, 044901. [CrossRef]

44. Bravina, L.; Gorenstein, M.; Belkacem, M.; Bass, S.; Bleicher, M.; Brandstetter, M.; Hofmann, M.; Soff, S.; Spieles, C.; Weber, H.; et al. Local thermodynamical equilibrium and the equation of state of hot, dense matter created in Au+Au collisions at AGS. *Phys. Lett. B* **1998**, *434*, 379–387. [CrossRef]

45. Bravina, L.; Gorenstein, M.; Belkacem, M.; Bass, S.; Bleicher, M.; Brandstetter, M.; Hofmann, M.; Soff, S.; Spieles, C.; Weber, H.; et al. Local thermal and chemical equilibration and the equation of state in relativistic heavy ion collisions. *J. Phys. G* **1999**, *25*, 351–362. [CrossRef]

46. Bravina, L.V.; Brandstetter, M.; Gorenstein, M.I.; Zabrodin, E.E.; Belkacem, M.; Bleicher, M.; Bass, S.; Ernst, C.; Hofmann, M.; Soff, S.; et al. Local equilibrium in heavy ion collisions: Microscopic model versus statistical model analysis. *Phys. Rev. C* **1999**, *60*, 024904. [CrossRef]

47. Bravina, L.V.; Zabrodin, E.E.; Gorenstein, M.I.; Bass, S.; Belkacem, M.; Bleicher, M.; Brandstetter, M.; Ernst, C.; Hofmann, M.; Neise, L.; et al. Chemical freezeout parameters at RHIC from microscopic model calculations. *Nucl. Phys. A* **2002**, *698*, 383–386. [CrossRef]

48. Bravina, L.V.; Zabrodin, E.E.; Bass, S.; Faessler, A.; Fuchs, C.; Gorenstein, M.I.; Greiner, W.; Soff, S.; Stöcker, H.; Weber, H. Equation of state of resonance rich matter in the central cell in heavy ion collisions at $S^{1/2} = 200$ AGeV. *Phys. Rev. C* **2001**, *63*, 064902. [CrossRef]

49. Bravina, L.V.; Zabrodin, E.E.; Bass, S.A.; Bleicher, M.; Brandstetter, M.; Faessler, A.; Fuchs, C.; Greiner, W.; Soff, S.; Stöcker, H. Microscopic models and effective equation of state in nuclear collisions in the vicinity of $E_lab = 30$ AGeV at the GSI Facility for Antiproton and Ion Research (FAIR) and beyond. *Phys. Rev. C* **2008**, *78*, 014907. [CrossRef]

50. Oliinychenko, D.; Petersen, H. Deviations of the Energy-Momentum Tensor from Equilibrium in the Initial State for Hydrodynamics from Transport Approaches. *Phys. Rev. C* **2016**, *93*, 034905. [CrossRef]

51. De, S.; De, S.; Chattopadhyay, S. Thermalization of dense hadronic matter in Au + Au collisions at energies available at the Facility for Antiproton and Ion Research. *Phys. Rev. C* **2016**, *94*, 054901. [CrossRef]

52. Belkacem, M.; Brandstetter, M.; Bass, S.A.; Bleicher, M.; Bravina, L.; Gorenstein, M.I.; Konopka, J.; Neise, L.; Spieles, C.; Soff, S.; et al. Equation of state, spectra and composition of hot and dense infinite hadronic matter in a microscopic transport model. *Phys. Rev. C* **1998**, *58*, 1727–1733. [CrossRef]

53. Bravina, L.V.; Zabrodin, E.E.; Bass, S.A.; Bleicher, M.; Brandstetter, M.; Soff, S.; Stöcker, H.; Greiner, W. Local equilibrium in heavy ion collisions: Microscopic analysis of a central cell versus infinite matter. *Phys. Rev. C* **2000**, *62*, 064906. [CrossRef]

54. Bratkovskaya, E.L.; Cassing, W.; Greiner, C.; Effenberger, M.; Mosel, U.; Sibirtsev, A. Aspects of thermal and chemical equilibration of hadronic matter. *Nucl. Phys. A* **2000**, *675*, 661–691. [CrossRef]

VI

VIII

MDPI

Article

Unruh Effect and Information Entropy Approach

Maksym Teslyk [1,2,†] , Olena Teslyk [2,†], Lidiia Zadorozhna [2,†], Larisa Bravina [1,†] and Evgeny Zabrodin [1,3,*,†]

1 Department of Physics, University of Oslo, PB 1048 Blindern, N-0316 Oslo, Norway; machur@ukr.net (M.T.); larissa.bravina@fys.uio.no (L.B.)
2 Faculty of Physics, Taras Shevchenko National University of Kyiv, UA-03022 Kyiv, Ukraine; ten@uni.kiev.ua (O.T.); zadorozhna_lida@ukr.net (L.Z.)
3 Skobeltsyn Institute of Nuclear Physics, Moscow State University, RU-119991 Moscow, Russia
* Correspondence: zabrodin@fys.uio.no
† These authors contributed equally to this work.

Abstract: The Unruh effect can be considered a source of particle production. The idea has been widely employed in order to explain multiparticle production in hadronic and heavy-ion collisions at ultrarelativistic energies. The attractive feature of the application of the Unruh effect as a possible mechanism of the multiparticle production is the thermalized spectra of newly produced particles. In the present paper, the total entropy generated by the Unruh effect is calculated within the framework of information theory. In contrast to previous studies, here the calculations are conducted for the finite time of existence of the non-inertial reference frame. In this case, only a finite number of particles are produced. The dependence on the mass of the emitted particles is taken into account. Analytic expression for the entropy of radiated boson and fermion spectra is derived. We study also its asymptotics corresponding to low- and high-acceleration limiting cases. The obtained results can be further generalized to other intrinsic degrees of freedom of the emitted particles, such as spin and electric charge.

Keywords: multiparticle production; Unruh effect; information theory

1. Introduction

As was demonstrated by Unruh [1], the observer comoving with the non-inertial reference frame (RF) with the acceleration a will detect particles thermalized at temperature

$$T = \frac{a}{2\pi}$$

in Planck units, whereas the observer in any inertial RF will see bare vacuum. If the acceleration a equals the surface gravity of some Schwarzschild black hole (BH), when the observer is at the horizon, T coincides with the temperature T_{BH} of the Bekenstein–Hawking radiation [2–4] of the horizon.

This peculiar non-invariance of the vacuum has raised a lot of interest in the topic (for review see, e.g., [5] and references therein). Recall that the Unruh effect was initially derived for scalar particles. Here, the change in the ratio between the negative and positive frequency modes of scalar fields in the noninertial RF was considered [1]. Generalizations to arbitrary trajectories of the observer is discussed in [6,7], whereas the generalization to the accelerated reference frames with rotation can be found in [8,9]. The emergence of the Unruh effect in the Rindler manifold of an arbitrary dimension and its relationship to the vacuum noise and stress are investigated in [10]. Various methods and approaches have been employed. For instance, an algebraic approach was used to extend the Unruh effect to theories with arbitrary spin and with interaction [11,12], whereas the path integral approach was applied to derive the effect for fermions within the framework of quantum field theory [13]. Among the recent studies, one can mention the relativistic quantum statistical

mechanics approach [14–16] based on the application of Zubarev's density operator [17,18]. Within this approach, the Unruh effect was obtained first for the scalar particles [14] and then generalized to the gas of massless fermions [16]. In the present study, we employ the approach based on the application of the information theory, which is a promising tool to study the black hole information dynamics, as one may see in [19] or reviews [20,21].

Usually, the non-inertial observer is assumed to accelerate forever. However, such an assumption implies the availability of an infinite energy supply and ever-lasting particle emission. The more sophisticated scenario, which considers the Unruh effect at finite time interval, is analyzed in papers [22–25].

There are a lot of proposals for the detection and application of the Unruh effect, see, e.g., [26–28]. The paper [29] discusses the possibility of eavesdropping in the non-inertial reference frame. The production of the entangled photon pairs from the vacuum with the help of the Unruh effect was investigated in [30], whereas, in [31], the creation of accelerated black holes by means of the Unruh effect was studied. In [32], the authors discuss the possibility of using accelerated electrons as thermometers; more on the topic can be found in Refs. [33,34]. Generated bosons and fermions were considered to be produced via the quantum tunneling mechanism at the Unruh horizon in [35,36].

The Unruh effect can be considered as a source for the creation of new particles. This idea has been widely employed [37–44] in order to explain multiparticle production in hadronic and heavy-ion collisions at ultrarelativistic energies. The attractive feature of the application of the Unruh effect as a possible mechanism of multiparticle production is the thermalized spectra of newly produced particles. Experiments with ultrarelativistic hadronic and heavy-ion collisions and their theoretical interpretations indicate that the produced matter seems to reach equilibrium extremely quickly, see, e.g., [45,46] for the present status of the field. The mechanism of this fast equilibration is still debated; therefore, the Unruh effect might be of great help. At the same time, since the Unruh source is thermal, it results in the observer-dependent entropy generation [47]. In the present paper, we also consider the Unruh horizon as a thermal source of particles. These particles are characterized by thermal distribution. Our aim is to estimate the entropy of the distribution and to define its dependence on any intrinsic degrees of freedom of the emitted particles.

In this paper, we consider Unruh radiation at some fixed energy E, which is assumed to be a parameter. It can be argued that such an analysis is incorrect because we should have taken into account the all-energy modes E_i via the product $\prod_{E_i}$ in the corresponding density matrix, see, e.g., [5]. This approach implies an independent emission of modes at different energies. In other words, in that case, one deals with the energy modes via the tensor product of the corresponding subspaces. However, such a generalization is not mandatory for the Unruh effect. For instance, in [35,36], the authors demonstrate that one can obtain the Unruh effect for some fixed energy without any need to take a product of all the modes to encompass the all-Unruh thermal bath states. This circumstance allows us to consider energy E of the mode as a parameter and, therefore, to take into account any correlations between the modes originating from the finite energy supply and restrictions imposed by energy conservation.

The paper is organized as follows. Section 2 presents the necessary basics from the probability theory and the information theory. Section 3 briefly describes the Unruh effect and the density matrix of the emitted quanta. The total entropy of the Unruh source is estimated in Section 4. Here, the general expression for the entropy of fermion and boson radiation is derived, as well as its analytic series expansion. In Section 5, one is dealing with the analysis of temperature asymptotics of the entropy. Two limiting cases corresponding to low and high temperatures, or, equivalently, the acceleration of the observer, are considered. Section 6 is devoted to the contribution of intrinsic degrees of freedom of the produced particles. Final remarks and conclusions can be found in Section 7.

2. Probability and Entropy

Let us consider some distribution $\{X\}$ with the unnormalized distribution probability $d(x)$. In other words, $d(x)$ is a number of events in which x is being observed. Shannon entropy $H(X)$ may be written as

$$H(X) = -\sum_x \frac{d(x)}{\mathcal{D}_X} \ln \frac{d(x)}{\mathcal{D}_X} = \ln \mathcal{D}_X - \frac{1}{\mathcal{D}_X} \sum_x d(x) \ln d(x), \tag{1}$$

where $\mathcal{D}_X = \sum_x d(x)$. $H(X)$ encodes the amount of information we need in order to completely describe $\{X\}$, i.e., this is amount of information we are lacking. Therefore, we should deal with the distribution $\{X\}$. It is scale-invariant, so it does not change under the transformations $d(x) \to \alpha d(x)$ for any $\alpha = $ const.

Similarly, for joint distribution $\{X, Y\}$ with the unnormalized distribution probability $d(x, y)$, one can write down Shannon entropy $H(X, Y)$ as

$$H(X,Y) = -\sum_{x,y} \frac{d(x,y)}{\mathcal{D}_{X,Y}} \ln \frac{d(x,y)}{\mathcal{D}_{X,Y}} = \ln \mathcal{D}_{X,Y} - \frac{1}{\mathcal{D}_{X,Y}} \sum_{x,y} d(x,y) \ln d(x,y), \tag{2}$$

where $\mathcal{D}_{X,Y} = \sum_{x,y} d(x,y)$.

In the joint case, one may define the conditional probability $d(x|y)$ as

$$d(x|y) = \frac{d(x,y)}{d(y)}, \qquad d(y) = \sum_x d(x,y). \tag{3}$$

It defines the amount of events with x from the set of events in which y occurs. Using Equation (1), Shannon entropy $H(X|y)$ becomes

$$H(X|y) = \ln \mathcal{D}_{X|y} - \frac{1}{\mathcal{D}_{X|y}} \sum_x d(x|y) \ln d(x|y) = -\sum_x d(x|y) \ln d(x|y), \tag{4}$$

where $\mathcal{D}_{X|y} = \sum_x d(x|y) = 1$, as follows from Equation (3).

Finally, substituting Equations (3) and (4) into Equation (2), one obtains

$$H(X,Y) = H(Y) + \langle H(X|y) \rangle_Y = H(X) + \langle H(Y|x) \rangle_X, \tag{5}$$

where averaging taken over X or Y reads

$$\langle \mathcal{A} \rangle_Z = \frac{1}{\mathcal{D}_Z} \sum_z d(z) \mathcal{A}, \qquad Z \equiv X, Y.$$

Recall that all the formulae above are valid for the discrete distributions only. In the continuous case, one should use the probability density function (PDF) $p(x)$ instead of $d(x)$. Shannon entropy becomes dimensionally incorrect and should be re-defined, as shown in [48,49].

For the distribution $\{X\}$ with the PDF $p(x)$, the entropy given by Equation (1) is generalized to

$$H(X_p) = \ln \mathcal{D}_{X_p} - \frac{1}{\mathcal{D}_{X_p}} \int p(x) \ln p(x) \mathrm{d}x - \langle \ln \mathrm{d}x \rangle_{X_p}, \tag{6}$$

where $\mathcal{D}_{X_p} = \int p(x) \mathrm{d}x$ is the norm and

$$\langle \mathcal{A} \rangle_{X_p} = \frac{1}{\mathcal{D}_{X_p}} \int p(x) \mathcal{A} \mathrm{d}x.$$

The last term in Equation (6) is related to the limiting density of discrete points and takes into account the amount of information encoding a discrete-continuum transition (see [48,49] for

details). The term originates from the fact that the PDF $p(x)$ is not dimensionally invariant compared to the discrete probability $d(x)$. The last one can be set to be dimensionless—see the explanation below Equation (1)—while $p(x)$ cannot. In any realistic computational task, the term determines the contribution of the bin widths dx of the distribution to the entropy. Note that one may formally reduce $H(X_p)$ to $H(X)$ by substituting $\int p(x)dx$ into $\sum_x d(x)$ and setting $\langle \ln dx \rangle_{X_p}$ to zero; the same procedure is valid in the opposite direction.

3. Unruh Effect

From here, we will use Planck (or natural) units, $c = G = \hbar = k_B = 1$. Furthermore, we restrict our analysis to $1 + 1$-dimensional space-time because two other spatial dimensions play no role and, therefore, can be neglected.

As was already mentioned in Section 1, vacuum is non-invariant with respect to the reference frame [1]. In the non-inertial RF determined with the acceleration a, one meets the appearance of horizon that separates space-time into the inside and outside domains. As a result, the non-inertial observer detects the radiation going out from the horizon, while the inertial one detects the Minkowski vacuum state $|0\rangle$ only. For bosons, the latter reads [5,35,36]

$$|0\rangle = \sqrt{\frac{1 - \exp(-E/T)}{1 - \exp(-NE/T)}} \sum_{n=0}^{N-1} \exp(-nE/2T)|n\rangle_{\text{in}}|n\rangle_{\text{out}}, \tag{7}$$

whereas, for fermions, one obtains

$$|0\rangle = \frac{1}{\sqrt{1 + \exp(-E/T)}} \sum_{n=0}^{1} \exp(-nE/2T)|n\rangle_{\text{in}}|n\rangle_{\text{out}} \tag{8}$$

Here, E is the energy of the quanta emitted at the Unruh horizon with the temperature $T = a/(2\pi)$. The denominator for bosons stands for the normalization reasons. Parameter N, as can be seen from Equation (7), encodes the maximum amount of quanta at energy E plus 1. Loosely speaking, N is the number of dimensions of the corresponding Fock space at the given energy E and temperature T of the source. The subscripts *in* and *out* denote the components of the field (Rindler modes) with respect to the horizon.

Usually, N is assumed to be infinite. One may argue that the finiteness of the parameter N in the boson case is incorrect from a mathematical point of view since one deals with the incomplete basis then. However, in any real physical situation, one is dealing with the finite number of produced particles, bosons and fermions. Taking $N \to \infty$ in Equation (7), as it is widely used in the literature on the topic, seems to be too strong of an assumption because the source produces an infinite amount of energy, $(N-1)E \to \infty$. This is valid in the case of everlasting acceleration or the non-zero probability of detecting $N \to \infty$ amount of particles at some finite time interval; both scenarios can be provided with the infinite energy supply only. This is because the infinite sum for bosonic modes—see Equation (7)—contains an arbitrary amount of particles: despite being exponentially suppressed, the probability for any $n \neq \infty$ in the sum for bosons is non-zero. Such a scenario seems to be rather unlikely from the physical point of view, especially when one considers the application of the Unruh effect for the description of particle production in relativistic hadronic or heavy ion collisions. Therefore, we assume the maximum number of particles to be finite in all calculations below.

Furthermore, let us consider only boson production in what follows because the expression for the fermions given by Equation (8) can be derived from Equation (7) by setting $N = 2$.

Expression (7) is the Schmidt decomposition [50]. The outgoing radiation is described by the density matrix

$$\rho_{\text{out}} = \text{Tr}_{\text{in}} |0\rangle \langle 0| = \frac{1 - \exp(-E/T)}{1 - \exp(-NE/T)} \sum_{n=0}^{N-1} \exp\left(-\frac{nE}{T}\right) |n\rangle_{\text{out}} \langle n|_{\text{out}} , \tag{9}$$

where we have traced over the inaccessible degrees of freedom (*in-* modes). Thus, the pure vacuum state from the inertial RF has transformed into the mixed one in the non-inertial RF. Here, the geometric origin of the Unruh effect appears. Namely, finiteness of the speed of light leads to the appearance of the horizon dividing the all modes in Hilbert space into the accessible (*out-*) and non-accessible (*in-*) ones. The complete state is obviously pure and follows unitary evolution. However, because one has limited access to it in the non-inertial RF, it looks like a decoherence. The eigenvalues of the density matrix ρ_{out} define the emission probability of a certain number of particles at energy E and temperature T. Therefore, Equation (9) describes the conditional multiplicity distribution $\{n|N, E, T\}$ at any given N, E and T.

One may assume that once we have the distribution, it is possible to calculate the corresponding Shannon entropy due to the formulae presented in Section 2. However, to deal with the density matrix ρ, one should use the von Neumann entropy $H(\rho)$ instead, which is defined as

$$H(\rho) = -\text{Tr}\rho \ln \rho.$$

The key difference of the von Neumann entropy from its classical analog, Shannon entropy, is related to its meaning: $H(\rho)$ defines the amount of information encoded with the correlations between the system described by ρ and the rest of the world. From this point of view, the density matrix ρ defines the projection of some larger system, which was determined in the larger Hilbert space, to the space in which the observed system is being defined. The projection might result in a loss of information encoded with the corresponding correlations between the Hilbert subspaces. The von Neumann entropy is the quantity to estimate the amount of this information. Due to its origin, it can be equal to zero for the entire space and non-zero for its subspace. This is not the case for the Shannon entropy because classical entropy of the whole system cannot be less than that of some part of it. However, the von Neumann entropy can be set as equal to its Shannon counterpart provided that the Schmidt decomposition coincides with the basis of the detector [51].

4. Unruh Entropy

For the emission probability ρ_{out} from Equation (9), the von Neumann entropy is defined as

$$H(\rho_{\text{out}}) = -\text{Tr}\rho_{\text{out}} \ln \rho_{\text{out}} = H(n|N, E, T) = \sigma(qE/T)\Big|_{q=N}^{q=1} , \tag{10}$$

where we use the following notations

$$\sigma(qE/T) = \frac{qE/T}{\exp(qE/T) - 1} - \ln\left[1 - \exp\left(-\frac{qE}{T}\right)\right], \tag{11}$$

$$f(x)\Big|_{x=b}^{x=a} = f(a) - f(b) . \tag{12}$$

As one may notice, $H(n|N, E/T)$ is an even function of E/T, i.e., $H(n|N, E/T) = H(n|N, -E/T)$. The asymptotic behavior of the entropy (10) with respect to E/T is the following

$$\lim_{E/T \to 0} H(n|N, E, T) = \ln N = \max(H) \lim_{E/T \to \infty} H(n|N, E, T) = 0 . \tag{13}$$

Expression (10) defines the entropy of the emitted quanta, as well as the quanta inside the horizon, for some mode of the radiated field only, which is determined by parameter N, energy E and temperature T. Parameter N depends on the amount of time during which the observer is being described by the non-inertial reference frame. It follows from the fact that the longer one is observing the horizon, the more particles at any fixed energy may

be detected. Therefore, we conclude that N should increase with time. Temperature T is completely determined by the acceleration a, see [1]. However, E cannot be considered as a fixed parameter. The non-inertial observer is expected to detect particles at different energies. The energy range for the particles may be written as

$$m \leq E \leq M \,, \tag{14}$$

where m is the invariant mass of the particles, and M is the maximum energy to be observed, respectively. We assume M to be limited by the acceleration a since the observation of the high-energy particles is very unlikely due to energy conservation law: one cannot extract more energy from the vacuum than is being spent to sustain the observer's acceleration.

Unfortunately, the definition of the energy range does not mean we know the spectrum distribution $\{E\}$. It is determined by the unnormalized PDF $p(E)$ of the emission of a particle from the vacuum at energy E.

In order to figure out $p(E)$ somehow, we use the following procedure. As can be noticed from Equation (9), for any particle number $n > 0$, the emission probability is proportional to the factor $\exp(-E/T)$. The case with $n = 0$ means no emission at all. Therefore, one should expect exponential behavior for $p(E)$

$$p(E) = C \exp(-E/T) \,, \tag{15}$$

where prefactor C is responsible for any corrections that might depend on the particle type and its quantum numbers. For the sake of simplicity, we assume $C = $ const and, therefore, drop it due to normalization reasons (see Section 2) in what follows. It is worth noting that such assumption results in Schwinger-like mechanism of particle production [52]. Thus, we recovered Schwinger-like particle production from the properties of Hilbert space and space-time only. Recall, however, that this result is generated by the Unruh effect after neglecting all possible corrections.

Now, we have the spectrum distribution $\{E\}$ as given by Equation (15). Without any loss of generality, we assume energy to be defined within the range $m \leq E \leq M$ (Equation (14)). From Equations (5) and (6), one obtains

$$
\begin{aligned}
H(n, E | N, T) = & -\langle \ln dE \rangle_{E_p} + \ln \mathcal{D}_{E_p} - \frac{1}{\mathcal{D}_{E_p}} \int_m^M p(E) \ln p(E) dE \\
& + \frac{1}{\mathcal{D}_{E_p}} \int_m^M p(E) H(n | N, E, T) dE \,,
\end{aligned} \tag{16}
$$

where the subscript E_p implies that the energy distribution is not discrete but rather a continuous one, i.e., it is defined with some PDF—see the text concerning Equation (6). In order to obtain the analytic expression, we substitute Equations (15) and (10) into Equation (16) and obtain, after the straightforward calculations, the total Unruh entropy $H(n, E | N, T)$ in a form

$$
\begin{aligned}
H(n, E | N, T) = & -\langle \ln dE \rangle_{E_p} + 1 + \ln \mathcal{D}_{E_p} + \frac{m \exp(-m/T) - M \exp(-M/T)}{\mathcal{D}_{E_p}} \\
& + \frac{T}{\mathcal{D}_{E_p}} \sum_{k=1}^{\infty} \left\{ \left[\frac{2kq+1}{k(kq+1)} + q\frac{E}{T} \right] \times \left. \frac{\exp[-(kq+1)E/T]}{kq+1} \right|_{E=M}^{E=m} \right\} \Bigg|_{q=N}^{q=1} \,,
\end{aligned} \tag{17}
$$

where

$$\mathcal{D}_{E_p} = \int_m^M p(E) dE = T \left[\exp\left(-\frac{m}{T}\right) - \exp\left(-\frac{M}{T}\right) \right] \tag{18}$$

and $\sigma(qE/T)$ from Equation (10) is represented by the following series

$$\sigma(qE/T) = \sum_{k=1}^{\infty} \left(\frac{1}{k} + q\frac{E}{T} \right) \exp\left(-\frac{kqE}{T} \right). \tag{19}$$

The first term in Equation (17) is responsible for encoding the discrete-continuum transition, see [48,49]. It is expected to depend neither on any quantum numbers of outgoing particles nor on the reference frame. Therefore, we assume $\langle \ln dE \rangle_{E_p}$ to be constant.

Expression (17) defines entropy for the distribution $\{n, E | N, T\}$ of the particles being detected by the observer associated with non-inertial RF moving with acceleration $a = 2\pi T$. Recall that in the case of fermions, one should use $N = 2$. For the bosons, N may take any positive integer value obeying the energy conservation law. The entropy calculated for the Unruh radiation of fermions and bosons is presented in Figures 1 and 2, respectively. One can see the distinct maximum in the region of small values of the m/T ratio. The maximum increases with rising the M/T ratio and becomes more pronounced with the increase in radiated particles (see Figure 2).
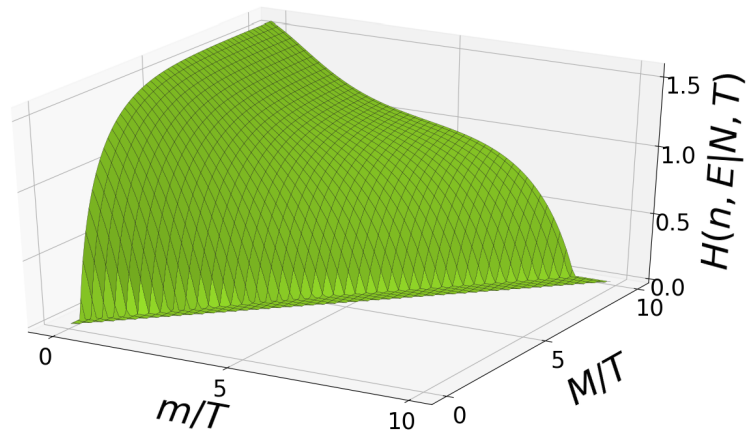
Figure 1. (Color online) The entropy $H(n, E | N, T)$ of Unruh radiation given by Equation (17) for fermions ($N = 2$) as function of m/T and M/T.

The considered example seems to be straightforward. However, one should keep in mind that the whole analysis above is valid for $1 + 1$-dimensional space-time. Other spatial dimensions do not contribute to the density matrix ρ_{out} or to its von Neumann entropy because the corresponding subspaces of the Hilbert space contribute to ρ_{out} via the direct tensor product and, therefore, can be traced out with no consequences to the analysis above. This simple direct extension to additional spatial dimensions for the Unruh effect may lead to the widely spread conclusion that the Unruh effect results in the appearance of thermal bath all over the space. In our opinion, this conclusion needs to be clarified. Namely, in the last case, the non-inertial observer, as well as the horizon itself, should be considered as an infinite plane in the additional spatial dimensions being accelerated alongside the normal to the plane. However, the observer should be finite and, therefore, cannot detect particles from the half-space defined by the horizon. Otherwise, it would lead to faster-than-light speed communication and causality violation because the transition to inertial RF cannot cause the immediate disappearance of the Unruh radiation from the horizon occupying the half-space.
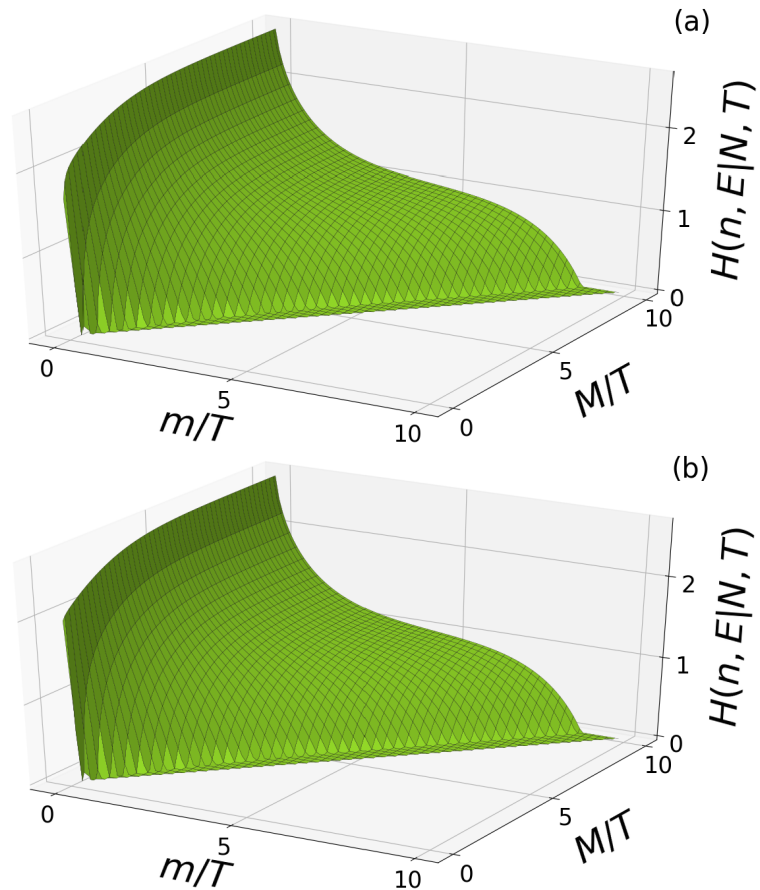
Figure 2. (Color online) The same as Figure 1 but for bosons. The spectrum of bosons contains (**a**) $N = 100$ and (**b**) $N = 1000$ particles.

To overcome the difficulties, we have to assume that

- In order to obey, the energy conservation law N should be finite;
- In the case of $(2 + 1)$ or $(3 + 1)$-dimensional space-time, the Unruh horizon should be considered as a radiation source of finite size.

Due to the axial symmetry of the non-inertial reference frame, the horizon should be a disk shape with some radius r. The radius can be determined by the observer's size and causality, i.e., the finiteness of light speed. Such an assumption leads to an observer-dependent size of r. The problem may be cured, e.g., if one considers the observer's acceleration a as a surface gravity of the corresponding black hole and obtain some efficient scale $r = (4\pi T)^{-1}$.

One might be confused by the fact that since the Unruh effect describes the thermal bath, its entropy should be maximal. As can be easily noticed from the eigenvalues of the density matrix (9), all of them exponentially depend on the total energy of the emitted number of particles and thus generate a well-known partition function. Note, however, that ρ_{out} is defined for some *fixed* value of energy. Therefore, E can be considered a parameter of the conditional distribution $\{n|N, E, T\}$. Dealing with the joint distribution $\{n, E|N, T\}$ over multiplicity n and energy E of the emitted quanta, one should take into account energy conservation. It results in some correlations between the possible number of emitted

particles and their energy. Thus, the entropy $H(n, E|N, T)$ describes not a completely thermal source but some other one.

5. Asymptotics of Unruh Entropy

Let us analyze the asymptotic behavior of the total Unruh entropy in Equation (16) for (i) small and (ii) large acceleration of the observer. The case of small acceleration is analogous to $T \to 0$; therefore, we will drop all but the leading term in Equation (16). At small temperatures, Equation (18) transforms into

$$\mathcal{D}_{E_p}\Big|_{T \to 0} \approx T \exp\left(-m/T\right),$$ (20)

where we have neglected the term $\exp\left(-M/T\right)$ since M is the upper bound for the energy spectrum; therefore, $M > m$. The Unruh entropy becomes

$$H(E)\Big|_{T \to 0} = \ln \mathcal{D}_{E_p} - \frac{1}{\mathcal{D}_{E_p}} \int_m^M p(E) \ln p(E) \mathrm{d}E \approx \ln T - \frac{m}{T} + 1 + \frac{m}{T} = \ln T + 1.$$ (21)

Because the entropy $H(n|N, E, T)$ equals zero when $N = 1$, we consider the case with $N > 1$ for $T \to 0$. Neglecting all the higher-order exponents, one obtains from Equation (10) that

$$H(n|N, E, T)\Big|_{T \to 0} \approx \frac{E}{T} \exp\left(-E/T\right).$$ (22)

Substituting Equations (21) and (22) into Equation (16), we obtain

$$H(n, E|N, T)\Big|_{T \to 0} \approx -\left\langle \ln \frac{\mathrm{d}E}{T} \right\rangle_{E_p} + 1 + \frac{1}{4}\left(1 + \frac{2m}{T}\right) \exp\left(-m/T\right),$$ (23)

where all the higher-order exponents are omitted. This distribution is displayed in Figure 3. The entropy reaches a quite distinct maximum at $m/T \approx 0.5$ and quickly drops to unity at larger values of this ratio.
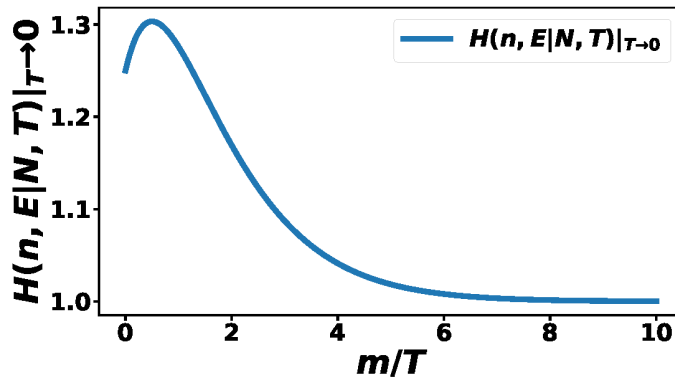

Figure 3. (Color online) Asymptotic behavior of entropy $H(n, E|N, T)$ given by Equation (23) at $T \to 0$ as function of m/T.

In the case of large acceleration $a \to \infty \Leftrightarrow T \to \infty$, one obtains from Equation (18)

$$
\begin{aligned}
\int_m^M p(E)\Big|_{T \to \infty} \mathrm{d}E &= \int_m^M \left(1 - \frac{E}{T} + \frac{E^2}{2T^2}\right) \mathrm{d}E + \mathcal{O}\left(1/T^3\right) \\
&= (M - m)\left(1 - \frac{M + m}{2T} + \frac{M^2 + Mm + m^2}{6T^2}\right) + \mathcal{O}\left(1/T^3\right),
\end{aligned}
$$ (24)

and, therefore,

$$H(E) = \ln \mathcal{D}_{E_p} - \frac{1}{\mathcal{D}_{E_p}} \int_m^M p(E) \ln p(E) \mathrm{d}E = \ln (M - m) - \frac{(M - m)^2}{24T^2} + \mathcal{O}\left(1/T^3\right). \quad (25)$$

Thus, the conditional entropy $H(n|N, E, T)$ from Equation (10) becomes

$$H(n|N, E, T)\Big|_{T\to\infty} = \ln N - \frac{N^2 - 1}{24T^2}E^2 + \mathcal{O}\left(1/T^4\right), \quad (26)$$

which, together with Equation (24), gives us

$$\frac{1}{\mathcal{D}_{E_p}} \int_m^M p(E) H(n|N, E, T) \mathrm{d}E = \ln N - \frac{M^2 + Mm + m^2}{72T^2}\left(N^2 - 1\right) + \mathcal{O}\left(1/T^3\right). \quad (27)$$

Finally, substituting Equations (25) and (27) into Equation (16), we obtain the desired asymptotics at high acceleration (or temperature)

$$\begin{aligned} H(n, E|N, T)\Big|_{T\to\infty} = & -\langle \ln \mathrm{d}E \rangle_{E_p} + 1 + \ln (M - m) + \ln N \\ & - \frac{(N^2 + 2)(M^2 + m^2) + (N^2 - 7)Mm}{72T^2} + \mathcal{O}\left(1/T^3\right). \end{aligned} \quad (28)$$

The entropy asymptotics at $T \to \infty$ calculated according to Equation (28) is presented in Figure 4 for fermions ($N = 2$) and in Figure 5 for the boson spectra with $N = 100$ and 1000 particles, respectively. At high temperatures, the entropy weakly depends on m and quickly increases with an increase in the value of M. The larger the number of particles, the steeper the rising slope. For $N = 1000$, the entropy seems to saturate at $M \geq 5$.
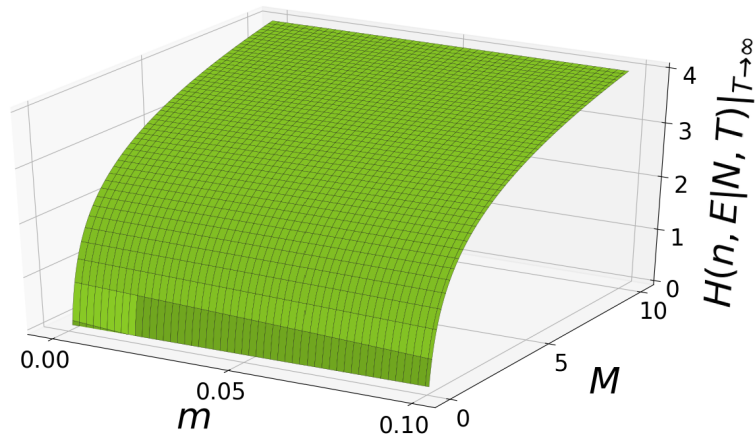
Figure 4. (Color online) High-temperature asymptotics of the entropy $H(n, E|N, T)$ of Unruh radiation given by Equation (28) for fermions ($N = 2$) as a function of m and M.
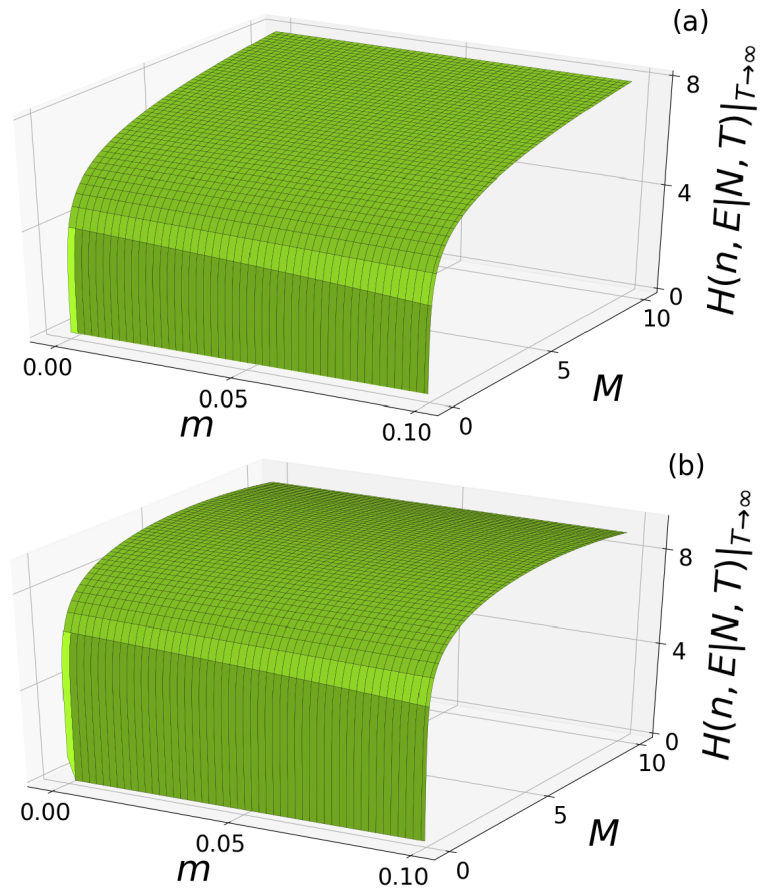
Figure 5. (Color online) The same as Figure 4 but for bosons with (**a**) $N = 100$ and (**b**) $N = 1000$ particles in the spectrum.

6. Generalization to Intrinsic Degrees of Freedom

Expression (17) is valid for some mode of the radiated field only, which is defined by the joint multiplicity-energy distribution $\{n, E\}$, temperature T and parameter N. However, since the emitted particles may have additional degrees of freedom $\{\lambda\}$, such as electric charge, spin, polarization, etc., they have to be taken into account too. This is equivalent to the following modification of the total distribution

$$\{n, E|N, T\} \to \{\lambda, n, E|N, T\} \, .$$

Using Equation (5), we then obtain

$$H(\lambda, n, E|N, T) = H(\lambda) + \langle H(n, E|N, T, \lambda) \rangle_\lambda \, . \tag{29}$$

However, such a generalization is not an easy task at all. Let us consider a simple example, while detecting a particle at some E, one should measure its energy. Such a process results in the consumption of the particle's momentum. One may argue that calorimetry is not required. The observer can build some source of similar particles and carry out interference experiments to determine the energy of the particle to be detected. However, any such interference will result in the re-distribution of the momenta during

the interference and therefore will change the observer's momentum as well. Thus, one concludes that measuring the particle's energy E leads to a change in the observer's acceleration a. It implies a change in the Unruh temperature $T = a/(2\pi)$ of the source the observer is dealing with.

One may also note that the Unruh effect is being considered within the quasi-classical approach. It means that the density matrix ρ_{out} in Equation (9) is obtained under the assumption that the outgoing radiation has no influence on the background metric (see [5,35,36]). Such a remark is correct, but what about other degrees of freedom λ? For instance, taking into account the spin of the particles emitted by the Unruh horizon may lead to a change in the observer's angular momentum. In this case, the observer's acceleration a can not be constant due to the conservation of the total angular momentum anyway and thus implies a change in T in Equation (29) during particle identification.

Thus, the situation seems to be simple only if one neglects *any* influence of the outgoing particles during the Unruh effect. In this case the entropy $H(n, E|N, T, \lambda)$ does not depend on $\{\lambda\}$, and Expression (29) is reduced to the sum

$$H(\lambda, n, E|N, T) = H(\lambda) + H(n, E|N, T). \tag{30}$$

7. Conclusions

The Unruh effect is considered from the point of view of the information theory. We estimated the total entropy of the radiation generated by the Unruh horizon in the non-inertial reference frame for the state verified as vacuum by any inertial observer. Usually such a case is treated as von Neumann entropy of the corresponding density matrix. However, this is just the starting point of our study because the density matrix of the outgoing radiation describes the conditional multiplicity distribution at the given energy and Unruh temperature. As a result, it allows one to estimate the *total* entropy of the Unruh source by taking into account both the multiplicity and energy distribution of the outgoing quanta. We show how it can be calculated even without the exact knowledge of the corresponding Hamiltonian. In particular, such a lack of information results in the Schwinger-like spectrum of the emission (see Equation (15)).

The case of a finite amount of particle emission is considered. It allows us to utilize the results for realistic particle emission spectra. The asymptotics of the general expression for entropy with respect to low and high values of the Unruh temperature are also investigated. We found that in the case of small acceleration corresponding to a low temperature, the entropy of the radiation does not depend on the maximal amount of emitted particles in the leading order (see Equation (23)). The dependence on N is recovered for large accelerations when $T \rightarrow \infty$ (see Equation (28)). It can be explained by the abundant emission of particles from the hot Unruh horizon when the amount of the emitted quanta may be considered as an extra degree of freedom contributing to the total entropy.

Another interesting point is that the total entropy $H(n, E|N, T)$ quickly drops to zero with the increase in the mass m of the quanta. It can be explained by the energy conservation law: the more energy is being spent on the creation of particle's mass, the less of it may be used to generate the total distribution. At the same time, total entropy of the Unruh source slightly increases with the maximum allowed energy M because the distribution widens with the increase in M, thus leading to the total entropy increase.

The obtained results can be applied to the analysis of particle distributions in inelastic scattering processes at high energies. Furthermore, they may be generalized to other degrees of freedom of the emitted particles, such as spin, charges, etc. However, such a generalization may significantly complicate the analysis. For instance, additional conservation laws originating from the other degrees of freedom might change the metric. Therefore, one may be forced to take a distribution $\{T\}$ into account too.

References

1. Unruh, W.G. Notes on black-hole evaporation. *Phys. Rev. D* **1976**, *14*, 870–892. [CrossRef]
2. Hawking, S.W. Particle creation by black holes. *Comm. Math. Phys.* **1975**, *43*, 199–220. [CrossRef]
3. Bekenstein, J.D. Black holes and entropy. *Phys. Rev. D* **1973**, *7*, 2333–2346. [CrossRef]
4. Bekenstein, J.D. Statistical black-hole thermodynamics. *Phys. Rev. D* **1975**, *12*, 3077–3085. [CrossRef]
5. Crispino, L.C.B.; Higuchi, A.; Matsas, G.E.A. The Unruh effect and its applications. *Rev. Mod. Phys.* **2008**, *80*, 787–838. [CrossRef]
6. Letaw, J.R. Stationary world lines and the vacuum excitation of noninertial detectors. *Phys. Rev. D* **1981**, *23*, 1709–1714. [CrossRef]
7. Obadia, N.; Milgrom, M. On the Unruh effect for general trajectories. *Phys. Rev. D* **2007**, *75*, 065006. [CrossRef]
8. Letaw, J.R.; Pfautsch, J.D. Quantized scalar field in rotating coordinates. *Phys. Rev. D* **1980**, *22*, 1345–1351. [CrossRef]
9. Korsbakken, J.I.; Leinaas, J.M. The Fulling-Unruh effect in general stationary accelerated frames. *Phys. Rev. D* **2004**, *70*, 084016. [CrossRef]
10. Takagi, S. Vacuum noise and stress induced by uniform acceleration: Hawking-Unruh effect in Rindler manifold of arbitrary dimension. *Prog. Theor. Phys. Suppl.* **1986**, *88*, 1–142. [CrossRef]
11. Bisognano, J.J.; Wichmann, E.H. On the duality connection for a Hermitian scalar field. *J. Math. Phys.* **1975**, *16*, 985–1007. [CrossRef]
12. Bisognano, J.J.; Wichmann, E.H. On the duality connection for quantum fields. *J. Math. Phys.* **1976**, *17*, 303–321. [CrossRef]
13. Unruh, W.G.; Weiss, N. Acceleration radiation in interacting field theories. *Phys. Rev. D* **1984**, *29*, 1656–1662. [CrossRef]
14. Becattini, F. Thermodynamic equilibrium with acceleration and the Unruh effect. *Phys. Rev. D* **2018**, *97*, 085013. [CrossRef]
15. Becattini, F.; Rindori, D. Extensivity, entropy current, area law and Unruh effect. *Phys. Rev. D* **2019**, *99*, 125011. [CrossRef]
16. Prokhorov, G.Y.; Teryaev, O.V.; Zakharov, V.I. Unruh effect for fermions from the Zubarev density operator. *Phys. Rev. D* **2019**, *99*, 071901. [CrossRef]
17. Zubarev, D.N.; Prozorkevich, A.V.; Smolyanskii, S.A. Derivation of nonlinear generalized equations of quantum relativistic hydrodynamics. *Theor. Math. Phys.* **1979**, *40*, 821–831. [CrossRef]
18. Becattini, F.; Buzzegoli, M.; Grossi, F. Reworking the Zubarev's approach to non-equilibrium quantum statistical mechanics. *Particles* **2019**, *2*, 197–207. [CrossRef]
19. Page, D.N. Information in black hole radiation. *Phys. Rev. Lett.* **1993**, *71*, 3473. [CrossRef]
20. Page, D.N. Hawking radiation and black hole thermodynamics. *New J. Phys.* **2005**, *7*, 203. [CrossRef]
21. Stoica, O.C. Revisiting the Black Hole Entropy and the Information Paradox. *Adv. High Energy Phys.* **2018**, *2018*, 4130417. [CrossRef]
22. Svaiter, B.F.; Svaiter, N.F. Inertial and noninertial particle detectors and vacuum fluctuations. *Phys. Rev. D* **1992**, *46*, 5267–5277. [CrossRef]
23. Sriramkumar, L.; Padmanabhan, T. Response of finite time particle detectors in noninertial frames and curved space-time. *Class. Quant. Grav.* **1996**, *13*, 2061–2079. [CrossRef]
24. Higuchi, A.; Matsas, G.E.A.; Peres, C.B. Uniformly accelerated finite-time detectors. *Phys. Rev. D* **1993**, *48*, 3731–3734. [CrossRef]
25. Kothawala, D.; Padmanabhan, T. Response of Unruh-DeWitt detector with time-dependent acceleration. *Phys. Lett. B* **2010**, *690*, 201–206. [CrossRef]
26. Chen, P.; Tajima, T. Testing Unruh radiation with ultraintense lasers. *Phys. Rev. Lett.* **1999**, *83*, 256–259. [CrossRef]
27. Louko, J.; Satz, A. Transition rate of the Unruh-DeWitt detector in curved spacetime. *Class. Quant. Grav.* **2008**, *25*, 055012. [CrossRef]

28. Akhmedova, V.; Pilling, T.; de Gill, A.; Singleton, D. Comments on anomaly versus WKB/tunneling methods for calculating Unruh radiation. *Phys. Lett. B* **2009**, *673*, 227–231. [CrossRef]

29. Bradler, K. Eavesdropping of quantum communication from a non-inertial frame. *Phys. Rev. A* **2007**, *75*, 022311. [CrossRef]

30. Han, M.; Olson, S.J.; Dowling, J.P. Generating entangled photons from the vacuum by accelerated measurements: Quantum information theory meets the Unruh-Davies effect. *Phys. Rev. A* **2008**, *78*, 022302. [CrossRef]

31. Parentani, R.; Massar, S. The Schwinger mechanism, the Unruh effect and the production of accelerated black holes. *Phys. Rev. D* **1997**, *55*, 3603–3613. [CrossRef]

32. Bell, J.S.; Leinaas, J.M. Electrons as accelerated thermometers. *Nucl. Phys. B* **1983**, *212*, 131–150. [CrossRef]

33. Bell, J.S.; Leinaas, J.M. The Unruh effect and quantum fluctuations of electrons in storage rings. *Nucl. Phys. B* **1987**, *284*, 488–508. [CrossRef]

34. Akhmedov, E.T.; Singleton, D. On the relation between Unruh and Sokolov-Ternov effects. *Int. J. Modern Phys. A* **2007**, *22*, 4797–4823. [CrossRef]

35. Banerjee, R.; Majhi, B.R. Hawking black body spectrum from tunneling mechanism. *Phys. Lett. B* **2009**, *675*, 243–245. [CrossRef]

36. Roy, D. The Unruh thermal spectrum through scalar and fermion tunneling. *Phys. Lett. B* **2009**, *681*, 185–189. [CrossRef]

37. Barshay, S.; Troost, W. A possible origin for temperature in strong interactions. *Phys. Lett.* **1978**, *73B*, 437–439. [CrossRef]

38. Grillo, A.F.; Srivastava, Y. Intrinsic temperature of confined systems. *Phys. Lett. B* **1979**, *85*, 377–380. [CrossRef]

39. Hosoya, A. Moving mirror effects in hadronic reactions. *Progr. Theor. Phys.* **1979**, *61*, 280–293. [CrossRef]

40. Barshay, S.; Braun, H.; Gerber, J.P.; Maurer, G. Possible evidence for fluctuations in the hadronic temperature. *Phys. Rev. D* **1980**, *21*, 1849–1853. [CrossRef]

41. Kharzeev, D.; Tuchin, K. From color glass condensate to quark gluon plasma through the event horizon. *Nucl. Phys. A* **2005**, *753*, 316–334. [CrossRef]

42. Castorina, P.; Kharzeev, D.; Satz, H. Thermal hadronization and Hawking-Unruh radiation in QCD. *Eur. Phys. J. C* **2007**, *52*, 187–201. [CrossRef]

43. Castorina, P.; Satz, H. Hawking-Unruh hadronization and strangeness production in high energy collisions. *Adv. High Energy Phys.* **2014**, *2014*, 376982. [CrossRef]

44. Biro, T.S.; Gyulassy, M.; Schram, Z. Unruh gamma radiation at RHIC? *Phys. Lett. B* **2012**, *708*, 276–279. [CrossRef]

45. Liu, F.; Wang, E.; Wang, X.-N.; Xu, N.; Zhang, B.-W. Proceedings, 28th International Conference on Ultrarelativistic Nucleus-Nucleus Collisions (Quark Matter 2019): Wuhan, China, November 3–9. 2019. *Nucl. Phys. A* **2021**, *1005*, 122104.

46. Antinori, F.; Dainese, A.; Giubellino, P.; Greco, V.; Lombardi, M.P.; Scomparin, E. Proceedings, 27th International Conference on Ultrarelativistic Nucleus-Nucleus Collisions (Quark Matter 2018): Venice, Italy, May 14–19. 2018. *Nucl. Phys. A* **2019**, *982*, 1–1066.

47. Marolf, D.; Minic, D.; Ross, S.F. Notes on spacetime thermodynamics and the observer dependence of entropy. *Phys. Rev. D* **2004**, *69*, 064006. [CrossRef]

48. Jaynes, E.T. Information theory and statistical mechanics. In *Lectures in Theoretical Physics*; Ford, K.W., Ed.; Benjamin: New York, NY, USA, 1963; Volume 3, pp. 181–218.

49. Jaynes, E.T. Prior probabilities. *IEEE Trans. Syst. Sci. Cybern.* **1968**, *4*, 227–241. [CrossRef]

50. Pathak, A. *Elements of Quantum Computation and Quantum Communication*, 1st ed.; Taylor & Francis: London, UK, 2013; pp. 1–340.

51. Kharzeev, D.E. Quantum information approach to high energy interactions. *Phil. Trans. R. Soc. A* **2021**, *380*, 20210063. [CrossRef]

52. Schwinger, J. On Gauge Invariance and Vacuum Polarization. *Phys. Rev.* **1951**, *82*, 664–679. [CrossRef]